Jagiellonian University in Kraków
Faculty of Physics, Astronomy and Applied Computer Science

Wojciech Tarnowski
Student number: 1079390

Eigenvectors of Random Matrices: Theory and Applications

PhD thesis

Thesis written under the supervision of
prof. dr hab. Maciej A. Nowak
Mark Kac Complex Systems Research Center

Kraków, July 2020

Wydział Fizyki, Astronomii i Informatyki Stosowanej
Uniwersytet Jagielloński

Oświadczenie

Ja niżej podpisany Wojciech Tarnowski (nr indeksu: 1079390) doktorant Wydziału Fizyki, Astronomii i Informatyki Stosowanej Uniwersytetu Jagiellońskiego oświadczam, że przedłożona przeze mnie rozprawa doktorska pt. „Eigenvectors of Random Matrices: Theory and Applications" jest oryginalna i przedstawia wyniki badań wykonanych przeze mnie osobiście, pod kierunkiem prof. dra hab. Macieja A. Nowaka. Pracę napisałem samodzielnie.

Oświadczam, że moja rozprawa doktorska została opracowana zgodnie z Ustawą o prawie autorskim i prawach pokrewnych z dnia 4 lutego 1994 r. (Dziennik Ustaw 1994 nr 24 poz. 83 wraz z późniejszymi zmianami).

Jestem świadom, że niezgodność niniejszego oświadczenia z prawdą ujawniona w dowolnym czasie, niezależnie od skutków prawnych wynikających z ww. ustawy, może spowodować unieważnienie stopnia nabytego na podstawie tej rozprawy.

Kraków, dnia .....

.....
(podpis doktoranta)

Acknowledgments

I would like to thank my family for their support during my entire studies and to direct special thanks to Janina Krzysiak for her continuous support and patience during the time of my PhD studies. She is also a silent hero of more than half of my scientific papers (including this thesis) to whom I owe their final shape.

I would like also to express my sincere gratitude to my supervisor, professor Maciej A Nowak, for guiding me through the journey across my PhD studies, and for the broad range of interdisciplinary research directions pursued together throughout this time. Special thanks to my colleagues from the Theory of Complex Systems Department and the Statistical Physics Department for the friendly and stimulating environment. I am indebted to my mentors at King's College London – Yan Fyodorov, Pierpaolo Vivo and Izaak Neri – for the warm hospitality and great collaboration during my scholarship there.

Special thanks to Staszek Jastrzębski for our squash games and discussions between them, during which the ideas of [A7] were conceived, fulfilling this way his wish from the second year of our undergraduate studies of having a paper together, in which I had not believed.

Last but not least, I would like to thank the funding agencies for the financial support during the time of my PhD studies. My work was supported by the Ministry of Science and Higher Education through the Diamond Grant 0225/DIA/2015/44, National Center for Science through the Etiuda scholarship UMO-2018/28/T/ST1/00470 and the MAESTRO Grant DEC-2011/02/A/ST1/00119, Foundation for Polish Science (FNP) through the project *Bio-inspired Artificial Neural Networks* POIR.04.04.00-00-14DE/18-00 and through the Marian Smoluchowski Research Consortium Matter Energy Future scholarship from KNOW funding.

Abstract

The thesis tackles the problem of non-orthogonal eigenvectors of non-Hermitian random matrices from two perspectives: theoretical and applicational. The first part is devoted to development of analytical tools allowing for effective calculation of one- and two-point correlation functions involving scalar products of left and right eigenvectors. The technique of Feynman diagrams is used for calculations in the limit of large matrix size. Eigenvector non-orthogonality is studied in the real elliptic ensemble, where a novel regime of weak non-normality is discovered. The developed formalism from the first part is then applied to two neural networks. One is a model of a biological network, where it is discovered that two biological rules – Dale's principle and excitatory/inhibitory balance – are the source of strong eigenvector non-orthogonality. The second is an artificial neural network with residual architecture, where the input-output Jacobian is analyzed. It is observed that its singular values in a universal way concentrate around one, explaining why such an architecture facilitates training neural networks.

Streszczenie

Przedstawiona praca porusza problem nieortogonalnych wektorów własnych niehermitowskich macierzy przypadkowych z punktu widzenia teorii oraz zastosowań. Pierwsza część pracy poświęcona jest rozwinięciu technik analitycznych pozwalających na obliczanie jedno- i dwupunktowej funkcji korelacji, które zawierają iloczyny skalarne lewych i prawych wektorów własnych. Obliczenia w granicy dużego rozmiaru macierzy są wykonane w oparciu o analizę diagramów Feynmana. Przeprowadzona jest analiza nieortogonalnych wektorów własnych w eliptycznym zespole statystycznym, gdzie odkryty zostaje nowy obszar tak zwanej słabej nienormalności. Wypracowany formalizm jest następnie zastosowany w dwóch modelach sieci neuronowych. W pierwszym modelu, który opisuje biologiczne sieci, zaobserwowano, że uwzględnienie reguły Dale'a oraz równowagi między neuronami wzmacniajacymi a hamującymi jest źrodłem silnej nieortogonalności wektorów własnych. Drugim analizowanym modelem jest sztuczna sieć neuronowa o architekturze residualnej, gdzie analizowany jest jakobian wejście-wyjście. Zaobserwowano, że jego wartości osobliwe w uniwersalny sposób koncentrują się wokół jedności, tym samym wyjaśniając, dlaczego taka architektura ułatwia trenowanie sieci neuronowych.

This thesis is based on the following publications. Their full texts are presented in the appendix

[A1] Serban Belinschi, Roland Speicher, Maciej A. Nowak and Wojciech Tarnowski, *Squared eigenvalue condition numbers and eigenvector correlations from the single ring theorem*, Journal of Physics A: Mathematical and Theoretical 50 (10), 105204 (2017).

[A2] Maciej A. Nowak and Wojciech Tarnowski, *Complete diagrammatics of the single-ring theorem*, Physical Review E 96 (4), 042149 (2017).

[A3] Maciej A. Nowak and Wojciech Tarnowski, *Probing non-orthogonality of eigenvectors in non-Hermitian matrix models: diagrammatic approach*, Journal of High Energy Physics 2018 (6), 152 (2018).

[A4] Yan V. Fyodorov and Wojciech Tarnowski, *Condition numbers for real eigenvalues in real Elliptic Gaussian ensemble*, arXiv:1910.09204 [math-ph] (2019). Submitted to Annales Henri Poincaré.

[A5] Maciej A. Nowak and Wojciech Tarnowski, *Narain transform for spectral deformations of random matrix models*, Nuclear Physics B 955, 115051 (2020).

[A6] Ewa Gudowska-Nowak, Maciej A. Nowak, Dante R. Chialvo, Jeremi K. Ochab and Wojciech Tarnowski, *From Synaptic Interactions to Collective Dynamics in Random Neuronal Networks Models: Critical Role of Eigenvectors and Transient Behavior* Neural Computation 32 (2), 395-423 (2020).

[A7] Wojciech Tarnowski, Stanisław Jastrzębski, Piotr Warchoł, Jacek Tabor and Maciej A. Nowak, *Dynamical Isometry is Achieved in Residual Networks in a Universal Way for any Activation Function*, Proceedings of Machine Learning Research 89, 2221–2230 (2019). Supplementary material available at `http://proceedings.mlr.press/v89/tarnowski19a/tarnowski19a-supp.pdf`

List of publications written during the time of PhD studies but not included in the thesis

[B1] Gabor Andras Almasi, Wojciech Tarnowski, Bengt Friman and Krzysztof Redlich, *Scaling violation and the magnetic equation of state in chiral models*, Physical Review D 95 (1), 014007 (2017).

[B2] Maciej A. Nowak and Wojciech Tarnowski, *Spectra of large time-lagged correlation matrices from Random Matrix Theory*, Journal of Statistical Mechanics: Theory and Experiment 2017 (6), 063405 (2017).

[B3] Sergey Denisov, Tetyana Laptyeva, Wojciech Tarnowski, Dariusz Chruściński and Karol Życzkowski, *Universal Spectra of Random Lindblad Operators*, Physical Review Letters 123 (14), 140403 (2019).

[B4] Jeremi K. Ochab, Wojciech Tarnowski, Maciej A. Nowak and Dante R. Chialvo, *On the pros and cons of using temporal derivatives to assess brain functional connectivity*, NeuroImage 184, 577–585 (2019).

[B5] Wojciech Tarnowski, Izaak Neri and Pierpaolo Vivo, *Universal transient behavior in large dynamical systems on networks*, Physical Review Research 2, 023333 (2020).

Contents

Chapter 1

Introduction

1.1 Mathematical preliminaries

In simple words, matrices are arrays of numbers. Like numbers, one can add and multiply them. The latter operation is different than for numbers, because the order of multiplication matters. In particular, matrices can multiply vectors, which are special instances of matrices, represented by a single column. For a given matrix A vectors $|v_i\rangle$ that satisfy

$$A\,|v_i\rangle = \lambda_i\,|v_i\rangle \tag{1.1}$$

are distinguished and called eigenvectors, while the corresponding numbers λ_i are called eigenvalues.

A lot of attention is focused on the spectral properties of symmetric (Hermitian) matrices due to their ubiquity in physics. Such matrices always have real eigenvalues and their eigenvectors form orthogonal basis. One of the physical examples is the moment of inertia. It is a rank-2 tensor, therefore represented by a matrix, which is symmetric by construction. Its orthogonal eigenvectors determine the principal axes of rotation, while eigenvalues define principal moments of inertia.

When the symmetry (Hermiticity) condition is dropped, these properties are lost. Eigenvalues can be complex in general. Moreover, due to the fact that the matrix and its transpose are not related, the eigenproblem is not uniquely defined. The matrix can be multiplied by the column vector from the right hand side or the row vector from the left hand side, therefore the need for the notion of left and right eigenvectors. They satisfy

$$\langle L_i|\,A = \langle L_i|\,\lambda_i, \qquad A\,|R_i\rangle = \lambda_i\,|R_i\rangle \tag{1.2}$$

for the same eigenvalue. Eigenvalues can be found by solving the algebraic equation $\det(\lambda - A) = 0$, which for an $N \times N$ matrix has N solutions, including multiplicities. When the eigenvalues are degenerate, it is, however, not always possible to find N eigenvectors, and then the matrix is said to be nondiagonalizable. If the matrix is diagonalizable, the eigenvectors form a biorthogonal set

$$\langle L_i|R_j\rangle = \delta_{ij}, \quad \text{for} \quad i,j = 1,\ldots,N, \tag{1.3}$$

but the eigenvectors are not orthogonal within sets, $\langle L_i|L_j\rangle \neq \delta_{ij} \neq \langle R_i|R_j\rangle$. Dual to the biorthogonality condition is the resolution of the identity matrix

$$\mathbb{1} = \sum_{k=1}^{N} |R_k\rangle\,\langle L_k|\,. \tag{1.4}$$

Relations (1.3) and (1.4) put constraints on the eigenvectors, but some freedom still remains. One can multiply each right eigenvector by a non-zero complex number c_i,

$|R_i\rangle \to c_i |R_i\rangle$ and the corresponding left eigenvector by the inverse $\langle L_i| \to c_i^{-1} \langle L_i|$, keeping (1.3) and (1.4) untouched, while still solving the eigenproblem (1.1). This further allows one to normalize lengths of either left or right eigenvectors, but we will not use this fact. Instead, we focus on objects that are insensitive to these rescalings.

The simplest possible quantities built from left and right eigenvectors that are invariant under their rescalings are the following scalar products introduced by Chalker and Mehlig [25, 77]:

$$O_{ij} = \langle L_i|L_j\rangle \langle R_j|R_i\rangle . \tag{1.5}$$

Here by $\langle R_j|$ we mean the Hermitian conjugate of the right eigenvector $|R_j\rangle$, which is now a row vector. Similarly, $|L_i\rangle = (\langle L_i|)^\dagger$ is a column vector. These scalar products can be collected into a matrix, which we refer to as the *matrix of overlaps* or the *overlap matrix*. The resolution of the identity (1.4) combined with the biorthogonality (1.3) put constrains on the elements of the overlap matrix - the sum rules

$$\sum_{j=1}^{N} O_{ij} = 1. \tag{1.6}$$

The matrix O is Hermitian by construction, but its spectral properties are beyond our interest. Instead, we pay attention to the elements of this this matrix.

A particular class of non-Hermitian matrices, called *normal matrices* is worth distinguishing. Such matrices commute with their Hermitian conjugate, $XX^\dagger = X^\dagger X$, and can always be diagonalized. Moreover, the transformation to the eigenbasis is unitary, therefore the eigenvectors are orthogonal, $\langle R_i|R_j\rangle = \delta_{ij}$. Left and right eigenvectors are associated by $\langle L_i| = (|R_i\rangle)^\dagger$. As a consequence, the overlap matrix is an identity matrix $O_{ij} = \delta_{ij}$, as it is for Hermitian matrices. Normal matrices can be therefore seen as objects in which non-Hermiticity affects only eigenvalues, while keeping eigenvectors still orthogonal.

1.2 Why eigenvectors?

After this a bit dry and succinct, but necessary mathematical introduction, it is time to explain why eigenvectors of non-Hermitian matrices are interesting at all.

Let us imagine a stock market in which prices of stocks evolve in time. Their evolution is not independent and one of the measures describing their interdependence is their correlation. Each pair of stocks has its own correlation, a number between -1 and 1, which says to what extent they coevolve. These numbers are stored in the *correlation matrix*. The numbers of stocks priced in decent stock markets often exceed thousands, therefore, in order to understand their dynamics, one needs to reduce the number of parameters, while losing as little information as possible. For correlation matrices this is obtained by diagonalizing the correlation matrix, which decomposes the system into principal components. The magnitude of the eigenvalue tells how important that component is, while the corresponding eigenvector tells how each stock participates in the principal. When this procedure is applied to stock markets, it naturally decomposes the market into sectors (see Fig 1.1). While the first principal component describes the overall evolution of the market, and each stock participates approximately equally, the next principal components are dominated by different types of stocks like banks, the oil industry, healthcare, and so on.

This type of analysis allows one to find correlations between stock prices at the same moment of time. From the investor's perspective it is more desired to find correlations between different moments of time and use this knowledge to make investment decisions. Such *time-lagged* correlations are no longer symmetric - prices of stocks in

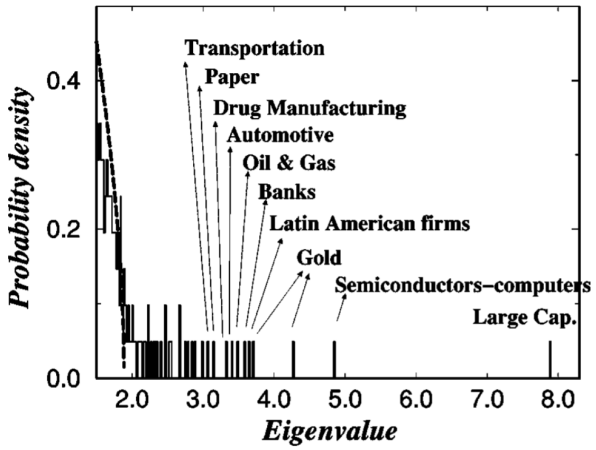

Figure 1.1: Principal component analysis of 30-min returns of 1000 US stocks for the 2-year period 1994–1995. The dashed line on the left represents random matrix model corresponding to the absence of any correlations. Eigenvectors associated with the outlying eigenvalues are strongly localized at stocks belonging to different market sectors. Analysis performed in [91], where this figure is also taken from.

the banking sector influence prices in the healthcare sector much more than vice versa. This naturally leads to asymmetric correlation matrices [75], but the methodology with decomposition into eigenvalues and eigenvectors remains the same [14, 86]. Again, eigenvectors encode participation of stocks in the principal components.

As another example, let us consider a random walk on a directed graph. For each node a walker moves with the same probability into any possible directions given by outgoing links from that node. If there is no outgoing link, one connects that node with all others, allowing the walker to go anywhere with the same probability. Further, regardless of the node the walker resides in, one also allows the walker to teleport to any possible node with a small probability. Probabilities of jumps from one node to another are stored in the *transition matrix*. The right eigenvector of this matrix to the eigenvalue equal to 1 encodes the stationary probability distribution of a random walker. Such a construction was used to develop an internet search engine, hence the name *Google matrix*. Websites that have larger probability to be reached by a walker are considered more relevant and appear first in the list of search results. Besides the Page Rank algorithm described here, eigenvectors play an essential role in many other algorithms in computer science, including spectral clustering [107, 99], community detection [85, 72] and spectral partitioning [94].

Many algorithms rely on the diagonalization of non-Hermitian matrices and precise numerical calculations of eigenvalues are important. In this context, eigenvalues of non-normal matrices are less stable and require more effort to maintain required precision because of the non-orthogonality of their eigenvectors. This phenomenon is illustrated by the following mathematical model.

Suppose that we want to numerically calculate eigenvalues of a matrix X, which is stored in memory with finite precision or its elements are determined with some uncertainty. Instead, we deal with slightly perturbed matrix $X' = X + \epsilon P$, where ϵP represents the deviation of our matrix from the true one. We can numerically compute only the eigenvalues of X', so one needs to know how close they are to the eigenvalues of X. If the deviation P is small, one can resort to the perturbation theory, which in the first order yields

$$\Delta\lambda_i = \epsilon \langle L_i | P | R_i \rangle . \tag{1.7}$$

The Cauchy-Schwartz inequality provides the upper bound

$$\langle L_i| P |R_i\rangle \leqslant ||P||_F \sqrt{\langle L_i|L_i\rangle \langle R_i|R_i\rangle}. \tag{1.8}$$

Here $||P||_F^2 = \mathrm{Tr}PP^\dagger$ is the Frobenius norm. The inequality is saturated if the perturbation is tuned to the eigenspace of that particular eigenvalue, which is of the form $P = |R_i\rangle \langle L_i|$. For normal matrices, this bound reduces to the norm of the perturbation, but non-orthogonal eigenvectors enhance the eigenvalue's sensitivity against perturbations. The quantity $\kappa_i = \sqrt{O_{ii}}$ is known in the numerical analysis community as the *eigenvalue condition number* [112]. In the early era of numerical computations it played an important role by telling how much the non-normal nature of the matrix enhances the uncertainty from finite precision.

As another example where the non-orthogonality of eigenvectors plays an important role, let us consider a dynamical system with N components evolving according to the system of nonlinear equations $\dot{x}_i = f_i(x)$. Close to a fixed point x^*, defined as $f_i(x^*) = 0$ for all i, the dynamics can be linearized

$$\frac{dy_i}{dt} = \sum_{j=1}^{N} J_{ik} y_k, \tag{1.9}$$

where $y_i = x_i - x_i^*$ and $J_{ik} = \left.\frac{\partial f_i}{\partial x_k}\right|_{x^*}$ is the Jacobian matrix at the fixed point. To quantitatively describe whether and how the system approaches its fixed point, it is convenient to consider the squared Euclidean distance from it, $||y(t)||^2 = \langle y(0)| e^{J^\dagger t} e^{Jt} |y(0)\rangle$. Here $|y(0)\rangle$ is the initial condition and we used the solution of the linear system in the form of a matrix exponential.

The above form is general and exact, but if the Jacobian can be diagonalized, $J = \sum_{i=1}^{N} |R_i\rangle \lambda_i \langle L_i|$, we gain a new interpretation, since we can now write

$$||y(t)||^2 = \sum_{j,k=1}^{N} e^{t(\bar{\lambda}_i + \lambda_j)} \langle y(0)|L_i\rangle \langle R_i|R_j\rangle \langle L_j|y(0)\rangle . \tag{1.10}$$

With this decomposition into eigenmodes, it is clearly visible that the fixed point is stable if real parts of all eigenvalues are smaller than 0, otherwise the system moves away from the fixed point. This characterizes the asymptotic behavior of the system, but the early-time dynamics is more complicated. If the Jacobian matrix is normal,

$$||y(t)||^2 = \sum_{j=1}^{N} e^{2t\mathrm{Re}\lambda_i} |\langle R_j|y(0)\rangle|^2, \tag{1.11}$$

the dynamics separate into eigenspaces and each eigenspace contributes independently. Eigenmodes decouple, and for stable systems the squared norm decays monotonically. In systems driven by non-normal matrices all eigenmodes are coupled with each other through the scalar product of eigenvectors and their overlap with the initial conditions. One therefore expects effects similar to interference. Indeed, the behavior of the squared norm can be nonmonotonic even for stable systems.

As an illustration, consider two 2×2 matrices representing Jacobians

$$J_1 = \begin{pmatrix} -1 & 10 \\ 0 & -2 \end{pmatrix}, \qquad J_2 = \begin{pmatrix} -1 & 1 \\ 0 & -2 \end{pmatrix}. \tag{1.12}$$

They have the same eigenvalues, but differ by their eigenvectors. The dynamics of the squared norm, presented in Fig. 1.2, are completely different. In the second case, the system initially drifts away from the fixed point, but after some time it eventually approaches it, since the fixed point is stable. When the system is observed in a short time interval, these *transient dynamics* may mislead the observer to conclude instability.

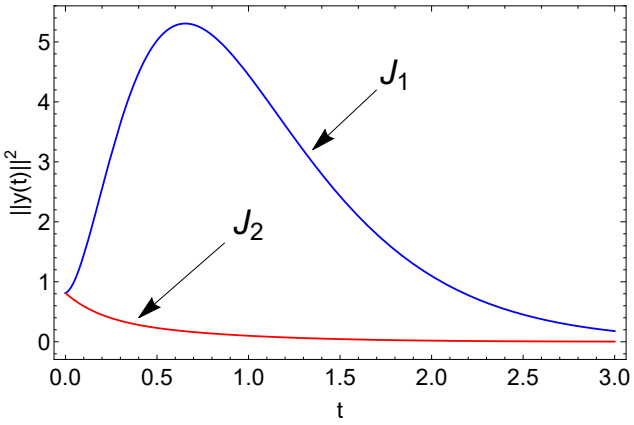

Figure 1.2: Evolution of the squared norm in the system (1.9) driven by two matrices with the same eigenvalues but different eigenvectors (1.12). The initial condition was chosen $|y(0)\rangle = (\frac{1}{2}, \frac{\sqrt{3}}{2})^T$. Eigenvectors of the matrix J_1 are more non-orthogonal.

1.3 Randomness in matrix elements

Each matrix is different, with its own properties. It is impossible to analyze all matrices. In many cases where the matrix represents interactions in the physical system, such as couplings between differential equations governing the dynamics or a Hamiltonian of a quantum system, one cannot even retrieve the exact form of that matrix. Since the properties of that specific system are impossible to calculate, one reverts the problem and asks: what is a 'typical' system, what properties does it have and whether the predictions from the 'typical' system can be verified in the system that one started with.

This line of reasoning led Eugene Wigner to introduce random matrices to physics. In the early 1950's there was a lot of data from nuclear scattering that unraveled the structure of energy levels in heavy nuclei, but constructed theories were correctly predicting only low-energy excitations, failing at more energetic collisions. Knowing that attempting to construct a Hamiltonian that will recover the spectrum is fruitless, Wigner proposed to treat it as a matrix filled with random numbers. The main constraint put on that matrix is its symmetry - the matrix must be symmetric, Hermitian or skew-symmetric to represent the physical Hamiltonian. Such a random object definitely cannot predict energies of excited states, so Wigner proposed to look at the statistics of the energy gap between consecutive levels and compare with the results obtained from a random matrix.

He started from the simplest example – a 2×2 random matrix with Gaussian entries – and found the spacing distribution $p(s) = \frac{\pi s}{2} e^{-\pi s^2/4}$, now called the *Wigner surmise*. If the data is normalized, that is mean and variance are equal to 1, there is no place for adjusting any parameters. When applied to empirical data from heavy nuclei, it shows remarkable agreement despite such a simplistic approach. This sparked heavy interest in applications of random matrix theory to other domain of physics. The Wigner surmise is used in quantum systems as a first check to see whether a system is integrable or chaotic. According to the Bohigas-Giannoni-Schmit conjecture [15], quantum systems, the classical counterpart of which is integrable, exhibit a Poissonian spacing distribution, while the Wigner surmise applies to systems with chaotic classical dynamics. Random matrix theory also found applications in quantum chromodynamics where it describes low-lying eigenvalues of the Dirac operator [3].

The Wigner surmise has also been found beyond physics. In number theory it describes spacings between large zeros on the critical line of the Riemann zeta function [87]. For this reason it was even speculated that there exists a Hamiltonian, the spectrum of which coincides with zeros of the Riemann zeta (Hilbert-Polya conjecture) and its Hermiticity will prove the Hilbert conjecture. Recently, such a Hamiltonian was constructed [11], but it is not Hermitian, so the conjecture still remains unproven. Further remarkable applications include the bus system in the Mexican city of Cuernavaca [68], where no schedule regulates the transportation system. Rather, bus drivers themselves decide when to start a route and how fast to drive in order to maximize their income. The statistics of time intervals between consecutive buses fit well to the Wigner surmise. Similar behavior was observed also in the subway system in New York City [61].

It is intriguing why the Wigner surmise obtained from a simple 2×2 matrix model can appear in so many places. There are two phenomena observed in random matrix theory explaining its remarkable success. One is fast convergence. In other words, results calculated for small matrices do not differ much from formulas obtained for large matrices. With a great analytical effort, the Wigner surmise was generalized to any matrix size, and the limiting case for infinitely large matrices involves solving nonlinear differential equations in the Painlevé hierarchy [36, 65], but, when plotted, it does not differ significantly from the Wigner surmise [47]. Calculating the distribution of the eigenvalues of finite-size random matrices is another demanding task, which in the limit of their large size can be performed using Feynman diagrams and $1/N$ expansion. This approach is often simpler to use, and results take a much simpler form, which nevertheless stays in a decent agreement with the exact finite N formulas, even for the size $N = 10$. The second phenomenon is universality. In simple words, it is not essential to consider matrix elements as Gaussian. Matrices with independent and identically distributed entries with finite variance, in the large N limit give the same spectral density as Gaussian matrices [102]. This phenomenon is known as *macroscopic universality*. Also, the behavior of eigenvalues at the scale of their typical separation is not very sensitive to the type of randomness, but more to the symmetry of matrices. This *microscopic universality* is responsible for ubiquity of the Wigner surmise. Universality explains why random matrices can describe certain properties of so many systems in nature, while fast convergence justifies the use of simpler asymptotic formulas, making random matrices handy to use.

There is another reason for introducing randomness – it is everywhere. Information is often corrupted with noise. Measurements are imperfect, and randomness models this imperfection. In interacting systems there are no two identical agents, and the populational variability is modeled by introducing randomness on top of certain deterministic structure. Random matrices are therefore not only null hypotheses or typical representants of an abstract class, but also important ingredient of reality.

1.4 Previous work on eigenvectors of non-Hermitian random matrices

Ten years after Wigner introduced random Hermitian matrices to physics, in 1965 Jean Ginibre studied random non-Hermitian Gaussian matrices [48]. He focused on their spectral properties and found the joint distribution of eigenvalues for real, complex and quaternionic random matrices. Since then, eigenvalues of random matrices have been intensively studied. There was also an interest in eigenvectors, mostly concentrated in their localization properties [42, 80] and relations to quantum chaos [74, 93].

In random matrix theory, the non-orthogonality was somehow overlooked until 1998,

when Chalker and Mehlig [25, 77] introduced the overlap matrix (1.5). It is such a complicated object, that even for the simplest ensemble studied by Ginibre, it was difficult to calculate its statistics beyond matrices of size $N = 2$. Instead, Chalker and Mehlig introduced correlation functions related to the overlap matrix:

$$\tilde{O}_1(z) = \left\langle \frac{1}{N} \sum_{i=1}^{N} O_{ii} \delta^{(2)}(z - \lambda_i) \right\rangle, O_2(z_1, z_2) = \left\langle \frac{1}{N} \sum_{\substack{i,j=1 \\ i \neq j}}^{N} O_{ij} \delta^{(2)}(z_1 - \lambda_i) \delta^{(2)}(z_2 - \lambda_j) \right\rangle. \tag{1.13}$$

Here and throughout the thesis $\langle ... \rangle$ denotes the average over the randomness with respect to the proper probability distribution function. Chalker and Mehlig were able to calculate $\tilde{O}_1(z)$ and $O_2(0, z)$ for the Ginibre ensemble for a finite size of the matrix, expressing the result in terms of a determinant of the band matrix. They also developed a way to calculate their asymptotics. It turns out that in order to obtain finite result in the large N limit, the one-point function must be rescaled to $O_1(z) = \frac{1}{N}\tilde{O}_1(z)$. Using Feynman diagrams, they also found the two-point function in the large N limit.

Around that time there was a quest to develop a technique for calculating the spectra of non-Hermitian random matrices. Such a task was completed [33, 63], and the resulting quaternionic formalism produces two outputs, one of them yielding the desired spectral density, the other more mysterious. Soon, it was realized that the additional piece of information that naturally emerges from the mathematical structure was exactly the one-point eigenvector correlation function [62].

Eigenvector non-orthogonality plays an important role in open quantum systems, in particular in the scattering in open chaotic cavities [37]. It also appears in random lasing, where the Petermann factor [90] modifies quantum limitations on the laser linewidth. These problems triggered research on eigenvectors in the specific model of the quantum scattering ensemble, resulting in the calculation of the one- and two-point functions [41, 78, 88, 97] and the full distribution in the case of a single channel coupling [88]. Furthermore, non-orthogonal eigenvectors were linked to the resonance width shifts in open quantum systems [43]. This fact was soon confirmed experimentally [53].

In late 2000's and early 2010's, transient amplification in systems driven by non-normal matrices was proposed as a possible mechanism of amplification of weak signals in balanced neural networks [58, 59, 81]. This topic created a wave of interest in random matrices and aspects of their non-normality in the neuroscience community.

During my undergraduate studies I was working on the problem of diffusion in non-Hermitian matrices. In such a process, matrix elements undergo Brownian motion, but since eigenvalues are complicated functions of matrix elements, their dynamics are highly nontrivial. In diffusing Hermitian matrices it was known since the early days of random matrix theory that the main force driving the eigenvalues was their mutual repulsion [30]. There was no such description in the case of non-Hermitian matrices and the Kraków group was working on the dynamics of the global density of eigenvalues. It turned out that the evolution of the spectral density requires also knowledge about the eigenvector correlation function. More specifically, it evolves according to the continuity equation

$$\partial_t \rho(z) = \partial_{z\bar{z}} O_1(z), \tag{1.14}$$

while the evolution of the eigenvector correlation function is not influenced by the eigenvalue density [20, 21]. Based on this result, it was speculated that it is the eigenvectors that are primary objects in this process.

1.5 What is this thesis about?

It was the lack of understanding of the mysterious correlation function playing a crucial role in diffusing matrices and scientific curiosity that drove me to enter this unexplored area and pursue the problems of non-orthogonal eigenvectors in random matrices. There are two main lines of research presented in this thesis - theoretical and applicational. The first approach aims at a better understanding of the overlap matrix and the development of new analytical tools that allow for calculating correlation functions. Given the scarcity of analytical results on this subject, even the asymptotic results that can be obtained from Feynman diagrams are of great value. The developed formalism is then applied to matrix models borrowed from theoretical neuroscience and machine learning.

The realm of random matrices is broad, and one can distinguish different types of them, depending on the criteria used. Random matrices can be dense, with almost all elements non-zero, or sparse, where only a small fraction of elements is non-zero. Matrix elements can be independent or dependent, but with various symmetries of their joint probability density. Each class of random matrices requires its own tools for their analysis. Here and throughout the thesis we focus on a class of unitarily invariant ensembles. Such matrices are dense, their elements are not independent, but the probability distribution function is invariant under the adjoint action of the unitary group, that is $P(X) = P(UXU^\dagger)$ for $U \in U(N)$. Such transformations are natural operations on matrices, making this class convenient for spectral analysis. We focus on complex random matrices, but the results obtained in the large N limit are the same if we also take real or quaternionic matrices. This fact is used in chapters 6 and 7 where the developed techniques are applied to real random matrices.

In chapters 2 and 3 we fill the gaps in calculations of one- and two-point eigenvector correlation functions. While the general procedure for the calculation of the one-point function is known, it leads to equations which often need to be solved numerically. We focus on the subclass of random matrices in which the enhanced unitary symmetry leads to remarkable simplifications, making these random matrices handy to use. The formalism of Feynman diagrams which was used for calculation of the two-point function in the Ginibre ensemble is extended to the general class of unitarily invariant random matrices. In such a case the summation of Feynman diagrams can be performed, allowing one to write a set of matrix equations for the two-point functions. These equations can be solved for the class of matrices with enhanced unitary symmetry.

We discussed Hermitian matrices with orthogonal eigenvectors and non-Hermitian random matrices with eigenvectors so strongly non-orthogonal that one needs additional rescaling in the definition of the one-point function $O_1(z)$. Is there anything in between? In chapter 4 we study an ensemble which allows for a smooth interpolation between a symmetric Gaussian matrix and a matrix with a complete lack of symmetry. Previously, in such an ensemble the regime of *weak non-Hermiticity* was found, where eigenvalues gain a tiny imaginary part. We find that in this regime eigenvectors become non-orthogonal, but only weakly, therefore the associated regime is called *weak non-normality*.

Universal microscopic correlations are at the heart of random matrix theory. However, calculations of their explicit forms are often technically challenging. Borodin and Olshanski offered a different perspective of the problem, which allows for fast calculations of microscopic limits. In chapter 5 we demonstrate this method and extend it for a broader class of ensembles, called *biorthogonal ensembles*. The biorthogonal structure there is strikingly similar to the biorthogonal structure of eigenvectors of non-Hermitian matrices. We demonstrate on a concrete example that the functions appearing there can be interpreted as left and right eigenfunctions of a non-self-adjoint differential op-

erator. This allows us to use Borodin and Olshanski's tools to obtain the microscopic universality in an effortless way.

In the last decade we have witnessed a surge of interest in neural networks, both biological and artificial. Recent progress in experimental techniques enables us to observe brain activity with unprecedented resolution, and the activity of single neurons can now be tracked. Due to the large number of neuronal cells in brains, data acquisition is still a challenging technical problem. Numerical simulations of their dynamics are still an important field of study, not only because this is the least invasive technique. Random matrices have also appeared in theoretical neuroscience as important ingredients of neural network models, which at the beginning were considered purely random, but with time acquired an increasingly deterministic structure. In chapter 6 we study a model which was introduced in 2006, but all following studies focused on the spectral properties of the associated random matrix and its influence on the dynamics. The work [A6] on which this chapter is based was the first to observe a particularly strong non-orthogonality of eigenvectors in such a model. The source of this effect is a combination of a deterministic structure, Dale's principle and excitatory-inhibitory balance.

Artificial neural networks suffered from many problems preventing them from effective learning. Major steps overcoming these difficulties were linked with developing new types of architecture. The work [A7], which heavily uses tools developed in [A1], is described in chapter 7 and provides a quantitative answer why and how residual neural networks overcame the problem of vanishing gradients. Remarkably, we find macroscopic universality of the spectral density in the associated random matrix model.

The aim of this thesis is to provide the Reader with a tentative introduction to the topic by briefly setting papers [A1-A7] in the context of previous developments, presenting the motivation for tackling these specific problems and briefly exposing the main results. A detailed derivation of the main results, more side results and applications of general formulas can be found in these papers, which are attached to the thesis.

1.6 Overview of recent progress in studies of eigenvectors

During the last four years we have witnessed a significant growth of interest in eigenvectors in the random matrix community. More research groups started tackling these problems. Renowned scientists who already have achievements in this field took another look at this topic, but also young researchers entered the field. The aim of this section is to give a brief overview on the progress that was made in parallel to my own research.

The problem of dynamics of eigenvalues in the process of the non-Hermitian diffusion was solved by Grela and Warchoł [52], and, independently, by Bourgade and Dubach [19]. The system of stochastic differential equations describes the evolution of eigenvalues at the microscopic level and indeed, the overlaps between eigenvectors are an essential ingredient in that process.

Knowledge about the one-point function has been growing. The expression obtained by Chalker and Mehlig for finite N as a determinant of a band matrix has been brought into a compact form that allowed for studying its edge asymptotics [109]. Later $O_1(z)$ was also found for products of Ginibre matrices of a small size [24]. Recently, Akemann et al. [6] considered slightly more general correlation functions than (1.13), with more than one eigenvalue conditioned by the Dirac delta, and found that such objects form determinantal point processes. Crawford and Rosenthal considered correlation functions that include overlaps of more than two different eigenvectors and found analytic results

in the large N limit for the Ginibre ensemble [26].

Bourgade and Dubach [19] have considered diagonal elements of the overlap matrix for the eigenvalues conditioned in the bulk of the spectrum (far from the edge). They found the full distribution of O_{ii} in the large N limit for the complex Ginibre ensemble, which turns out to be the same as of $\frac{1}{\gamma_2}$, where γ_2 is a random variable from the gamma distribution, $p_{\gamma_k}(x) \sim x^{k-1}e^{-x}$. The distribution of O_{ii} is heavy-tailed with only its first moment finite. Dubach further applied his technique to other complex [27] and quaternion [28] non-Hermitian matrix ensembles . Fyodorov [39], using the supersymmetry technique, found the full distribution of O_{ii} for finite N in complex Ginibre and for real eigenvalues in the real Ginibre ensemble. His approach allows also to obtain the asymptotics at the edge of the spectrum. In the real Ginibre ensemble, O_{ii} for real eigenvalues in the bulk is given by the inverse γ_1 distribution in the large N limit. Eigenvector overlaps of eigenvalues that come in complex conjugate pairs even in real Ginibre remain an open problem at the stage of writing the thesis.

Chapter 2

One-point correlation functions. Based on [A1,A2].

2.1 Random Hermitian matrices

The joint probability density function of elements of Hermitian matrices that belong to the class of unitarily invariant ensembles can be written in the form

$$P(H)dH = Z_N \exp\left(-N\mathrm{Tr}V(H)\right) dH, \tag{2.1}$$

where dH denotes the flat Lebesgue measure over all independent matrix elements and Z_N denotes the normalization constant. Trace in the exponent ensures invariance under the transformation $U \to UHU^\dagger$. Also, the integration measure transforms as $dH \to dH\,\det(UU^\dagger)$. Hermitian matrices can be brought to the diagonal form by unitary transformations, and it turns out that also the Jacobian of the change of variables to the diagonal basis $H = U\Lambda U^\dagger$ factorizes into the eigenvalues and the eigenvector variables. For that reason eigenvalues capture relevant information of the ensemble, while the eigenvectors are uniformly distributed on the $U(N)$ group.

The primary object of interest in these ensembles is the average density of eigenvalues

$$\rho(x) = \left\langle \frac{1}{N}\sum_{i=1}^{N} \delta(x-\lambda_i) \right\rangle. \tag{2.2}$$

The Dirac delta is impractical in direct calculations, so instead one resorts to its representations. Particularly convenient is the Sochocki-Plemelj formula

$$\delta(x) = -\frac{1}{\pi}\lim_{\epsilon\to 0}\mathrm{Im}\frac{1}{x+i\epsilon}. \tag{2.3}$$

To find the eigenvalue density, one introduces the Green's function – a traced resolvent of a matrix

$$G(z) = \left\langle \frac{1}{N}\mathrm{Tr}\frac{1}{z\mathbb{1}-H} \right\rangle. \tag{2.4}$$

When the Green's function is considered as a function on the complex plane, its expansion around $z=\infty$ generates all spectral moments

$$G(z) = \sum_{k=0}^{\infty}\frac{1}{z^{k+1}}\left\langle \frac{1}{N}\mathrm{Tr}H^k \right\rangle = \sum_{k=0}^{\infty}\frac{1}{z^{k+1}}\int_{\mathbb{R}}\rho(\lambda)\lambda^k d\lambda. \tag{2.5}$$

Its behavior in the vicinity of the real line, where eigenvalues reside, stores information about their mean density, which is recovered by the virtue of the Sochocki-Plemelj formula

$$\rho(x) = -\frac{1}{\pi}\lim_{\epsilon\to 0}\mathrm{Im}G(x+i\epsilon). \tag{2.6}$$

The Green's function is more handy to evaluate. Due to the $U(N)$ invariance, the averaged resolvent is proportional to the identity matrix, while for z close to infinity it can be expanded into a power series, yielding the following:

$$G\mathbb{1} = \frac{\mathbb{1}}{z} + \left\langle \frac{\mathbb{1}}{z} H \frac{\mathbb{1}}{z} \right\rangle + \left\langle \frac{\mathbb{1}}{z} H \frac{\mathbb{1}}{z} H \frac{\mathbb{1}}{z} \right\rangle + \dots . \tag{2.7}$$

The averages are then performed with the use of tools from statistical field theory – Feynman diagrams. The potential $V(H)$ in (2.1) is split into the Gaussian part yielding the propagator and the residual part bringing vertices into the calculations. One distinguishes the class of one-line irreducible (1LI) diagrams, which are the building blocks of this diagrammatic calculus. Each diagram can be drawn as a composition of 1LI diagrams glued together by terms coming from $1/z$. This gives the first Schwinger-Dyson equation

$$G(z) = \frac{1}{z} + \frac{1}{z}\Sigma(z)\frac{1}{z} + \frac{1}{z}\Sigma(z)\frac{1}{z}\Sigma(z)\frac{1}{z} + \ldots = \frac{1}{z - \Sigma(z)}, \tag{2.8}$$

where $\Sigma(z)$ denotes sum of all 1LI diagrams.

For large matrix size, the dominant contribution comes from planar diagrams, simplifying their combinatorics. One defines cumulants $c_k = \left\langle \frac{1}{N} \mathrm{Tr} X^k \right\rangle_c$ as the sum of all connected diagrams appearing in calculation of k-th moment. Each 1LI diagram can be then decomposed as a certain cumulant c_k encompassing diagrams that are not necessarily 1LI. On the other hand, such diagrams contribute to the Green's function, and one can write the second Schwinger-Dyson equation

$$\Sigma(z) = c_1 + c_2 G(z) + c_3 G(z)^2 + \ldots = R(G(z)), \tag{2.9}$$

where $R(z) = \sum_{k=1}^{N} c_k z^{k-1}$ is the cumulant-generating function.

The form of the cumulant-generating function depends on the potential, but its knowledge is sufficient to solve the problem. In short, the non-perturbative object, that is the Dirac delta, is regularized via the resolvent, which is then evaluated using the perturbative method of Feynman diagrams. The spectral density is then recovered from the behavior of the Green's function in close proximity to the real line.

Here the complex argument z plays the role of a regularizer, the imaginary part of which moves us away from the problematic real axis, where the resolvent is not defined. When z is promoted to a full-fledged complex variable, it uncovers additional features of this formalism that stay in direct analogy to classical probability.

Consider the problem of addition of two random matrices A and B. What is the spectrum of $A + B$? In general, it depends not only on the eigenvalues, but also on the mutual orientations of the eigenvectors of A and B. If these matrices are random, generated from the unitarily invariant distribution, their eigenvectors are in a random position. This independent orientation of eigenbases is the noncommutative counterpart of classical independence in random matrix theory. In such a case, similarly to classical probability, cumulants are additive. In other words, their cumulant-generating functions are additive:

$$R_{A+B}(z) = R_A(z) + R_B(z). \tag{2.10}$$

The function R plays the same role as the logarithm of the characteristic function in classical probability and is also known as the R-transform. The relation between the R-transform and the Green's function is more complicated than their classical counterparts, because they satisfy functional equations

$$R(z) = B(z) - \frac{1}{z}, \qquad R(G(z)) = z - \frac{1}{G(z)}, \tag{2.11}$$

where $B(z)$ is the functional inverse of the Green's function, $B(G(z)) = z$. The mathematical theory describing the probability calculus on large random matrices was discovered by Voiculescu and is now known as *free probability* [105, 106], since the notion of independence is replaced by freeness, which corresponds to random orientation of eigenbases. Interestingly, for six years free probability existed as a separate mathematical theory, before the connection to random matrices was discovered [104].

Similarly to addition, one may consider the problem of multiplication of random matrices. Such a problem is not always well posed, because the product of two Hermitian matrices is not Hermitian, $(AB)^\dagger = BA \neq AB$. However, if one of them (let us say A) is positive definite, its square root $A^{1/2}$ is Hermitian. The spectrum of AB is the same as the spectrum of $A^{1/2}BA^{1/2}$, which is now Hermitian and therefore the spectrum of AB is real. The object that is multiplicative under the multiplication of random matrices is called the S-transform and it is related to the R-transform by the following functional relations

$$R(z)S(zR(z)) = 1, \qquad S(z)R(zS(z) = 1. \tag{2.12}$$

2.2 Non-Hermitian random matrices

When the Hermiticity condition is relaxed, there are many more admissible probability distribution functions, which can now be written in the generic form

$$P(X, X^\dagger)dXdX^\dagger = Z_N \exp\left(-N\mathrm{Tr}V(X, X^\dagger)\right) dXdX^\dagger. \tag{2.13}$$

The flat measure contains all independent elements $dXdX^\dagger = \prod_{j,k=1}^N dx_{jk}dy_{jk}$. Again, one wants to find the density of eigenvalues, but now eigenvalues can be complex, and one deals with a 2-dimensional Dirac delta. The Sochocki-Plemelj formula ceases to work, and another representation is needed. It is convenient to use

$$\delta^{(2)}(z) = \frac{1}{\pi}\lim_{\epsilon\to 0}\frac{\epsilon^2}{(|z|^2+\epsilon^2)^2} = \frac{1}{\pi}\lim_{\epsilon\to 0}\partial_{\bar z}\frac{\bar z}{|z|^2+\epsilon^2}. \tag{2.14}$$

The second differentiation reduces the power in the denominator. In order to apply this formula, one is tempted to use

$$\left\langle \frac{1}{N}\mathrm{Tr}\frac{\bar z\mathbb{1} - X^\dagger}{(z\mathbb{1}-X)(\bar z\mathbb{1}-X^\dagger)+\epsilon^2\mathbb{1}}\right\rangle, \tag{2.15}$$

but this form contains quadratic terms in the denominator, which are impractical in diagrammatic calculations. A remedy for this problem is to consider (2.15) as a part of a bigger object. In order to solve the spectral problem of $N\times N$ matrices, one introduces the generalized Green's function, which is a 2×2 matrix [33, 63]

$$\mathcal{G} = \begin{pmatrix}\mathcal{G}_{11} & \mathcal{G}_{1\bar 1}\\ \mathcal{G}_{\bar 1 1} & \mathcal{G}_{\bar 1\bar 1}\end{pmatrix} = \left\langle \mathrm{bTr}\begin{pmatrix} z\mathbb{1}-X & i\bar w\mathbb{1}\\ iw\mathbb{1} & \bar z\mathbb{1}-X^\dagger\end{pmatrix}^{-1}\right\rangle. \tag{2.16}$$

Here bTr is the block trace operation which acts on a space of $2N\times 2N$ matrices and yields 2×2 matrices:

$$\mathrm{bTr}\begin{pmatrix}A & B\\ C & D\end{pmatrix} = \begin{pmatrix}\mathrm{Tr}A & \mathrm{Tr}B\\ \mathrm{Tr}C & \mathrm{Tr}D\end{pmatrix}. \tag{2.17}$$

The Schur complement formula shows that $\mathcal{G}_{11}$ is precisely equal to (2.15). Moreover, the generalized Green's function can be rewritten as follows:

$$\mathcal{G} = \left\langle \frac{1}{N}\mathrm{bTr}(Q\otimes \mathbb{1}_N - \mathcal{X})^{-1}\right\rangle, \tag{2.18}$$

where Q is the 2×2 matrix representation of a quaternion, while $\mathcal{X}$ is a duplicated matrix

$$Q = \begin{pmatrix} z & i\bar{w} \\ iw & \bar{z} \end{pmatrix}, \qquad \mathcal{X} = \begin{pmatrix} X & 0 \\ 0 & X^\dagger \end{pmatrix}. \tag{2.19}$$

The form (2.18) resembles the standard resolvent, but now it is a 2×2 matrix. Symmetries of this matrix are the same as of the quaternion Q, therefore we refer to it as the quaternionic Green's function [64].

The tools used for Hermitian matrices can be easily generalized with one complication, namely when performing averages with respect to the ensemble, due to the block structure, we need to deal with two types of indices - one set enumerates blocks, and the other enumerates matrix element within blocks, running from 1 to N. We use the convention where the first set of indices takes values in $\{1, \bar{1}\}$ instead of $\{1, 2\}$ because of the structure of the matrix $\mathcal{X}$. Its first block is always associated with X, while the second block with its conjugate, hence $\bar{1}$.

The methodology behind calculations remains the same. One starts with the averaged quaternionic resolvent, which, again, has trivial structure in matrix elements due to the unitary invariance. Expanding it as a geometric series, one obtains

$$\mathcal{G}(Q) \otimes \mathbb{1} = \mathcal{Q}^{-1} + \left\langle \mathcal{Q}^{-1}\mathcal{X}\mathcal{Q}^{-1} \right\rangle + \left\langle \mathcal{Q}^{-1}\mathcal{X}\mathcal{Q}^{-1}\mathcal{X}\mathcal{Q}^{-1} \right\rangle + \dots \tag{2.20}$$

where we denoted $\mathcal{Q} = Q \otimes \mathbb{1}$. Now the order of terms in the expansion matters, because $\mathcal{Q}\mathcal{X} \neq \mathcal{X}\mathcal{Q}$.

Because of non-normality, the structure of cumulants is much richer – there are several different cumulants of the same order, for example

$$c^{(4)}_{11\bar{1}\bar{1}} = \left\langle \frac{1}{N}\mathrm{Tr}XXX^\dagger X^\dagger \right\rangle_c \neq \left\langle \frac{1}{N}\mathrm{Tr}XX^\dagger XX^\dagger \right\rangle_c = c^{(4)}_{1\bar{1}1\bar{1}}. \tag{2.21}$$

Thanks to noncommutativity of $\mathcal{X}$ and $\mathcal{Q}$, all cumulant are stored in the R-transform, which is now a quaternion. Its expansion reads [21] [A2]

$$\mathcal{R}(Q) \otimes \mathbb{1} = \langle \mathcal{X} \rangle_c + \langle \mathcal{X}\mathcal{Q}\mathcal{X} \rangle_c + \langle \mathcal{X}\mathcal{Q}\mathcal{X}\mathcal{Q}\mathcal{X} \rangle_c + \dots \tag{2.22}$$

or, more explicitly, component-wise

$$\mathcal{R}(Q)_{\alpha\beta} = c^{(1)}_\alpha \delta_{\alpha\beta} + c^{(2)}_{\alpha\beta} Q_{\alpha\beta} + \sum_\gamma c^{(3)}_{\alpha\gamma\beta} Q_{\alpha\gamma} Q_{\gamma\beta} + \sum_{\gamma,\epsilon} c^{(4)}_{\alpha\gamma\epsilon\beta} Q_{\alpha\gamma} Q_{\gamma\epsilon} Q_{\epsilon\beta} + \dots . \tag{2.23}$$

Again the quaternionic R-transform is additive when two independent random matrices are added.

Schwinger-Dyson equations are generalized to the quaternionic setting and read

$$\mathcal{G}(Q) = [Q - \Sigma(Q)]^{-1}, \tag{2.24}$$

$$\Sigma(Q) = \mathcal{R}(\mathcal{G}(Q)). \tag{2.25}$$

The knowledge of all cumulants determines the form of the R-transform and therefore allows one to fully solve the non-Hermitian random matrix model.

2.3 Eigenvectors

After solving the model, at the end of the day, one obtains the quaternionic Green's function, which in turn yields the spectral density via $\rho(z, \bar{z}) = \lim_{|w|\to 0} \frac{1}{\pi} \partial_{\bar{z}} \mathcal{G}_{11}$. The Green's function as a 2×2 matrix has 4 entries, but its quaternionic nature constrains two entries $\mathcal{G}_{\bar{1}\bar{1}} = \overline{\mathcal{G}}_{11}$ and $\mathcal{G}_{1\bar{1}} = -\overline{\mathcal{G}}_{\bar{1}1}$. This means that besides the spectral density

one obtains an additional piece of information for free. It was observed that the product of off-diagonal elements of the quaternionic Green's function yields the one-point eigenvector correlation function [62]. An alternative derivations was presented in [A1].

The definition of the correlation function as presented in (1.13) does not have a clear interpretation. From the discussion in Section 1.2 it is now clear that O_{ii} is the square of the eigenvalue condition number, $\kappa^2(\lambda_i)$. The correlation function by itself is not very informative, as it is a density of eigenvalues, but each eigenvalue is weighted by the associated overlap. Rather, the ratio $\frac{O_1(z)}{\rho(z)}$ carries information because it is a conditional expectation of $\kappa^2(\lambda_i)/N$, where the corresponding eigenvalue λ_i is conditioned to take the value z. This simply follows from the sequence of equalities [A1]

$$\mathbb{E}\left(\frac{\kappa^2(\lambda_i)}{N}\middle|\,\lambda_i=z\right)=\int\frac{O_{ii}}{N}\frac{\rho(O_{ii},\lambda_i=z)}{\rho(\lambda_i=z)}=\frac{1}{N\rho(z)}\int O_{ii}\delta^{(2)}(z-\lambda_i)p(X)dX=\frac{O_1(z)}{\rho(z)}. \tag{2.26}$$

Here $\rho(O_{ii},\lambda_i=z)$ denotes the joint probability density of finding O_{ii} and λ_i at O_{ii} and z, respectively. In the second inequality we used the fact that this density can be obtained from the joint density of all matrix elements by integrating all variables except for the two interesting ones. An additional factor of $1/N$ and the summation appear when one symmetrizes this expression over eigenvalues, which directly leads to the last equality.

This result, despite its simplicity, tells important fact about condition numbers of eigenvalues of random matrices. The additional $1/N$ in the normalization of $O_1(z)$ was introduced to obtain finite results in the large N limit. This means that condition numbers of eigenvalues of random matrices grow like $\sqrt{N}$ and O_{ii} grows linearly with their size.

2.4 Biunitarily invariant ensembles

In principle, the formalism presented above solves all non-Hermitian matrix models with unitary symmetry, but due to its 2×2 matrix structure it leads to systems of algebraic equations. Therefore, the number of analytically solved examples of matrix models is rather small. There is, however, a certain class of non-Hermitian random matrices, the treatment of which is effectively one-dimensional. The potential that determines the probability density function is not a function of X and $X^\dagger$ separately, but of their product, $V(XX^\dagger)$. Such ensembles admit enhanced symmetry, because multiplication by two unitary matrices U,V from both sides, $X\to UXV^\dagger$, does not alter the probability density. Moreover, using transformations belonging to the symmetry group, the matrix can be brought to the diagonal form with its singular values on the diagonal. With this argument one expects *all* observables in this ensemble to be determined solely by the singular values.

Due to the enhanced symmetry, eigenvalue density is rotationally symmetric, that is $\rho(z,\bar{z})=\rho(|z|)$. For that reason it is convenient to consider the radial cumulative distribution function $F(r)=2\pi\int_0^r\rho(r)rdr$, counting the fraction of the eigenvalues within a disk of radius r. When analyzing the biunitarily invariant ensemble, Feinberg and Zee [31, 32] not only found the relation between the density of eigenvalues and singular values in terms of the Green's function of $XX^\dagger$, but also discovered that the spectrum of such random matrices is either a disk or an annulus, hence the name *the single ring theorem*. It is characterized by internal and external radii

$$r_{ext}^2=\int x\rho_{XX^\dagger}(x)dx,\qquad r_{int}^{-2}=\int x^{-1}\rho_{XX^\dagger}(x)dx, \tag{2.27}$$

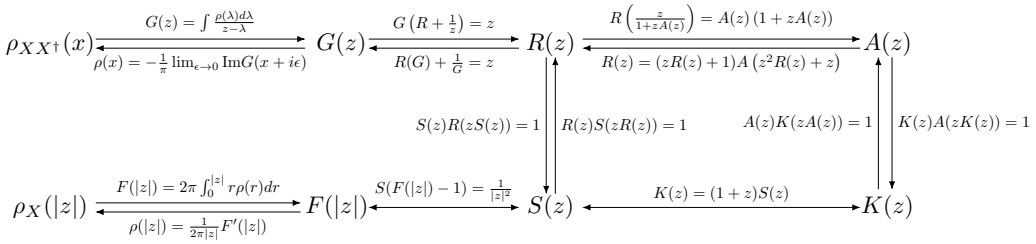

Figure 2.1: A diagrams presenting relations between transforms which appear in free probability in the context of large biunitarily invariant random matrices. The bottom-left leg of the diagram is the essence of the Haagerup-Larsen theorem. The cycle on the right-hand side presents relations between the function $A(z)$ representing cumulants in the expansion of X and the R-transform generating cumulants in the expansion of $XX^\dagger$. We also used an auxiliary function $K(z)$, which is related to $A(z)$ in the same way as $S(z)$ is related to $R(z)$.

where $\rho_{XX^\dagger}$ is the density of squared singular values of X. If the latter integral is infinite, $r_{int}=0$, which corresponds to the case of a disk. Later, this ensemble was studied in the framework of free probability by Hageruup and Larsen [54], who found a particularly simple mapping between the S-transform of squared singular values and the radial cumulative distribution function in terms of a functional equation

$$S_{XX^\dagger}(F(r)-1)=\frac{1}{r^2}, \tag{2.28}$$

which is now known as the Haagerup-Larsen theorem.

The eigenvector correlation function is also directly linked to the distribution of singular values. Having solved (2.28) for $F(r)$ one immediately obtains the one point function via [A1,A2]

$$O(r)=\frac{F(r)(1-F(r))}{\pi r^2}. \tag{2.29}$$

From the diagrammatic point of view, the effective reduction to one dimension stems from the fact that the non-vanishing cumulants in this ensemble are of the form $\alpha_k=\left\langle \frac{1}{N}\mathrm{Tr}(XX^\dagger)^k\right\rangle_c = c^{(2k)}_{1\bar{1}\ldots 1\bar{1}} = c^{(2k)}_{\bar{1}1\ldots\bar{1}1}$. Therefore, they can be stored in a single scalar generating function $A(z)=\sum_{k=1}^{\infty}\alpha_k z^{k-1}$. Thus, the quaternionic R-transform takes the particularly simple form [A2]

$$\mathcal{R}(Q)=A(-|w|^2)\begin{pmatrix}0 & i\bar{w}\\ iw & 0\end{pmatrix}. \tag{2.30}$$

A direct analysis of one-line irreducible Feynman diagrams contributing to the Green's function of $XX^\dagger$ leads to the functional relation between the R-transform of $XX^\dagger$ and the generating function $A(z)$ in terms of the Green's function [A2]

$$R(G(z))=zG(z)A(zG^2(z)). \tag{2.31}$$

One can further manipulate this relation to find further relations between all relevant transforms [A2]. They are summarized in Fig. 2.1.

2.5 A brief summary

Based on the work [10], the relation (2.29) was derived for the first time in [A1]. The connection between the conditional expectation of the squared eigenvalue condition number and the ratio between O_1 and the density (2.26) was also established therein.

The work [A2] provides an alternative derivation of the relation (2.29) based on the diagrammatic approach. To this end the quaternionic R-transform for biunitarily invariant ensembles (2.30) and its relations with R ans S transforms for their squared singular value density, are needed.

Chapter 3

Two-point eigenvector correlation functions. Based on [A3].

3.1 Motivation

Let us return to the example of a dynamical system operating near a fixed point, discussed in section 1.2. The time dependence of the squared norm is expressed in terms of eigenvalues and corresponding left and right eigenvectors

$$||y(t)||^2 = \sum_{j,k=1}^{N} e^{t(\bar{\lambda}_i+\lambda_j)} \langle y(0)|L_i\rangle \langle R_i|R_j\rangle \langle L_j|y(0)\rangle . \tag{3.1}$$

It clearly depends also on the choice of the initial condition $|y(0)\rangle$. If the system is perturbed in many different directions, it is reasonable to consider its dynamics averaged over all possible directions. Since each direction is equiprobable, one may take N basis vectors from the orthogonal canonical basis, $e_1 = (1, 0, \ldots)^T$, ..., $e_N = (0, \ldots, 0, 1)^T$ and average over them. This results in

$$\overline{||y(t)||^2} = \frac{1}{N} \sum_{j,k=1}^{N} e^{t(\bar{\lambda}_i+\lambda_j)} O_{ji}. \tag{3.2}$$

These dynamics in turn depend on the choice of the matrix, therefore – in the spirit of the thesis – we consider it random and average over the randomness. This leads to the expression which can be written in a compact form

$$S(t) = \left\langle \overline{||y(t)||^2} \right\rangle = \left\langle \frac{1}{N} \mathrm{Tr} e^{X^\dagger t} e^{Xt} \right\rangle . \tag{3.3}$$

This is an instance of a more general problem, namely of evaluating averages of type $\left\langle \frac{1}{N} \mathrm{Tr} f(X) g(X^\dagger) \right\rangle$, where f, g are arbitrary functions. Its Hermitian counterpart, which is known under the name *linear statistics*, has been intensively studied in random matrix theory, mainly due to its applications. The non-normal version, however, has not attracted attention so far. With the use of the identity $f(\lambda) = \int_{\mathbb{C}} \delta^{(2)}(z-\lambda) f(z) d^2 z$ and interchanging the order of integration and summation, (3.3) can be rewritten as follows:

$$S(t) = \int_{\mathbb{C}} d^2 z_1 \int_{\mathbb{C}} d^2 z_2 e^{t(z_1+\bar{z}_2)} \left\langle \frac{1}{N} \sum_{i,j=1}^{N} O_{ij} \delta^{(2)}(z_1 - \lambda_i) \delta^{(2)}(z_2 - \lambda_j) \right\rangle . \tag{3.4}$$

On the right-hand side we recognize the object resembling (1.13). Indeed, by extracting the singular part, it is naturally decomposed into one- and two-point functions

$$D(z_1, z_2) = O_2(z_1, z_2) + \tilde{O}_1(z_1) \delta^{(2)}(z_1 - z_2). \tag{3.5}$$

While the eigenvector correlation functions appear naturally when one calculates expectations of functions of matrices and their Hermitian conjugates, explicit calculations using the representation (3.4) are impossible. To make analytical progress, we use Cauchy's integral formula, which can be easily generalized to functions of matrices and which then reads

$$f(X) = \frac{1}{2\pi i} \oint_\gamma \frac{f(z)}{z\mathbb{1} - X} dz. \tag{3.6}$$

The contour γ encircles all eigenvalues counterclockwise. Inserting this into (3.3) and interchanging the order of integrals, one obtains the following representation [A2,B5]

$$S(t) = \frac{1}{(2\pi i)^2} \oint_\gamma \oint_\gamma dz_1 dz_2 e^{t(z_1+\bar{z}_2)} \left\langle \frac{1}{N} \mathrm{Tr} \frac{1}{z_1\mathbb{1} - X} \frac{1}{\bar{z}_2\mathbb{1} - X^\dagger} \right\rangle. \tag{3.7}$$

This reduces the problem to the calculation of another correlation function, which is a traced product of resolvents that later needs to be integrated with exponentials.

3.2 Setup for two-point functions

In the same manner as the resolvent yields spectral density, the correlation function

$$\mathfrak{h}(z_1, \bar{z}_2) = \left\langle \frac{1}{N} \mathrm{Tr} \frac{1}{z_1\mathbb{1} - X} \frac{1}{\bar{z}_2\mathbb{1} - X^\dagger} \right\rangle \tag{3.8}$$

is directly related to the eigenvector correlation function due to another representation of the two-dimensional Dirac delta

$$\delta^{(2)}(z) = \frac{1}{\pi} \partial_{\bar{z}} \frac{1}{z}. \tag{3.9}$$

In principle

$$D(z_1, z_2) = \frac{1}{\pi^2} \partial_{\bar{z}_1} \partial_{z_2} \mathfrak{h}(z_1, \bar{z}_2), \tag{3.10}$$

but one needs to know $\mathfrak{h}$ inside the spectrum, where resolvents are not defined, thus this relation does not provide the correct formula. In order to perform calculations, one needs to remove singularities at the location of eigenvalues by appropriately regularizing the resolvent. A correct prescription is already provided by the second equality in (2.14), which was later successfully used to evaluate eigenvalue density. Each resolvent that appears in formulas needs to be replaced as follows

$$(z - X)^{-1} \to (\bar{z} - X^\dagger) M(z, w)^{-1}, \tag{3.11}$$

with $M(z, w) = (z - X)(\bar{z} - X^\dagger) + |w|^2$. Then the expectations with respect to the randomness can be calculated, and finally the regularization is removed by taking the limit $|w| \to 0$. To this end we consider the following object [77][A3]

$$h(z_1, w_1, z_2, w_2) = \left\langle \frac{1}{N} \mathrm{Tr} (\bar{z}_1 - X^\dagger) M(z_1, w_1)^{-1} M(z_2, w_2)^{-1} (z_2 - X) \right\rangle, \tag{3.12}$$

which will lead to the desired correlation function via [77]

$$D(z_1, z_2) = \lim_{|w_1|, |w_2| \to 0} \frac{1}{\pi^2} \partial_{\bar{z}_1} \partial_{z_2} h(z_1, w_1, z_2, w_2). \tag{3.13}$$

In fact, the average over randomness is calculated using Feynman diagrams, which is a perturbative technique. Such methods are insensitive to objects that are nonperturbative like the Dirac delta, therefore the singular term in (3.5) will not be captured within this formalism, and $D(z_1, z_2) = O_2(z_1, z_2)$.

3.3 Linearization

After properly regularizing resolvents, we encounter the same problem as in calculations of one-point functions, namely we deal with the inverse of a matrix that is a quadratic form of X and $X^\dagger$. To overcome this difficulty, we linearize the expression by introducing twice bigger matrices. The most general object that can be built from two resolvents is their Kronecker product [77]

$$\mathcal{H} = \left\langle (\mathcal{Q} - \mathcal{X})^{-1} \otimes (\mathcal{P}^T - \mathcal{X}^T)^{-1} \right\rangle . \tag{3.14}$$

Here $\mathcal{Q} = Q \otimes \mathbb{1}$ and $\mathcal{P} = P \otimes \mathbb{1}$, while Q, P and $\mathcal{X}$ are different quaternions and the duplicated matrix

$$Q = \begin{pmatrix} z_1 & i\bar{w}_1 \\ iw_1 & \bar{z}_1 \end{pmatrix}, \quad P = \begin{pmatrix} z_2 & i\bar{w}_2 \\ iw_2 & \bar{z}_2 \end{pmatrix}, \quad \mathcal{X} = \begin{pmatrix} X & 0 \\ 0 & X^\dagger \end{pmatrix}. \tag{3.15}$$

Transposition in (3.14) anticipates the final results, and this convention makes them more consistent. $\mathcal{H}$, a $4N^2 \times 4N^2$ matrix, is equipped with 8 indices enumerating blocks of each term in a Kronecker product (Greek indices) and matrix elements within each block (Latin indices). Explicitly,

$$\mathcal{H}^{\alpha\beta,ij}_{\mu\nu,kl} = \left\langle (\mathcal{Q} - \mathcal{X})^{-1}_{\alpha\beta,ij} (\mathcal{P} - \mathcal{X})^{-1}_{\nu\mu,lk} \right\rangle . \tag{3.16}$$

Previously, when dealing with a single resolvent, there was a unique way to contract Latin indices leading to the block trace. Now there are two different possibilities generating the following objects [A3]:

$$K^{\alpha\beta}_{\mu\nu} = \frac{1}{N} \sum_{i,j=1}^{N} \mathcal{H}^{\alpha\beta,ij}_{\mu\nu,ij}, \qquad L^{\alpha\beta}_{\mu\nu} = \frac{1}{N^2} \sum_{i,j=1}^{N} \mathcal{H}^{\alpha\beta,ii}_{\mu\nu,jj}. \tag{3.17}$$

These two objects are different due to another reason - the way how indices are contracted determines which diagrams are planar, thus each of them requires separate treatment.

The second contraction corresponds to the block trace withing each term in the Kronecker product. Such correlation functions involving products of traces are also relevant in random matrix theory. We, though, need an object that leads to the multiplication of resolvents. Therefore, we turn our attention to K, which is a 4×4 matrix. The simplest way to identify the correct entry that corresponds to $h(z_1, w_1, z_2, w_2)$ is to set $w_1 = 0 = w_2$, calculate the entries and check which one generates $\mathfrak{h}(z_1, \bar{z}_2)$, which is devoid of regularization. It turns out that the desired component is $K^{11}_{\bar{1}\bar{1}}$, or, in standard notation, K_{22}.

3.4 Diagrammatics

In the large N limit the dominant contribution to K comes from ladder-type planar diagrams. Two rails of the ladder are generated by two resolvents in (3.14) and all vertices must be located between these rails. Diagrammatic equations now bear the name of Bethe-Salpeter, but their structure is similar to Schwinger-Dyson equation for one-point functions. K is expressed as a geometric series, which can be written as [A3]

$$K(Q, P) = \mathcal{G}(Q) \otimes \mathcal{G}(P)^T + [\mathcal{G}(Q) \otimes \mathcal{G}(P)^T] B(Q, P) K(Q, P). \tag{3.18}$$

Here $\mathcal{G}$ is the one-point Green's function, while B is the counterpart of one-line irreducible diagrams. Loosely speaking, $B(Q, P)$ is the sum of connected diagrams that

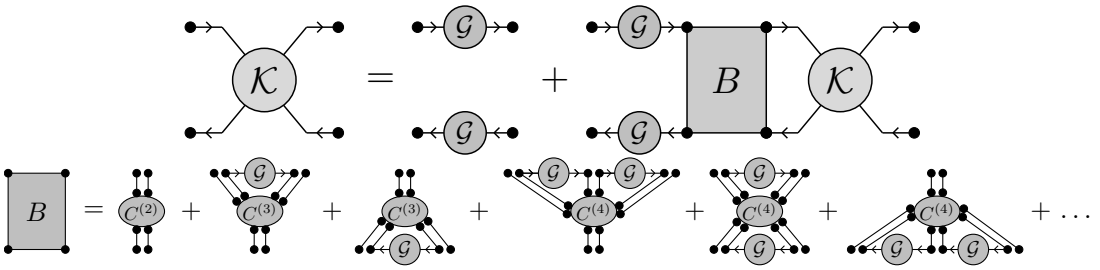

Figure 3.1: Diagrammatic representations of the Bethe-Salpeter equations for the two-point functions. (top) Relation (3.18) between $\mathcal{K}$ and irreducible diagrams B connecting two rails of the ladder. (bottom) Sum of irreducible diagrams expressed in terms of cumulants and the one-point Green's function (3.19).

build rungs of the ladder. It is expressed in terms of cumulants and the Green's functions in the following way [A3]

$$B^{\alpha\beta}_{\mu\nu}(Q,P) = \sum_{k,l=1}^{\infty} \sum_{\substack{\sigma_1,\ldots,\sigma_k \\ \rho_1,\ldots,\rho_l}} \delta^{\alpha\sigma_1}\delta^{\beta\sigma_k}\delta_{\mu\rho_l}\delta_{\nu\rho_1} c^{(k+l)}_{\sigma_1\ldots\sigma_k\rho_1\ldots\rho_l} \mathcal{G}^{\sigma_1\sigma_2}(Q)\ldots\mathcal{G}^{\sigma_{k-1}\sigma_k}(Q)\mathcal{G}_{\rho_1\rho_2}(P)\ldots\mathcal{G}_{\rho_{l-1}\rho_l}(P). \quad (3.19)$$

This expansion is similar to the expansion of $\Sigma(Q)$ for one-point functions, but now certain Green's function are replaced by the Green's functions of a second quaternionic argument, making the above form more complicated. The knowledge of one-point functions, which can be determined beforehand, and all cumulants is sufficient to solve the model by equations (3.18) and (3.19). First one needs to find the form of the B function and then solve the algebraic equation for the 4×4 matrix. It is a daunting task, so it is worth looking at problems with a simplified structure.

3.5 Traced product of resolvents

Outside of the spectrum, the regularization in the resolvents can be removed, and then $h(z_1, 0, z_2, 0) = \mathfrak{h}(z_1, \bar{z}_2)$. Setting $w_1 = 0 = w_2$ simplifies formulas significantly, because then quaternions are diagonal, and (3.18) reduces to decoupled scalar equations with the immediate solution [A3]

$$K^{1\bar{1}}_{1\bar{1}} = \frac{G(z_1)\bar{G}(\bar{z}_2)}{1 - G(z_1)\bar{G}(\bar{z}_2)B^{1\bar{1}}_{1\bar{1}}}, \quad (3.20)$$

where $G(z) = \left\langle \frac{1}{N}\mathrm{Tr}(z-X)^{-1} \right\rangle$ is the one-point Green's function like in the Hermitian case, but for non-Hermitian matrices it is not informative about the spectrum. $\bar{G}(\bar{z})$ is its complex conjugate. The double series yielding the appropriate element of B also simplifies and can be summed up. All cumulants appearing therein can be recovered from the quaternionic R-transform. If we denote $\tilde{\mathcal{R}}_{1\bar{1}} = \mathcal{R}_{1\bar{1}}/Q_{1\bar{1}}$ (such division is always possible and does not lead to rational expressions), then

$$B^{1\bar{1}}_{1\bar{1}} = \tilde{\mathcal{R}}_{1\bar{1}}(\mathrm{diag}(G(z_1), \bar{G}(\bar{z}_2)). \quad (3.21)$$

3.6 Biunitarily invariant ensembles

For matrices with enhanced symmetry to $U(N) \times U(N)$ the expressions above simplify even further. The traced product of resolvents takes the particularly simple

form [A3]

$$\mathfrak{h}(z_1, \bar{z}_2) = \frac{1}{z_1\bar{z}_2 - r_{out}^2}. \tag{3.22}$$

This means that the expression $\left\langle \frac{1}{N}\mathrm{Tr} f(X)g(X^\dagger) \right\rangle$ depends only on the spectral radius r_{out}. The entire dependence of eigenvalues and eigenvectors for such a class of expressions is reduced to a single parameter, showing the remarkable degree of universality of transient dynamics.

Inside the spectrum, due to the simplified structure of cumulants, (3.19) can be brought into a compact form, and it turns out that out of 16 elements of B, only 4 are non-zero. This allows us to find a formula for the two-point function [A3]

$$O_2(z_1, z_2) = \frac{1}{\pi}\partial_{\bar{z}_1}\partial_{z_2}\frac{\bar{z}_1(z_1 - z_2)O_1(r_1) + z_2(\bar{z}_1 - \bar{z}_2)O_1(r_2)}{|z_1 - z_2|^2[F(r_1) - F(r_2)]}, \tag{3.23}$$

where $r_j = |z_j|$ and F is the radial cumulative distribution function. The two-point function is not rotationally symmetric (except for $O_2(0, z)$) because choosing one point in the spectrum distinguishes a particular direction. Equation (3.23) can be considered as the next generalization of the Haagerup-Larsen theorem to eigenvector correlation functions.

3.7 Microscopic universality?

The two considered correlation functions are not independent. Sum rules (1.6) satisfied by the overlap matrix impose the sum rule $\int d^2z_2 D(z_1, z_2) = \rho(z_1)$, which in turn implies

$$\rho(z_1) = NO_1(z_1) + \int_{\mathbb{C}} O_2(z_1, z_2)d^2z_2. \tag{3.24}$$

At first glance, this equation seems contradictory, because all functions – ρ, O_1, O_2 – are of order 1 in the large N limit, while the one-point function is multiplied by a factor of N. Without doubting its correctness, one expects some cancellations on the right-hand side.

It is not immediately evident how this may take place, but after calculating several examples, a certain pattern emerges. The two-point function takes the form [A3]

$$O_2(z, w) = -\frac{1}{\pi^2}\frac{P(z, w)}{|z - w|^4}, \tag{3.25}$$

where $P(z, w)$ is some function. Moreover, it can be checked that for biunitarily invariant ensembles $P(z, z) = \frac{O_1(z)}{\rho(z)}$. This repeating singularity in the denominator suggests that when the two argument get close to each other something new happens. Such singularities in two-point functions in Hermitian ensembles are the signs of a microscopic universality, and different universality classes correspond to different types of singularity. Microscopic universality is observed at scales of typical separation between eigenvalues, which for non-Hermitian models is of the order $\frac{1}{\sqrt{N}}$. Introducing the variable probing the microscopic scale as $w = z + \frac{u}{\sqrt{N\rho(z)}}$, one sees that the denominator in (3.25) combined with the Jacobian of a change of variables produces additional factor of N, which may provide the needed cancellation in the sum rule (3.24). Based on the importance of the microscopic scaling and ubiquity of the $|z - w|^{-4}$ singularity it was conjectured that there exists a universal miscroscopic scaling of the eigenvector correlation function [A3]

$$\lim_{N\to\infty} N^{-2}O_2\left(z + \frac{x}{\sqrt{N}}, z + \frac{y}{\sqrt{N}}\right) = -\frac{O_1(z)}{\pi^2|x - y|^4}\left(1 - (1 + |x - y|^2)e^{-|x-y|^2}\right). \tag{3.26}$$

The exact form of the universal function is not accessible from Feynman diagrams, but it was deduced based on the exact calculations and the asymptotic limit of $O_2(0, z)$ calculated by Chalker and Mehlig [77].

3.8 A brief summary

The setup for the two-point eigenvector correlation functions was proposed by Chalker and Mehlig [77], where it was used to solve the Gaussian model. The work [A3] presents its significant extension, solving all ensembles in large N by the summation of planar Feynman diagrams. Bethe-Salpeter equations (3.18 – 3.19) provide the general solution. Biunitarily invariant ensembles admit further simplifications with the explicit formula for the two-point function (3.23), the analysis of which supports hypothesized microscopic universality in eigenvector correlations (3.26). Another important result of [A3] is the procedure for calculations of traced product of two resolvents (3.8), with the general solution given by (3.20 – 3.21).

Chapter 4

Eigenvectors in a partially symmetric ensemble. Based on [A4].

4.1 Motivation

For a long time the study of non-orthogonal eigenvectors in random matrices was limited to the analysis of one- and two-point functions, with a single exception [88]. Only very recently, Bourgade and Dubach [19] considered the complex Ginibre ensemble and studied the full distribution of the diagonal overlap O_{ii} with the corresponding eigenvalue $\lambda_i = z$. They found that the rescaled variable $u = \frac{O_{ii}}{N(1-|z|^2)}$ in the large N limit tends to the inverse γ_2 distribution given by the probability density function

$$p(u) = \frac{1}{u^3} e^{-\frac{1}{u}}. \tag{4.1}$$

The heavy tail $p(u) \sim u^{-3}$ of the distribution has already been conjectured by Chalker and Mehlig [25, 77] on the basis of calculations for 2×2 matrices and numerical simulations for larger sizes. The rescaling factor in u is the conditional expectation of the overlap $\frac{NO_1(z)}{\rho(z)}$, so this procedure merely shifts the mean of the distribution.

Fyodorov [39], using a different technique, obtained the joint distribution of the eigenvalue and the associated overlap for any matrix size in the complex Ginibre ensemble and for real eigenvalues in the real Ginibre ensemble. He confirmed the inverse γ_2 distribution in the complex Ginibre ensemble, and also found that in the real Ginibre the joint density of the rescaled overlap $O_{ii} = Ns$ and the corresponding bulk eigenvalue $\lambda_i = x\sqrt{N}$ reads

$$\mathcal{P}_{bulk}(s, x) = \frac{1 - x^2}{2\sqrt{2\pi}} \frac{e^{-\frac{1-x^2}{2s}}}{s^2} \text{ for } |x| < 1. \tag{4.2}$$

This distribution is so heavy-tailed that it even does not have the mean, so the correlation function $O_1(z)$ does not exist on the real line for the real Ginibre ensemble. The rescaling $u = \frac{2s}{1-x^2}$ brings (4.2) to the canonical form of the inverse γ_1 distribution.

Dubach [27] analyzed diagonal overlaps in truncated unitary matrices [113] and in the so-called spherical ensemble [69]. Matrices in both ensembles are complex and possess unitary invariance. Again, after rescaling by the conditional expectation $\frac{NO_1(z)}{\rho(z)}$, the distribution of diagonal overlaps is the inverse γ_2 distribution. In the ensemble of quaternionic Gaussian matrices, which was also studied by Dubach, the distribution of properly rescaled overlaps turns out to be the inverse γ_4 distribution [28]. His results

point at possible bulk universality in the distribution of eigenvector overlaps, which is given by the inverse γ_β distribution with the parameter β determined by the number of degrees of freedom in matrix elements, $\beta = 1$ for real, $\beta = 2$ for complex, $\beta = 4$ for quaternion matrices.

Eigenvalues of studied non-Hermitian matrices are ill-conditioned – diagonal overlaps grow linearly with their size. On the other hand, eigenvalue condition numbers in Hermitian matrices are all equal to one. One expects an intermediate regime existing between these two extremes. The elliptic ensemble allows one to smoothly interpolate between the Gaussian Unitary Ensemble of Hermitian matrices and the Ginibre ensemble of non-Hermitian matrices by varying one parameter. This ensemble was studied by Girko [49], who concentrated on the limiting spectral density, which is an ellipse, degenerating to an interval for Hermitian matrices. Fyodorov, Khoruzhenko and Sommers [40, 44] studied this ensemble at a finite size and discovered an intermediate regime of weakly non-Hermitian matrices, where some of the eigenvalues become complex, but their imaginary part is of the same order as the spacing between their real parts. Knowing that the non-Hermiticity affects also the eigenvectors, we conjectured that there exists an analogous regime of weak non-Hermiticity, which we called the weak non-normality.

4.2 The real elliptic ensemble

Eigenvector overlaps are simpler to analyze when real eigenvalues of real ensembles are considered. Therefore, we focus our attention on the real elliptic ensemble, in which the joint probability density function for the elements reads

$$P(X)dX = C_N^{-1} \exp\left[-\frac{1}{2(1-\tau^2)}\mathrm{Tr}(XX^T - \tau X^2)\right] dX. \tag{4.3}$$

Here $dX = \prod_{i,j=1}^{N} dX_{ij}$ is the flat Lebesgue measure over all matrix elements. The normalization constant reads $C_N = (2\pi)^{N^2/2}(1+\tau)(1-\tau^2)^{N(N-1)/4}$. An important ingredient in the model is the parameter $\tau \in [0,1]$, which allows for interpolating between the Gaussian Orthogonal Ensemble ($\tau = 1$) and the real Ginibre ensemble $\tau = 0$. More specifically, it governs the correlations between elements on the opposite side of the diagonal $\langle X_{ij}X_{ji}\rangle = \tau$. The weak non-Hermiticity regime in this model is obtained in the limit $N \to \infty$, $\tau \to 1$, but keeping the product $N(1-\tau)$ of order unity.

4.3 Eigenvectors in the elliptic ensemble

The Cauchy-Schwartz inequality asserts that $O_{ii} \geqslant 1$, so Fyodorov proposed to consider the shifted overlaps $t_i = O_{ii} - 1$. He defined the joint probability density function [39]

$$\mathcal{P}_N(z,t) = \left\langle \sum_{i=1}^{r} \delta(z-\lambda_i)\delta(O_{ii}-1-t) \right\rangle. \tag{4.4}$$

The summation runs over all real eigenvalues. The joint density defined this way differs from the standard definitions of correlation functions by the normalization factor. After integrating over all variables, it yields the average number of real eigenvalues.

It turns out that for the elliptic ensemble it is convenient to absorb a factor that drives the departure from Hermiticity by introducing the variable $q = (1-\tau)t$. Then

the joint density takes the form of [A4]

$$\mathcal{P}(z,q)=\frac{1}{2(1+\tau)\sqrt{2\pi}\Gamma(N-1)}\frac{e^{-\frac{z^2}{2(1+\tau)}\left(1+\frac{q}{1+q}\right)}}{\sqrt{q(1+q)}}\left(\frac{q}{1+\tau+q}\right)^{\frac{N}{2}-1}\left[\frac{P_{N-2}z^2}{(1+q)^2}+\right.$$
$$\frac{(1+\tau-2z^2)P_{N-2}+2z[R_{N-2}+\tau(N-2)R_{N-3}]}{1+q}+\frac{\tau^2(1+\tau)^2N(N-2)P_{N-3}}{(1+\tau+q)^2}+$$
$$\left.\frac{(1+\tau)(1-\tau^2)(N-2)((N-2)P_{N-3}-T_{N-3})}{1+\tau+q}-\frac{2\tau(1+\tau)(N-2)zR_{N-3}}{(1+q)(1+\tau+q)}\right] \quad (4.5)$$

The auxiliary functions P_N, R_N and T_N are defined in the following way:

$$P_N=N!\sum_{k=0}^{N}\frac{\tau^k}{k!}\left((k+1)\mathrm{He}_k^2\left(\frac{z}{\sqrt{\tau}}\right)-k\mathrm{He}_{k-1}\left(\frac{z}{\sqrt{\tau}}\right)\mathrm{He}_{k+1}\left(\frac{z}{\sqrt{\tau}}\right)\right), \quad (4.6)$$

$$R_N=\frac{N!}{2}\sum_{k=0}^{N}\frac{\tau^{k+\frac{1}{2}}}{k!}\left((k+2)\mathrm{He}_{k+1}\left(\frac{z}{\sqrt{\tau}}\right)\mathrm{He}_k\left(\frac{z}{\sqrt{\tau}}\right)-k\mathrm{He}_{k+2}\left(\frac{z}{\sqrt{\tau}}\right)\mathrm{He}_{k-1}\left(\frac{z}{\sqrt{\tau}}\right)\right), \quad (4.7)$$

$$T_N=N!\sum_{k=0}^{N}\frac{k\tau^k}{k!}\left((k+1)\mathrm{He}_k^2\left(\frac{z}{\sqrt{\tau}}\right)-k\mathrm{He}_{k-1}\left(\frac{z}{\sqrt{\tau}}\right)\mathrm{He}_{k+1}\left(\frac{z}{\sqrt{\tau}}\right)\right), \quad (4.8)$$

where $\mathrm{He}_k(z)$ denotes the Hermite polynomials

$$\mathrm{He}_k(z)=\frac{(\pm i)^k}{\sqrt{2\pi}}e^{\frac{z^2}{2}}\int_{-\infty}^{\infty}t^k e^{-\frac{t^2}{2}\mp izt}dt. \quad (4.9)$$

The expression (4.5) is exact for any matrix size, but in order to draw conclusions it is beneficial to take the asymptotic limits.

1. *Bulk*. We fix $\tau\in[0,1)$ and rescale $z\to z\sqrt{N}$, $t\to Nt$. We define the limiting distribution $\mathcal{P}_{Bulk}(z,t)=\lim_{N\to\infty}N\mathcal{P}_N(\sqrt{N}z,Nt)$, which for $|z|<1+\tau$ takes the form [A4]

$$\mathcal{P}_{Bulk}(z,t)=\frac{\sqrt{1-\tau^2}}{2\sqrt{2\pi}}\frac{\left[1-\frac{z^2}{(1+\tau)^2}\right]}{t^2}e^{-\frac{1-\tau^2}{2t}\left[1-\frac{z^2}{(1+\tau)^2}\right]}. \quad (4.10)$$

   The way the asymptotic limit is taken shows that in the bulk the eigenvector overlap grows linearly with the matrix size N. Moreover, in the rescaled variable $\frac{1}{u}=\frac{1-\tau^2}{2t}[1-\frac{z^2}{(1+\tau)^2}]$ the joint density $\mathcal{P}_{Bulk}$ takes the form of the inverse γ_1 distribution.

2. *Edge*. Keeping $\tau\in[0,1)$ fixed, we probe the edge of the distribution by parameterizing $z=\sqrt{N}(1+\tau)+\delta_\tau\sqrt{1-\tau^2}$. The overlap is further reparamerized as $q=\sigma\sqrt{N(1-\tau^2)}$. The limit $\mathcal{P}_{Edge}(\delta_\tau,\sigma)=\lim_{N\to\infty}\mathcal{P}_N(z,q)$ reads [A4]

$$\mathcal{P}_{Edge}(\delta_\tau,\sigma)=\frac{1}{4\pi\sigma^2(1-\tau^2)}e^{-\frac{1}{4\sigma^2}+\frac{\delta_\tau}{\sigma}}\left[e^{-2\delta_\tau^2}+\left(\frac{1}{\sigma}-2\delta_\tau\right)\int_{2\delta_\tau}^{\infty}e^{-\frac{u^2}{2}}du\right]. \quad (4.11)$$

   Eigenvector overlaps corresponding to the eigenvalues located close to the edge of the spectrum scale now as $O_{ii}\sim N^{1/2}$, so the eigenvectors are less non-orthogonal than for bulk eigenvalues.

3. *Weak non-normality.* Rescaling $z \to z\sqrt{N}$ we take the large N limit, but keeping $a^2 = 2N(1-\tau)$ fixed, and thus approaching also the Hermitian limit. The limiting distribution $\mathcal{P}_{Weak}(z,t) = \lim_{N\to\infty} N^{-1/2}\mathcal{P}_N(z\sqrt{N},t)$ reads [A4]

$$\mathcal{P}_{Weak}(z,t) = \frac{A}{2}\rho_{sc}(z)\frac{e^{-\frac{A}{2t}}}{t^2}\int_0^1 e^{-\frac{1}{2}As^2}\left(1+A+\frac{A}{t}-As^2\right)s^2 ds, \qquad (4.12)$$

where we denoted $A = (\pi a \rho_{sc}(z))^2$, and $\rho_{sc}(z) = \frac{1}{2\pi}\sqrt{4-z^2}$ is the Wigner semi-circle distribution, which is a density of eigenvalues in the fully Hermitian limit. In the regime of weak non-Hermiticity O_{ii} are of order one, but their distribution is heavy-tailed.

The bulk and edge limiting distributions after an appropriate rescaling are given by the same form as obtained by Fyodorov for the real Ginibre ensemble [39], providing further evidence for the universality in the bulk and the edge. The expression in the weak non-normality limit interpolates between the Hermitian limit $\mathcal{P}(z,t) = \rho_{sc}(z)\delta(t)$ and strong non-normality. In the entire range, the distribution $\mathcal{P}_{Weak}$ is heavy tailed, so we conclude that the tail $\mathcal{P}(z,t) \sim t^{-2}$ is the most robust feature of the distribution of overlaps.

4.4 About the proofs

A key technical tool in the derivation of (4.5) is the partial Schur decomposition. A real $N \times N$ matrix X_N with a real eigenvalue λ can be decomposed as

$$X_N = O\begin{pmatrix}\lambda & w^T \\ 0 & X_{N-1}\end{pmatrix}O^T = O\tilde{X}_N O^T. \qquad (4.13)$$

Here w is a column vector with $N-1$ components and the matrix X_{N-1} has the size reduced by 1. The matrix O is orthogonal. With this decomposition the eigenvector overlap associated with λ can be written as [39]

$$O_{ii} = 1 + w^T(\lambda - X_{N-1})^{-1}(\lambda - X_{N-1}^T)^{-1}w. \qquad (4.14)$$

The Jacobian of the change of variables is the modulus of the characteristic determinant, $|\det(\lambda - X_{N-1})|$. Instead of the direct density, it is convenient to work with the Laplace transform in the eigenvector variable and consider $\mathcal{L}(z,p) = \left\langle \delta(z-\lambda)e^{-p(O_{ii}-1)}\right\rangle$. The orthogonal matrix O decouples, while the integral over w is Gaussian, so it can be evaluated explicitly, yielding [A4]

$$\mathcal{L}(z,p) = \frac{e^{-\frac{z^2}{2(1+\tau)}}}{2^{N/2}\Gamma\left(\frac{N}{2}\right)\sqrt{1+\tau}}\left\langle \frac{\det(z-X_{N-1})(z-X_{N-1}^T)}{\det{}^{1/2}[2p(1-\tau^2)+(z-X_{N-1})(z-X_{N-1}^T)]}\right\rangle. \qquad (4.15)$$

The Laplace transform is expressed in terms of the ratio of two determinants averaged over the same elliptic ensemble (4.3), but with size reduced by 1. Ratios of characteristic polynomials were intensively studied in random matrix theory and several tools for their study have been worked out [7, 8, 38, 45]. One of them uses the Gaussian representation of the characteristic polynomials and its inverse square root

$$\det X = \int d\chi d\eta e^{-\chi^T X \eta}, \qquad \det{}^{-1/2} X = (2\pi)^{-N/2}\int_{\mathbb{R}} e^{-y^T X y} d^n y, \qquad (4.16)$$

where y is a real N-component vector, while χ, η are two different vectors with anti-commuting (Grassmann) numbers which satisfy the algebra $\chi_j\chi_k = -\chi_k\chi_j$.

The bulk, edge and weak non-normality limits are obtained via the integral representation of the Hermite polynomials (4.9) followed by saddle point analysis.

4.5 A brief summary

The paper [A4] relies on the technique developed by Fyodorov [39], applying it to the real elliptic ensemble. The main results are the exact finite N formula (4.5) and its asymptotic limits in three regimes (4.10 – 4.12), including the weak non-normality regime, which was identified for the first time.

Chapter 5

Fast route to microscopic universality. Based on [A5].

5.1 Integrability of Hermitian random matrices

Random Hermitian matrices with a unitarily invariant probability density function (given by (2.1)) are solvable not only in large N limit, but also for any matrix size. By solvability we understand that for $1 \leqslant m \leqslant N$, all m-point eigenvalue correlation functions [34]

$$R_m(x_1, \ldots, x_m) = \left\langle \sum_{i_1 \neq \ldots \neq i_m} \prod_{j=1}^{m} \delta(x_j - \lambda_{i_j}) \right\rangle \tag{5.1}$$

can be calculated. The one-point function is the spectral density times the number of eigenvalues, while the N-point function is the joint density of eigenvalues. The k-point functions are obtained by integrating out one variable from the $(k+1)$-point function. Changing variables as $H = U\Lambda U^\dagger$, we move to the eigenbasis, and the joint pdf now reads [34]

$$P(\Lambda, U) d\Lambda dU = Q_N^{-1} e^{-\sum_{j=1}^{N} V(\lambda_j)} \prod_{1 \leqslant i < j \leqslant N} |\lambda_i - \lambda_j|^2 d\Lambda dU. \tag{5.2}$$

Here $d\Lambda = \prod_{i=1}^{N} d\lambda_i$ is the flat Lebesgue measure, while dU denotes the Haar measure on the unitary group. We also removed a factor of N in the exponent in (2.1) since this is the standard convention in the literature on finite random matrices. This scaling will be brought back when taking the scaling limits.

One sees that U – the matrix of eigenvectors – is uniformly distributed on the $U(N)$ group. Eigenvectors decouple from the eigenvalues, so they can be integrated out, changing only the overall normalization constant. An additional factor $|\Delta(\lambda)|^2 = \prod_{1 \leqslant i < j \leqslant N} |\lambda_i - \lambda_j|^2$ is the Jacobian of the change of variables. It is the square of the Vandermonde determinant

$$\Delta(\lambda) = \begin{vmatrix} 1 & 1 & \ldots & 1 \\ \lambda_1 & \lambda_2 & \ldots & \lambda_N \\ \lambda_1^2 & \lambda_2^2 & \ldots & \lambda_N^2 \\ \vdots & \vdots & \ddots & \vdots \\ \lambda_1^{N-1} & \lambda_2^{N-1} & \ldots & \lambda_N^{N-1} \end{vmatrix} = \det[\lambda_l^{k-1}]_{k,l=1}^{N}. \tag{5.3}$$

Adding a multiplicity of one row to another one does not change the value of the determinant, so monomials as entries of this matrix are not the only choice. In fact, in the k-th row one can put any polynomial with the leading term λ^{k-1} (monic polynomial), thus $\Delta(\lambda) = \det[P_{k-1}(\lambda_l)]_{k,l=1}^{N}$, where P_k denotes such a polynomial. Moreover,

the term in the potential can be incorporated into the matrix, so the joint probability density function is proportional to

$$\Big(\det[\psi_{k-1}(\lambda_l)]_{k,l=1}^{N}\Big)^2 = \det[K_N(\lambda_k,\lambda_l)]_{k,l=1}^{N}, \tag{5.4}$$

where $\psi_k(\lambda) = e^{-V(\lambda)/2}P_k(\lambda)$. In the second equality we used the fact that the transposition of the determinant does not change its value and performed matrix multiplication explicitly, which results in the following function:

$$K_N(x,y) = \sum_{k=0}^{N-1} \psi_k(x)\psi_k(y). \tag{5.5}$$

In principle, P_k can be any monic polynomial, but it is most convenient to choose it to be orthogonal with respect to the weight given by the potential. Moreover, the combination of normalization constants allows one to further rescale monic polynomials so that they are *orthonormal*

$$\int_{-\infty}^{+\infty} e^{-V(x)}P_j(x)P_k(x)dx = \delta_{jk}, \tag{5.6}$$

but no longer monic. With the choice of orthonormal polynomials, the function K_N is called the *correlation kernel* and satisfies the self-reproducing property

$$\int_{-\infty}^{\infty} K_N(x,z)K_N(z,y)dz = K_N(x,y). \tag{5.7}$$

It can be shown [79] that all m-point correlation functions can be written as

$$R_m(x_1,\ldots,x_m) = \det[K_N(x_i,x_j)]_{i,j=1}^{m}, \tag{5.8}$$

which provides a solution for any matrix model. It is a remarkable simplification that all correlation function are expressed in terms of a single two-point function.

5.2 Spectral projection method

To describe the main concept, we focus now on a specific choice of the potential $V(\lambda) = \lambda - \alpha\log(x)$. Such a potential is realized in the Wishart ensemble. Consider X to be a matrix of size $N \times T$ with elements generated from the complex Gaussian distribution of zero mean and $\langle |X_{ij}|^2\rangle = 1$. Then, the matrix $H = XX^\dagger$ belongs to the Wishart ensemble. The choice of the potential corresponds to the weight $e^{-\lambda}\lambda^\alpha$ in (5.6). Polynomials orthogonal to this weight are the modified Laguerre polynomials, which appear also in the hydrogen atom problem. Indeed, upon the identification of constants and parameters, $\psi_k(\lambda)$ can be mapped onto the radial part of the wavefunction (see the details of that mapping in [A5]).

Moreover, the first determinant in (5.4) is the Slater determinant, which means that the eigenvalues of random matrices behave like non-interacting fermions. This fact explains why all correlation functions are expressed by the correlation kernel – it plays the role of a propagator in non-interacting theories. The function $\psi_k(x)$ satisfies the Schrödinger equation

$$\frac{d^2\psi_k}{dx^2} + \frac{1}{x}\frac{d\psi_k}{dx} + \frac{1+2k+\alpha}{2x}\psi_k - \frac{\alpha^2}{4x^2}\psi_k = \frac{1}{4}\psi_k. \tag{5.9}$$

It is even more instructive to use the bra-ket notation, in which the kernel can be written as $\hat{K}_N = \sum_{k=0}^{N-1} |\psi_k\rangle\langle\psi_k|$. Besides orthonormality, eigenfunctions $|\psi_k\rangle$ provide

also the resolution of identity $\mathbb{1} = \sum_{k=0}^{\infty} |\psi_k\rangle \langle\psi_k|$. The kernel is represented by a similar sum, but truncated at first N terms, so it is a projection operator. Interestingly, the self-reproducing property (5.7) reflects this fact, $\hat{K}_N^2 = \hat{K}_N$, but it is written in the coordinate representation $K_N(x,y) = \langle x| \hat{K}_N |y\rangle$. Formally, the kernel projects the Hilbert space to its subspace spanned by eigenfunctions satisfying $\langle\psi| \hat{H} |\psi\rangle \leqslant E_{N-1}$, where $\hat{H}$ is the Hamiltonian associated with the Schrödinger equation (5.9). We write this less formally as [A5]

$$\frac{d^2}{dx^2} + \frac{1}{x}\frac{d}{dx} + \frac{1+2k+\alpha}{2x} - \frac{\alpha^2}{4x^2} \geqslant \frac{1}{4}, \tag{5.10}$$

and we will be looking for a convenient representation of functions spanning this space.

In order to have a finite support of the limiting density of eigenvalues for large N, it is convenient to rescale the Wishart matrix as $H \to \frac{1}{T}H$. Then in the double scaling limit $N, T \to \infty$ with $c = \frac{N}{T}$ fixed, one obtains the Marčenko-Pastur distribution [76]

$$\rho(x) = \frac{1}{2\pi c x}\sqrt{(r_+ - x)(x - r_-)}, \tag{5.11}$$

where $r_\pm = (1 \pm \sqrt{c})^2$ are the two endpoints of the spectrum.

Universal correlations of eigenvalues are probed on the scale of the typical separation between them. Based on the limiting form of the density, one can distinguish three possibilities of microscopic universality, depending on the behavior of $\rho(x)$. The scale s, at which the correlations are probed, is obtained by demanding that within an interval of length s one expects one eigenvalue to occur. The three regimes are:

1. *Bulk.* Between endpoints in the close vicinity of the considered point x_0 the density can be approximated as constant $\rho(x_0)$, so we are looking for s in which

$$1 \sim N \int_{x_0 - s/2}^{x_0 + s/2} \rho(x_0) dx = N s \rho(x_0). \tag{5.12}$$

   Therefore the proper scale is $s \sim \frac{1}{N\rho(x_0)}$.

2. *Soft edge.* Close to the edges of the spectrum the density vanishes like $\sqrt{|r_\pm - x|}$, so the condition determining the proper scale now reads

$$1 \sim N \int_0^s \sqrt{x} dx \sim N s^{2/3}, \tag{5.13}$$

   and the microscopic scale at the edge is $s \sim N^{-2/3}$.

3. *Hard edge.* When $c = 1$ the left endpoint of the spectrum is $r_- = 0$, drastically changing the spectral density, which is now singular at the origin and behaves like $x^{-1/2}$. A similar analysis leads to the microscopic scale $s \sim \frac{1}{N^2}$.

The above rough calculations allow one only to determine the microscopic scale at which the behavior of the eigenvalues can be probed. The existence and exact form of the microscopic correlations need to be found by taking the appropriate limits. Since all correlation functions are determined by the kernel, it is sufficient to study its scaling. This is a difficult task as it involves studying the Plancherel-Rotach asymptotics of orthogonal polynomials in which the argument of the polynomial is rescaled by its order, which goes to infinity. Typically, such calculations are performed by finding the integral representation of the kernel, followed by careful saddle point analysis. In all interesting regimes, representations involve at least two integrals, and the saddle point is degenerate, complicating calculations even more.

Borodin and Olshanski [18] introduced a method which simplifies the calculations considerably. It uses the fact that the kernel is a projection built from eigenfunctions of a certain Hamiltonian. The microscopic scaling often simplifies the form of the Hamiltonian. Instead of an abstract description, we demonstrate it by recalculating three microscopic universalities, which can be found in the Wishart ensemble. This analysis in a more general setting was performed by Bornemann [16].

1. *Bulk.* We probe the microscopic scale by introducing the variable s defined as $\frac{x}{T} = x_0 + \frac{s}{N\rho(x_0)}$. The factor $1/T$ is needed to ensure a finite support of the spectrum, while $\frac{1}{N\rho(x_0)}$ provides proper probing of the microscopic regime. This change of variables, followed by taking the limit $N, T \to \infty$ with $c = N/T$ fixed, turns the condition (5.10) into

$$-\frac{d^2}{ds^2} \leqslant \pi^2. \tag{5.14}$$

On the left-hand side we see the Hamiltonian of a free particle, so it is convenient to move to the momentum space via the Fourier transform. We introduce $F(q)$, the Fourier transform of $f(y)$. These functions are related via

$$F(q) = \int_{-\infty}^{\infty} e^{2\pi i q y} f(y) dy, \qquad f(x) = \int_{-\infty}^{\infty} e^{-2\pi i x q} F(q) dq. \tag{5.15}$$

The Fourier transform and its inverse provide also the resolution of the identity

$$f(x) = \int_{-\infty}^{\infty} \int_{-\infty}^{\infty} e^{-2\pi i x q} e^{2\pi i q y} dq f(y) dy. \tag{5.16}$$

The Kernel is a projection operator acting on the space of functions via

$$P[f(x)] = \int_{-\infty}^{\infty} K(x, y) f(y) dy. \tag{5.17}$$

In the Fourier space the condition (5.14) takes the form of $q^2 \leqslant \frac{1}{4}$. This means that only momenta in the range $-\frac{1}{2} \leqslant q \leqslant \frac{1}{2}$ contribute to the kernel, so

$$P[f(x)] = \int_{-\infty}^{\infty} \left[\int_{-\frac{1}{2}}^{\frac{1}{2}} e^{-2\pi i x q} e^{2\pi i q y} dq \right] f(y) dy. \tag{5.18}$$

Comparing (5.18) with (5.17), we immediately read out the form of the kernel

$$K_{Bulk}(x, y) = \frac{\sin(\pi(x - y))}{\pi(x - y)}. \tag{5.19}$$

2. *Edge scaling.* To probe the microscopic behavior at the soft edge, we introduce the following scaling variable: $\frac{x}{T} = r_\pm \pm \frac{s}{\sqrt{c}(r_\pm N)^{2/3}}$, which in the large N limit turns (5.10) into

$$-\frac{d^2}{ds^2} + s \leqslant 0. \tag{5.20}$$

The trick with the Fourier space does not lead to simplifications, because it restricts the region of integration to a parabola. Instead, we observe that (5.20) represents a Hamiltonian of a particle in a linear potential, the eigenfunctions of which are the Airy functions. Therefore, we resort to the Airy transform

$$F(z) = \int_{-\infty}^{\infty} Ai(y - z) f(y) dy, \qquad f(x) = \int_{-\infty}^{\infty} Ai(x - z) F(z) dz. \tag{5.21}$$

The Airy transform and its inverse provide the resolution of the identity

$$f(x) = \int_{-\infty}^{\infty} \int_{-\infty}^{\infty} Ai(x-z)Ai(y-z)dz f(y)dy, \tag{5.22}$$

The condition (5.20) in this representation leads to $z < 0$, which truncates the range of admissible values of z, therefore the kernel, understood as a projection, reads

$$K_{Edge}(x,y) = \int_{-\infty}^{0} Ai(x-z)Ai(y-z)dz = \frac{Ai(x)Ai'(y) - Ai(y)Ai'(x)}{x-y}. \tag{5.23}$$

3. *Hard edge.* The hard edge occurs only when $c = 1$, that is, when N goes with the same speed to infinity as T, so their difference $\alpha = T - N$ may remain constant, which plays an important role in the microscopic regime. Upon the scaling $\frac{x}{T} = \frac{s}{N^2}$ the condition (5.10) is transformed into

$$\frac{d^2}{ds^2} + \frac{1}{s}\frac{d}{ds} + \frac{1}{s} - \frac{\alpha^2}{4s^2} \geqslant 0. \tag{5.24}$$

With the variable $z = 2\sqrt{s}$ it takes a more familiar form

$$-\frac{d^2}{dz^2} - \frac{1}{z}\frac{d}{dz} + \frac{\alpha^2}{z^2} \leqslant 1. \tag{5.25}$$

On the left-hand side we recognize the Bessel operator, so we use the Hankel transform, which provides the resolution of the identity

$$f(z) = \int_0^{\infty} \int_0^{\infty} z' t J_\alpha(zt) J_\alpha(tz') dt f(z') dz'. \tag{5.26}$$

The condition (5.20) in the variable of the Bessel transform reads $t \leqslant 1$, which turns the identity (5.26) into the projection

$$P[f(z)] = \int_0^{\infty} \left[\int_0^1 zt J_\alpha(zt) J_\alpha(tz') dt \right] f(z) dz'. \tag{5.27}$$

Returning to the original Hamiltonian by introducing variables $t = \sqrt{s}$, $z = \sqrt{x}$, $z' = \sqrt{y}$, we read out the form of the kernel

$$K_{Hard}(x,y) = \frac{1}{4} \int_0^1 J_\alpha(\sqrt{xs}) J_\alpha(\sqrt{ys}) ds. \tag{5.28}$$

The above calculations show how the projection method, combined with the clever choice of the integral transform, allows one to calculate the microscopic scaling of the kernel in just a few lines, without the need of integral representations and saddle point analysis.

5.3 Biorthogonal ensembles

Having in mind integrable structure of Hermitian matrices, Muttalib [82], motivated by physical applications, and later Borodin [17] introduced a new class of ensembles which also have determinantal structure. In this case the joint probability density function is given by the product of two determinants

$$P(x_1, \ldots, x_N) \sim \det[\eta_i(x_j)]_{i,j=1}^N \det[\chi_i(x_l)]_{k,l=1}^N, \tag{5.29}$$

where η_i and χ_i are some functions. The choice $\eta_i(x) = x^{i-1}$ and $\chi_i(x) = e^{-V(x)}x^{i-1}$ corresponds to ensembles solved by orthogonal polynomials. Assume now that it is possible to biorthogonalize these functions, that is, to construct P_k's as linear combinations of χ_i's and Q_k's as linear combinations of η_i's in such a way that P_k's and Q_k's form a biorthogonal set

$$\int_{-\infty}^{\infty} Q_j(x)P_k(x)dx = \delta_{jk}. \tag{5.30}$$

Then, all correlation functions are expressed in terms of a determinant of a matrix, the elements of which are given by the correlation kernel, which reads

$$K_N(x,y) = \sum_{k=0}^{N} P_k(x)Q_k(y). \tag{5.31}$$

Beyond the example considered by Muttalib and Borodin, biorthogonal ensembles were later found in multi-matrix models [13, 12, 29, 35] and recently in products of random matrices [4, 5, 66, 73].

The biorthogonal structure of functions Q_k and P_k reminds us of the biorthogonal eigenvectors of non-Hermitian matrices, where Q_k's play the role of left and P_k's of right eigenvectors. In the method of orthogonal polynomials it was possible to choose $P_k = Q_k$, which were the eigenfunctions of a self-adjoint operator. In the case of Wishart model, it was the Hamiltonian. This raises a question whether a non-self-adjoint counterpart of the Hamiltonian can be found in biorthogonal ensembles. Below we provide an example of a biorthogonal ensemble, where such a structure is realized. Moreover, the spectral projection method allows one to simply calculate the microscopic scaling.

5.4 Products of Gaussian matrices

Let X_k be a rectangular matrix of size $(N+\nu_{k-1})\times(N+\nu_k)$, the entries of which are Gaussian of zero mean and variance $\langle|X_{ij}|^2\rangle = 1$. One may assume $\nu_0 = 0$ and $\nu_k > 0$ for all $k > 0$ without losing generality. The squared singular values of the product $Y_M = X_1X_2\dots X_M$ form a biorthogonal ensemble with the correlation kernel (5.31). The biorthogonal functions read [4]

$$P_k(x) = G^{1,0}_{1,M+1}\left(\begin{matrix} k+1 \\ 0, -\nu_M, \dots, -\nu_1 \end{matrix}\middle| x\right), \tag{5.32}$$

$$Q_k = G^{M,1}_{1,M+1}\left(\begin{matrix} -k \\ \nu_M, \dots, \nu_1, 0 \end{matrix}\middle| x\right), \tag{5.33}$$

where G denotes the Meijer-G function (see Appendix C of [A5] for the definition and basic properties). More importantly, due to the differential equation satisfied by the Meijer-G function, functions $P_k(x)$, which are in fact polynomials, satisfy the eigenequation $\mathcal{H}_M P_k = kP_k$ with the differential operator

$$\mathcal{H}_M = x\frac{d}{dx} - \frac{d}{dx}\prod_{j=1}^{M}\left(x\frac{d}{dx} + \nu_j\right). \tag{5.34}$$

Its adjoint operator, in a sense that it satisfies $\int g(x)\mathcal{H}_M f(x)dx = \int(\mathcal{H}^*_M g(x))f(x)dx$, can be obtained by the integration by parts and noticing that the boundary terms vanish. It reads explicitly [A5]

$$\mathcal{H}^*_M = -x\frac{d}{dx} - 1 + (-1)^M\frac{d}{dx}\prod_{j=1}^{M}\left(x\frac{d}{dx} - \nu_j\right). \tag{5.35}$$

It can be checked that indeed Q_k satisfies the eigenequation $\mathcal{H}_M^* Q_k = kQ_k$ for the same eigenvalue. This stays in the full analogy with the left and right eigenvectors of non-Hermitian matrices.

The limiting spectral density of $\frac{1}{N^M} Y_M Y_M^\dagger$ cannot be presented in an explicit form, but in the vicinity of zero it behaves as $\rho(x) \sim x^{-\frac{M}{M+1}}$ [22]. For $M > 1$ this is a new type of singular behavior, so one expects different microscopic universality to occur. Introducing the scaling variable $x = \frac{z}{N}$ turns the eigenequation for P_k into

$$\left[\frac{1}{N} z \frac{d}{dz} - \frac{d}{dz} \prod_{j=1}^{M} \left(z \frac{d}{dz} + \nu_j \right) \right] P_k = \frac{k}{N} P_k. \tag{5.36}$$

The summation index in the kernel (5.31) is always smaller than N, which provides a bound on the eigenfunctions which can be less formally written as [A5]

$$- \frac{d}{dz} \prod_{j=1}^{M} \left(z \frac{d}{dz} + \nu_j \right) \leqslant 1. \tag{5.37}$$

Narain [84] introduced a class of asymmetric integral transforms that generalize 'classical' transforms. A special instance of the transform that is relevant for our problem is the following

$$g(s) = \int_0^\infty k(s,y) f(y) dy, \qquad f(x) = \int_0^\infty h(x,s) g(s) ds, \tag{5.38}$$

with

$$k(s,y) = G^{M,0}_{0,M+1}\left(\begin{matrix} - \\ \nu_1, \ldots, \nu_M, 0 \end{matrix} \middle| sy \right), \tag{5.39}$$

$$h(x,s) = G^{1,0}_{0,M+1}\left(\begin{matrix} - \\ 0, -\nu_1, \ldots, -\nu_M \end{matrix} \middle| xs \right). \tag{5.40}$$

These transforms provide a convenient representation of the condition (5.37), because in the dual variable it simply reads $s \leqslant 1$. In the resolution of the identity

$$f(x) = \int_0^\infty \int_0^\infty h(x,s) k(s,y) ds f(y) dy \tag{5.41}$$

the condition (5.37) restricts the range of the inner integral to $0 \leqslant s \leqslant 1$, so one easily reads out the form of the limiting kernel [A5], which was obtained for the first time in [73]

$$K^M_{Hard}(x,y) = \int_0^1 G^{1,0}_{0,M+1}\left(\begin{matrix} - \\ 0, -\nu_1, \ldots, -\nu_M \end{matrix} \middle| xs \right) G^{M,0}_{0,M+1}\left(\begin{matrix} - \\ \nu_1, \ldots, \nu_M, 0 \end{matrix} \middle| sy \right) ds. \tag{5.42}$$

It is worth noting that the case $M = 1$ corresponds to the Wishart ensemble, so this result generalizes the Bessel kernel. However, the exact form of that kernel reads

$$K^1_{Hard}(x,y) = \left(\frac{y}{x} \right)^{\nu/2} \int_0^1 J_\nu(2\sqrt{sx}) J_\nu(2\sqrt{sy}) ds, \tag{5.43}$$

which is almost the same as (5.28), but with a different prefactor. This discrepancy is explained by the fact that the functions P_k and Q_k building the kernel are not unique. Like left and right eigenvectors are defined up to rescaling, one can rescale $P_k(x) \to \frac{1}{f(x)} P_k(x)$ and $Q_k(y) \to f(y) Q_k(y)$ without altering the orthogonality relations. Then the kernel transforms as $K(x,y) \to \frac{f(y)}{f(x)} K(x,y)$.

5.5 A brief summary

The spectral projection method, introduced by Borodin and Olshanski [18] is extended to the case of biorthogonal ensembles in paper [A5], where an analogous structure to left and right eigenvectors of non-Hermitian matrices was noticed. The Narain transform was identified as the source of projections obtained in the microscopic limit at the hard edge in products of Gaussian random matrices.

Chapter 6

Non-orthogonal eigenvectors in models of neural networks. Based on [A6].

6.1 Models of randomly coupled neural networks

In 1988, Sompolinsky, Crisanti and Sommers [100] introduced a model of a neural network evolving in time according to the system of first order coupled nonlinear differential equations

$$\dot{y}_i = -y_i + \sum_{j=1}^{N} J_{ij}\phi(y_j). \tag{6.1}$$

Here y_i denotes the local membrane potential of the i-th neuron, while $\phi(y_i)$ denotes its activity. The nonlinear function $\phi(y)$ is sigmoidal and for concreteness chosen to be $\phi(x) = \tanh(gx)$, with parameter g adjusting its degree of nonlinearity. Equations (6.1) are Kirchhoff equations in which the first term represents leaking current due to membrane capacity, $-y_i$ is the current flow through the membrane resistance, while the last term is the inflowing current from other connected cells. J_{ij} are synaptic efficacies coupling the output of the j-th neuron with the input of the i-th neuron. In this model they are chosen as Gaussian random variables with zero mean and variance σ^2/N. The synaptic weight matrix J is therefore a random matrix generated from the real Ginibre ensemble.

The model can be solved in the large N limit with the use of the dynamical mean field theory. There are two parameters g and σ in the model, but the dynamics depend on their combination $g\sigma$, and one can distinguish two regimes. The system has a fixed point $y^* = 0$, and by linearizing (6.1) one can see that when $g\sigma < 1$ this fixed point is stable. If neurons are externally excited by some stimulus, their activity will be finally damped. Therefore, in this regime the system cannot operate for a long time. When $g\sigma < 1$ the fixed point y^* is unstable, and the system is in the chaotic phase in the sense that its response to two very similar external stimuli will differ in time, and this difference will grow exponentially in time.

The stability-instability transition of the fixed point is related to the rightmost eigenvalue (that is, the eigenvalue with the largest real part) of a random matrix gJ – whether it is greater or smaller than 1. At the microscopic level, it is related to the transition between a single fixed point and the proliferation of fixed points, the number of which grows exponentially with the number of the system's components N [108].

If the system is to be operative, none of these two phases is desired. Instead, the system should be posed at the edge of the stability or slightly below in order to main-

tain its activity for a long time, while still responding in a non-chaotic manner. The network is excited by external stimuli coming from other networks coupled to the considered network or from the surroundings, so it needs to stay active until the next external excitation comes. In systems with a non-normal synaptic connectivity matrix, the transient dynamics was proposed as a mechanism, which keeps the system active for a longer time by amplifying neural responses to weak stimuli [46, 81, 51].

6.2 The Rajan-Abbott model

The aim of modeling neural networks is to gain some insights into how biological networks may operate. The main drawback of the model (6.1) is that the connections between real neurons are definitely not random. A way out of this problem was proposed by Rajan and Abbott [95], who proposed modifications by changing only the synaptic weight matrix. They introduced two types of neurons: excitatory (E) and inhibitory (I). Synaptic strengths of $f_E N$ excitatory neurons are generated from a Gaussian distribution with mean $\mu_E > 0$ and variance σ_E^2/N. Similarly, weights of the remaining $f_I N$ inhibitory neurons have a Gaussian distribution with $\mu_I < 0$ mean and σ_I^2/N variance. For large matrix sizes, it is unlikely for an excitatory neuron to have a negative weight, therefore this model reflects the Dale's principle stating that each neuron either inhibits or excites all connected neurons.

The synaptic weight matrix can be naturally decomposed as $J = M + W$. The deterministic matrix M represents the average strengths of neuronal connection and it consists of $f_E N$ identical columns filled with μ_E followed by $f_I N$ columns with elements μ_I. W represents the populational variability of synaptic strengths and is decomposed as $W = G\Lambda$, where G is a random matrix from the Ginibre ensemble. The diagonal matrix Λ with first $f_E N$ elements equal to σ_E and last $f_I N$ elements equal to σ_I is responsible for rescaling the variance within columns.

The spectrum of the matrix W is a disk of radius $r^2 = f_I\sigma_I^2 + f_E\sigma_E^2$, so in order to pose the system at the edge of stability, one slightly modifies the model, introducing another parameter μ, and shifting the spectrum. Now the dynamics can be written as

$$\dot{y}_i = -\beta y_i + \sum_{j=1}^{N} (\mu_j + G_{ij}\sigma_j)\phi(y_j), \tag{6.2}$$

where μ_j is either μ_E or μ_I depending of the type of neuron and similarly for σ_j. This additional parameter β can be obtained by recovering the time-scale of the dynamics.

When the deterministic matrix M is introduced to the model, the spectrum of the synaptic weight matrix changes drastically, and several outliers emerge. Such outliers cause chaos in the model by making the fixed point $y^* = 0$ unstable. In principle, this can be cured by appropriately adjusting μ to shift all eigenvalues to the left, but then the contribution from the eigenvalues in the bulk will by quickly damped.

It was observed in experiments that the amount of excitation and inhibition to a single neuron is the same [55, 98, 103]. This so-called E/I balance is maintained on the time-scale of several milliseconds [60, 110]. Rajan and Abbott incorporated this phenomenon in the model by demanding that the strengths of incoming synapses add to zero both on the average, $f_I\mu_I + f_E\mu_E = 0$ (global balance), and for each neuron separately, $\sum_{j=1}^{N} W_{ij} = 0$ (local balance). The global balance is set by restricting one parameter in the model, while the local balance is imposed numerically by subtracting the same number from all elements within each row so that their sum is zero. This procedure leads to only a small modification of the original matrix W, therefore, besides one eigenvalue equal to 0, its spectrum is not affected much, and the results obtained

from random matrix theory approximate it very well. The E/I balance, however, has a drastic change on the spectrum of the entire synaptic strength matrix, making it insensitive to the presence of the deterministic part. Spectra of $M + W$ and M are exactly the same, which also means that the E/I balance cures the model by bringing outliers back to the disk.

6.3 Spectrum in the Rajan-Abbott model

The Rajan-Abbott model is easily generalized to m types of neurons, the synaptic weights of which are generated from q Gaussian distribution with μ_k mean and σ_k^2/N variance. There are $f_k N$ neurons of each type, with participations adding to one, $\sum_{k=1}^m f_k = 1$. The diagonal matrix, which rescales variances, can be written as $W = \mathrm{diag}(\sigma_1 \mathbb{1}_{f_1 N}, \ldots, \sigma_m \mathbb{1}_{f_m N})$, while the deterministic part has a dyadic structure $M = |u\rangle \langle m|$ with

$$|u\rangle = (1, \ldots, 1)^T, \qquad \langle m| = (\underbrace{\mu_1, \ldots, \mu_1}_{f_1 N \text{ times}}, \ldots, \underbrace{\mu_m, \ldots, \mu_m}_{f_m N \text{ times}}). \tag{6.3}$$

Spectral properties of the synaptic weight matrix in such a model has already been considered, and the Feynman diagram technique allows one to find spectral densities [2, 111]. Such results can be obtained in a much simpler way, because in the large N limit biunitarily invariant ensembles behave like an ideal. This means that W, which is the product of a deterministic matrix with a biunitarily invariant one, is also a subject of the Haagerup-Larsen theorem. The radial cumulative distribution function satisfies an algebraic equation [A6]

$$1 = \sum_{i=1}^m \frac{f_i \sigma_i^2}{r^2 - \sigma_i^2 (F(r) - 1)}, \tag{6.4}$$

which for $m \leqslant 4$ types of neurons can be solved analytically. The spectrum of the synaptic weight matrix is then obtained via $\rho(r) = \frac{1}{2\pi r} \frac{dF}{dr}$, since it is insensitive to the presence of the deterministic part. Eigenvector correlations are also easily accessible, $O_1(r) = \frac{F(r)(1-F(r))}{\pi r^2}$, but only of the matrix W modeling populational variability. The applicability of the Haagerup-Larsen theorem has further advantages, because it allows one to consider other types of randomness than Gaussian. The case when G represents Cauchy randomness cannot be treated with diagrammatic techniques, but it nicely fits with the Haagerup-Larsen theorem, and the spectral density with the eigenvector correlation function of W can be written explicitly [A6]

$$\rho(r) = \frac{1}{\pi} \sum_{i=1}^m \frac{f_i \sigma_i^2}{(r^2 + \sigma_i^2)^2}, \tag{6.5}$$

$$O_1(r) = \frac{1}{\pi} \sum_{i=1}^m \frac{f_i}{r^2 + \sigma_i^2} \sum_{j=1}^m \frac{f_j \sigma_j^2}{r^2 + \sigma_j^2}. \tag{6.6}$$

6.4 Eigenvector non-orthogonality in the Rajan-Abbott model

While, due to the E/I balance maintained in the model, the presence of deterministic synaptic strengths does not affect the spectrum, it strongly influences eigenvectors, in particular their non-orthogonality. Assuming that left and right eigenvectors of the matrix W with the E/I balance condition imposed are known, one can explicitly construct eigenvectors of $W + M$. In fact, left eigenvectors of W and $W + M$ are the

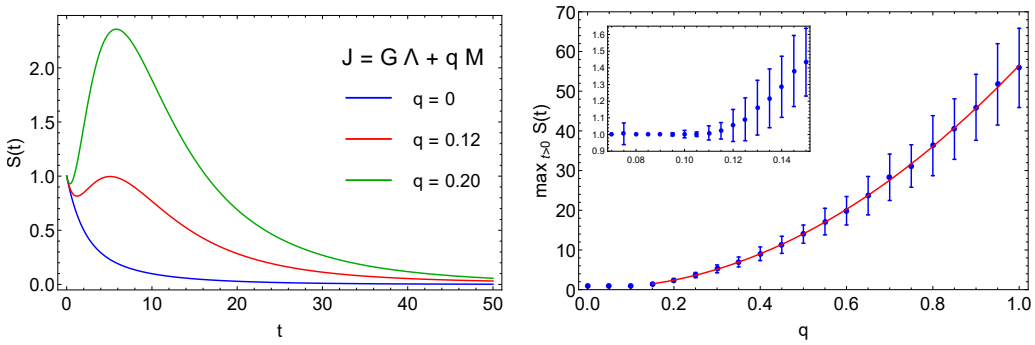

Figure 6.1: (left) Averaged squared norm in the model interpolating between the Rajan-Abbott model and the model without deterministic weights. As the interpolating parameter q grows, $S(t)$ is amplified with the maximum exceeding the initial value 1. (right) Maximum of the squared norm throughout the entire dynamics as a function of q. Inset shows a close-up for the range $0.07 < q < 0.15$, where the transition between the maximum attaining its initial value and the maximum growing quadratically with q (red line) occurs. Error bars denote standard deviation in the numerical simulations.

same and $|u\rangle$ is always a right eigenvector to the eigenvalue $\lambda_1 = 0$ because of the E/I balance. The remaining right eigenvectors are then

$$\left|R'_j\right\rangle = |R_j\rangle + \frac{\alpha_j}{\lambda_j}|u\rangle\,, \tag{6.7}$$

where $\alpha_j = \langle m|R_j\rangle$. The diagonal elements of the overlap matrix O' of $M+W$ read [A6]

$$O'_{jj} = O_{jj} + 2\,\langle L_j|L_j\rangle\,\mathrm{Re}\left(\frac{\langle m|R_j\rangle\,\langle R_j|u\rangle}{\lambda_j}\right) + N\,\langle L_j|L_j\rangle\,\frac{|\,\langle m|R_j\rangle\,|^2}{|\lambda_j|^2}. \tag{6.8}$$

By the freedom of rescaling left and right eigenvectors (see section 1.1) one can also set $\langle L_j|L_j\rangle = 1$. Diagonal elements of the overlap matrix get a contribution from the deterministic weight, and, moreover, this surplus grows linearly with the size of the matrix. The denominator in the last term shows that this effect is stronger for eigenvalues of smaller magnitude. Although the condition of the E/I balance brings outliers back to the circle saving the dynamics, it makes all eigenvalues extremely sensitive. Small changes in synaptic weights may result in a complete reshuffling of the eigenvalues.

6.5 Transient dynamics in the Rajan-Abbott model

Through the same mechanism the off-diagonal overlaps become larger, the leading contribution of which reads [A6]

$$O'_{ij} - O_{ij} \sim N\,\langle L_i|L_j\rangle\,\frac{\langle m|R_i\rangle\,\langle R_j|m\rangle}{\lambda_i\bar{\lambda}_j}. \tag{6.9}$$

Due to such a strong non-normality, reflected in the high values of all elements of the overlap matrix, we expect transient effects in the linearized dynamics. Moreover, despite the fact that the contribution to the squared norm from eigenvalues of a small magnitude is decaying faster than the one from eigenvalues close to the rightmost eigenvalue, non-normality affects such eigenvalues more. Strong coupling between eigenmodes results in the oscillatory dynamics of the squared norm, which correspond to moving back

and forth towards the fixed points. These effects can be observed for almost all initial conditions [A6]. In the absence of the deterministic matrix M, the initial conditions need to be carefully tuned for transient amplification to occur.

To quantitatively study the effects of the presence of the deterministic matrix, we consider a family of models, $J = W + qM$, where the parameter $q \in [0, 1]$ interpolates between purely random weights and the Rajan-Abbott model. The E/I balance is always imposed. We analyze the squared norm of the solution, averaged over initial conditions and over the randomness in matrix elements, $S(t)$. The oscillations average out, but above the threshold value q^* we observe the growth of the norm, as presented in Fig. 6.1. As a measure of amplification we consider the maximum attained throughout the entire process, $\max_{t \geqslant 0} S(t)$. For low values of q stays at 1, when the amplification is not strong enough to overcome the exponential damping. When the threshold value q^* is exceeded, the maximum squared norm grows quadratically with q (see Fig. 6.1), which is expected from (6.9), where the vector $|m\rangle$ appears twice.

6.6 A brief summary

In [A6] it was observed that in the model introduced by Rajan and Abbott [95] the Dale's principle and the excitatory/inhibitory balance are the source of strong non-orthogonality of eigenvectors. This phenomenon, which was not studied in previous research, leads to high sensitivity of the spectrum against changes in synaptic weights and leads to the strong transient effects in the linearized dynamics close to the fixed point.

Chapter 7

Universal spectra of input-output Jacobians in residual neural networks. Based on [A7].

7.1 What are artificial neural networks?

One of the steps towards artificial intelligence is to get machines 'understanding' the content of images from the surrounding environment. This is, definitely, too difficult a task to start with. Instead, in computer vision one considers a simplified version of this problem, namely an image is presented to a computer, which is supposed to choose a word or a sentence to describe its content. The choice is then compared to the ground truth. For a long time this type of problem posed a serious challenge to computer scientists until 2012, when deep neural networks sparked a revolution in this field [71].

Mathematically, this problem relies on finding a mapping between a collection of pixels representing an image and a set of labels describing the possible content of images. Neural networks provide a model of that mapping by the composition of simple operations realized by layers. Each layer as an entry gets a vector of numbers, which is then multiplied by a matrix of weights W, and another vector of biases b is added. Then a nonlinear function ϕ, called the activation function, is applied entry-wise to this affine transformed vector. The output x_i of the layer becomes then an input of the next layer. This set of operations can be mathematically written as a set of recursive equations

$$x_i^l = \phi(h_i^l), \quad h_i^l = \sum_{j=1}^{N} W_{ij}^l x_j^{l-1} + b_i^l. \tag{7.1}$$

We also used h to denote preactivations – the numbers to which the activations function is applied. The upper indices enumerate layers, while the lower indices enumerate elements within a layer.

There are many technical details related with practical neural networks. For example, the last layer performs classification and transforms a vector of preactivations into probabilities for each labels. Also, the number of neurons may be different for each layer, and often this is the case because the size of an image (number of pixels) is larger than the number of labels. To focus on important aspects, we neglect these subtleties and consider a simplified neural network in which all layers have the same number N of neurons, and layers perform similar operations.

7.2 Training neural networks

In neural networks, weights and biases are the adjustable parameters, and the training process relies on tuning them so that the networks perform well on the sets of training and test data. One defines an error function, which tells how bad a network is. An example of such a function is $E = \frac{1}{M}\sum_{k=1}^{M} ||x^L_{(k)} - \hat{x}_{(k)}||^2$, where k enumerates pictures in the training set, x^L is the output of the network and $\hat{x}$ is the desired output. The choice of the error function determines a landscape in the high-dimensional space of adjustable parameters, and better performing networks correspond to a lower elevation in this landscape. In each training step parameters are adjusted, so that the error function decreases the most, that is, in the direction of the steepest descent in the landscape. There are many variants of the learning algorithm devised to avoid getting stuck in bad local minima, but for simplicity we focus on a simple gradient descent algorithm. Weights in the l-th layer are incremented according to

$$\Delta W^l_{ij} = -\eta \frac{\partial E}{\partial W^l_{ij}}, \tag{7.2}$$

where the parameter η is the learning rate. Biases are updated in a similar way, but for concreteness we focus on weights only.

7.3 Problems with gradients

Using the chain rule, the derivative can be decomposed into 3 terms

$$\Delta W^l_{ij} = -\eta \sum_{k,m} \frac{\partial x^l_k}{\partial W^l_{ij}} \frac{\partial x^L_m}{\partial x^l_k} \frac{\partial E}{\partial x^L_m}. \tag{7.3}$$

The first term represents the derivative of an output of the l-th layer with respect to the weights of this layer, and the last term is the derivative of the error function with respect to the output of the last layer. For stable learning, all terms cannot be too small or too large and the middle one is the most problematic. This is a matrix of derivatives of the output of the last layer with respect to the output of the l-th layer, which reads

$$\frac{\partial x^L_j}{\partial x^l_i} = \left[\prod_{m=l+1}^{L} D^m W^m \right]_{ij}. \tag{7.4}$$

Here $D^m_{ij} = \phi'(h^m_i)\delta_{ij}$ is a diagonal matrix with a derivative of the activation function evaluated at preactivations of the m-th layer. The derivatives in (7.4) are decomposed as products of matrices, which can be more problematic, as more matrices are multiplied. One therefore considers the most extreme object – the input-output Jacobian

$$J = \prod_{m=1}^{L} D^m W^m. \tag{7.5}$$

In general, it can be a rectangular matrix, so its eigenvalues are not always defined, thus we shift our attention to the analysis of its singular values. Singular value decomposition $J = U\Sigma V^\dagger$ yields two unitary matrices and a diagonal matrix with positive entries. Columns of unitary matrices have unit norm, and thus singular values are the only objects with clearly defined magnitudes. In the analysis of deep linear networks Saxe et al. [96] found that training the neural network is the fastest when all singular values of the input-output Jacobian are equal to 1. Otherwise, the training goes in an uneven

pace – the network learns fast in directions associated with large singular values and slowly in directions associated with small singular values. This is a severe problem in deep networks, since, typically, the largest (smallest) singular value grows (decays) fast with the depth. Such an issue even makes very deep networks impossible to train, and thus it is desired to keep the singular values as close to unity as possible. In the case when all singular values are equal to 1, the network adjust its weights and biases in all directions of the parameter space at the same pace and is a phenomenon called *dynamical isometry*.

7.4 Spectral properties of the Jacobian

Training a network is a dynamical process, so besides the dataset and the choice of the learning algorithm, the network's accuracy also depends on how the network is initialized. It was empirically observed that networks pretrained on simpler tasks and taken as a starting point for more sophisticated datasets learn faster. On the other hand, networks which learn very slowly at the beginning are highly unlikely to be trained at all. It is therefore desired to find initializations of neural networks which do not hinder the training process.

In practice, neural networks are initialized at random. Weights and biases are independently sampled from some probability distribution, usually Gaussian. The distribution of preactivations h_i, which are sums of independent random numbers, approximates the Gaussian distribution, due to the central limit theorem. Therefore, the main quantity describing their behavior is variance. Glorot and Bengio [50] studied the forward propagation of the signal across the randomly initialized networks with sigmoidal nonlinearity and found that depending on the variances of weights, the variance of preactivations grows or decays exponentially with depth. This pushes preactivations to 0 or to large values. In the first regime the signal decays, while in the second regime the sigmoid function saturates. In both cases nonlinearity is insensitive to its inputs. This phenomenon prevents efficient training of deep networks. Glorot and Bengio proposed an initialization scheme that poses the network in the 'sweet spot' where the variance stays approximately constant across depth. This choice of initialization significantly decreases the time needed to train the networks. Later, a similar analysis was performed for the rectified linear unit (ReLU) as an activation function, where it was proposed to initialize weights from a Gaussian distribution of variance $\frac{2}{N}$ [57].

Stabilization of the variance of forwardly propagated signal is not sufficient to stabilize the backwardly propagated gradients, as the latter form a matrix, while the former is a single number. Poole et al. [92] studied backpropagation by means of the layer-to-layer Jacobian, $\frac{\partial x_k^{l+1}}{\partial x_i^l}$. The analysis of the second moment of its singular value density led them to the discovery of a transition between regimes of exploding and vanishing gradients. Since the parameters are initialized as Gaussian, only variances of weights σ_W^2 and biases σ_b^2 are relevant, and the phase portrait is two-dimensional. The condition that the mean squared singular value is located at 1 separates these two regimes. Choosing the initialization parameters in order to stay at the critical line indeed significantly speeds up learning.

Demanding that the mean of the distribution of the layer-to-layer Jacobian is, though, quite a weak condition, because it only prevents exponential growth or decay of the mean of the input-output Jacobian. It may happen that, when adding more layers to the network, small singular values become smaller, and large singular values grow even more, with the mean singular value remaining constant. Pennington, Shoenholz and Ganguli [89] studied also the full distribution of squared singular values of the input-output Jacobian with special emphasis on the location of the right edge of the

spectrum. They found that for Gaussian weights it is not possible to achieve dynamical isometry at any depth of the network. However, if the weight matrices are chosen as scaled orthogonal matrices, that is $WW^T = \sigma_w^2 \mathbb{1}$, and sigmoidal nonlinearity is used, the spectrum concentrates around 1, and the network is close to perfect dynamical isometry. Such a situation cannot be realized for the ReLU activation function.

7.5 Residual networks

A couple years before introducing the concept of dynamical isometry and discovering its role in the trainability of deep neural networks, scientists have found a way to train networks with more than one hundred layers [56]. It became possible with introducing a novel architecture, which relies on skip connections. In standard feedforward networks described in previous sections, at each layer the signal undergoes affine transformation followed by the element-wise evaluation of the nonlinear activation function. Skip connections bypass one or more layers directly sending the original signal. In the simplest setting, where each layer is equipped with skip connections, the signal is propagated according to the recursion

$$x_i^l = x_i^{l-1} + \phi(h_i^l), \quad h_i^l = b_i^l + \sum_{j=1}^{N} W_{ij}^l x_j^{l-1}, \tag{7.6}$$

which differs from (7.1) by a single term. This changes also the form of the input-output Jacobian, which now reads

$$J = \prod_{l=1}^{L} (\mathbb{1} + D^l W^l). \tag{7.7}$$

It was also observed that, in order to maintain stable forward signal propagation, such an architecture requires different normalization of weights [9, 101]. Their variance needs to be rescaled both by the width N and the depth L of the network.

7.6 Spectra of Jacobians in residual networks

The formalism presented in chapter 2, upon tiny modifications, allows one to deduce the distribution of singular values of Jacobians in residual architecture.

Let us define the layer-to-layer Jacobian as $Y_l = (\mathbb{1} + D^l W^l)$ and the Jacobian between output of the L-th layer to the input as J_L. Then, $J_L J_L^T = Y_L J_{L-1} J_{L-1}^T Y_L^T$, which has the same spectrum as $Y_L^T Y_L J_{L-1} J_{L-1}^T$. For large random matrices, their S-transforms are multiplicative, that is $S_{JJ^T}(z) = S_{Y_L^T Y_L}(z) S_{J_{L-1} J_{L-1}^T}(z)$. Decomposing recursively, one immediately obtains the factorization in terms of S-transforms [23]

$$S_{J_L J_L^T}(z) = \prod_{l=1}^{L} S_{Y_L^T Y_L}(z), \tag{7.8}$$

despite the fact that $J_L J_L^T$ does not factorize. This reduces the problem to the calculation of squared singular values of the layer-to-layer Jacobian and the associated S-transform. Let us introduce two block matrices [A7]

$$\mathcal{Z} = \begin{pmatrix} -1 & 1 \\ z & -1 \end{pmatrix}, \quad \mathcal{X} = \begin{pmatrix} X & 0 \\ 0 & X^T \end{pmatrix}, \tag{7.9}$$

with $X = D^l W^l$. They are used for constructing the generalized Green's function

$$\mathcal{G} = \begin{pmatrix} G_{11} & G_{12} \\ G_{21} & G_{22} \end{pmatrix} = \left\langle \frac{1}{N} \mathrm{bTr}(\mathcal{Z} \otimes \mathbb{1} - \mathcal{X})^{-1} \right\rangle = \left\langle \frac{1}{N} \mathrm{bTr} \begin{pmatrix} -\mathbb{1} - X & \mathbb{1} \\ z\mathbb{1} & -\mathbb{1} - X^T \end{pmatrix}^{-1} \right\rangle. \tag{7.10}$$

The G_{12} entry is precisely the Green's function of $Y_l Y_l^T$:

$$G_{12} = \left\langle \frac{1}{N} \mathrm{Tr}(z\mathbb{1} - Y_l Y_l^T)^{-1} \right\rangle = G(z). \tag{7.11}$$

The generalized Green's function defined this way is not a quaternion, but solely because of its symmetries. The diagrammatic formalism presented in chapter 2 works in the same way. If the weight matrix W is biunitarily invariant, which includes the cases of Gaussian and scaled orthogonal matrices, its product with an arbitrary matrix is also the subject of the Haagerup-Larsen theorem. This leads to the functional equation for the Green's function [A7]

$$G = \frac{GA(zG^2) - 1}{1 - z(1 - GA(zG^2))^2}. \tag{7.12}$$

Using formulas (2.11) and (2.12), the above can be transformed into the equation for the S transform. When the additional $1/\sqrt{L}$ rescaling proposed for residual networks is taken into account, the S transform can be expanded [A7]

$$S_{Y_l Y_l^T}(z) = 1 - \frac{c_2^l}{L}(1 + 2z) + \mathcal{O}(L^{-2}). \tag{7.13}$$

Here

$$c_2^l = \left\langle \frac{1}{N} \mathrm{Tr} X X^\dagger \right\rangle = \frac{\sigma_w^2}{N} \sum_{i=1}^{N} \left(\phi'(h_i^l) \right)^2 \tag{7.14}$$

is the second cumulant of X, which is also the spectral radius of the matrix $D^l W^l$. Assuming that c_2^l does not vary much across the depth, the logarithm of the S transform of the input-output Jacobian reads

$$\ln S_{JJ^T}(z) = -(1 + 2z)c + \mathcal{O}(L^{-1}), \tag{7.15}$$

where $c = \frac{1}{L} \sum_{k=1}^{L} c_2^l$. In the large L limit the subleading terms can neglected, and thus the S transform takes the form of an exponent. The Green's function of the input-output Jacobian satisfies the transcendental equation [A7]

$$G(z) = (zG(z) - 1)e^{c(1 - 2zG(z))}, \tag{7.16}$$

which formally is solved by the Lambert W function, but in practice it is solved numerically to obtain the singular value density.

In general, the spectrum depends on weights and the activation function, which in turn determine the forward propagation, but the above calculations show that this entire dependence is encapsulated in a single parameter c. Moreover, a direct evaluation of the spectral density shows that the singular values of the Jacobian concentrate around 1 for small values of c (see Fig. 7.1). Hence, residual neural networks are close to the dynamical isometry, provided that the variance of weights is proportional to $\frac{1}{NL}$. Note that the spectrum concentration holds both for Gaussian and scaled orthogonal weights, regardless of the activation function used. Contrary to the feedforward architecture, one does not need to fine-tune the parameters of the networks to ensure its trainability.

In order to relate the parameter c with parameters of neural networks, one needs to know how the signal propagates across the network. It was already argued that the preactivations are Gaussian, so we denote by q^l their variance in the l-th layer. Then

$$c_2^l = \sigma_W^2 \int_{-\infty}^{+\infty} \mathcal{D}z \phi'^2 \left(z\sqrt{q^l} \right), \tag{7.17}$$

where we denoted the Gaussian measure by $\mathcal{D}z = \frac{dz}{\sqrt{2\pi}} e^{-z^2/2}$. An analysis of the signal propagation shows that variances satisfy the recurrence [A7]

$$q^{l+1} = q^l + \frac{\sigma_W^2}{L} \int_{-\infty}^{\infty} \mathcal{D}z \phi^2(z\sqrt{q^l}) + 2\frac{(\sigma_W)^2}{L} \left[\sum_{k=1}^{l-1} \int_{-\infty}^{\infty} \mathcal{D}z \phi(z\sqrt{q^{l-k}}) \right] \int_{-\infty}^{\infty} \mathcal{D}z \phi(z\sqrt{q^l}), \tag{7.18}$$

with the initial condition $q^1 = \sigma_b^2 + \frac{\sigma_W^2}{L}$. Note that the last term vanishes for antisymmetric activation functions, such as hyperbolic tangent.

7.7 Numerical experiments

To test the predictions of the theory, we used the CIFAR-10 dataset [70], which is one of popular benchmarks in image classification. It consists of 60000 color images of size 32×32 pixels. There are 10 classes of images in this dataset. We used the residual architecture, with $L = 10$ and $L = 20$ layers and with an additional classification layer at the end. The following activation functions were considered: ReLU ($\phi(x) = x$ for $x > 0$ and $\phi(x) = 0$ for $x < 0$) [83], hyperbolic tangent, Hard Tanh ($\phi(x) = x$ for $|x| < 1$ and $\phi(x) = \text{sign}(x)$ otherwise), sigmoid ($\phi(x) = \frac{1}{1+e^{-x}}$), Leaky ReLU ($\phi(x) = x$ for $x > 0$ and $\phi(x) = \alpha x$ for $x < 0$) with the leaking constant $\alpha = 0.05$ and 0.25, and Scaled Exponential Linear Unit (SELU) [67].

In the first experiment, all weights are initialized as Gaussian with zero mean and variance $\frac{\sigma_W}{\sqrt{NL}}$, while biases are set to zero. For a given activation function and the number of blocks L we set σ_W in such a way that, upon solving the recurrence (7.18) numerically, the parameter c is equal to 0.125, in order to ensure the concentration of the spectrum. Then, an image from the dataset is directed as an input to the network. The signal is propagated, and, finally, the input-output Jacobian of residual blocks (the classification layer is neglected) is calculated. The spectra of Jacobians, as presented in Fig. 7.1, coalesce, and the theoretical predictions describe the empirical Jacobian very well. This validates the prediction of the theory that a single parameter c determines the shape of the spectrum. Remarkably, despite the fact that the formula (7.16) was derived in the limit $L \to \infty$, it works also for relatively small values $L = 10$.

The theoretical considerations were focused on the Jacobian at the initialization. We hypothesize that the universality in the spectra of Jacobians is also reflected in the early stages of learning. To verify this claim, we trained networks for 200 epochs and observed the accuracy of the network, measured as a fraction of correctly classified images. Networks were initialized like in the previous experiment. We observe that the learning curves follow the same trajectory for almost all activation functions. Only the sigmoid detaches with much worse accuracy. This is caused by the instability of the forward signal propagation, resulting in a saturation of the nonlinearity. To further investigate the effect of the Jacobian universality, we considered a different initialization scheme in which variances of weights were set to be $\frac{1}{\sqrt{NL}}$, irrespective of the activation function. In such a case the curves detach at the very beginning of the learning process [A7], confirming the importance of initialization in the learning dynamics.

In many experiments the initialization of the network is a confounding factor. Our second numerical experiments shows that this factor can be eliminated by appropriately

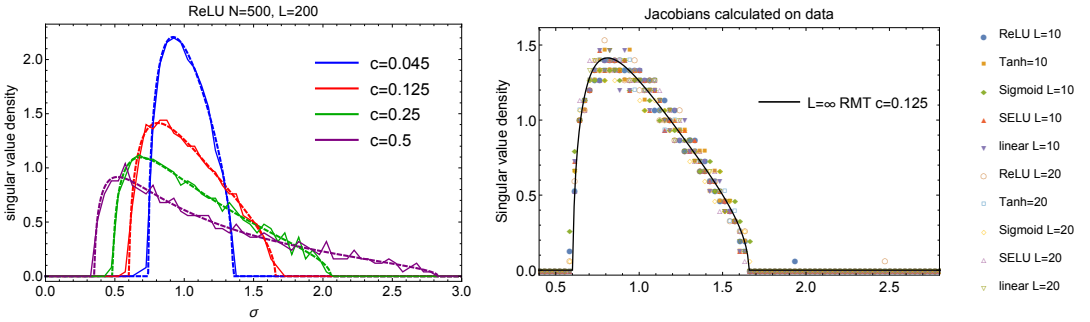

Figure 7.1: (left) Singular value densities of the input-output Jacobians for several values of the parameter c. Solid lines represent numerical simulations, while the dashed lines are obtained by numerically obtaining the density from (7.16). One sees that singular values concentrate around 1 for small values of c. (right) Distribution of singular values of the input-output Jacobian evaluated on the data from CIFAR10. The parameters of the network were chosen in such a way that $c = 0.125$. Distributions for all activation functions are described by the same curve (solid line).

initializing networks. Then, other effects than the input-output Jacobians can be studied, as it was already observed that the sigmoid activation function follows completely different learning trajectory.

7.8 A brief summary

The work [A7] uses the formalism developed in [A2] to describe the spectra of input-output Jacobians. It is shown that, after the rescaling of weights by the square root of the depth of a network, singular values concentrate around 1 and the network is close to the dynamical isometry. This phenomenon explains why the residual architecture makes deep networks easier to train. Theoretical predictions are then verified in numerical experiments.

Summary of the thesis

This thesis presents studies of properties of non-orthogonal eigenvectors of random matrices. First, the one- and two-point eigenvector correlation functions are studied in the large N limit for unitarily invariant ensembles by means of Feynman diagrams. Then, the joint density of the diagonal overlap O_{ii} and the associated real eigenvalue in the real elliptic ensemble is studied. It is also observed that the mathematical structure resembling left and right eigenvectors appears in biorthogonal ensembles, which opens a way for immediate calculations of the universal microscopic correlations of eigenvalues.

The main results are:

- The relation (2.26) between the one-point function and the conditional expectation of the squared eigenvalue condition number controlling the stability of eigenvalues.
- The relation (2.29) determining the one-point function for the biunitarily invariant ensembles in terms of the spectral density. It can considered as the generalization of the Haagerup-Larsen theorem [54] from functional analysis.
- The formalism of Bethe-Salpeter equations (3.18) and (3.19) for finding the two-point function for unitarily invariant ensembles with its special case (3.23) for biunitarily invariant ensembles.
- Finite N formula (4.5) with the study of its asymptotic regimes (4.10), (4.11) and (4.12), with the discovery of the *weak non-normality* regime.
- The extension of the spectral projection method to the biorthogonal ensembles, allowing for calculations of microscopic universalities in a new way.

The theoretical developments are then applied to theoretical neuroscience and machine learning.

It is shown that in the Rajan-Abbott model of a neural network the proposed Dale's principle combined with the excitatory/inhibitory balance leads to strong non-orthogonality of eigenvectors of the weight matrix, which in turn causes high sensitivity of the network to the changes in weights, and strong transient effects in the linearized dynamics close to the fixed point.

The distribution of the squared singular values of the input-output Jacobian in residual neural networks is analyzed. It is shown that, after appropriate rescaling of weights, this distribution is universal, depends only on a single parameter, and, more importantly, concentrates around one. The network is then close to the *dynamical isometry*. This phenomenon explains why this specific architecture allows one to effectively train very deep networks.

Bibliography

[1] Adel Y Abul-Magd, *Modelling gap-size distribution of parked cars using random-matrix theory*, Physica A: Statistical Mechanics and its Applications 368 (2), 536–540 (2006).

[2] Yashar Ahmadian, Francesco Fumarola, and Kenneth D Miller, *Properties of networks with partially structured and partially random connectivity*, Physical Review E 91 (1), 012820 (2015).

[3] Gernot Akemann, Poul Henrik Damgaard, Kim Splittorff, and Jacobus JM Verbaarschot, *Spectrum of the Wilson Dirac operator at finite lattice spacings*, Physical Review D 83 (8), 085014 (2011).

[4] Gernot Akemann, Jesper R Ipsen, and Mario Kieburg, *Products of rectangular random matrices: singular values and progressive scattering*, Physical Review E 88 (5), 052118 (2013).

[5] Gernot Akemann, Mario Kieburg, and Lu Wei, *Singular value correlation functions for products of Wishart random matrices*, Journal of Physics A: Mathematical and Theoretical 46 (27), 275205 (2013).

[6] Gernot Akemann, Roger Tribe, Athanasios Tsareas, and Oleg Zaboronski, *On the determinantal structure of conditional overlaps for the complex Ginibre ensemble*, Random Matrices: Theory and Applications (Online ready Jul 2019). URL: `https://doi.org/10.1142/S201032632050015X`.

[7] Gernot Akemann and Graziano Vernizzi, *Characteristic polynomials of complex random matrix models*, Nuclear Physics B 660 (3), 532–556 (2003).

[8] Jinho Baik, Percy Deift, and Eugene Strahov, *Products and ratios of characteristic polynomials of random Hermitian matrices*, Journal of Mathematical Physics 44 (8), 3657–3670 (2003).

[9] David Balduzzi, Marcus Frean, Lennox Leary, John P Lewis, Kurt Wan-Duo Ma, and Brian McWilliams, *The shattered gradients problem: If resnets are the answer, then what is the question?*, in: Proceedings of the 34th International Conference on Machine Learning, 2017, 342–350.

[10] Serban T Belinschi, Piotr Śniady, and Roland Speicher, *Eigenvalues of non-Hermitian random matrices and Brown measure of non-normal operators: Hermitian reduction and linearization method*, Linear Algebra and its Applications 537, 48–83 (2018).

[11] Carl M Bender, Dorje C Brody, and Markus P Müller, *Hamiltonian for the zeros of the Riemann zeta function*, Physical Review Letters 118 (13), 130201 (2017).

[12] Marco Bertola and Thomas Bothner, *Universality conjecture and results for a model of several coupled positive-definite matrices*, Communications in Mathematical Physics 337 (3), 1077–1141 (2015).

[13] Marco Bertola, Michael Gekhtman, and Jacek Szmigielski, *The Cauchy two-matrix model*, Communications in Mathematical Physics 287 (3), 983–1014 (2009).

[14] Christoly Biely and Stefan Thurner, *Random matrix ensembles of time-lagged correlation matrices: derivation of eigenvalue spectra and analysis of financial time-series*, Quantitative Finance 8 (7), 705–722 (2008).

[15] Oriol Bohigas, Marie-Joya Giannoni, and Charles Schmit, *Characterization of chaotic quantum spectra and universality of level fluctuation laws*, Physical Review Letters 52 (1), 1 (1984).

[16] Folkmar Bornemann, *On the scaling limits of determinantal point processes with kernels induced by Sturm-Liouville operators*, SIGMA. Symmetry, Integrability and Geometry: Methods and Applications 12, 083 (2016).

[17] Alexei Borodin, *Biorthogonal ensembles*, Nuclear Physics B 536 (3), 704–732 (1998).

[18] Alexei Borodin and Grigori Olshanski, *Asymptotics of Plancherel-type random partitions*, Journal of Algebra 313 (1), 40–60 (2007).

[19] Paul Bourgade and Guillaume Dubach, *The distribution of overlaps between eigenvectors of Ginibre matrices*, Probability Theory and Related Fields, 1–68 (2019).

[20] Zdzisław Burda, Jacek Grela, Maciej A Nowak, Wojciech Tarnowski, and Piotr Warchoł, *Dysonian dynamics of the Ginibre ensemble*, Physical Review Letters 113 (10), 104102 (2014).

[21] Zdzisław Burda, Jacek Grela, Maciej A Nowak, Wojciech Tarnowski, and Piotr Warchoł, *Unveiling the significance of eigenvectors in diffusing non-Hermitian matrices by identifying the underlying Burgers dynamics*, Nuclear Physics B 897, 421–447 (2015).

[22] Zdzisław Burda, Andrzej Jarosz, Giacomo Livan, Maciej A Nowak, and Artur Święch, *Eigenvalues and singular values of products of rectangular Gaussian random matrices*, Physical Review E 82 (6), 061114 (2010).

[23] Zdzisław Burda, Maciej A Nowak, and Artur Święch, *Spectral relations between products and powers of isotropic random matrices*, Physical Review E 86 (6), 061137 (2012).

[24] Zdzisław Burda, Bartłomiej J Spisak, and Pierpaolo Vivo, *Eigenvector statistics of the product of Ginibre matrices*, Physical Review E 95 (2), 022134 (2017).

[25] John T Chalker and Bernhard Mehlig, *Eigenvector statistics in non-Hermitian random matrix ensembles*, Physical Review Letters 81 (16), 3367 (1998).

[26] Nicholas Crawford and Ron Rosenthal, *Eigenvector correlations in the complex Ginibre ensemble*, arXiv preprint arXiv:1805.08993 (2018).

[27] Guillaume Dubach, *On eigenvector statistics in the spherical and truncated unitary ensembles*, arXiv preprint arXiv:1908.06713 (2019).

[28] Guillaume Dubach, *Symmetries of the quaternionic Ginibre ensemble*, Random Matrices: Theory and Applications (Online ready Jan 2020). URL: `https://doi.org/10.1142/S2010326321500131`.

[29] Maurice Duits and Arno BJ Kuijlaars, *Universality in the two-matrix model: a Riemann-Hilbert steepest-descent analysis*, Communications on Pure and Applied Mathematics 62 (8), 1076–1153 (2009).

[30] Freeman J Dyson, *A Brownian-motion model for the eigenvalues of a random matrix*, Journal of Mathematical Physics 3 (6), 1191–1198 (1962).

[31] Joshua Feinberg, Richard Scalettar, and Anthony Zee, *"Single ring theorem" and the disk-annulus phase transition*, Journal of Mathematical Physics 42 (12), 5718–5740 (2001).

[32] Joshua Feinberg and Anthony Zee, *Non-Gaussian non-Hermitian random matrix theory: phase transition and addition formalism*, Nuclear Physics B 501 (3), 643–669 (1997).

[33] Joshua Feinberg and Anthony Zee, *Non-hermitian random matrix theory: Method of hermitian reduction*, Nuclear Physics B 504 (3), 579–608 (1997).

[34] Peter J Forrester, *Log-gases and random matrices*, Princeton University Press, 2010.

[35] Peter J Forrester and Mario Kieburg, *Relating the Bures measure to the Cauchy two-matrix model*, Communications in Mathematical Physics 342 (1), 151–187 (2016).

[36] Peter J Forrester and Nicholas S Witte, *Exact Wigner surmise type evaluation of the spacing distribution in the bulk of the scaled random matrix ensembles*, Letters in Mathematical Physics 53 (3), 195–200 (2000).

[37] Klaus M Frahm, Henning Schomerus, Michael Patra, and Carlo WJ Beenakker, *Large Petermann factor in chaotic cavities with many scattering channels*, Europhysics Letters 49 (1), 48 (2000).

[38] Yan V Fyodorov, *Negative moments of characteristic polynomials of random matrices: Ingham–Siegel integral as an alternative to Hubbard–Stratonovich transformation*, Nuclear Physics B 621 (3), 643–674 (2002).

[39] Yan V Fyodorov, *On statistics of bi-orthogonal eigenvectors in real and complex ginibre ensembles: combining partial schur decomposition with supersymmetry*, Communications in Mathematical Physics 363 (2), 579–603 (2018).

[40] Yan V Fyodorov, Boris A Khoruzhenko, and Hans-Jürgen Sommers, *Almost Hermitian random matrices: crossover from Wigner-Dyson to Ginibre eigenvalue statistics*, Physical Review Letters 79 (4), 557 (1997).

[41] Yan V Fyodorov and Bernhard Mehlig, *Statistics of resonances and nonorthogonal eigenfunctions in a model for single-channel chaotic scattering*, Physical Review E 66 (4), 045202 (2002).

[42] Yan V Fyodorov and Alexander D Mirlin, *Statistical properties of eigenfunctions of random quasi 1d one-particle Hamiltonians*, International Journal of Modern Physics B 8 (27), 3795–3842 (1994).

[43] Yan V Fyodorov and Dmitry V Savin, *Statistics of resonance width shifts as a signature of eigenfunction nonorthogonality*, Physical Review Letters 108 (18), 184101 (2012).

[44] Yan V Fyodorov, Hans-Jürgen Sommers, and Boris A Khoruzhenko, *Universality in the random matrix spectra in the regime of weak non-Hermiticity*, Annales de l'IHP Physique théorique 68 (4), 449–489 (1998).

[45] Yan V Fyodorov and Eugene Strahov, *Characteristic polynomials of random Hermitian matrices and Duistermaat–Heckman localisation on non-compact Kähler manifolds*, Nuclear Physics B 630 (3), 453–491 (2002).

[46] Surya Ganguli, Dongsung Huh, and Haim Sompolinsky, *Memory traces in dynamical systems*, Proceedings of the National Academy of Sciences 105 (48), 18970–18975 (2008).

[47] Michel Gaudin, *Sur la loi limite de l'espacement des valeurs propres d'une matrice aléatoire*, Nuclear Physics 25, 447–458 (1961).

[48] Jean Ginibre, *Statistical ensembles of complex, quaternion, and real matrices*, Journal of Mathematical Physics 6 (3), 440–449 (1965).

[49] Vyacheslav L Girko, *Elliptic law*, Theory of Probability & Its Applications 30 (4), 677–690 (1986).

[50] Xavier Glorot and Yoshua Bengio, *Understanding the difficulty of training deep feedforward neural networks*, in: Proceedings of the 13th International Conference on Artificial Intelligence and Statistics (AISTATS), 2010, 249–256.

[51] Mark S Goldman, *Memory without feedback in a neural network*, Neuron 61 (4), 621–634 (2009).

[52] Jacek Grela and Piotr Warchoł, *Full Dysonian dynamics of the complex Ginibre ensemble*, Journal of Physics A: Mathematical and Theoretical 51 (42), 425203 (2018).

[53] Jean-Baptiste Gros, Ulrich Kuhl, Olivier Legrand, Fabrice Mortessagne, Elodie Richalot, and Dimitry V Savin, *Experimental width shift distribution: a test of nonorthogonality for local and global perturbations*, Physical Review Letters 113 (22), 224101 (2014).

[54] Uffe Haagerup and Flemming Larsen, *Brown's Spectral Distribution Measure for R-Diagonal Elements in Finite von Neumann Algebras*, Journal of Functional Analysis 176 (2), 331–367 (2000).

[55] Bilal Haider, Alvaro Duque, Andrea R Hasenstaub, and David A McCormick, *Neocortical network activity in vivo is generated through a dynamic balance of excitation and inhibition*, Journal of Neuroscience 26 (17), 4535–4545 (2006).

[56] Kaiming He, Xiangyu Zhang, Shaoqing Ren, and Jian Sun, *Deep residual learning for image recognition*, in: Proceedings of the IEEE conference on computer vision and pattern recognition, 2016, 770–778.

[57] Kaiming He, Xiangyu Zhang, Shaoqing Ren, and Jian Sun, *Delving deep into rectifiers: Surpassing human-level performance on imagenet classification*, in: Proceedings of the IEEE international conference on computer vision, 2015, 1026–1034.

[58] Guillaume Hennequin, Tim P Vogels, and Wulfram Gerstner, *Non-normal amplification in random balanced neuronal networks*, Physical Review E 86 (1), 011909 (2012).

[59] Guillaume Hennequin, Tim P Vogels, and Wulfram Gerstner, *Optimal control of transient dynamics in balanced networks supports generation of complex movements*, Neuron 82 (6), 1394–1406 (2014).

[60] Michael J Higley and Diego Contreras, *Balanced excitation and inhibition determine spike timing during frequency adaptation*, Journal of Neuroscience 26 (2), 448–457 (2006).

[61] Aukosh Jagannath and Thomas Trogdon, *Random matrices and the New York City subway system*, Physical Review E 96 (3), 030101 (2017).

[62] Romuald A Janik, Wolfgang Nörenberg, Maciej A Nowak, Gábor Papp, and Ismail Zahed, *Correlations of eigenvectors for non-Hermitian random-matrix models*, Physical Review E 60 (3), 2699 (1999).

[63] Romuald A Janik, Maciej A Nowak, Gábor Papp, and Ismail Zahed, *Non-hermitian random matrix models*, Nuclear Physics B 501 (3), 603–642 (1997).

[64] Andrzej Jarosz and Maciej A Nowak, *Random Hermitian versus random non-Hermitian operators—unexpected links*, Journal of Physics A: Mathematical and General 39 (32), 10107 (2006).

[65] Michio Jimbo, Tetsuji Miwa, Yasuko Môri, and Mikio Sato, *Density matrix of an impenetrable Bose gas and the fifth Painlevé transcendent*, Physica D: Nonlinear Phenomena 1 (1), 80–158 (1980).

[66] Mario Kieburg, Arno BJ Kuijlaars, and Dries Stivigny, *Singular value statistics of matrix products with truncated unitary matrices*, International Mathematics Research Notices 2016 (11), 3392–3424 (2016).

[67] Günter Klambauer, Thomas Unterthiner, Andreas Mayr, and Sepp Hochreiter, *Self-normalizing neural networks*, in: Advances in neural information processing systems, 2017, 971–980.

[68] Milan Krbálek and Petr Seba, *The statistical properties of the city transport in Cuernavaca (Mexico) and random matrix ensembles*, Journal of Physics A: Mathematical and General 33 (26), L229 (2000).

[69] Manjunath Krishnapur, *Zeros of random analytic functions*, Ph.D. thesis, U.C. Berkeley (2006). Preprint available at arXiv:math/0607504v1 [math.PR].

[70] Alex Krizhevsky, *Learning multiple layers of features from tiny images*, Technical report. University of Toronto. 2009. URL: `https://www.cs.toronto.edu/~kriz/learning-features-2009-TR.pdf`.

[71] Alex Krizhevsky, Ilya Sutskever, and Geoffrey E Hinton, *Imagenet classification with deep convolutional neural networks*, in: Advances in neural information processing systems, 2012, 1097–1105.

[72] Florent Krzakala, Cristopher Moore, Elchanan Mossel, Joe Neeman, Allan Sly, Lenka Zdeborová, and Pan Zhang, *Spectral redemption in clustering sparse networks*, Proceedings of the National Academy of Sciences 110 (52), 20935–20940 (2013).

[73] Arno BJ Kuijlaars and Dries Stivigny, *Singular values of products of random matrices and polynomial ensembles*, Random Matrices: Theory and Applications 3 (03), 1450011 (2014).

[74] Marek Kuś, Jan Mostowski, and Fritz Haake, *Universality of eigenvector statistics of kicked tops of different symmetries*, Journal of Physics A: Mathematical and General 21 (22), L1073 (1988).

[75] Jarosław Kwapień, Stanisław Drożdż, Andrzej Z Górski, and Paweł Oświęcimka, *Asymmetric matrices in an analysis of financial correlations*, Acta Physica Pol. B 36 (11), 3039–3048 (2006).

[76] Vladimir A Marčenko and Leonid A Pastur, *Distribution of eigenvalues for some sets of random matrices*, Mathematics of the USSR-Sbornik 1 (4), 457 (1967).

[77] Bernhard Mehlig and John T Chalker, *Statistical properties of eigenvectors in non-Hermitian Gaussian random matrix ensembles*, Journal of Mathematical Physics 41 (5), 3233–3256 (2000).

[78] Bernhard Mehlig and Melvin Santer, *Universal eigenvector statistics in a quantum scattering ensemble*, Physical Review E 63 (2), 020105 (2001).

[79] Madan Lal Mehta, *Random matrices*, Elsevier, 2004.

[80] Alexander D Mirlin, *Statistics of energy levels and eigenfunctions in disordered systems*, Physics Reports 326 (5-6), 259–382 (2000).

[81] Brendan K Murphy and Kenneth D Miller, *Balanced amplification: a new mechanism of selective amplification of neural activity patterns*, Neuron 61 (4), 635–648 (2009).

[82] Khandker A Muttalib, *Random matrix models with additional interactions*, Journal of Physics A: Mathematical and General 28 (5), L159 (1995).

[83] Vinod Nair and Geoffrey E Hinton, *Rectified linear units improve restricted Boltzmann machines*, in: Proceedings of the 27th International Conference on Machine Learning, 2010.

[84] Roop Narain, *The G-Functions as Unsymmetrical Fourier Kernels. I*, Proceedings of the American Mathematical Society 13 (6), 950–959 (1962).

[85] Mark EJ Newman, *Finding community structure in networks using the eigenvectors of matrices*, Physical review E 74 (3), 036104 (2006).

[86] Maciej A Nowak and Wojciech Tarnowski, *Spectra of large time-lagged correlation matrices from random matrix theory*, Journal of Statistical Mechanics: Theory and Experiment 2017 (6), 063405 (2017).

[87] Andrew M Odlyzko, *On the distribution of spacings between zeros of the zeta function*, Mathematics of Computation 48 (177), 273–308 (1987).

[88] Michael Patra, Henning Schomerus, and Carlo WJ Beenakker, *Quantum-limited linewidth of a chaotic laser cavity*, Physical Review A 61 (2), 023810 (2000).

[89] Jeffrey Pennington, Samuel Schoenholz, and Surya Ganguli, *Resurrecting the sigmoid in deep learning through dynamical isometry: theory and practice*, in: Advances in neural information processing systems, 2017, 4785–4795.

[90] Klaus Petermann, *Calculated spontaneous emission factor for double-heterostructure injection lasers with gain-induced waveguiding*, IEEE Journal of Quantum Electronics 15 (7), 566–570 (1979).

[91] Vasiliki Plerou, Parameswaran Gopikrishnan, Bernd Rosenow, Luis A Nunes Amaral, Thomas Guhr, and H Eugene Stanley, *Random matrix approach to cross correlations in financial data*, Physical Review E 65 (6), 066126 (2002).

[92] Ben Poole, Subhaneil Lahiri, Maithra Raghu, Jascha Sohl-Dickstein, and Surya Ganguli, *Exponential expressivity in deep neural networks through transient chaos*, in: Advances in neural information processing systems, 2016, 3360–3368.

[93] Charles E Porter, *Statistical theories of spectra: fluctuations*, Academic, New York, 1965.

[94] Alex Pothen, Horst D Simon, and Kang-Pu Liou, *Partitioning sparse matrices with eigenvectors of graphs*, SIAM journal on matrix analysis and applications 11 (3), 430–452 (1990).

[95] Kanaka Rajan and Larry F Abbott, *Eigenvalue spectra of random matrices for neural networks*, Physical Review Letters 97 (18), 188104 (2006).

[96] Andrew M Saxe, James L McClelland, and Surya Ganguli, *Exact solutions to the nonlinear dynamics of learning in deep linear neural networks*, in: Proceedings of the International Conference on Learning Representations (ICLR) 2014,

[97] Henning Schomerus, Klaus M Frahm, Michael Patra, and Caarlo WJ Beenakker, *Quantum limit of the laser line width in chaotic cavities and statistics of residues of scattering matrix poles*, Physica A: Statistical Mechanics and its Applications 278 (3-4), 469–496 (2000).

[98] Michael N Shadlen and William T Newsome, *Noise, neural codes and cortical organization*, Current opinion in neurobiology 4 (4), 569–579 (1994).

[99] Jianbo Shi and Jitendra Malik, *Normalized cuts and image segmentation*, IEEE Transactions on pattern analysis and machine intelligence 22 (8), 888–905 (2000).

[100] Haim Sompolinsky, Andrea Crisanti, and Hans-Jurgen Sommers, *Chaos in random neural networks*, Physical Review Letters 61 (3), 259 (1988).

[101] Masato Taki, *Deep residual networks and weight initialization*, arXiv preprint arXiv:1709.02956 (2017).

[102] Terence Tao, Van Vu, and Manjunath Krishnapur, *Random matrices: Universality of ESDs and the circular law*, The Annals of Probability 38 (5), 2023–2065 (2010).

[103] Todd W Troyer and Kenneth D Miller, *Physiological gain leads to high ISI variability in a simple model of a cortical regular spiking cell*, Neural computation 9 (5), 971–983 (1997).

[104] Dan Voiculescu, *Limit laws for random matrices and free products*, Inventiones mathematicae 104 (1), 201–220 (1991).

[105] Dan Voiculescu, *Symmetries of some reduced free product C*-algebras*, in: Operator algebras and their connections with topology and ergodic theory, Springer, 1985, 556–588.

[106] Dan V Voiculescu, Ken J Dykema, and Alexandru Nica, *Free random variables*, CRM monograph series. American Mathematical Society, 1992.

[107] Ulrike Von Luxburg, *A tutorial on spectral clustering*, Statistics and computing 17 (4), 395–416 (2007).

[108] Gilles Wainrib and Jonathan Touboul, *Topological and dynamical complexity of random neural networks*, Physical Review Letters 110 (11), 118101 (2013).

[109] Meg Walters and Shannon Starr, *A note on mixed matrix moments for the complex Ginibre ensemble*, Journal of Mathematical Physics 56 (1), 013301 (2015).

[110] Michael Wehr and Anthony M Zador, *Balanced inhibition underlies tuning and sharpens spike timing in auditory cortex*, Nature 426 (6965), 442–446 (2003).

[111] Yi Wei, *Eigenvalue spectra of asymmetric random matrices for multicomponent neural networks*, Physical Review E 85 (6), 066116 (2012).

[112] James Hardy Wilkinson, *The algebraic eigenvalue problem*, vol. 662. Oxford Clarendon, 1965.

[113] Karol Życzkowski and Hans-Jürgen Sommers, *Truncations of random unitary matrices*, Journal of Physics A: Mathematical and General 33 (10), 2045 (2000).

Chapter 8

Appendix

The appendix contains papers [A1-A7] contributing to the thesis in the style and formatting of the publishing journals. The paper [A4], which at the stage of writing the thesis is still under review, is presented in the style in which it was submitted to *Annales Henri Poincaré* and posted in the ArXiv repository.

IOP Publishing Journal of Physics A: Mathematical and Theoretical

J. Phys. A: Math. Theor. **50** (2017) 105204 (11pp) doi:10.1088/1751-8121/aa5451

Squared eigenvalue condition numbers and eigenvector correlations from the single ring theorem

Serban Belinschi[1], Maciej A Nowak[2], Roland Speicher[3] and Wojciech Tarnowski[2]

[1] CNRS, Institut de Mathématiques de Toulouse, 118 Route de Narbonne, F-31062 Toulouse Cedex 09, France
[2] M. Smoluchowski Institute of Physics and Mark Kac Complex Systems Research Centre, Jagiellonian University, PL–30348 Kraków, Poland
[3] Universität des Saarlandes, Fachrichtung Mathematik, Postfach 151150, 66041 Saarbrücken, Germany

E-mail: serban.belinschi@math-univ.toulouse.fr, nowak@th.if.uj.edu.pl, speicher@math-uni.sb.de and wojciech.tarnowski@uj.edu.pl

Received 27 September 2016, revised 12 December 2016
Accepted for publication 16 December 2016
Published 6 February 2017

Abstract

We extend the so-called 'single ring theorem' (Feinberg and Zee 1997 *Nucl. Phys.* B **504** 579), also known as the Haagerup–Larsen theorem (Haagerup and Larsen 2000 *J. Funct. Anal.* **176** 331). We do this by showing that in the limit when the size of the matrix goes to infinity a particular correlator between left and right eigenvectors of the relevant non-hermitian matrix X, being the spectral density weighted by the squared eigenvalue condition number, is given by a simple formula involving only the radial spectral cumulative distribution function of X. We show that this object allows the calculation of the conditional expectation of the squared eigenvalue condition number. We give examples and provide a cross-check of the analytic prediction by the large scale numerics.

Keywords: non-hermitian random matrix models, eigenvector correlations, single ring theorem, Haagerup–Larsen theorem

(Some figures may appear in colour only in the online journal)

1. Introduction

Recently, Belinschi, Speicher and Śniady [3] provided a rigorous mathematical justification of the method of the so-called generalized Green's functions [1, 4–7], broadly exploited in the physics literature in relation to the spectral problems of non-hermitian operators. In particular, as one of the examples of their construction, they showed explicitly how the generalized Green's functions reproduce the Haagerup–Larsen theorem [2], valid for the case when the non-hermitian operator X can be decomposed as $X = PU$, where P is a positive hermitian operator, U is a Haar unitary operator and P and U are mutually free in the sense of free random variables [8]. Such operators are named 'R-diagonal' in the mathematical literature [9]. It was shown [10] that random matrices drawn from a probability distribution function of the form $P(X, X^\dagger) \sim \exp(-N\mathrm{Tr}V(XX^\dagger))$ (biunitarily invariant ensembles) in the limit $N \to \infty$ become R-diagonal. The Haagerup–Larsen theorem for such R-diagonal operators states that the spectrum possesses radial symmetry is localized within the two circles with known radii $r_{\min}, r_{\max}$ (including the possibility $r_{\min} = 0$, $r_{\max} = \infty$), and the radial spectral cumulative distribution function $F(r) = 2\pi \int_0^r s\rho(s)\mathrm{d}s$ can be derived from the simple functional equation $S_{P^2}(F(r) - 1) = \frac{1}{r^2}$, where $S_{P^2}(z)$ is the Voiculescu S-transform for the square of the positive operator P and r is the modulus of the complex eigenvalue λ. The Haagerup–Larsen theorem gives the mapping between spectral densities of eigenvalues and singular values for biunitarily invariant ensembles in the large N limit. Recently, the correspondence between eigenvalues and singular values was extended to the exact mapping between their joint probability density functions [11]. In this letter we demonstrate that the function $F(r)$ yields, for these biunitarily invariant ensembles, also (in the limit $N \to \infty$) the eigenvector correlation function, namely we show that

$$O(r) \equiv \lim_{N\to\infty} \frac{1}{N^2} \left\langle \sum_\alpha O_{\alpha\alpha} \delta^{(2)}(\lambda - \lambda_\alpha) \right\rangle = \frac{1}{\pi} \frac{F(r)(1 - F(r))}{r^2}, \tag{1}$$

where $\langle \ldots \rangle$ denotes expectation value, $O_{\alpha\beta} = \langle L_\alpha | L_\beta \rangle \langle R_\beta | R_\alpha \rangle$, where $|L_\alpha\rangle$ and $|R_\alpha\rangle$ are left and right eigenvectors of X, respectively. We make use of free probability tools, thus the result is valid at the $N \to \infty$ limit. In case of finite but large matrices the formula describes the correlator in the bulk of the spectrum quite well, however the transient phenomena near the spectral edge (typically of size $1/\sqrt{N}$) are not accessible within this formalism.

This paper is organized as follows. Section 2 recalls the definition of the generalized Green's functions [4]. The relevance of the correlation function and its connection with the eigenvalue condition number are discussed in section 3. Section 4 exploits the formalism and results of [3], in order to provide a short, direct proof of the main result (1). Section 5 includes a few examples where our formula can be easily applied and provides the verification of these results with the large scale numerical simulations. We derive in section 6 a mapping between the spectral density and the eigenvector correlator, showing that they play an equal role in the biunitarily invariant ensembles. Section 7 concludes the paper.

2. Generalized Green's functions

In this section we briefly summarize the method of the generalized Green's function for non-hermitian random matrix models in the limit $N \to \infty$. The method is based on the 'electrostatic' analogy [12–14]. One defines a quantity

$$\Phi(z,\bar{z},w,\bar{w}) = \frac{1}{N}\Big\langle \mathrm{Tr}\log\Big((z\mathbf{1}_N - X)(\bar{z}\mathbf{1}_N - X^\dagger) + |w|^2\,\mathbf{1}_N\Big)\Big\rangle, \tag{2}$$

which can be interpreted in the limit $|w| \to 0$ as an electrostatic potential of a cloud of N identical electric charges interacting on the z-complex plane. The corresponding electric field is a gradient of the potential

$$G(z,\bar{z},w,\bar{w}) = \partial_z\Phi(z,\bar{z},w,\bar{w}) = \frac{1}{N}\left\langle \mathrm{Tr}\frac{\bar{z}\mathbf{1}_N - X^\dagger}{(z\mathbf{1}_N - X)(\bar{z}\mathbf{1}_N - X^\dagger) + |w|^2\,\mathbf{1}_N}\right\rangle. \tag{3}$$

We study first the distribution of eigenvalues

$$\rho(z,\bar{z}) \equiv \frac{1}{N}\left\langle \sum_i \delta^{(2)}(z-\lambda_i)\right\rangle, \tag{4}$$

where λ_i's are the eigenvalues of X. The limiting eigenvalue density comes from the Gauss law

$$\rho(z,\bar{z}) = \lim_{|w|\to 0}\frac{1}{\pi}\partial_{\bar{z}}G(z,\bar{z},w,\bar{w}). \tag{5}$$

This relation follows from a standard representation of the complex Dirac delta function

$$\pi\delta^{(2)}(z-\lambda_i) = \lim_{|w|\to 0}\frac{|w|^2}{(|w|^2 + |z-\lambda_i|^2)^2}. \tag{6}$$

The expression in the brackets on the r.h.s. of (3) can take formally the standard form of the resolvent $(z-X)^{-1}$ at the price of introducing $2N\times 2N$ matrices

$$Q\otimes\mathbf{1}_N = \begin{pmatrix} z\mathbf{1}_N & -\bar{w}\mathbf{1}_N \\ w\mathbf{1}_N & \bar{z}\mathbf{1}_N\end{pmatrix}, \quad \mathcal{X} = \begin{pmatrix} X & 0 \\ 0 & X^\dagger\end{pmatrix}, \tag{7}$$

in place of the original $N\times N$ ones. The generalized resolvent is represented by a 2×2 matrix

$$\mathcal{G}(z,\bar{z},w,\bar{w}) \equiv \begin{pmatrix}\mathcal{G}_{11} & \mathcal{G}_{12}\\ \mathcal{G}_{21} & \mathcal{G}_{22}\end{pmatrix} = \frac{1}{N}\left\langle \mathrm{bTr}\frac{1}{Q\otimes\mathbf{1}_N - \mathcal{X}}\right\rangle = \begin{pmatrix}\partial_z\Phi & \partial_w\Phi \\ -\partial_{\bar{w}}\Phi & \partial_{\bar{z}}\Phi\end{pmatrix}, \tag{8}$$

where the block-trace is defined as

$$\mathrm{bTr}\begin{pmatrix} A & B\\ C & D\end{pmatrix} = \begin{pmatrix}\mathrm{Tr}A & \mathrm{Tr}B\\ \mathrm{Tr}C & \mathrm{Tr}D\end{pmatrix}.$$

We note that $\mathcal{G}$ from (8) has the algebraic structure of quaternions and we refer to it as the generalized Green's function or the quaternionic Green's function [4, 5, 15], since both $\mathcal{G}(z,\bar{z},w,\bar{w})$ and Q are quaternions. Similarly, one can define the quaternionic R-transform, $\mathcal{R}[\mathcal{G}(Q)] + [\mathcal{G}(Q)]^{-1} = Q$, which is additive under the free convolution of non-hermitian ensembles and generates also the non-hermitian multiplication laws [17]. We mention that the quaternionic extension is equivalent to another approach known under the name of hermitization method [1, 7, 16], in which the diagonal and off-diagonal blocks of matrices Q and $\mathcal{X}$ are flipped before the block-trace operation.

The upper-left element of the quaternionic resolvent $\mathcal{G}_{11}$ is equal to $G(z,\bar{z},w,\bar{w})$ (3), the second diagonal element $\mathcal{G}_{22}$ is just its complex conjugated copy, but one may wonder what role is played by the off-diagonal elements of the 2 by 2 matrix $\mathcal{G}$?

If a non-normal matrix X is diagonalizable via a similarity transformation, it possesses distinct left and right eigenvectors $X = \sum_\alpha \lambda_\alpha |R_\alpha\rangle\langle L_\alpha|$, where $X|R_\alpha\rangle = \lambda_\alpha|R_\alpha\rangle$ and $\langle L_\alpha|X = \lambda_\alpha\langle L_\alpha|$ with the normalization $\langle L_\alpha|R_\beta\rangle = \delta_{\alpha\beta}$. However, neither the left and right eigenvectors are normalized to unity $\langle L_\alpha|L_\alpha\rangle \neq 1 \neq \langle R_\alpha|R_\alpha\rangle$ nor they are orthogonal to each other $\langle L_\alpha|L_\beta\rangle \neq 0 \neq \langle R_\alpha|R_\beta\rangle$ (for $\alpha \neq \beta$). The orthogonality relations hold only for normal matrices. We define a bra of the right eigenvector in the standard way $\langle R_i| = \big(|R_i\rangle\big)^\dagger$, and analogously a ket of the left eigenvector.

The biorthogonality condition leaves the freedom of rescaling each eigenvector by an arbitrary non-zero complex number $|R_i\rangle \to c_i|R_i\rangle$, $\langle L_i| \to \langle L_i|c_i^{-1}$. Another allowed transformation is the multiplication by a unitary matrix $|R_i\rangle \to U|R_i\rangle$, $\langle L_i| \to \langle L_i|U^\dagger$. The simplest non-trivial quantities invariant under these transformations form the matrix of overlaps $O_{\alpha\beta} \equiv \langle L_\alpha|L_\beta\rangle\langle R_\beta|R_\alpha\rangle$. One can define a correlation function [18] (being the special case of the Bell–Steinberger matrix [19–21])

$$O(z,\bar z) \equiv \frac{1}{N^2}\left\langle \sum_\alpha O_{\alpha\alpha}\delta^{(2)}(z-\lambda_\alpha)\right\rangle. \tag{9}$$

Below we show that the product of off-diagonal elements of $\mathcal{G}$ in the limit $|w| \to 0$ gives the eigenvector correlator, simplifying the proof, originally given in [6].

We rewrite the electrostatic potential (2) in terms of the regularized Fuglede–Kadison determinant [22], using the relation $\mathrm{Tr}\log A = \log\det A$ and linearize it by bringing it to a block structure

$$\Phi(z,\bar z,w,\bar w) = \frac{1}{N}\Big\langle \log\det\Big((z-X)(\bar z - X^\dagger) + |w|^2\Big)\Big\rangle = \frac{1}{N}\langle \log\det(Q-\mathcal{X})\rangle. \tag{10}$$

We assume that the matrix X can be diagonalized by a similarity transformation $X = S\Lambda S^{-1}$, which enables us to rewrite the Fuglede–Kadison determinant as

$$\det(Q-\mathcal{X}) = \det[\mathcal{S}^{-1}(Q-\mathcal{X})\mathcal{S}] = \det\begin{pmatrix} z\mathbf{1}_N - \Lambda & -\bar w\langle L|L\rangle \\ w\langle R|R\rangle & \bar z\mathbf{1}_N - \bar\Lambda\end{pmatrix} = \det(A+F), \tag{11}$$

where $\mathcal{S} = \mathrm{diag}(S,(S^{-1})^\dagger)$ is a block-diagonal matrix. Here $S(S^{-1})$ are built from N right (left) eigenvectors of X. In the last equality we represent the matrix as a sum of diagonal A and block off-diagonal F. Making use of the result in ([23], theorem 2.3) we expand the determinant as follows

$$\det(A+F) = \det A + \det F + S_1 + S_2 + \ldots + S_{2N-1}, \tag{12}$$

where

$$S_k = \sum_{1\leqslant i_1<\ldots<i_k\leqslant 2N} \frac{\det A}{a_{i_1}\ldots a_{i_k}}\det F_{i_1,\ldots,i_k}, \tag{13}$$

a_i denotes the ith element on the diagonal of A, and $F_{i_1,\ldots,i_k}$ is a $k\times k$ submatrix the element of which lie at the intersections of $i_1,\ldots,i_k$th rows and columns.

If z is far from any of the eigenvalues of X, the regularization in (10) is not needed and one can safely set $|w| \to 0$. In the $|w| \to 0$ limit the non-vanishing contribution to the correlator comes when during the averaging procedure z is close to a certain eigenvalue λ_i. We remark that in matrix models with unitary symmetry the probability of coalescence of two eigenvalues

is zero due to the presence of the Vandermonde determinant. Since $S_1 = 0$, the dominant term in the expansion is

$$S_2 = \sum_{k,l=1}^{N} \frac{\det A}{(z-\lambda_k)(\bar{z}-\bar{\lambda}_l)} \det \begin{pmatrix} 0 & -\bar{w}\langle L_k|L_l\rangle \\ w\langle R_l|R_k\rangle & 0 \end{pmatrix}$$
$$= \frac{\det A}{|z-\lambda_i|^2}|w|^2 O_{ii} + |w|^2 \mathcal{O}(|z-\lambda_i|). \tag{14}$$

In the first equality we used the fact that F is off-diagonal and the only non-zero terms correspond to $i_1 \leqslant N$ and $i_2 \geqslant N$ in (13). Since $\det A$ contains a factor $|z-\lambda_i|^2$, we regrouped terms into the ones that $(z-\lambda_i)$ has canceled $(k=l)$, and others $(k \neq l)$ which include a factor of $z-\lambda_i$ or its conjugate, denoting the sum over them by $\mathcal{O}(|z-\lambda_i|)$.

In the leading term we obtain

$$\partial_w \log\det(Q-\mathcal{X}) = \frac{\bar{w}}{\frac{|z-\lambda_i|^2}{O_{ii}} + |w|^2}, \tag{15}$$

therefore it is easy to see that

$$\pi O(z,\bar{z}) = \lim_{|w|\to 0} \left\langle \frac{1}{N^2} \partial_w \log\det(Q-\mathcal{X}) \partial_{\bar{w}} \log\det(Q-\mathcal{X}) \right\rangle, \tag{16}$$

where we used the representation of the two-dimensional Dirac delta (6). Equation (16) is exact for any N. It is a characteristic property of probability density functions which are invariant under the action of the $U(N)$ group that in the large N limit the average of two quantities A and B preserving the $U(N)$ symmetry factorizes. More precisely, we denote

$$f_N \equiv \frac{1}{N}\partial_w \log\det(Q-\mathcal{X}), \qquad g_N \equiv \frac{1}{N}\partial_{\bar{w}} \log\det(Q-\mathcal{X}).$$

As indicated in section 5 of [10] it is enough to prove concentration of measure on the unitary group (i.e. assume deterministic singular values for X). Then, as in equation (34) in section 3.2 of [10], by relying on corollary 4.4.28 of [24], we have that f_N, g_N, as well as that $f_N g_N$ are almost surely close to their respectve expected values as $N \to \infty$.

Applying this to (16), we finally obtain

$$\pi O(z,\bar{z}) = \lim_{|w|\to 0} \partial_w \Phi \partial_{\bar{w}} \Phi = -\mathcal{G}_{12}\mathcal{G}_{21}\big|_{w=0}. \tag{17}$$

3. Diagonal overlaps and the stability of the spectrum

The diagonal elements of the matrix of overlaps play an important role in the stability of the spectrum of non-normal matrices as can be seen in the following example. Consider a diagonalizable matrix X which is slightly perturbed by P: $X(\epsilon) = X + \epsilon P$. The first order perturbation yields the leading term in ϵ

$$|\lambda_i(\epsilon) - \lambda_i(0)| = |\epsilon\langle L_i|P|R_i\rangle| \leqslant |\epsilon| \sqrt{\langle L_i|L_i\rangle\langle R_i|R_i\rangle}\, \|P\|, \tag{18}$$

and the bound is reached if the perturbation is of rank one $P = |L_i\rangle\langle R_i|$. The square root of O_{ii} is known in the numerical analysis community as the eigenvalue condition number $\kappa(\lambda_i)$, introduced in [25] (see also [26] for a review). The Cauchy–Schwartz inequality asserts that $O_{ii} \geqslant 1$.

Generically, $O_{ii} \sim N$ in the bulk (see example 5 for the behavior at the edge), but for normal matrices $O_{ij} = \delta_{ij}$, showing explicitly that the eigenvalues of normal matrices are the most stable. The definition (9) of $O(z, \bar{z})$ differs from the original one in [18] by the factor of N^{-1} so that in the large N limit $O(z, \bar{z})$ remains finite. As a consequence of this normalization, for normal matrices there holds a relation $O(z, \bar{z}) = N^{-1}\rho(z, \bar{z})$.

The eigenvector correlator and the mean spectral density give a partial access to the conditional probability of the eigenvalue condition numbers, namely their ratio is the conditional mean of the eigenvalue condition number

$$c(z,\bar{z}) = \mathbb{E}\left(\kappa^2(\lambda_i)N^{-1}|\lambda_i = z\right) = \int \frac{O_{ii}}{N}\frac{p(O_{ii},\lambda_i = z)}{p(\lambda_i = z)}\mathrm{d}O_{ii} = \frac{1}{\rho(z,\bar{z})}\int \frac{O_{ii}}{N}\delta^{(2)}(z-\lambda_i)p(X)\mathrm{d}X = \frac{O(z,\bar{z})}{\rho(z,\bar{z})}. \tag{19}$$

Here we used the fact that the joint probability density for O_{ii} and λ_i can be calculated by integrating out all other variables from the joint pdf for the matrix elements. The additional N^{-1} factor and the summation over the eigenvalues appears if one symmetrizes the integrand. Last, but not least, we mention that $c(z, \bar{z})$ is also known in physics as a Petermann factor (excess noise factor), reflecting the non-orthogonality of the cavity modes in open chaotic scattering [27–29].

4. The eigenvector correlator from the single ring theorem

In the previous section we have stressed that the full solution of the spectral non-hermitian problem requires the simultaneous knowledge of its eigenvalues and eigenvectors, since they mutually interact with each other already at the leading terms of the $1/N$ expansion. Considering now the case of the Haagerup–Larsen theorem, one may therefore wonder what has happened to the information about the correlator $O(z, \bar{z})$. Certainly, R-diagonal operators are not normal in general, so such correlators are different from zero. Luckily, the direct construction of Belinschi, Speicher and Śniady can easily give the answer, we just read off the product of the appropriate elements of the Green's function ([3], equation (31))

$$\mathcal{G}_{12}(z,\bar{z},\mathrm{i}\epsilon,-\mathrm{i}\epsilon)\mathcal{G}_{21}(z,\bar{z},\mathrm{i}\epsilon,-\mathrm{i}\epsilon) = \frac{\omega^2(\mathrm{i}\epsilon)}{(\omega^2(\mathrm{i}\epsilon)-|z|^2)^2}. \tag{20}$$

The function $\omega(\mathrm{i}\epsilon)$ is specified in [3], however its exact form is not necessary for our purpose, since the upper diagonal element of the Green's function satisfies the relation ([3], equation (32))

$$zG(z,\bar{z},\mathrm{i}\epsilon,-\mathrm{i}\epsilon) = \frac{|z|^2}{|z|^2-\omega^2(\mathrm{i}\epsilon)}. \tag{21}$$

In the limit $\epsilon \to 0$ the lhs tends to $zG(z, \bar{z}, 0, 0) \equiv F(|z|)$ which is the radial cumulative distribution function [1, 3] $F(r) = 2\pi\int_0^r r'\rho(r')\mathrm{d}r'$. It satisfies the functional equation $S_{P^2}(F(r)-1) = r^{-2}$ [2]. For simplicity we use the notation $r = |z|$. Combining (20) and (21) with (17), we finally obtain

$$O(r) = \frac{1}{\pi}\frac{F(r)\,[1-F(r)]}{r^2}, \tag{22}$$

which represents the main result of this paper.

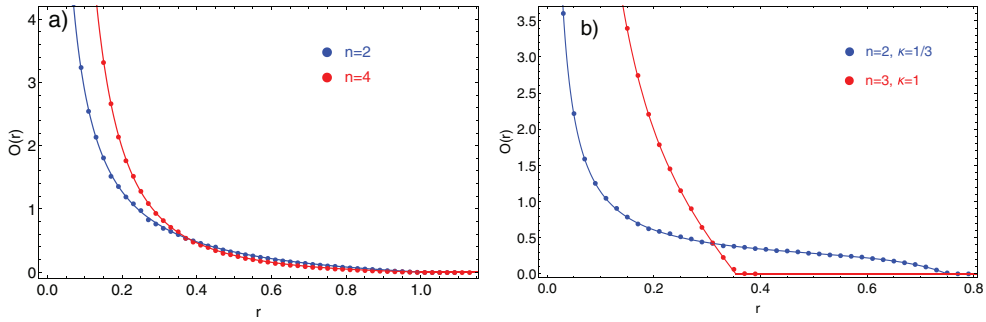

Figure 1. A numerical simulation (dots) of the eigenvector correlator for the product of (a) $n = 2, 4$ complex Ginibre matrices of the size 1000 by 1000, averaged over the sample of 2000 matrices; (b) $n = 2, 3$ truncated unitary matrices of the size $L = 1000$, $N = \kappa L$ done on the samples of 2000 matrices. The solid lines represent the analytic prediction. The fact that one observes datapoints outside the limiting spectrum is the effect of the finite size of matrices. Their agreement with the theoretical prediction ($O(r) = 0$ outside) is related to the scaling of the diagonal overlap O_{ii} (see also example 5).

5. Examples

In this section we provide five examples: (1) free product of n complex Ginibre ensembles, (2) free product of n truncated Haar matrices, (3) free quotient of complex Ginibre ensembles, (4) free sum of k Haar measures, and (5) mean condition number for the Ginibre ensemble. Taking into account the simplicity of the main formula (1), generalizations to any domain of applicability of the single ring theorem are straightforward.

1. Let us first take $Y = X_1X_2...X_n$, where X_i are free complex Ginibre ensembles. In this case the Haagerup–Larsen theorem yields $F_Y(r) = r^{\frac{2}{n}}$ for $r < 1$ and 1 otherwise [30, 31], hence

$$O_{Y,n}(r) = \frac{1 - r^{2/n}}{\pi r^{2-2/n}}\theta(1 - r), \tag{23}$$

where θ denotes the Heaviside (step) function. For completeness we note that [32]

$$\rho_{Y,n}(r) = \frac{1}{\pi n} r^{\frac{2}{n}-2}\theta(1 - r). \tag{24}$$

Interestingly, even for the case $n = 1$ the result for $O_{Y,1}(r) = \pi^{-1}(1 - r^2)\theta(1 - r)$ was obtained for the first time 33 years [6, 18] after the spectral density result $\rho_{Y,1} = \pi^{-1}\theta(1 - r)$ derived in the seminal paper by Ginibre [33]. Figure 1(a) confronts our prediction with the numerical calculations. Recently, (23) was confirmed by independent calculation using diagrammatic methods [34].

2. Let us also take $Y = X_1X_2 \ldots X_n$, where X_i are truncated unitary matrices, i.e. Haar matrices of the size $(N + L) \times (N + L)$, in which L columns and rows are removed. In the limit where both L and N tend to infinity in such a way that $\kappa = L/N$ is fixed, $F_Y = \kappa\frac{r^{2/n}}{1 - r^{2/n}}$ for $r < (1 + \kappa)^{-n/2}$ and 1 otherwise [30], hence

$$O_{Y,n,\kappa}(r) = \frac{\kappa}{\pi}\frac{1 - r^{2/n}(1 + \kappa)}{r^{2(n-1)/n}(1 - r^{2/n})^2}\theta\left(\frac{1}{(1 + \kappa)^{n/2}} - r\right). \tag{25}$$

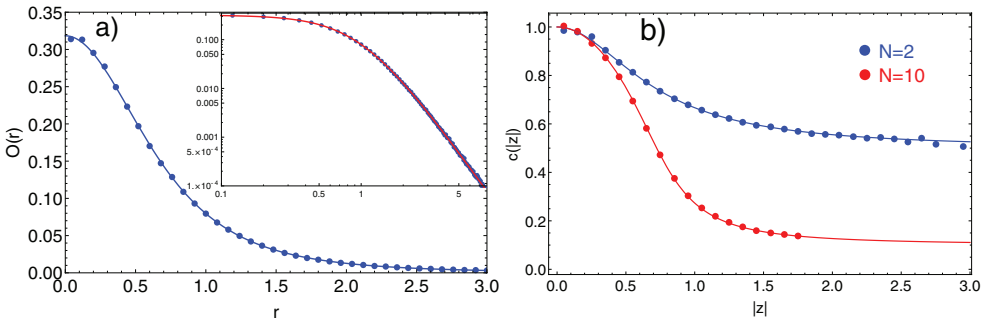

Figure 2. (a) The eigenvector correlator calculated by a numerical diagonalization of 4000 matrices that are ratio of two Ginibres (also known as the spherical ensemble) of size $N = 1000$ presented on linear and double logarithmic (inset) scales. (b) Mean eigenvalue condition number of the Ginibre ensemble. The complex plane was divided into the hollowed cylinders of radii r and $r + \Delta r$, eigenvalues and their condition numbers were assigned to cylinders, according to the modulus of the eigenvalue. The dots denote the average eigenvalue condition number within each cylinder, the lines present formula (28). Numerical distribution was obtained by the diagonalization of 10^6 matrices of size $N = 2$ and $4 \cdot 10^5$ matrices of size $N = 10$.

Figure 1(b) confronts our prediction with the numerical calculations.

3. Let us consider k Ginibre ensembles X_i and the same number of inverse Ginibre ensembles $\tilde{X}_i^{-1}$. Defining Y as the product $Y = X_1 \dots X_k \tilde{X}_1^{-1} \dots \tilde{X}_k^{-1}$, one easily obtains [35] $S_{P^2}(z) = (-z)^k/(1+z)^k$. If we argue that the eigenvector correlator formula holds also for the unbounded measures, using the Haagerup–Larsen theorem we get a rather unexpected result:

$$\begin{aligned} \rho_{Y,k}(r) &= \frac{1}{\pi k} \frac{r^{\frac{2}{k}-2}}{(1+r^{2/k})^2}, \\ O_{Y,k}(r) &= \frac{1}{\pi r^2} \frac{r^{\frac{2}{k}}}{(1+r^{2/k})^2}, \end{aligned} \tag{26}$$

i.e. the spectral density and the eigenvector correlator satisfy a very simple relation $O_{Y,k}(r) = k\rho_{Y,k}(r)$, which means that the eigenvalues are (on average) uniformly conditioned. The formula for the spectral density agrees with the recent results [36]. In figure 2(a) we confront our result for the eigenvector correlator with numerical simulations.

4. Let us consider free convolution of k Haar-distributed matrices U_k, i.e. $Y = U_1 + U_2 + \dots + U_k$. Then, $F_Y = \frac{r^2(k-1)}{k^2 - r^2}$ [2, 37] for $r < \sqrt{k}$ and 1 otherwise, hence

$$\begin{aligned} \rho_{Y,k}(r) &= \frac{1}{\pi} \frac{k^2(k-1)}{(k^2-r^2)^2} \theta(\sqrt{k} - r), \\ O_{Y,k}(r) &= \left(1 - \frac{r^2}{k}\right) \rho_{Y,k}(r). \end{aligned} \tag{27}$$

5. Our formula (1) is valid only in the limit $N \to \infty$. In order to access condition numbers in the Ginibre ensemble in the finite N, we superimpose the results from [18] and [38], derived with the use of different techniques. We obtain the formula for the averaged squared eigenvalue condition number

$$c(z,\bar{z}) = 1-|z|^2+\frac{1}{N}\frac{\mathrm{e}^{-N|z|^2}(N|z|^2)^N}{\Gamma(N,N|z|^2)}, \tag{28}$$

valid for any size of a matrix. Here $\Gamma(N,x)$ stands for the incomplete gamma function. The accordance with the numerical results is presented in figure 2(b).
Formulas (23), (25) and (27) predict that the eigenvector correlator vanishes at the edges of the spectrum. It neither means that the eigenvectors become orthogonal to each other nor that the condition number is smaller than 1, rather the diagonal overlap grows slower than linearly with the size of a matrix. Indeed, an asymptotic analysis of the formula (28) yields the conditional expectation

$$\mathbb{E}(O_{ii}|1=|\lambda_i|) = \sqrt{\frac{2}{\pi}}N^{1/2}+\frac{2}{3\pi}+\mathcal{O}(N^{-1/2}) \tag{29}$$

6. Eigenvector-eigenvalue mapping

Combining (1) with the definition of the radial spectral density $\rho(r)=\frac{1}{2\pi r}\frac{\mathrm{d}F(r)}{\mathrm{d}r}$, we can obtain a general relation between $\rho(r)$ and $O(r)$. Solving a quadratic equation we arrive at

$$F(r) = \frac{1}{2}(1\mp\sqrt{1-4\pi r^2 O(r)}). \tag{30}$$

We remark that both signs are relevant. At the inner rim of the ring, $F(r)=0$, which corresponds to the negative sign in (30). At the outer rim of the ring, $F(r)=1$, corresponding to the positive sign in (30). Differentiation of (30) with respect to r yields

$$\rho(r) = \pm\frac{1}{2\sqrt{1-4\pi r^2 O(r)}}\left(2O(r)+r\frac{\mathrm{d}O(r)}{\mathrm{d}r}\right). \tag{31}$$

It is instructive to consider the Ginibre case. The spectral density calculated from (31), with the use of $O(r)=\frac{1}{\pi}(1-r^2)\theta(1-r)$, reads

$$\rho(r) = \pm\frac{1}{\pi}\mathrm{sgn}(1-2r^2)\theta(1-r) = \frac{1}{\pi}\theta(1-r), \tag{32}$$

where the switch from the branches of the square root in (30) takes place at $r=1/\sqrt{2}$.

7. Conclusions

We have augmented the single ring theorem with the additional prediction for certain eigenvector correlations. We pointed out a link between the main object of this paper and the sensitivity of eigenvalues to perturbations. The considered correlation function, which is the spectral density weighted by the squared eigenvalue condition number, gives partial access to the distribution of eigenvalue condition numbers. We have shown that the ratio of the eigenvector correlation function and the spectral density gives the conditional expectation of the squared eigenvalue condition number. This ratio varies on the complex plane, indicating that the eigenvalues are not uniformly conditioned.

In a series of recent papers [39, 40] it was argued that the consistent description of non-hermitian ensembles requires the knowledge of the detailed dynamics of the co-evolving

eigenvalues and eigenvectors. Unexpectedly, in the Gaussian case (Ginibre ensemble), the dynamics of eigenvectors seemed to play even a superior role (at least in the $N \to \infty$ limit) and leads directly to the inference of the spectral properties solely from the knowledge of the eigenvector correlator. The case considered here, the Haagerup–Larsen theorem, seems to agree with this scenario. We conjecture therefore that in generic non-hermitian ensembles the correlations between left and right eigenvectors play an equally important role as the spectral information. Historically, in the literature on non-hermitian random matrix models, our parameter w always played the role of a regulator of the Fuglede–Kadison determinant, and was usually put to zero in an incautious way, and thus loosing a track of eigenvectors. That practice was a consequence of the duplication of the paradigm of hermitian random matrix models, which concentrates on the spectrum, since the $U(N)$ invariance of the probability density function leads to the decoupling of the eigenvectors. We suggest that this paradigm has to be challenged in the case of non-normal random matrix models, where the unitary transformations are not sufficient to diagonalize a matrix. In particular, our formula (8) explicitly points at the symmetric nature of z and w as complex variables, controlling the spectra and eigenvectors, respectively. In particular, $\partial_w \mathcal{G}_{11} = \partial_z \mathcal{G}_{12}$.

The presented new relation for eigenvectors in the single ring theorem is just the consequence of the above-mentioned symmetry applied to R-diagonal operators.

On more general grounds, it is tempting to speculate that the interplay between eigenvector correlators and spectral measures may play a role in generalizations of the Brown measure, which will be free of pathological discontinuities, as observed in [41].

Acknowledgments

MAN and WT were supported by the Grant DEC-2011/02/A/ST1/00119 of the National Centre of Science. WT also appreciates the support from the Ministry of Science and Higher Education through the Diamond Grant 0225/DIA/2015/44. The work of RS was supported by the ERC Advanced Grant NCDFP 339760. We are grateful to Jacek Grela, Ewa Gudowska-Nowak, Romuald A Janik and Piotr Warchoł for discussions.

References

[1] Feinberg J and Zee A 1997 *Nucl. Phys.* B **504** 579
Feinberg J, Scalettar R and Zee A 2001 *J. Math. Phys.* **42** 5718
Feinberg J and Zee A 1997 *Nucl. Phys.* B **501** 643
[2] Haagerup U and Larsen F 2000 *J. Funct. Anal.* **176** 331
[3] Belinschi S T, Śniady P and Speicher R 2015 arXiv:1506.02017v2 [math.OA]
[4] Janik R A, Nowak M A, Papp G and Zahed I 1997 *Nucl. Phys.* B **501** 603
[5] Janik R A, Nowak M A, Papp G, Wambach J and Zahed I 1997 *Phys. Rev.* E **55** 4100
[6] Janik R A, Noerenberg W, Nowak M A, Papp G and Zahed I 1999 *Phys. Rev.* E **60** 2699
[7] Chalker J T and Jane Wang Z 2000 *Phys. Rev.* E **6** 196
[8] Voiculescu D V, Dykema J J and Nica A 1992 *Free Random Variables* (*CRM Monograph Series* vol 1) (Providence, RI: American Mathematical Society)
[9] Nica A and Speicher R 2006 *Lectures on the Combinatorics of Free Probability* (Cambridge: Cambridge University Press)
[10] Guionnet A, Krishnapur M and Zeitouni O 2011 *Ann. Math.* **174** 1189
[11] Kieburg M and Kösters H 2016 (arXiv:1601.02586) [math.CA]
[12] Sommers H J, Crisanti A, Sompolinsky H and Stein Y 1988 *Phys. Rev. Lett.* **60** 1895
[13] Fyodorov Y V and Sommers H-J 1997 *J. Math. Phys.* **38** 1918
[14] Brown L G 1983 *Res. Notes Math. Ser.* **123** 1

[15] Jarosz A and Nowak M A 2006 *J. Phys. A: Math. Gen.* **39** 10107
[16] Girko V L 1984 *Teor. Veroyatn. Primen.* **29** 669
[17] Burda Z, Janik R A and Nowak M A 2011 *Phys. Rev.* E **84** 061125
[18] Chalker J T and Mehlig B 1998 *Phys. Rev. Lett.* **81** 3367
Mehlig B and Chalker J T 2000 *J. Math. Phys.* **41** 3233
[19] Bell J S and Steinberger J 1966 *Proc. of the Oxford Int. Conf. on Elementary particles (Rutherford Laboratory, UK)* ed R G Moorhouse *et al*
[20] Savin D V and Sokolov V V 1997 *Phys. Rev.* E **56** R4911
[21] Fyodorov Y V and Savin D V 2012 *Phys. Rev. Lett.* **108** 184101
[22] Fuglede B and Kadison R V 1952 *Ann. Math.* **55** 520
[23] Ipsen I C F and Rehman R 2008 *SIAM. J. Matrix Anal. Appl.* **30** 762776
[24] Anderson G, Guionnet A, Zeitouni O 2010 *An Introduction to Random Matrices* (Cambridge: Cambridge University Press)
[25] Wilkinson J H 1965 *Algebraic Eigenvalue Problem* (Oxford: Oxford University Press)
[26] Trefethen L N and Embree M 2005 *Spectra and Pseudospectra: The Behavior of Nonnormal Matrices and Operators* (Princeton, NJ: Princeton University Press)
[27] Frahm K, Schomerus H, Patra M and Beenakker C W J 2000 *Europhys. Lett.* **49** 48
Schomerus H, Frahm K M, Patra M, Beenakker C W J 2000 *Physica* A **278** 469–6
[28] Fyodorov Y V and Mehlig B 2002 *Phys. Rev.* E **66** 045202
[29] Berry M V 2003 *J. Mod. Opt.* **50** 63
[30] Burda Z, Nowak M A and Święch A 2012 *Phys. Rev.* E **86** 061137
[31] Alexeev N, Goetze F and Tikhomirov A N 2010 *Dokl. Math.* **82** 505
[32] Burda Z, Janik R A and Waclaw B 2010 *Phys. Rev.* E **81** 041132
[33] Ginibre J 1965 *J. Math. Phys.* **6** 440
[34] Burda Z 2016 *Talk at the workshop Random Product Matrices—New Developments and Applications (ZiF, Bielefeld, 22–26 August 2016)*
[35] Haagerup U and Schultz H 2007 *Math. Scand.* **100** 209
[36] Zeng X 2016 *J. Phys. A: Math. Theor.* **49** 235201
[37] Jarosz A 2011 *Phys. Rev.* **E 84** 011146
[38] Walters M, Starr S 2015 *J. Math. Phys.* **56** 013301
[39] Burda Z, Grela J, Nowak M A, Tarnowski W and Warchoł P 2014 *Phys. Rev. Lett.* **113** 104102
Burda Z, Grela J, Nowak M A, Tarnowski W and Warchoł P 2015 *Nucl. Phys.* B **897** 421
[40] Tribe R and Zaboronski O 2014 *J. Math. Phys.* **55** 063304
[41] Śniady P 2002 *J. Funct. Anal.* **193** 291

PHYSICAL REVIEW E **96**, 042149 (2017)

Complete diagrammatics of the single-ring theorem

Maciej A. Nowak* and Wojciech Tarnowski†
M. Smoluchowski Institute of Physics and Mark Kac Complex Systems Research Center, Jagiellonian University, S. Łojasiewicza 11, PL 30-348 Kraków, Poland
(Received 9 May 2017; published 24 October 2017)

Using diagrammatic techniques, we provide explicit functional relations between the cumulant generating functions for the biunitarily invariant ensembles in the limit of large size of matrices. The formalism allows us to map two distinct areas of free random variables: Hermitian positive definite operators and non-normal R-diagonal operators. We also rederive the Haagerup-Larsen theorem and show how its recent extension to the eigenvector correlation function appears naturally within this approach.

DOI: 10.1103/PhysRevE.96.042149

I. INTRODUCTION

Over half a century ago, Jean Ginibre [1], driven solely by the mathematical curiosity,[1] considered a first non-normal random matrix model. He proposed an ensemble, where the elements of a random matrix were drawn from real (complex, quaternion-valued) Gaussian distribution without imposing any restriction on the symmetry of the ensemble. Such a simple random matrix model (named today the Ginibre ensemble) exhibited two main features distinguishing it from earlier considered Hermitian or unitary ensembles, which made a great impact in various fields of mathematics, physics, statistics, and interdisciplinary applications. First, the spectrum was complex, filling, in the limit when size of the matrix tends to infinity, a uniform disk on the complex plane. Second, the ensemble is non-normal, therefore possesses two sets of left and right eigenvectors. It took several decades to understand the role of left and right eigenvectors. In late 1990s, in a series of papers by Fyodorov, Savin, Sokolov, Chalker, and Mehlig [2] showed that for non-normal matrices another type of observable, built out of right and left eigenvectors, plays a crucial role in understanding non-Hermitian ensembles, especially in the study of stability of the ensemble under small perturbations. Nowadays, the non-normal random matrices turned out to be beneficial for a plethora of problems involving chaotic scattering in quantum physics [3,4], lagged cross correlations [5,6], search algorithms [7], non-Hermitian quantum mechanics [8,9], and many others.

From the perspective of this work, it is worthy of notice that the Ginibre ensemble has another distinctive feature. The probability measure of the above-mentioned ensemble is invariant under the biunitary transformation, in contrast to single unitary invariance in the case of the Dysonian threefold way [10]. Since the unitary transformations related with the singular value decomposition fall into the symmetry group of the considered matrices, one expects that all spectral properties are given by the (squared) singular values. Symmetry of the ensemble assures also that the spectrum does not depend on the azimuthal angle ϕ, but is a function of a radial variable $|z|$ only.

In the limiting case of the size of the matrix $N \to \infty$, the Ginibre ensemble was also the first case of the later-termed **R**-diagonal random matrices. The concept of the **R**-diagonal operator was introduced formally by Nica and Speicher [11], in the framework of Voiculescu's theory of free random variables [12]. We say that the operator X (or its matricial representation) is **R** diagonal, if it can be decomposed as $X = PU$, where P is Hermitian positive definite, U represents the Haar measure, and P and U are mutually free. These are the natural extension of the isotropic complex random variables, the probability density function of which depends only of the modulus. Since the **R**-diagonal operators play a vital role in several applications of RMT—e.g., in MIMO telecommunication [13] and quantum information problems [14], the study of **R**-diagonal operators is not only an interesting subject from the viewpoint of formal mathematics.

An early result for spectra of biunitarily invariant matrices (but without explicit relation to the concept of **R**-diagonality) was formulated in a paper by Feinberg and Zee [15], who discovered the so-called "single-ring theorem"—the spectrum of the biunitary invariant measure in the limit when the $N \to \infty$ is always confined between two rings, r_{in} and r_{out}. This theorem was elaborated later in more detail by Feinberg, Scalettar, and Zee in Ref. [16]. The single-ring theorem includes also the cases when $r_{\text{in}} = 0$ (disk, like the Ginibre case) or $r_{\text{out}} = \infty$. Independently, in the more general framework of operator algebras Haagerup and Larsen [17] have mathematically formulated the single-ring theorem in terms of Voiculescu multiplicative S transform [18] for the square of the polar operator P. Then the topic of **R**-diagonal operators became the subject of intense research in mathematics. Another proof relying on the characteristic determinant and integration over the unitary groups was given by Fyodorov and Khoruzenko [19]. The direct and mathematically complete link to random matrices was established quite late by Guionnet, Krishnapur, and Zeitouini [20]. In 2015, Belinschi, Speicher, and Śniady [21] have rigorously proven how the single-ring theorem emerges as a result of the reduction of "Hermitization" ("quaternionization") approaches, proposed in the context of physical problems involving non-Hermitian operators [22–26]. All these works were concentrating on spectral properties of the single-ring theorem and did not address the issue of eigenvector correlations. Very recently, the single-ring

*maciej.a.nowak@uj.edu.pl
†wojciech.tarnowski@student.uj.edu.pl
[1]In his own words, "Apart from the intrinsic interest of the problem, one may hope that the methods and results will provide further insight in the cases of physical interest or suggest as yet lacking applications."

theorem was augmented, using analytic methods, with the part predicting also the generic form of a certain eigenvector correlation function [27].

Historically, Voiculescu formulated the free probability theory in the analytical language, but several years later, Speicher and Nica reformulated it as a combinatorial theory of noncrossing partitions, corresponding to planar diagrams in physicists language. Despite that the **R**-diagonal concept was originally introduced in a combinatorial language, all known mathematical proofs and generalization of the Haagerup-Larsen theorem were performed using the analytic methods of free random variables, sometimes quite involved. Moreover, despite that the original Feinberg and Zee's approach to the single-ring theorem relies on the resummation of planar diagrams, they do not focus on their combinatorial aspects.

The intention of this work is to fill this gap and provide the simple diagrammatic arguments leading directly to the Haagerup-Larsen theorem, for both the spectra and the left-right eigenvector correlator. In this way we build *an explicit* relation between the R transform of the square of the Hermitian operator P and the quaternionic R transform of **R**-diagonal matrices.

The paper is organized as follows. In Sec. II, we recall the diagrammatics of Hermitian ensembles leading to the Voiculescu additive R transform for free convolution. We note here that to avoid confusion coming from too many R's used traditionally in the free random variable calculus, we denote the **R**-diagonal feature using the bold font. Section III generalizes this diagrammatic construction to the case of non-Hermitian operators, following quaternionization construction [22,23]. Section IV shows the main result of the paper, i.e., the procedure of effective reduction of generic non-Hermitian diagrammatics to the case of **R**-diagonal operators. The main result is the diagrammatic derivation of the full (spectra and eigenvectors) Haagerup-Larsen theorem. We also stress the analogy between the Hermitian and **R**-diagonal cases, by presenting the mapping between various transformations used in free probability. We elucidate also an infinite resummation of the corresponding diagrams emerging from the change of the variables and leading to the change of the topology of the interlocked one-line irreducible diagrams. This observation is crucial for the proof. Finally, in Sec. V we consider three explicit examples applying our construction for a simple rederivation of the quaternionic R transform for the Haar measure, the **R**-diagonal analog of free Poisson distribution, and we study cumulants of the products of Ginibre matrices, which turn out to be the so-called Raney numbers. Section VI concludes the paper.

II. HERMITIAN RANDOM MATRICES

Before we focus on diagrams for non-Hermitian **R**-diagonal matrices we present briefly the diagrammatic approach to large Hermitian matrices and their integrable structure. We consider random matrices, the probability density function (pdf) of which is given by

$$P(H)dH = Z^{-1}\exp[-N\mathrm{Tr}V(H)]dH. \tag{1}$$

Here $dH = \prod_{j=1}^{N} d\mathrm{Re}H_{jj}\prod^{N}_{\substack{j,k=1\\ j<k}} d\mathrm{Re}H_{jk}d\mathrm{Im}H_{jk}$ and $H_{jk} = \bar{H}_{kj}$. The potential $V(H) = \sum_{k=1}^{\infty} g_k H^k$ is chosen such that the pdf is normalizable. We also include a possibility that some of g's are zero. The normalizing constant ensures that $\int P(H)dH = 1$. The pdf is invariant under the unitary transformations $H \to UHU^{\dagger}$, where $U \in U(N)$.

Since these transformations can bring H to the diagonal form, the only invariant quantities are built out of its eigenvalues. The simplest possible such object is the one-point correlation function, the spectral density

$$\rho(x) := \left\langle \frac{1}{N}\sum_{j=1}^{N}\delta(x-\lambda_i)\right\rangle, \tag{2}$$

where $\langle\ldots\rangle$ denotes the average over the pdf (1),

$$\langle f(H)\rangle = \int f(H)\exp[-N\mathrm{Tr}V(H)]dH. \tag{3}$$

In practice, the spectral density is inconvenient to handle directly, thus one considers its Stieltjes transform (Green's function),

$$G(z) := \left\langle \frac{1}{N}\mathrm{Tr}\frac{1}{z\mathbf{1}-H}\right\rangle, \tag{4}$$

which is more tractable. The spectral density can be recovered from G by means of the Sochocki-Plemelj formula

$$\rho(x) = -\frac{1}{\pi}\lim_{\epsilon\to 0}\mathrm{Im}G(x+i\epsilon). \tag{5}$$

The Green's function is also the generating function for moments of the spectral density, as can be seen from the power series expansion at $z=\infty$,

$$G(z) = \sum_{k=0}^{\infty}\frac{1}{z^{k+1}}\left\langle\frac{1}{N}\mathrm{Tr}H^k\right\rangle = \sum_{k=0}^{\infty}\frac{1}{z^{k+1}}\int\rho(\lambda)\lambda^k d\lambda. \tag{6}$$

For large matrices calculations of G can be done perturbatively. Consider the averaged resolvent $\hat{G} = \langle(z\mathbf{1}-H)^{-1}\rangle$. The unitary invariance of the pdf asserts that any quantity calculated as an average of matrices H has a trivial matrix structure, i.e., it is a multiple of the identity matrix (see [28,29] for calculations of averages with respect to the unitary group and [30,31] for a modern approach). We therefore treat them as scalars, which also enables us to freely interchange the resolvent with its traced version, the Green's function. The resolvent can be expanded into the geometric series

$$G\mathbf{1} = \frac{\mathbf{1}}{z} + \left\langle\frac{\mathbf{1}}{z}H\frac{\mathbf{1}}{z}\right\rangle + \left\langle\frac{\mathbf{1}}{z}H\frac{\mathbf{1}}{z}H\frac{\mathbf{1}}{z}\right\rangle + \cdots \tag{7}$$

and the average in each term can be evaluated independently. Sometimes it is convenient to rephrase the expansion into moments around $z=0$, then the useful generating function reads

$$\tilde{M}(z) := \frac{1}{z}G\left(\frac{1}{z}\right)\frac{1}{z} - \frac{1}{z} = \sum_{k=1}^{\infty} m_k z^{k-1}. \tag{8}$$

For calculation of the averages in Eq. (7) we use the diagrammatic representation, borrowing from standard field-theoretical tools—Feynman diagrams. The main ingredient is

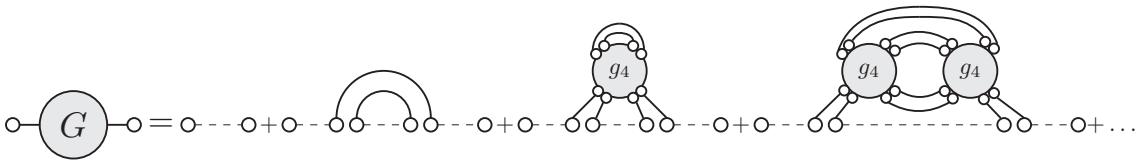

FIG. 1. Several exemplary planar diagrams which appear in the expansion of the complex resolvent for the potential $V(H) = g_2H^2 + g_4H^4$. Double dots denote a matrix H and each dot carries an index (not shown explicitly) which refers to the entries of the matrix. A dashed horizontal line with single dots at its ends represents $\frac{1}{z}$ terms in the expansion (7). Gray circles denote the coefficients of the power expansion of the potential (9), while budding white circles are the matrices in this expansion. For the simplicity, trivial summations of the identity matrix with the relevant matrices in the expansion are presented as already merged circles.

the representation of the Kronecker δ function by a single line. In the case of random matrix models the graphs have a particularly simple form, since they basically control only the flow of the indices of the averaged strings of matrices. We distinguish the Gaussian part in the potential, while the remaining part of the potential we expand into a series

$$\exp[-N\mathrm{Tr}V(H)] = \exp(-Ng_2\mathrm{Tr}H^2)\sum_{l=0}^{\infty}\frac{1}{l!}\left(-N\sum_{k\neq 2}^{\infty}g_kH^k\right)^l. \quad (9)$$

Then we integrate it, term by term, with respect to the Gaussian measure, making use of the Wick's (Isserlis') theorem, which reduces the calculation of expectations of H's to the all possible pairings. The price for the simplification of the integrals is the proliferation of the terms in the integrand. In order to cope with the multitude of expressions, we represent them graphically as diagrams; see Fig. 1. A pairing of two matrices we call a propagator, which brings a factor

$$\langle H_{ab}H_{cd}\rangle_G = \frac{1}{g_2N}\delta_{ad}\delta_{bc}, \quad (10)$$

which is represented by the double line. The terms on the right-hand side of (9) bring additional factors: Ng_k and k matrices to be paired. The final expressions are represented by diagrams obtained from all possible pairing of vertices and matrices from the expansion (7) by the propagators (10).

Remarkably, in the large N limit only the planar diagrams give the $\mathcal{O}(1)$ contribution, while the sum of all remaining diagrams vanishes in this limit, which simplifies the theory. This fact was observed by t'Hooft [32] in the context of non-Abelian gauge theories. We remark here that the subleading terms are successively accessible in the framework of loop equations (see, e.g., [33]) and the $\mathcal{O}(N^{-2g})$ corrections are encoded in diagrams that are planar when drawn on the surface of genus g.

A. *R* transform and 1LI diagrams

Among the planar diagrams we distinguish a class of one-line irreducible (1LI), i.e., the ones that cannot be split into two by a single cut of a horizontal line. We denote by Σ a sum of all 1LI diagrams and refer to this as self-energy. Further, among the 1LI diagrams we distinguish the connected subdiagrams which originate from the expectations $\langle H^n\rangle$, where H's are separated by dashed horizontal lines. The sum of such diagrams with the traced trivial matrix structure we call the nth cumulant $\kappa_n := \langle\frac{1}{N}\mathrm{Tr}H^n\rangle_c$ and endow the corresponding average with the index c. We consider also a generating function of all cumulants $R(z) := \sum_{n=1}^{\infty}\kappa_nz^{n-1}$, called the R transform.

The self-energy is the building block of the Green's function which can be expressed as a geometric series of Σ's [see Fig. 2(a)],

$$G(z) = \frac{1}{z} + \frac{1}{z}\Sigma(z)\frac{1}{z} + \frac{1}{z}\Sigma(z)\frac{1}{z}\Sigma(z)\frac{1}{z} + \cdots, \quad (11)$$

written in a closed form,

$$G(z) = [z - \Sigma(z)]^{-1}. \quad (12)$$

The relation between the Green's function and the self-energy is known by the name of the Schwinger-Dyson equation. Moreover, the planarity of diagrams allows us also to express the self-energy through the Green's function by means of the R transform [see Fig. 2(b)]

$$\Sigma(z) = R(G(z)) = \sum_{k=1}^{\infty}\kappa_kG^{k-1}(z) \quad (13)$$

Combining (12) with (13) we arrive at the relation

$$R(G(z)) + \frac{1}{G(z)} = z, \quad (14)$$

which, after introducing the auxiliary function $B(z) = R(z) + 1/z$ (sometimes nicknamed Blue's function), leads to the relation of the functional inverse type, i.e.,

$$G(B(z)) = B(G(z)) = z. \quad (15)$$

Knowledge of the R transform is sufficient to solve the matrix model in the large N limit. We remark that the combinatorics standing behind the planar diagrams is equivalent to the axiomatic framework of the lattice of noncrossing partitions in the free probability theory [34].

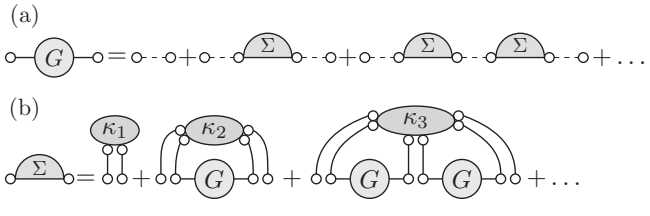

FIG. 2. (a) Relation between the Green's function and the sum over all 1LI diagrams. (b) Self-energy represented by the cumulants and the Green's function.

B. Addition and multiplication of Hermitian random matrices

It is natural to ask a question about the spectral density of a sum of two large matrices. In general, this is a very hard task since the matrices can be correlated. In classical probability of real variables, one has to know their joint distribution in advance. The problem simplifies if they are independent and the logarithm of the Fourier transform of the probability density function is the quantity, which is additive when we add two independent random variables.

In the noncommutative world of large random matrices the notion of independence is replaced by freeness, a concept introduced by Voiculescu [12]. We do not go into detail concerning the free probability, we just mention the important fact that the matrices A and $UBU^\dagger$, where U is Haar unitary, are free in the limit when their size tends to infinity [35,36]. In this framework, the R transform, which has already appeared in the description of Feynman diagrams, is additive under the addition of free random variables. The additivity of the R transform in the language of Feynman diagrams was shown in Ref. [37].

Although the product AB of two Hermitian matrices is not Hermitian in general, assuming that at least one of these matrices, let us say A, is positive definite, the construction for multiplication is possible. Since A is Hermitian positive definite, its square root $A^{1/2}$ is also Hermitian, therefore the matrix AB, isospectral to the Hermitian matrix $A^{1/2}BA^{1/2}$, has real eigenvalues. The problem of multiplying large unitarily invariant random matrices in the sense above is solved by the S transform, which is related to the R transform via

$$R(z)S(zR(z)) = 1, \quad S(z)R(zS(z)) = 1. \tag{16}$$

These relations are particularly simple, if we use "tilded" functions $\tilde{S}(z) = zS(z)$ and $\tilde{R}(z) = zR(z)$. Then $\tilde{S}(z)$ is the functional inverse of $\tilde{R}(z)$

$$\tilde{R}(\tilde{S}(z)) = \tilde{S}(\tilde{R}(z)) = z. \tag{17}$$

This formulation requires $R_A(0) \neq 0 \neq R_B(0)$, i.e., that the first moments of both distributions do not vanish, for the S transform to exist. This assumption can be further weakened to the case when one of the distributions has zero mean [38]. There exists a different formulation of the multiplication rule in terms of the R transforms solely [39],

$$R_{AB}(z) = R_A(x)R_B(y), \tag{18}$$

where x and y are related to z via

$$x = zR_B(y), \quad y = zR_A(x). \tag{19}$$

III. NON-HERMITIAN RANDOM MATRICES

A. Preliminaries

In this section we focus on the spectral properties of non-Hermitian random matrices, the entries of which, $X_{jk} = x_{jk} + iy_{jk}$, are generated from the probability distribution

$$P(X,X^\dagger)dXdX^\dagger \sim \exp[-N\mathrm{Tr}V(X,X^\dagger)]dXdX^\dagger, \tag{20}$$

where the measure reads

$$dXdX^\dagger = \prod_{j,k=1}^{N} dx_{jk}dy_{jk}. \tag{21}$$

Since X is not Hermitian, the potential depends also on $X^\dagger$ and non-normality of X allows for a much richer structure of the potential than in the Hermitian case. We demand that V is chosen such that the probability density function is normalizable and real valued. The pdf is again invariant under the unitary transformations.

Non-Hermitian matrices have in general complex eigenvalues. In such a case the Sochocki-Plemelj formula ceases to work, therefore in order to find a spectral density one has to resort to different methods. In the spirit of the electrostatic analogy one introduces a potential [40–42]

$$\Phi(z,\bar{z},w,\bar{w}) := \left\langle \frac{1}{N}\ln\det[(z\mathbf{1}-X)(\bar{z}\mathbf{1}-X^\dagger)+|w|^2\mathbf{1}]\right\rangle \tag{22}$$

and its z gradient

$$g(z,\bar{z},w,\bar{w}) := \partial_z\Phi = \left\langle \frac{1}{N}\mathrm{Tr}\frac{\bar{z}\mathbf{1}-X^\dagger}{(z\mathbf{1}-X)(\bar{z}\mathbf{1}-X^\dagger)+|w|^2\mathbf{1}}\right\rangle. \tag{23}$$

The spectral density $\rho(z,\bar{z}) := \langle \frac{1}{N}\sum_{i=1}^{N}\delta^{(2)}(z-\lambda_i)\rangle$ is then given by the Poisson law

$$\rho(z,\bar{z}) = \frac{1}{\pi}\lim_{|w|\to 0}\partial_{\bar{z}}g(z,\bar{z},w,\bar{w}) = \lim_{|w|\to 0}\frac{1}{\pi}\partial_{z\bar{z}}\Phi(z,\bar{z},w,\bar{w}), \tag{24}$$

which simply follows from the representation of the two-dimensional Dirac δ (Poisson kernel)

$$\delta^{(2)}(z) = \lim_{\epsilon\to 0}\frac{1}{\pi}\frac{\epsilon^2}{(|z|^2+\epsilon^2)^2}. \tag{25}$$

The z gradient of the potential contains a quadratic expression in the denominator, which makes it inconvenient to calculate in the perturbative expansion. For the price of doubling the size of a considered matrix one can linearize g [22,24,26], introducing the generalized Green's function, which is a 2×2 matrix

$$\mathcal{G} = \begin{pmatrix}\mathcal{G}_{11} & \mathcal{G}_{1\bar{1}}\\ \mathcal{G}_{\bar{1}1} & \mathcal{G}_{\bar{1}\bar{1}}\end{pmatrix} := \left\langle \frac{1}{N}\mathrm{bTr}\begin{pmatrix} z\mathbf{1}-X & i\bar{w}\mathbf{1}\\ iw\mathbf{1} & \bar{z}\mathbf{1}-X^\dagger\end{pmatrix}^{-1}\right\rangle, \tag{26}$$

where we introduced a block trace operation, which, acting on $2N\times 2N$ matrices, yields a 2×2 matrix

$$\mathrm{bTr}\begin{pmatrix}A & B\\ C & D\end{pmatrix} = \begin{pmatrix}\mathrm{Tr}A & \mathrm{Tr}B\\ \mathrm{Tr}C & \mathrm{Tr}D\end{pmatrix}. \tag{27}$$

The components of the generalized Green's function read explicitly

$$\mathcal{G}_{11} = \left\langle \frac{1}{N}\mathrm{Tr}\frac{\bar{z}\mathbf{1}-X^\dagger}{(z\mathbf{1}-X)(\bar{z}\mathbf{1}-X^\dagger)+|w|^2\mathbf{1}}\right\rangle = \bar{\mathcal{G}}_{\bar{1}\bar{1}},$$
$$\mathcal{G}_{1\bar{1}} = \left\langle \frac{1}{N}\mathrm{Tr}\frac{-i\bar{w}}{(z\mathbf{1}-X)(\bar{z}\mathbf{1}-X^\dagger)+|w|^2\mathbf{1}}\right\rangle = -\bar{\mathcal{G}}_{\bar{1}1}. \tag{28}$$

One easily recognizes that the $\mathcal{G}_{11}$ entry of the generalized Green's function is exactly equal to (23). Moreover, the generalized Green's function can be written in the form

which resembles the complex Green's function for Hermitian matrices,

$$\mathcal{G}(Q) = \left\langle \frac{1}{N} \mathrm{bTr}(Q \otimes \mathbf{1}_N - \mathcal{X})^{-1} \right\rangle, \tag{29}$$

where Q is a 2×2 matrix representation of a quaternion and $\mathcal{X}$ is a duplicated matrix

$$Q := \begin{pmatrix} z & i\bar{w} \\ iw & \bar{z} \end{pmatrix}, \quad \mathcal{X} := \begin{pmatrix} X & 0 \\ 0 & X^\dagger \end{pmatrix}. \tag{30}$$

The generalized Green's function as a 2×2 matrix has a structure of a quaternion, therefore we refer to this also as the quaternionic Green's function [23].

Solving the random matrix problem for the spectral density, one always gets the entire generalized Green's function, obtaining the additional information stored in the off-diagonal elements of $\mathcal{G}$, which is as important as the spectral density itself.

A non-Hermitian matrix, if it is diagonalizable, possesses sets of left ($\langle L|$) and right ($|R\rangle$) eigenvectors, solving the eigenproblem

$$X|R_i\rangle = \lambda_i |R_i\rangle, \quad \langle L_i|X = \langle L_i|\lambda_i. \tag{31}$$

The eigenvectors are biorthogonal, i.e., they are constrained by the condition $\langle L_i|R_j\rangle = \delta_{ij}$, but they are not orthogonal among themselves $\langle L_i|L_j\rangle \neq \delta_{ij}$. The biorthogonality condition leaves freedom of rescaling each eigenvector by a nonzero complex number $|R_i\rangle \to c_i|R_i\rangle$ with $\langle L_i| \to \langle L_i|c_i^{-1}$, and of multiplication by a unitary matrix $|R_i\rangle \to U|R_i\rangle$ with $\langle L_i| \to \langle L_i|U^\dagger$. The vectors obtained by the latter transformation are no longer the eigenvectors of X, but of another matrix $UXU^\dagger$, which lies on the orbit of X under the symmetry group of the joint pdf (20). The simplest nontrivial quantity invariant under these transformations is the matrix of overlaps $O_{\alpha\beta} := \langle L_\alpha|L_\beta\rangle\langle R_\beta|R_\alpha\rangle$. Only for normal matrices $O_{ij} = \delta_{ij}$, therefore the overlaps can be thought of as a measure of non-normality of a matrix.

Chalker and Mehlig introduced in Ref. [43] a one-point correlation function associated with the diagonal part of the overlap matrix, being the special case of the Bell-Steinberger matrix [44]

$$O_N(z,\bar{z}) := \left\langle \frac{1}{N^2} \sum_{\alpha=1}^{N} O_{\alpha\alpha} \delta^{(2)}(z - \lambda_\alpha) \right\rangle. \tag{32}$$

In the large N limit the eigenvector correlation function is given by the product of off-diagonal elements of the quaternionic Green's function [27,45],

$$O(z,\bar{z}) := \lim_{N\to\infty} O_N(z,\bar{z}) = -\frac{1}{\pi} \lim_{|w|\to 0} \lim_{N\to\infty} \mathcal{G}_{1\bar{1}}\mathcal{G}_{\bar{1}1}. \tag{33}$$

The diagonal overlaps $O_{\alpha\alpha}$ are the squares of the eigenvalue condition numbers, $O_{\alpha\alpha} = \kappa^2(\lambda_\alpha)$, known in the numerical analysis community to play the significant role in the stability of the spectrum against additive perturbations [46,47]. The Cauchy-Schwartz inequality gives a bound $O_{ii} \geqslant 1$ and the inequality is saturated for normal matrices. The ratio $O_N(z,\bar{z})/\rho(z,\bar{z})$ gives a conditional expectation of the squared eigenvalue condition number [27]

$$\frac{O_N(z,\bar{z})}{\rho(z,\bar{z})} = \mathbb{E}\left(\frac{1}{N}\kappa^2(\lambda_\alpha) \middle| z = \lambda_\alpha \right). \tag{34}$$

B. Large N expansion of the quaternionic Green's function and Feynman diagrams

The procedure for the calculation of the quaternionic Green's function is only slightly modified, compared to the Hermitian case. Again, the unitary invariance of the pdf asserts that the untraced resolvent has a trivial structure $\langle (Q \otimes \mathbf{1} - \mathcal{X})^{-1}\rangle = \mathcal{G} \otimes \mathbf{1}$. We write the geometric series

$$\begin{aligned} &\mathcal{G}(Q) \otimes \mathbf{1} \\ &\quad = \mathcal{Q}^{-1} + \langle \mathcal{Q}^{-1}\mathcal{X}\mathcal{Q}^{-1}\rangle + \langle \mathcal{Q}^{-1}\mathcal{X}\mathcal{Q}^{-1}\mathcal{X}\mathcal{Q}^{-1}\rangle + \cdots, \end{aligned} \tag{35}$$

where $\mathcal{Q} = Q \otimes \mathbf{1}$. Now, due to the block structure originating from the linearization, all objects in the above expansion, apart from the matrix indices, possess additional indices $(1,\bar{1})$ enumerating the blocks of $\mathcal{X}$ and the elements of the quaternion. The block trace operation taken at the end of the calculations is in fact the partial trace over the matrix space.

To calculate the averages, we decompose the pdf into Gaussian and residual parts. The most general, allowed by the Hermiticity condition, Gaussian part of the potential (20) can be written in a convenient form with $\sigma > 0$ and $\tau \in (-1,1)$,

$$\begin{aligned} &P_G(X,X^\dagger) \\ &\quad \sim \exp\left[-\frac{N}{\sigma^2} \frac{1}{1-\tau^2} \left(\mathrm{Tr} X X^\dagger - \frac{\tau}{2} \mathrm{Tr}[X^2 + (X^\dagger)^2] \right) \right]. \end{aligned} \tag{36}$$

The propagator therefore reads

$$\left\langle \mathcal{X}_{ab}^{\alpha\beta} \mathcal{X}_{cd}^{\mu\nu} \right\rangle_G = \frac{\sigma^2}{N} [1 + (\tau - 1)\delta_{\alpha\mu}] \delta_{\alpha\beta}\delta_{\mu\nu}\delta_{ad}\delta_{bc}, \tag{37}$$

where the Greek indices take values from $\{1,\bar{1}\}$ and the Latin ones from $\{1,2,\ldots,N\}$. The residual part is expanded into a power series, bringing additional matrices (vertices in the diagrammatic representation), and all averages are then calculated with respect to the Gaussian measure, which by means of the Wick's theorem reduces to the summation over all possible pairings. The diagrammatic rules are exactly the same as in the Hermitian case, apart from the additional Greek indices, carried by each dot. In this paper we do not exploit the index structure explicitly; for a thorough calculation involving Gaussian matrices we refer to [6].

C. Quaternionic R transform

The structure of the Feynman diagrams is exactly the same as for Hermitian matrices, but now the objects that we calculate are 2×2 matrices. The Schwinger-Dyson equation relating the quaternionic Green's function with the self-energy composed of 1LI diagrams then reads

$$\mathcal{G}(Q) = [Q - \Sigma(Q)]^{-1}. \tag{38}$$

Now, due to the fact that in general X is not related with $X^\dagger$, there are many types of cumulants in the expansion

TABLE I. Comparison between corresponding quantities in Hermitian vs non-Hermitian ensembles.

	Hermitian	Non-Hermitian
Spectrum	real	complex
Green's	complex valued	quaternion valued
function	$G(z)=\frac{1}{N}\langle \mathrm{Tr}(z-H)^{-1}\rangle$	$\mathcal{G}(Q)=\frac{1}{N}\langle \mathrm{bTr}(Q-\mathcal{X})^{-1}\rangle$
Moments	$\tilde{M}(z)=\frac{1}{z}G\left(\frac{1}{z}\right)\frac{1}{z}-\frac{1}{z}$	$\tilde{\mathcal{M}}(Q)=Q^{-1}\mathcal{G}(Q^{-1})Q^{-1}-Q^{-1}$
Cumulants	$R(z)=\sum_n \kappa_n z^{n-1}$	$[\mathcal{R}(Q)]_{\alpha\beta}=\sum_{k,\{i_1\ldots i_{k-2}\}} c^{(k)}_{\alpha i_1\ldots i_{k-2}\beta} Q_{\alpha i_1}\ldots Q_{i_{k-2}\beta}$
S-D eqs.	$R(G(z))+\frac{1}{G(z)}=z$	$\mathcal{R}(\boldsymbol{\mathcal{G}}(Q))+(\mathcal{G}(Q))^{-1}=Q$

of $\mathcal{G}$, corresponding to the connected averages of different words, separated by a horizontal line (appropriate component of Q^{-1}), e.g., $c_{1\bar{1}1\bar{1}}=\langle\frac{1}{N}\mathrm{Tr}XX^\dagger XX^\dagger\rangle_c\neq\langle\frac{1}{N}\mathrm{Tr}XXX^\dagger X^\dagger\rangle_c=c_{11\bar{1}\bar{1}}$. Remarkably, all possible cumulants are stored in a single object, the quaternionic R transform, which itself is a 2×2 matrix representation of the quaternion, defined as follows:

$$\mathcal{R}(Q)\otimes\mathbf{1}=\langle\mathcal{X}\rangle_c+\langle\mathcal{X}Q\mathcal{X}\rangle_c+\langle\mathcal{X}Q\mathcal{X}Q\mathcal{X}\rangle_c+\cdots, \tag{39}$$

more explicitly

$$\mathcal{R}(Q)_{\alpha\beta}=c^{(1)}_{\alpha}\delta_{\alpha\beta}+c^{(2)}_{\alpha\beta}Q_{\alpha\beta}+\sum_{\gamma\in\{1,\bar{1}\}}c^{(3)}_{\alpha\gamma\beta}Q_{\alpha\gamma}Q_{\gamma\beta}+\sum_{\gamma,\epsilon\in\{1,\bar{1}\}}c^{(4)}_{\alpha\gamma\epsilon\beta}Q_{\alpha\gamma}Q_{\gamma\epsilon}Q_{\epsilon\beta}+\cdots. \tag{40}$$

This definition is quite compact and deserves a more intuitive explanation. Suppose that we know all cumulants and we want to construct the $\mathcal{R}$ transform. We naturally associate $\bar{1}$ in the index of the cumulant with $\dagger$ in the corresponding expression in X's. The first and the last index of the cumulant give us the appropriate component of $\mathcal{R}$. Starting from the first index, we move towards the rightmost one and each time we make a step between two indices, we pick the component of Q given by the indices we encounter. Q therefore can be considered as a transfer matrix. The cumulant $c^{(4)}_{\alpha\beta\gamma\epsilon}=\langle\frac{1}{N}\mathrm{Tr}X^\alpha X^\beta X^\gamma X^\epsilon\rangle_c$ comes with the expression $Q_{\alpha\beta}Q_{\beta\gamma}Q_{\gamma\epsilon}$ in $\mathcal{R}_{\alpha\beta}$. For example, $c_{111\bar{1}}$ appears with $Q_{11}Q_{11}Q_{1\bar{1}}=z^2(i\bar{w})$ in $\mathcal{R}_{1\bar{1}}$. The ability to store all mixed cumulant in a single object relies on the fact that $\mathcal{Q}$ and $\mathcal{X}$ do not commute. The mapping between $\mathcal{R}$ transform and the cumulants is not bijective, there are different cumulants, which bring the same expression in the components of Q to the quaternionic R transform.[2] For the one-to-one mapping, one has to consider either different Q's in the expansion (39) or a single Q, but with entries from a noncommutative algebra.

The relation between the self-energy and the quaternionic Green's function through the connected diagrams can be expressed via the quaternionic R transform $\Sigma(Q)=\mathcal{R}(\mathcal{G}(Q))$. A direct relation between the generalized Green's function and the quaternionic R transform can be written in terms of the auxiliary function, nicknamed Blue's function, which is the functional inverse of the quaternionic Green's function $\mathcal{B}(\mathcal{G}(Q))=Q=\mathcal{G}(\mathcal{B}(Q))$. The $\mathcal{R}$ transform is then given by $\mathcal{R}(Q)=\mathcal{B}(Q)-Q^{-1}$. The inverse of Q is understood as the matrix inverse.

The R transform for non-Hermitian matrices was discovered in Refs. [15,22] as a function generating all 1LI diagrams. The quaternionic structure was discovered much later [23].

We remark here that the mixed moments are encoded in the same way in the quaternionic moment generating function

$$\tilde{\mathcal{M}}(Q)=Q^{-1}\mathcal{G}(Q^{-1})Q^{-1}-Q^{-1}. \tag{41}$$

We conclude this section by a comparison of two formalisms (Table I), using calligraphic notation in the case of non-Hermitian analogs of Hermitian entries.

In the next section we demonstrate how, in the case of **R**-diagonal operators, the general formalism for non-Hermitian ensembles reduces to quasi-Hermitian formalism for biunitary invariant ensembles.

IV. BIUNITARILY INVARIANT RANDOM MATRICES

The presented construction for non-Hermitian random matrices, despite its neatness, suffers from a limited practical usage due to the procedure of functional inversion on route from the R transform to the quaternionic Green's function. Even in the calculation for Hermitian matrices we are limited by the degree of the polynomial equation that we have to solve.

There are classes of random matrices, the quaternionic R transform of which can be calculated from simpler objects, because the spectrum of such matrices is one dimensional and matrices are normal. An embedding of complex transforms of Hermitian matrices to the general setting of quaternionic transforms in the non-Hermitian world was rendered by [23]. Later, an analogous embedding has been conducted for unitary matrices [48].

In this section we discuss another class of random matrices, the spectrum of which, despite being complex, is effectively one dimensional, because the spectral problem has an azimuthal symmetry. We consider matrices generated according to the probability distribution function $P(X,X^\dagger)\sim\exp[-N\mathrm{Tr}V(XX^\dagger)]$. The symmetry in this case is enhanced from $U(N)$ to $U(N)\times U(N)$. The spectrum of X is rotationally symmetric on the complex plane $\rho(z,\bar{z})=\rho_r(|z|)$ and the entire information is encoded in the radial cumulative distribution function $F(s)=\int_{|z|\leqslant s}\rho(z,\bar{z})d^2z=2\pi\int_0^s s'\rho_r(s')ds'$. Such matrices are the natural extensions of the so called isotropic complex random variables, the distribution of which

[2]For example a pair $c^{(6)}_{11\bar{1}1\bar{1}1}$ and $c^{(6)}_{1\bar{1}11\bar{1}1}$.

depends only on their modulus. Moreover, the symmetry transformations can bring the matrix to the diagonal form with the singular values on the diagonal. It is natural, therefore, to expect all spectral properties of X to be determined by its singular values.

In the free probability community such objects are called **R** diagonal; the meaning of this notion shall become clear later. The **R**-diagonal operators have a polar decomposition $X = PU$, where P is Hermitian positive definite, U is Haar unitary, and P and U are mutually free. In the limit $N \to \infty$ biunitarily invariant random matrices become the R-diagonal operators, which was shown by Hiai and Petz [49, Theorem 4.4.5].

The first relation between the Green's function of $XX^\dagger$, encoding the distribution of the squares of the singular values, and the radial cumulative distribution was found by Feinberg and Zee [15]. They also found a very intriguing property that the support of the spectrum of such matrix is either a disk or an annulus, which bears the name of the single-ring theorem. Later, Haagerup and Larsen [17] within the framework of free probability derived a simple relation between the S transform of $XX^\dagger$ and the radial cumulative distribution function

$$S_{XX^\dagger}[F(s) - 1] = \frac{1}{s^2}. \tag{42}$$

Recently [27], this theorem has been extended to describe also the eigenvector correlation function

$$O(s) = \frac{F(s)[1 - F(s)]}{\pi s^2}. \tag{43}$$

The relation between eigenvalues and squared singular values of biunitarily invariant random matrices has been pushed much further by Kieburg and Kösters who found an explicit integral transform between their joint pdfs [50].

We remark here that the expression on the right-hand side of the equality above has already appeared in the pioneering paper by Feinberg and Zee [15], but without any connection to eigenvectors.

A. 1PI diagrams

Due to the particular form of the potential, namely that X and $X^\dagger$ appear alternately, and the planarity of diagrams in the large N limit, the structure of diagrams simplifies considerably.

The only nonvanishing cumulants correspond to the expressions where X and $X^\dagger$ are alternating, i.e., $\alpha_n := \langle \frac{1}{N}\mathrm{Tr}(XX^\dagger)^n\rangle_c = c^{(2n)}_{1\bar{1}1\bar{1}\ldots1\bar{1}} = c^{(2n)}_{\bar{1}1\bar{1}1\ldots\bar{1}1}$. Let us consider a generating function for all such cumulants $A(x) := \sum_{k=1}^{\infty} \alpha_k z^{k-1}$. In the free probability context it is also known as the determining sequence [11]. Due to the very simple structure of nonvanishing cumulants, only one (commuting) variable is sufficient to encode all cumulants.

According to the prescription (40), the quaternionic R transform for biunitarily invariant random matrices reads

$$\mathcal{R} = A(-|w|^2)\begin{pmatrix} 0 & i\bar{w} \\ iw & 0 \end{pmatrix}. \tag{44}$$

The R transform depends only on the off-diagonal elements of the quaternion, which is a consequence of the fact that $X^\dagger$ has to be sandwiched between X's and vice versa. In the "hermitization" approach to non-Hermitian matrices, the corresponding R transform is diagonal.

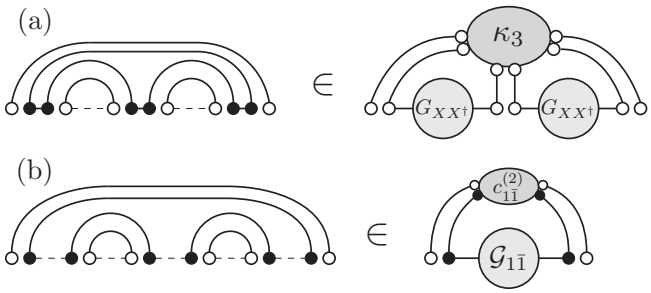

FIG. 3. The average $\langle (XX^\dagger)^3\rangle$ with respect to the Gaussian measure $\exp(-N\mathrm{Tr}XX^\dagger)$ produces the same vertices which are classified to different types of 1LI diagrams, depending on at which expansion it appears. Diagram (a) appears in the expansion of the complex resolvent of $XX^\dagger$, while (b) is in the expansion of the quaternionic Green's function of X. To distinguish between X and $X^\dagger$ we denote the first by double dots with white on the left, while for $X^\dagger$ it is the other way around. Two neighboring black dots joined by a solid line denote matrix multiplication. The loop formed from the black dots and propagators in (a) becomes an internal line of the cumulant κ_3 of $XX^\dagger$. The appearance of additional horizontal dashed lines (appropriate components of Q^{-1}) in (b) classifies this diagram to a different class of 1LI diagrams.

B. Relation between R transform of $XX^\dagger$ and the quaternionic R transform of X

Before we find a relation between the R transforms, let us briefly explain why the alternating cumulants in the expansion of the quaternionic Green's function of X are not the same as the corresponding ones of $XX^\dagger$. In both cases we consider moments like $\langle \frac{1}{N}\mathrm{Tr}(X^\dagger X)^k\rangle$ in the moment expansion of the Green's function of $XX^\dagger$. The average is taken over the probability measure proportional to $\exp[-N\mathrm{Tr}V(X^\dagger X)]dXdX^\dagger$. There are two ways of calculating such an object.

First, making use of the symmetry of the potential, one changes the integration measure from $dXdX^\dagger$ into $d(XX^\dagger)$ and uses the tools for Hermitian matrices. In this approach, however, the resulting Jacobian modifies the form of the potential, which changes the structure of the vertices in the expansion of the Green's function.

In the diagrammatic approach for non-Hermitian problems, we circumvent the calculation of the Jacobian, calculating the averages with respect to the original measure. We remind that the connected diagrams contributing to the kth cumulant originate from the k matrices separated by horizontal lines. In the expansion of the Green's function of $XX^\dagger$ the matrices X and $X^\dagger$ are merged and treated as a new single object, which gives rise to the new connected diagrams. Some propagators become internal lines, changing the topology of the diagrams and producing effectively new types of vertices. The notion of 1LI diagrams is always tied to the Green's function, the expansion of which is taken under consideration.

In Fig. 3 we present how the third cumulant of $XX^\dagger$ emerges from propagators, which are the only allowed lines for the quadratic potential. Such a mechanism is at the heart of the

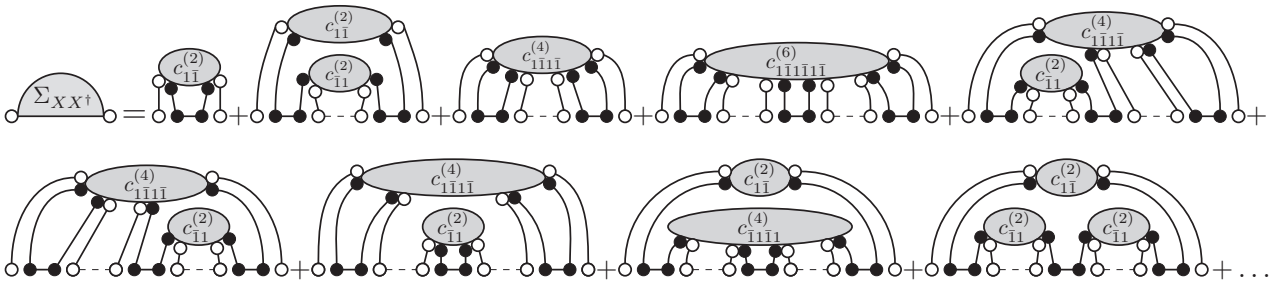

FIG. 4. Several lowest order 1PI diagrams contributing to $\Sigma_{XX^\dagger}$.

powerful linearization technique, which allows for calculation of spectra of products [39,51–53], polynomials [54,55], and even of the rational expressions of random matrices [56].

Let us consider the expansion of the complex resolvent of $XX^\dagger$,

$$G_{XX^\dagger}(z)\mathbf{1} = \frac{\mathbf{1}}{z} + \left\langle \frac{\mathbf{1}}{z} XX^\dagger \frac{\mathbf{1}}{z} \right\rangle + \left\langle \frac{\mathbf{1}}{z} XX^\dagger \frac{\mathbf{1}}{z} XX^\dagger \frac{\mathbf{1}}{z} \right\rangle + \cdots . \tag{45}$$

Let us focus on 1PI diagrams, the simplest of which are presented in Fig. 4. All vertices are already summed, such that we depicted cumulants. Let us notice that in order to have a 1LI diagram, the leftmost X has to be connected with the rightmost $X^\dagger$ through some cumulant. The matrices in between legs of the outermost cumulant can be connected in any manner. Further, we use the fact that the term $\frac{\mathbf{1}}{z}$ commutes with X and $X^\dagger$, therefore we can rearrange diagrams, so that the resulting diagrams in between legs are the ones of the Green's function of either $XX^\dagger$ or $X^\dagger X$. The missing $\mathbf{1}/z$ terms are encapsulated by considering $zG(z)$. The general structure of the diagrams, presented graphically in Fig. 5, is now clear. The equation generated by these diagrams reads

$$\begin{aligned}\Sigma_{XX^\dagger}(z) &= c^{(2)}_{1\bar{1}} zG_{X^\dagger X}(z) + c^{(4)}_{1\bar{1}1\bar{1}} zG_{X^\dagger X}(z) \\ &\quad \times G_{XX^\dagger}(z) zG_{X^\dagger X}(z) + \cdots \qquad (46)\\ &= zG_{X^\dagger X}(z) \sum_{k=1}^{\infty} \alpha_k [zG_{X^\dagger X}(z) G_{XX^\dagger}(z)]^{k-1} \\ &= zG_{X^\dagger X}(z) A[zG_{X^\dagger X}(z) G_{XX^\dagger}(z)]. \qquad (47)\end{aligned}$$

Using the general relation between the self-energy and the Green's function (13), we arrive at

$$R_{XX^\dagger}(G_{XX^\dagger}(z)) = zG_{X^\dagger X}(z) A(zG_{X^\dagger X}(z) G_{XX^\dagger}(z)). \tag{48}$$

Knowing that for square matrices $G_{XX^\dagger} = G_{X^\dagger X}$, which follows from cyclicity of the trace, we can associate these objects and skip the subscript for simplicity. Let us also make a substitution $z \to B(z)$ and make use of the fact that B is a functional inverse of G, to finally obtain

$$R(z) = zB(z) A(z^2 B(z)). \tag{49}$$

This relation is convenient if knowing the quaternionic R transform of X one wants to calculate the complex R transform of $XX^\dagger$. To invert this relation, let us introduce an auxiliary variable $y := z^2 B(z)$. Note that $zR(z) + 1 = zB(z) = yA(y) + 1$.

Introducing yet another variable t given by $z =: tS(t)$, where $S(z)$ is the S transform and using the relation between R and S transforms (16), we obtain

$$t = yA(y) \quad \text{and} \quad y = t(t+1)S(t). \tag{50}$$

Let us introduce another auxiliary transform $K(z)$ related to A in a similar way as R is related with S, namely

$$A(z)K(zA(z)) = 1, \quad K(z)A(zK(z)) = 1. \tag{51}$$

This definition says that $zK(z)$ is a functional inverse of $zA(z)$. Such an inversion is always possible for nonzero **R**-diagonal operators, since $A(0) = c^{(2)}_{1\bar{1}} = \langle \frac{1}{N} \mathrm{Tr} XX^\dagger \rangle$. The last auxiliary variable u, which we define via $y =: uK(u)$, transfers (50) into

$$t = u \quad \text{and} \quad uK(u) = t(t+1)S(t). \tag{52}$$

This gives us the simple relation between K and S,

$$S(t) = \frac{1}{1+t} K(t). \tag{53}$$

The S transform of $XX^\dagger$ is therefore related to the determining sequence of X via

$$S(zA(z)) = \frac{1}{A(z)[1 + zA(z)]}. \tag{54}$$

This relation is crucial in the derivation of the Haagerup-Larsen theorem, as we demonstrate in the next section. One can apply the relation between R and S transforms (16) to obtain an

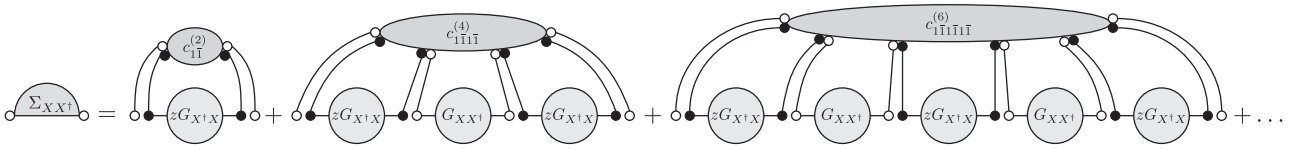

FIG. 5. General structure of 1PI diagrams in the resolvent expansion of $XX^\dagger$.

equation which allows us to calculate A from R,

$$R\left(\frac{z}{1+zA(z)}\right) = [1+zA(z)]A(z). \tag{55}$$

We remark that the relations (49) and (55) were known earlier in terms of coefficients of their expansions around $z=0$ [34, Proposition 15.6]. The functional relation, which is more operational, and all intermediate steps are the alternative approach.

To summarize this part, we have introduced a set of auxiliary transforms in order to relate the R transform of $XX^\dagger$ with the determining sequence $A(z)$, being the cornerstone of the quaternionic R transform of **R**-diagonal matrices. In Fig. 6 we provide a guide through all transformations.

C. Haagerup-Larsen theorem

Using the above formalism we rederive in a compact way Eqs. (42) and (43).

Making use of the form of the quaternionic R transform (44) and the relation $\mathcal{R}(\mathcal{G})+\mathcal{G}^{-1}=\mathcal{B}(\mathcal{G})=\mathcal{Q}$, we obtain the matrix equation

$$A(\mathcal{G}_{1\bar{1}}\mathcal{G}_{\bar{1}1})\begin{pmatrix}0 & \mathcal{G}_{1\bar{1}}\\ \mathcal{G}_{\bar{1}1} & 0\end{pmatrix} + \frac{1}{\mathcal{G}_{11}\mathcal{G}_{\bar{1}\bar{1}}-\mathcal{G}_{1\bar{1}}\mathcal{G}_{\bar{1}1}} \times \begin{pmatrix}\mathcal{G}_{\bar{1}\bar{1}} & -\mathcal{G}_{1\bar{1}}\\ -\mathcal{G}_{\bar{1}1} & \mathcal{G}_{11}\end{pmatrix} = \begin{pmatrix}z & i\bar{w}\\ iw & \bar{z}\end{pmatrix}. \tag{56}$$

We are now interested in calculating the spectral density and the eigenvector correlator, so we set $|w|\to 0$. Let us first consider the upper-left component of matricial Eq. (56):

$$\frac{\mathcal{G}_{\bar{1}\bar{1}}}{\mathcal{G}_{11}\mathcal{G}_{\bar{1}\bar{1}}-\mathcal{G}_{1\bar{1}}\mathcal{G}_{\bar{1}1}} = z. \tag{57}$$

The $\bar{1}\bar{1}$ component gives the complex conjugate of the above. Combining them we easily deduce that $z\mathcal{G}_{11}=\bar{z}\mathcal{G}_{\bar{1}\bar{1}}$. Denoting $F:=z\mathcal{G}_{11}$ [15], we immediately obtain from (57) that

$$O(z,\bar{z}) = -\frac{1}{\pi}\mathcal{G}_{1\bar{1}}\mathcal{G}_{\bar{1}1} = \frac{F-F^2}{\pi|z|^2}. \tag{58}$$

Considering now the $1\bar{1}$ component we obtain two possibilities. First $\mathcal{G}_{1\bar{1}}=0$ and in consequence $\mathcal{G}_{11}=\frac{1}{z}$, which is a trivial solution, valid outside the spectrum. Second, assuming $\mathcal{G}_{1\bar{1}}\neq 0$ we use (58) to arrive at

$$A(\mathcal{G}_{1\bar{1}}\mathcal{G}_{\bar{1}1})\mathcal{G}_{1\bar{1}}\mathcal{G}_{\bar{1}1} = F-1. \tag{59}$$

Now, evaluating the S transform at both sides of the equation above, exploiting the relation between S and A (54), and using (58) once again, we finally get

$$S(F-1) = \frac{1}{A(\mathcal{G}_{1\bar{1}}\mathcal{G}_{\bar{1}1})[1+\mathcal{G}_{1\bar{1}}\mathcal{G}_{\bar{1}1}A(\mathcal{G}_{1\bar{1}}\mathcal{G}_{\bar{1}1})]} = \frac{1}{|z|^2}, \tag{60}$$

which is the statement of the original formulation of the Haagerup-Larsen theorem. One deduces that F depends on z and $\bar{z}$ only through their modulus, therefore the spectral density can be calculated by [15]

$$\rho(z,\bar{z}) = \frac{1}{\pi}\partial_{\bar{z}}\mathcal{G}_{11} = \frac{1}{2\pi|z|}F'(|z|). \tag{61}$$

Moreover, outside the support of the spectral density, the trivial solution gives $F=1$, therefore F is indeed the radial cumulative distribution function. The inner and outer radii of the spectrum can be calculated by imposing $F=1$ (outer) or that F is equal to the fraction of the zero modes (inner) and solving the resulting equation for $|z|$. In general, (60) can yield several solutions for F. The uniqueness of the radial cumulative distribution function has been shown within the framework of the analytic subordination function theory [21].

Multiplying (60) by $(F-1)$, evaluating the R transform on both sides of the equation and making use of (16), we obtain

$$R_{XX^\dagger}\left(\frac{F-1}{r^2}\right) = r^2. \tag{62}$$

Substituting $F=1$ and taking into account that $R(0)=\kappa_1=m_1$, we relate the external radius with the first moment of $XX^\dagger$.

Using the relation $S_X(z)S_{X^{-1}}(-1-z)=1$ [57] and performing analogous computations, we arrive at

$$R_{(XX^\dagger)^{-1}}(-Fr^2) = \frac{1}{r^2}. \tag{63}$$

Substitution $F=0$ relates the first inverse moment of $XX^\dagger$ with the internal radius. To summarize, the internal and external radii are given by

$$r_{\text{ext}}^2 = \int x\rho_{XX^\dagger}(x)dx, \quad r_{\text{in}}^{-2} = \int x^{-1}\rho_{XX^\dagger}(x)dx, \tag{64}$$

which was observed independently in Refs. [16,17].

D. Addition and multiplication of *R*-diagonal matrices

The problem of addition of unitarily invariant non-Hermitian random matrices was posed and solved a long time ago [15,22]. It turns out that the quaternionic R transform is additive under the addition of non-Hermitian matrices, generalizing the result from free probability. Due to the particular form of the quaternionic R transform for biunitarily invariant large random matrices **R**-diagonal operators, their addition boils down to the addition of the corresponding determining sequences.

The multiplication is also straightforward for the reason that the entire one-point spectral information is encoded in the S transform of $XX^\dagger$, by virtue of the Haagerup-Larsen theorem. Yet, the matrix $ABB^\dagger A^\dagger$ has the same eigenvalues as $BB^\dagger A^\dagger A$, and if A and B are free, then $S_{ABB^\dagger A^\dagger}(z)=S_{A^\dagger A}(z)S_{BB^\dagger}(z)$, which shows that the S transform of $XX^\dagger$ is multiplicative.

We remark here that the rules for multiplication and addition of **R**-diagonal operators were known in free probability, but were given in terms of a boxed convolution of determining sequences with an auxiliary Möbius sequence [11]. Our approach, which uses functions instead of the coefficients of their expansion is more operational. Together with the Haagerup-Larsen theorem this allows us to calculate spectral densities and the eigenvector correlator easily. The presented functional approach is complementary to the special case of the rectangular free probability [58]. Within the latter formalism, when adding **R**-diagonal operators, one deals with a symmetrized distribution of $X^\dagger X$, while our approach provides a very simple prescription for calculation of an additive quantity. Moreover, the explicit form of the quaternionic R transform enables us also for addition with non-Hermitian random matrices which are not biunitarily invariant.

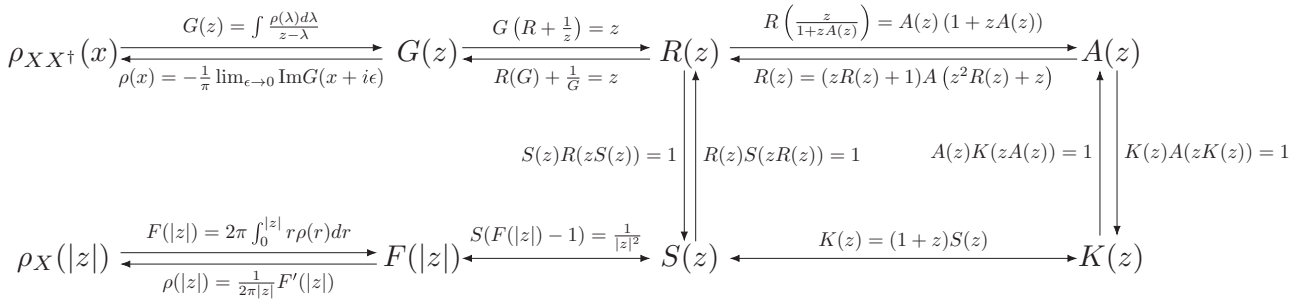

FIG. 6. Diagram of intermediate transforms, linking the spectral density of squared singular values and the radial profile of the eigenvalue density. The diagram also present the relation and all intermediate steps between the R-transform of squared singular values and the determining sequence of an **R**-diagonal operator. The lower left branch is discussed in Sec. IV C.

E. Abelization

One way of generating complex isotropic variables is given in terms of the radial profile of the corresponding pdf. Its natural extension for noncommutative random variables is given by the Haagerup-Larsen theorem.

The radial distribution $\rho_r(|z|)$ of an isotropic complex random variable $z=x+iy$ can be also recovered from the marginal distribution of its real part,

$$\rho_x(x)=\int_{-\sqrt{R^2-x^2}}^{\sqrt{R^2-x^2}}\rho(|z|)dy=2\int_x^\infty \frac{\rho(r)rdr}{\sqrt{r^2-x^2}}. \tag{65}$$

Here R is the radius of the support of the distribution, which can be infinite. The last integral is the Abel transform of the radial profile, which can be inverted via

$$\rho(r)=-\frac{1}{\pi}\int_r^\infty \frac{d\rho_x(x)}{dx}\frac{dx}{\sqrt{x^2-r^2}}, \tag{66}$$

giving the exact one-to-one mapping between radial density profile of a complex number and the distribution of its real part.

One can ask whether a counterpart of this relation exists in the noncommutative free probability. Biely and Thurner [5] conjectured that the Abel transform directly transfers to matrices. Later, it was pointed out that the Abel transform does not give a proper spectral density for the product of two GUE matrices [51]. Recently, the authors has shown that such a procedure, coined as Abelization, works for normal matrices, the spectrum of which possesses an azimuthal symmetry [6]. The biunitarily invariant matrices are in general not normal, which can be seen from the fact that the eigenvector correlation function $O(|z|)$ does not vanish.

Consider now the R transform of the matrix $X+X^\dagger$, which is twice the Hermitian part of X. This matrix appears in the description of the transient regime of a linear dynamical system [59]. Its cumulants can be related to the non-Hermitian cumulants, encoded in the determining sequence, via

$$\begin{aligned} R_{X+X^\dagger}(z)&=\sum_{k=1}^\infty z^{k-1}\left\langle\frac{1}{N}\mathrm{Tr}(X+X^\dagger)^k\right\rangle_c \\ &=\sum_{k=1}^\infty 2z^{2k-1}\left\langle\frac{1}{N}\mathrm{Tr}(XX^\dagger)^k\right\rangle_c=2zA_X(z^2). \end{aligned} \tag{67}$$

In the second equality we have used the fact that the only nonvanishing cumulants of the **R**-diagonal operators are $\alpha_k=\langle\frac{1}{N}\mathrm{Tr}(XX^\dagger)^k\rangle_c$, which can be extracted from the even powers of $X+X^\dagger$ exactly in two ways. The connected cumulants are encoded in the determining sequence A instead of the R transform of $XX^\dagger$, because in the expansion of the Green's function of $X+X^\dagger$ matrices X and $X^\dagger$ are separated by either $\frac{1}{z}$ term or a plus sign.

V. APPLICATIONS OF THIS FORMALISM

A. Quaternionic R transform of Haar unitary matrix

We consider a unitary matrix $UU^\dagger=\mathbf{1}$, the spectral density of which is uniform on the unit circle. Due to unitarity, $R_{UU^\dagger}(z)=1$ and from (16) $S(z)=1$, hence $K(z)=1+z$. Substituting $z\to xA(x)$ and using (51), we obtain the quadratic equation

$$xA^2(x)+A(x)-1=0. \tag{68}$$

Knowing that $A(0)=c_{1\bar{1}}=\langle\frac{1}{N}\mathrm{Tr}UU^\dagger\rangle_c=1$, we choose the appropriate branch of the solution. From (44) we deduce the quaternionic R transform, which reads

$$\mathcal{R}(Q)=\frac{1-\sqrt{1-4|w|^2}}{2|w|^2}\begin{pmatrix}0 & i\bar{w}\\ iw & 0\end{pmatrix}. \tag{69}$$

The same result was derived in Ref. [48] using a different technique. We remark that the free cumulants are $\alpha_n=(-1)^{n-1}C_{n-1}$, where $C_{n-1}=\frac{1}{n+1}\binom{2n}{n}$ are the Catalan numbers, in agreement with [60].

B. Free non-Hermitian Poisson

In Hermitian free probability, the counterpart of the Poisson distribution is the Wishart distribution, which has all cumulants the same, equal to q. The matrix model corresponding to this distribution is constructed as follows. Take X a $N\times T$ rectangular matrix with independent identically distributed (iid) normal complex entries. The spectral density of $\frac{1}{T}XX^\dagger$ in the limit $N,T\to\infty$ with $T/N=q$ fixed is given by the Wishart law.

Let us consider now the isotropic ensemble with all $\alpha_n=\lim_{N\to\infty}\langle\frac{1}{N}\mathrm{Tr}(XX^\dagger)^n\rangle_c=q$ the same for any $n\geqslant 1$ and vanishing all other mixed cumulants. The generating sequence is therefore $A(z)=\sum_{k=1}^\infty qz^{k-1}=\frac{q}{1-z}$. The S trans-

form reads $S(z) = [(1+z)(q+z)]^{-1}$ and the application of the Haagerup-Larsen theorem yields $F(r) = \frac{1-q+\sqrt{(q-1)^2+4r^2}}{2}$, where the positive branch of the solution was taken, so that the cumulative distribution function (cdf) is increasing. We easily recover the spectral density and the eigenvector correlator,

$$\rho(r) = \max(0,1-q)\delta^{(2)}(z) + \frac{1}{\pi\sqrt{(1-q)^2+4r^2}}\theta(\sqrt{q}-r), \tag{70}$$

$$O(r) = \frac{q\sqrt{(q-1)^2+4r^2} - q^2 + q - 2r^2}{2\pi r^2}\theta(\sqrt{q}-r). \tag{71}$$

Remarkably, the spectral density corresponds to the density of eigenvalues in the model $\frac{1}{T}XY^\dagger$, where X and Y are independent $N \times T$ matrices the entries of which are iid normal complex, considered in the limit $N,T \to \infty$, with $q = T/N$ fixed [53], generalizing the result from the Hermitian case.

C. Cumulants of products of Ginibre matrices

Let X be a complex Ginibre matrix. The S transform of $XX^\dagger$ reads $S(z) = (1+z)^{-1}$. Let us consider a product of k independent Ginibre matrices. The multiplication law leads to $S_k = (1+z)^{-k}$. Using the relation (54) we obtain the algebraic equation for the determining sequence,

$$[zA_k(z)+1]^{k-1} = A_k(z). \tag{72}$$

The solution can be written in a power series [61]

$$A_k(z) = \sum_{n=1}^{\infty} A_{n-1}(k-1,k-1)z^{n-1}, \tag{73}$$

where

$$A_n(p,r) = \frac{r}{np+r}\binom{np+r}{m} = \frac{r}{n!}\prod_{i=1}^{n-1}(mp+r-i) \tag{74}$$

are the two parameter Fuss-Catalan numbers, also known as Raney numbers. The **R**-diagonal cumulants are therefore $\alpha_n^{(k)} = A_{n-1}(k-1,k-1) = A_n(k,1)$. Such numbers have appeared in the free probability many times [62–64] and densities associated with them have been extensively studied [65,66].

D. Commutator $[X,X^\dagger]$

One of many measures of non-normality of a matrix (see, e.g., [67]) is defined through the spectral properties of a Hermitian matrix $C := XX^\dagger - X^\dagger X$. Usually it is a square root of its Frobenius norm or the square root of the largest eigenvalue. Substituting the polar decomposition $X = PU$, one obtains $C = P^2 + U(-P^2)U^\dagger$. The unitary matrices assert that in the large N limit the summands are free and their addition reduces to the addition of the corresponding R transforms,

$$R_C(z) = R_{P^2}(z) + R_{-P^2}(z) = R_{P^2}(z) - R_{P^2}(-z), \tag{75}$$

since $R_{aX}(z) = aR_X(az)$.

In the simplest instance, the Ginibre matrix, the R transform of the commutator reads $R_C(z) = \frac{z}{1-z^2}$, which corresponds to the distribution known as the Tetilla law, derived in Ref. [68]. It was proven to be the limiting law for the anticommutator of Hermitian Wigner matrices [69]. Recently, it has also found an application in quantum information [70].

VI. SUMMARY

In this work, we have formulated a diagrammatic construction for **R**-diagonal operators or, equivalently, biunitary invariant random matrices in the limit when the size of the matrix tends to infinity. Relations between individual cumulants and moments were known, but were expressed usually in terms of ζ functions and their inverses (Möbius functions), and the explicit functional relation between the corresponding generating function was so far unknown. Then, adapting the formalism of free random variables for the Hermitian and the non-Hermitian ensembles to the case of **R**-diagonal operators, we have obtained a concise proof of the original Haagerup-Larsen theorem for the isotropic spectra (single-ring theorem) and of its recent extension for the case of the correlation function, which involves overlaps of left and right eigenvectors of non-normal matrices.

Hitherto, all proofs of the single-ring theorem in the formalism of free random variables were based on the analytic methods, so providing the concise diagrammatic proof is an interesting result. It is also interesting to speculate why the eigenvector part of single-ring theorem was missed for almost 20 years (counting from the original formulation by Feinberg and Zee), despite several followups and generalizations in physical and mathematical literature. We dare to link this fact to the very subtle and underappreciated role of the complex parameter w in the "electrostatic potential" (or the regularized Fuglede-Kadison determinant in mathematical language) in Eq. (22). When considering the spectra, this parameter serves solely as the infinitesimal regulator, which is put to zero after performing the average over the ensemble. However, since it appears also in a nontrivial way in off-diagonal components of the quaternionic Greens' function (28), contributing to the left-right eigenvector correlations, particular care has to be taken during the limiting procedure. Actually, looking at our prescription for R transform for biunitarily invariant ensembles (44) one clearly sees that taking the limit $|w| \to 0$ in a hasty way makes our construction meaningless. Moreover, keeping $w \neq 0$ causes that $\mathcal{Q}$ do not commute with the linearized matrix $\mathcal{X}$, which in turn is crucial in encoding all mixed cumulant in the quaternionic R transform.

Last but not least, taking into account the rapidly growing impact of free random variable calculus onto so many branches of modern applications [13,14,71] we hope that the operational construction presented here will contribute to further interweaving of both communities of mathematicians and practitioners.

ACKNOWLEDGMENTS

W.T. is grateful to Prof. M. Bożejko for fruitful discussions and for posing the problem of the non-Hermitian free Poisson, which initiated this work. The authors appreciate also the discussions with R. Speicher. The research was supported by the MAESTRO DEC-2011/02/A/ST1/00119 grant of the National Center of Science. W.T. also appreciates the financial support

from the Polish Ministry of Science and Higher Education through "Diamond Grant" No. 0225/DIA/2015/44 and the scholarship of Marian Smoluchowski Research Consortium Matter Energy Future from KNOW funding.

[1] J. Ginibre, J. Math. Phys. **6**, 440 (1965).
[2] D. V. Savin and V. V. Sokolov, Phys. Rev. E **56**, R4911 (1997); J. T. Chalker and B. Mehlig, Phys. Rev. Lett. **81**, 3367 (1998); Y. V. Fyodorov and B. Mehlig, Phys. Rev. E **66**, 045202 (2002).
[3] Y. V. Fyodorov and H.-J. Sommers, JETP Lett. **63**, 1026 (1996), and references therein.
[4] S. E. Skipetrov and A. Goetschy, J. Phys. A **44**, 065102 (2011).
[5] S. Thurner and C. Biely, Acta Phys. Pol. B **38**, 4111 (2007); C. Biely and S. Thurner, Quant. Finance **8**, 705 (2008).
[6] M. A. Nowak and W. Tarnowski, J. Stat. Mech.: Theor. Exp. (2017) 063405, and references therein.
[7] F. Krzakala *et al.*, Proc. Natl. Acad. Sci. USA **110**, 20935 (2013).
[8] N. Moiseyev, *Non-Hermitian Quantum Mechanics* (Cambridge University Press, New York, 2011).
[9] C. Bender and P. N. Meisinger, J. Math. Phys. **40**, 2201 (1999).
[10] F. J. Dyson, J. Math. Phys. **3**, 1199 (1962).
[11] A. Nica and R. Speicher, Fields Inst. Commun. **12**, 149 (1997).
[12] D. V. Voiculescu, A. Nica, and K. Dykema, *Free Random Variables*, CRM Monograph Series (CRM, Providence, 1992).
[13] R. Couillet and M. Debbah, *Random Matrix Methods for Wireless Communications* (Cambridge University Press, New York, 2011).
[14] B. Collins and I. Nechita, J. Math. Phys. **57**, 015215 (2016).
[15] J. Feinberg and A. Zee, Nucl. Phys. B **501**, 643 (1997).
[16] J. Feinberg, R. Scalettar, and A. Zee, J. Math. Phys. **42**, 5718 (2001).
[17] U. Haagerup and F. Larsen, J. Funct. Anal. **176**, 331 (2000).
[18] D. Voiculescu, J. Operator Theory **18**, 223 (1987).
[19] Y. V. Fyodorov and B. A. Khoruzhenko Acta Phys. Pol. B**38**, 4067 (2007).
[20] A. Guionnet, M. Krishnapur, and O. Zeitouni, Ann. Math. **174**, 1189 (2011).
[21] S. Belinschi, P. Śniady, and R. Speicher, Linear Algebra and its Applications **537**, 48 (2018).
[22] R. A. Janik, M. A. Nowak, G. Papp, and I. Zahed, Nucl. Phys. B **501**, 603 (1997); R. A. Janik, M. A. Nowak, G. Papp, J. Wambach, and I. Zahed, Phys. Rev. E **55**, 4100 (1997).
[23] A. Jarosz and M. A. Nowak, J. Phys. A: Math. Gen. **39**, 10107 (2006).
[24] J. Feinberg and A. Zee, Nucl. Phys. B **504**, 579 (1997).
[25] J. T. Chalker and Z. J. Wang, Phys. Rev. E **61**, 196 (2000).
[26] J. T. Chalker and Z. J. Wang, Phys. Rev. Lett. **79**, 1797 (1997).
[27] S. Belinschi, M. A. Nowak, R. Speicher, and W. Tarnowski, J. Phys. A: Math. Theor. **50**, 105204 (2017).
[28] D. Weingarten, J. Math. Phys. **19**, 999 (1978).
[29] P. W. Brouwer and C. W. J. Beenakker, J. Math. Phys. **37**, 4904 (1996).
[30] B. Collins, Int. Math. Res. Not. **2003**, 953 (2003).
[31] B. Collins and P. Śniady, Commun. Math. Phys. **264**, 773 (2006).
[32] G. t'Hooft, Nucl. Phys. B **72**, 461 (1974).
[33] B. Eynard, *Counting Surfaces: Combinatorics, Matrix Models and Algebraic Geometry*, Progress in Mathematical Physics No. 114 (Birkhäuser, Basel, 2016).
[34] A. Nica and R. Speicher, *Lectures on the Combinatorics of Free Probability* (Cambridge University Press, New York, 2006).
[35] D. Voiculescu, Int. Math. Res. Not. **1998**, 41 (1998).
[36] F. Xu, Commun. Math. Phys. **190**, 287 (1997).
[37] A. Zee, Nucl. Phys. B **474**, 726744 (1996).
[38] R. Speicher and N. R. Rao, Elect. Comm. Prob. **12**, 248 (2007).
[39] Z. Burda, R. A. Janik, and M. A. Nowak, Phys. Rev. E **84**, 061125 (2011).
[40] H. J. Sommers, A. Crisanti, H. Sompolinsky, and Y. Stein, Phys. Rev. Lett. **60**, 1895 (1988).
[41] Y. V. Fyodorov and H.-J. Sommers, J. Math. Phys. **38**, 1918 (1997).
[42] L. G. Brown, Res. Notes Math. Ser. **123**, 1 (1983).
[43] J. T. Chalker and B. Mehlig, J. Math. Phys. **41**, 3233 (2000).
[44] J. S. Bell and J. Steinberger, in *Proceedings of the Oxford International Conference on Elementary Particles 1965*, edited by R. G. Moorhouse, A. E. Taylor, and T. R. Walsh (Rutherford High Energy Laboratory, England, 1966), pp. 195–222.
[45] R. A. Janik, W. Nörenberg, M. A. Nowak, G. Papp, and I. Zahed, Phys. Rev. E **60**, 2699 (1999).
[46] J. H. Wilkinson, *Algebraic Eigenvalue Problem* (Oxford University Press, New York, 1965).
[47] L. N. Trefethen and M. Embree, *Spectra and Pseudospectra: The Behavior of Nonnormal Matrices and Operators* (Princeton University Press, Princeton, 2005).
[48] A. Jarosz, Phys. Rev. E **84**, 011146 (2011).
[49] F. Hiai and D. Petz, *The Semicircle Law, Free Random Variables and Entropy*, Mathematical Surveys and Monographs Vol. 77 (American Mathematical Society, Providence, Rhode Island, 2000).
[50] M. Kieburg and H. Kösters, Random Matrices: Theory Appl. **5**, 1650015 (2016).
[51] Z. Burda, R. A. Janik, and B. Wacław, Phys. Rev. E **81**, 041132 (2010).
[52] E. Gudowska-Nowak, R. A. Janik, J. Jurkiewicz, and M. A. Nowak, Nucl. Phys. B **670**, 479 (2003).
[53] Z. Burda, A. Jarosz, G. Livan, M. A. Nowak, and A. Świech, Phys. Rev. E **82**, 061114 (2010).
[54] S. T. Belinschi, R. Speicher, J. Treilhard, and C. Vargas, Int. Math. Res. Not. **14**, 5933 (2014).
[55] S. T. Belinschi, T. Mai, and R. Speicher, Journal für die reine und angewandte Mathematik, doi:10.1515/crelle-2014-0138.
[56] J. W. Helton, T. Mai, and R. Speicher, arXiv:1511.05330.
[57] U. Haagerup and H. Schultz, Math. Scand. **100**, 209 (2007).
[58] F. Benaych-Georges, Probab. Theory Relat. Fields **144**, 471 (2009).
[59] J. Grela, Phys. Rev. E **96**, 022316 (2017).
[60] R. Speicher, Mem. Am. Math. Soc. **132**, 627 (1998).
[61] R. L. Graham, D. E. Knuth, and O. Patashnik, *Concrete Mathematics* (Addison-Wesley, Reading, MA, 1994).
[62] W. Młotkowski, Doc. Math. **15**, 939 (2010).
[63] W. Młotkowski, K. A. Penson, and K. Życzkowski, Doc. Math. **18**, 1573 (2013).
[64] W. Młotkowski, M. A. Nowak, K. A. Penson, and K. Życzkowski, Phys. Rev. E **92**, 012121 (2015).
[65] P. J. Forrester and D. Z. Liu, J. Stat. Phys. **158**, 1051 (2015).

[66] K. A. Penson and K. Życzkowski, Phys. Rev. E **83**, 061118 (2011).
[67] L. Elsner and M. H. C. Paardekooper, Linear Algebra Appl. **92**, 107 (1987).
[68] A. Nica and R. Speicher, Duke Math. J. **92**, 553 (1998).
[69] A. Deya and I. Nourdin, Lat. Am. J. Probab. Math. Stat. **9**, 101 (2012).
[70] Z. Puchała, Ł. Pawela, and K. Życzkowski, Phys. Rev. A **93**, 062112 (2016).
[71] A. W. Marcus, D. A. Spielman, and N. Srivastava, arXiv:1504.00350.

Published for SISSA by Springer

Received: *February 2, 2018*
Revised: *May 25, 2018*
Accepted: *June 12, 2018*
Published: *June 27, 2018*

Probing non-orthogonality of eigenvectors in non-Hermitian matrix models: diagrammatic approach

Maciej A. Nowak and Wojciech Tarnowski

M. Smoluchowski Institute of Physics and Mark Kac Complex Systems Research Center, Jagiellonian University,
S. Łojasiewicza 11, PL 30-348 Kraków, Poland

E-mail: maciej.a.nowak@uj.edu.pl, wojciech.tarnowski@uj.edu.pl

Abstract: Using large N arguments, we propose a scheme for calculating the two-point eigenvector correlation function for non-normal random matrices in the large N limit. The setting generalizes the quaternionic extension of free probability to two-point functions. In the particular case of biunitarily invariant random matrices, we obtain a simple, general expression for the two-point eigenvector correlation function, which can be viewed as a further generalization of the single ring theorem. This construction has some striking similarities to the freeness of the second kind known for the Hermitian ensembles in large N. On the basis of several solved examples, we conjecture two kinds of microscopic universality of the eigenvectors — one in the bulk, and one at the rim. The form of the conjectured bulk universality agrees with the scaling limit found by Chalker and Mehlig [JT Chalker, B Mehlig, Phys. Rev. Lett. **81** (1998) 3367] in the case of the complex Ginibre ensemble.

Keywords: Matrix Models, Random Systems

ArXiv ePrint: 1801.02526v2

https://doi.org/10.1007/JHEP06(2018)152

JHEP06(2018)152

Contents

1 Introduction

Non-normal operators are ubiquitous in physical models. Examples include hydrodynamics, open quantum systems, PT-symmetric Hamiltonians, Dirac operators in the presence of a chemical potential or finite angle θ. Non-normality is responsible for the transient dynamics, sensitivity of the spectrum to perturbations, pseudoresonant behavior and rapid growth of the perturbations of the system [1]. These effects are relevant in plasma physics [2], fluid mechanics [3], ecology [4, 5], laser physics [6], atmospheric science [7], and magnetohydrodynamics [8], just to mention a few. Non-normality is common in dynamical systems as its simplest source is the asymmetry of coupling between components.

JHEP06(2018)152

Historically, most of the studied properties of non-normal random operators dealt with the eigenvalues. The eigenvalues of such operators are usually complex, requiring new calculational techniques, at the level of both macroscopic and microscopic correlations. Surprisingly, this quest for complex eigenvalues has eclipsed the study of eigenvectors, which are perhaps most distinctive features of non-normal operators. In particular, non-normal operators have two sets of eigenvectors, left and right, which are non-orthogonal among themselves, but can be chosen to be bi-orthogonal, provided that the non-normal operator can be diagonalized at all.

One of the first attempts to develop a systematic understanding of the non-orthogonality of eigenvectors in non-Hermitian random matrices was made by Chalker and Mehlig [9, 10]. Despite their study concentrated on the complex Ginibre ensemble, perhaps the simplest non-normal random operator, the results turned out quite non-trivial and revealed the possibilities of well-hidden universal properties of eigenvectors of non-normal operators. Another connection of the properties of non-normal operators and their eigenvectors to free probability was established soon after [11], but the systematic study of this topic has not followed. Only very recently, the topic of eigenvectors of non-normal operators was picked back up. First, the transient growth driven by eigenvector non-orthogonality was proposed as a mechanism of amplification of neural signals in balanced neural networks [12–14] and giant amplification of noise crucial in the formation of Turing patterns [15–17]. Second, the non-orthogonality of eigenfunctions was related to the statistics of resonance width shifts in open quantum systems [18], which was soon confirmed experimentally [19]. Third, the essential role of eigenvectors in stochastic motion of eigenvalues was revealed [20–22]. Last but not least, the topic has triggered the attention of the mathematical community [23, 24].

In this work we focus on statistical ensembles of complex non-Hermitian matrix models, the probability density of which is invariant under the action of the unitary group $P(X) = P(UXU^\dagger)$. We also assume that in the $N \to \infty$ limit, at which we are working, the eigenvalues of X concentrate on a compact domain of a complex plane. Our results are valid for $|z - w|$ of order 1. We will study one-point and two-point Green functions built out of left and right eigenvectors. Here we recall, that if a non-normal matrix X can be diagonalized by a similarity transformation $X = S\Lambda S^{-1}$, it possesses two eigenvectors for each eigenvalue λ_i: right $|R_i\rangle$ (a column in the matrix notation) and left $\langle L_i|$ (row), satisfying the eigenequations

$$X\,|R_i\rangle = \lambda_i\,|R_i\rangle\,, \quad \langle L_i|\,X = \langle L_i|\,\lambda_i. \tag{1.1}$$

These eigenvectors are not orthogonal $\langle L_i|L_j\rangle \neq \delta_{ij} \neq \langle R_i|R_j\rangle$, but normalized by the biorthogonality condition $\langle L_i|R_j\rangle = \delta_{ij}$. They also satisfy the completeness relation $\sum_{k=1}^{N} |R_k\rangle\,\langle L_k| = \mathbf{1}$. These two properties leave a freedom of rescaling each eigenvector by a non-zero complex number, $|R_i\rangle \to c_i\,|R_i\rangle$ with $\langle L_i| \to \langle L_i|\,c_i^{-1}$. They also allow for multiplication by a unitary matrix $|R_i\rangle \to U\,|R_i\rangle$ and $\langle L_i| \to \langle L_i|\,U^\dagger$. Upon the second transformation the new vectors are not the eigenvectors of the original matrix but of one given by the adjoint action of the unitary group $X \to UXU^\dagger$, which suggests that a natural probability measure should assign these two matrices the same probability density

JHEP06(2018)152

function (pdf). The simplest object, which is invariant under these transformations, is the matrix of overlaps $O_{ij} = \langle L_i|L_j\rangle \langle R_j|R_i\rangle$ [9, 10].

To see how the eigenvector correlation functions appear naturally, let us consider an average $\left\langle \frac{1}{N}\mathrm{Tr} f(X)g(X^\dagger)\right\rangle$, where f, g are two functions analytic in the spectrum of X and $\langle f(X)\rangle = \int f(X)P(X)dX$ denotes the average with respect to the pdf $P(X)$. Taking $f = g$, we get the (normalized) Frobenius norm of a function of matrix. The $1/N$ normalization was taken to get a finite quantity in the $N \to \infty$ limit. Using the spectral decomposition $X = \sum_{k=1}^{N} |R_k\rangle \lambda_k \langle L_k|$ and inserting the identity, $1 = \int d\mu(z)\delta^{(2)}(z - \lambda_k)$ twice, we obtain the expression

$$\left\langle \frac{1}{N}\mathrm{Tr} f(X)g(X^\dagger)\right\rangle = \int d\mu(z)d\mu(w)f(z)g(\bar{w})D(z,w), \tag{1.2}$$

with

$$D(z,w) = \left\langle \frac{1}{N}\sum_{k,l=1}^{N} O_{kl}\delta^{(2)}(z-\lambda_k)\delta^{(2)}(w-\lambda_l)\right\rangle. \tag{1.3}$$

The two dimensional Dirac delta is understood as two deltas for real and imaginary parts $\delta^{(2)}(z) = \delta(\mathrm{Re}z)\delta(\mathrm{Im}z)$, and the measure $d\mu(z) = dxdy$ for $z = x + iy$. $D(z,w)$ introduced in [9, 10] is the density of eigenvalues weighted by the invariant overlap of the corresponding eigenvectors. It is split into a regular and singular part $D(z,w) = \tilde{O}_1(z)\delta^{(2)}(z-w) + O_2(z,w)$, where

$$\tilde{O}_1(z) = \left\langle \frac{1}{N}\sum_{k=1}^{N} O_{ii}\delta^{(2)}(z-\lambda_i)\right\rangle, \qquad O_2(z,w) = \left\langle \frac{1}{N}\sum_{\substack{k,l=1\\k\neq l}}^{N} O_{kl}\delta^{(2)}(z-\lambda_k)\delta^{(2)}(w-\lambda_l)\right\rangle. \tag{1.4}$$

A one-point function, defined this way, in the bulk and far from the rims of the complex spectra grows linearly with the size of a matrix. To have a finite limit in large N, one considers the scaled function $O_1(z) = \frac{1}{N}\tilde{O}_1(z)$. Throughout the paper we shall use only the 'untilded' function.

The one-point function O_1 plays an important role in scattering in open chaotic cavities [18, 25] and random lasing [26, 27], where the so-called Petermann factor [28] modifies the quantum-limited linewidth of a laser. It is also crucial in the description of the diffusion processes on matrices [21, 22] and gives the expectation of the squared eigenvalue condition number [29], an important quantity governing the stability of eigenvalues [1, 30]. The exact calculations are possible for Gaussian matrices [9, 10, 23], in the matrix model for open chaotic scattering [26, 27, 31] and for products of small Gaussian matrices [32]. For the Ginibre matrix the full distribution of the diagonal overlap is available and turns out to be heavy-tailed, as discovered by Bourgade and Dubach [24] with the use of probabilistic techniques, and investigated later using integrable structure and sypersymmetry by Fyodorov [33].

Despite that the overlap between eigenvectors are crucial in the description of the dynamic of the linear system [34] and in the decay laws in open quantum systems [35], the two-point function is much less known. The exact results are obtained only for the Ginibre

JHEP06(2018)152

matrix [9, 10, 24] and for open chaotic scattering with a single channel coupling [31]. Even the asymptotic results are known only for Gaussian matrices [9, 10] and the quantum scattering ensemble [36]. The aim of this paper is to extend the known asymptotic results and develop a diagrammatic technique for calculation of the two-point function in the large N limit.

The paper is organized as follows. In section 2 we briefly recall the cornerstones of diagrammatic calculus [11] for one-point Green's functions in the large non-Hermitian ensembles, to show an analogy between the formalism developed in this paper and the diagrammatic approach to one-point functions. This encapsulates both the mean spectral density and the one-point eigenvector correlation function O_1. Appendix A shows concrete calculations within this formalism for the elliptic ensemble.

Section 3 contains the main body of the paper — a formalism for the calculation of O_2 in the large N limit. We extend the diagrammatic technique introduced by Chalker and Mehlig for Gaussian matrices to any probability distribution with unitary symmetry. Regularizing and linearizing the product of resolvents, we embed them into the quaternionic space. The analysis of planar Feynman diagrams leads us to the matrix Bethe-Salpeter equation (3.15), which relates the product of resolvents with the one-point Green's function and planar cumulants. The latter are encoded in their generating function — quaternionic R-transform, see (3.16). As a result, the two-point eigenvector correlation function is completely determined by the one-point functions encoding the spectral density and O_1. This result resembles the Ambjørn-Jurkiewicz-Makeenko universality for Hermitian ensembles [37].

We also study the traced product of resolvents $\mathfrak{h}(z,\bar{w}) = \left\langle \frac{1}{N}\mathrm{Tr}(z\mathbf{1}-X)^{-1}(\bar{w}\mathbf{1}-X^\dagger)^{-1}\right\rangle$, which allows for the calculation of the average (1.2) as a Dunford-Taylor integral [38, 39]

$$\left\langle \frac{1}{N}\mathrm{Tr} f(X)g(X^\dagger)\right\rangle = \frac{1}{(2\pi i)^2}\int_\gamma dz \int_{\bar{\gamma}} d\bar{w} f(z)g(\bar{w})\mathfrak{h}(z,\bar{w}), \tag{1.5}$$

where contours $\bar{\gamma}$,γ encircle all eigenvalues of X clockwise and counterclockwise, respectively. We derive the equation for $\mathfrak{h}$, expressing it in terms of quaternionic R-transform and traced resolvents, see (3.18) and (3.19).

An important and still quite large subclass of non-Hermitian ensembles for which the main equations (3.15)(3.16) admit further simplifications consists of matrices, the pdf of which is invariant under the transformation by two independent unitary matrices $U, V \in \mathrm{U}(N)$, i.e. $P(X) = P(UXV^\dagger)$, thus called the biunitarily invariant ensemble [40]. In this case we obtain a compact formula for the two-point eigenvector correlation function

$$O_2(z_1,z_2) = \frac{1}{\pi}\partial_{\bar{z}_1}\partial_{z_2}\frac{\bar{z}_1(z_1-z_2)O_1(r_1)+z_2(\bar{z}_1-\bar{z}_2)O_1(r_2)}{|z_1-z_2|^2\left[F(r_1)-F(r_2)\right]}. \tag{1.6}$$

Here F is the radial cumulative distribution function (cdf), defined as $F(r) = 2\pi\int_0^r \rho(s)sds$, with $\rho(s)$ the spectral density circularly symmetric on the complex plane. The one-point eigenvector function is related to F via [29]

$$O_1(r) = \frac{F(r)(1-F(r))}{\pi r^2}, \tag{1.7}$$

JHEP06(2018)152

and $r = |z|$. The traced product of resolvents is shown to take a universal form

$$\mathfrak{h}(z, \bar{w}) = \frac{1}{z\bar{w} - r_{\text{out}}^2}, \tag{1.8}$$

where r_{out} is the spectral radius. This result has been already obtained for the Ginibre ensemble [10] and, recently, for matrices with independent identically distributed (iid) entries [41].

Applications of the developed formalism are presented in section 4, where we consider an elliptic ensemble, some instances from the biunitarily invariant class: truncated unitary, induced Ginibre, the product of two Ginibres and their ratio. As the last example we consider a pseudohermitian matrix — a product of two shifted GUE matrices. In section 5, we discuss the consequences of our large N results on the microscopic regime. We conjecture, on the basis of the few examples solved in the literature and using our own results, that the two-point eigenvector correlation functions may exhibit universal bulk scaling, as what happens for the microscopic spectral two-pointers in Hermitian matrix models. More precisely, we conjecture that in generic complex non-Hermitian matrices for all points in the bulk at which the spectral density does not develop singularities there exists a limit

$$\lim_{N\to\infty} N^{-2} O_2\left(z + \frac{x}{\sqrt{N}}, z + \frac{y}{\sqrt{N}}\right) = O_1(z)\Phi(|x-y|), \tag{1.9}$$

where

$$\Phi(|\omega|) = -\frac{1}{\pi^2|\omega|^4}\left(1 - (1+|\omega|^2)e^{-|\omega|^2}\right). \tag{1.10}$$

Section 6 concludes the paper and points at some possible further developments.

2 Non-Hermitian random matrices

In non-Hermitian random matrix theory one is primarily interested in the distribution of the eigenvalues $\rho(z) = \left\langle \frac{1}{N}\sum_{i=1}^{N} \delta^{(2)}(z-\lambda_i)\right\rangle$. The 2-dimensional Dirac delta can be recovered using the relation $\partial_{\bar{z}}\frac{1}{z} = \pi\delta^{(2)}(z)$. Unfortunately, the average over the ensemble of the trace of the resolvent $\mathfrak{g}(z) = \left\langle \frac{1}{N}\mathrm{Tr}(z\mathbf{1} - X)^{-1}\right\rangle$ does not yield the correct result inside the spectrum, as one would naively expect. The reason for this failure is that differentiation and taking the ensemble average are not interchangeable. This phenomenon was termed the spontaneous breaking of holomorphic symmetry [42].

A way to circumvent this obstacle is to consider a regularization of the Dirac delta. In RMT one mostly considers the 2D Poisson kernel

$$\pi\delta^{(2)}(z) = \lim_{\epsilon\to 0}\frac{\epsilon^2}{(|z|^2+\epsilon^2)^2} = \lim_{\epsilon\to 0}\partial_{\bar{z}}\frac{\bar{z}}{|z|^2+\epsilon^2}. \tag{2.1}$$

The expression on the right hand side provides a prescription for how the resolvent in the spectrum of X should be regularized. Having this hint in mind, one defines

$$g(z,\bar{z},w,\bar{w}) = \left\langle \frac{1}{N}\mathrm{Tr}(\bar{z}\mathbf{1} - X^\dagger)[(z\mathbf{1}-X)(\bar{z}\mathbf{1}-X^\dagger) + |w|^2\mathbf{1}]^{-1}\right\rangle. \tag{2.2}$$

The spectral density can be now calculated via

$$\rho(z,\bar{z}) = \frac{1}{\pi}\lim_{|w|\to 0}\partial_{\bar{z}} g(z,\bar{z},w,\bar{w}), \tag{2.3}$$

which can be also understood as a Poisson law in 2D electrostatics, since

$$\rho(z,\bar{z}) = \lim_{|w|\to 0}\frac{1}{\pi}\partial_z\partial_{\bar{z}}\Phi(z,\bar{z},w,\bar{w}), \tag{2.4}$$

where

$$\Phi(z,\bar{z},w,\bar{w}) = \left\langle \frac{1}{N}\ln\det[(z\mathbf{1}-X)(\bar{z}\mathbf{1}-X^\dagger)+|w|^2\mathbf{1}]\right\rangle \tag{2.5}$$

is the (regularized) electrostatic potential of charges interacting via repulsive central force $F(r)\sim\frac{1}{r}$.

2.1 Linearization

Due to the quadratic expression in X in the denominator, the average in (2.2) is intractable when non-normal matrices are considered. To circumvent this problem one introduces the $2N\times 2N$ matrix [42–45]

$$\mathcal{G} = \left\langle \begin{pmatrix} z\mathbf{1}-X & i\bar{w}\mathbf{1} \\ iw\mathbf{1} & \bar{z}\mathbf{1}-X^\dagger \end{pmatrix}^{-1}\right\rangle \tag{2.6}$$

and the block trace operation, mapping $2N\times 2N$ matrices onto 2×2 ones

$$\mathrm{bTr}\begin{pmatrix} A & B \\ C & D\end{pmatrix} = \begin{pmatrix} \mathrm{Tr}A & \mathrm{Tr}B \\ \mathrm{Tr}C & \mathrm{Tr}D\end{pmatrix}. \tag{2.7}$$

Then, one defines the 2×2 Green's function

$$G(z,\bar{z},w,\bar{w}) = \begin{pmatrix} G_{11} & G_{1\bar{1}} \\ G_{\bar{1}1} & G_{\bar{1}\bar{1}}\end{pmatrix} = \frac{1}{N}\mathrm{bTr}\mathcal{G}(z,\bar{z},w,\bar{w}). \tag{2.8}$$

Its upper-left entry is exactly the desired function g (cf. (2.2)). Once Green's function is known, one gets four elements of G. The entry $G_{\bar{1}\bar{1}}$ is just the complex conjugate of G_{11}, thus does not provide any additional information. The off-diagonal entries $G_{1\bar{1}} = -\bar{G}_{\bar{1}1}$ in the large N limit give the one-point eigenvector correlation function [11]

$$O_1(z) = \lim_{|w|\to 0} -\frac{1}{\pi}G_{1\bar{1}}G_{\bar{1}1}. \tag{2.9}$$

2.2 Quaternionic structure

Green's function can be conveniently written as

$$G = \left\langle \frac{1}{N}\mathrm{bTr}(\mathcal{Q}-\mathcal{X})^{-1}\right\rangle = \begin{pmatrix} \partial_{Q_{11}}\Phi & \partial_{Q_{\bar{1}1}}\Phi \\ \partial_{Q_{1\bar{1}}}\Phi & \partial_{Q_{\bar{1}\bar{1}}}\Phi\end{pmatrix}, \tag{2.10}$$

JHEP06(2018)152

with

$$\mathcal{X} = \begin{pmatrix} X & 0 \\ 0 & X^\dagger \end{pmatrix}, \quad \mathcal{Q} = Q \otimes \mathbf{1}, \quad Q = \begin{pmatrix} z & i\bar{w} \\ iw & \bar{z} \end{pmatrix}. \tag{2.11}$$

This form of Green's function resembles its traditional form as a traced resolvent, but now its argument is a 2×2 matrix and the matrix X is duplicated to incorporate also $X^\dagger$. The matrix Q is a representation of a quaternion $q = x + iy + ju + kv$ with the identification $z = x + iy$ and $w = v + iu$ [46]. The entries of G satisfy the same algebraic constraints as Q, therefore G is itself a quaternion and we refer to it as the quaternionic Green's function, similarly $\mathcal{G}$ is called the quaternionic resolvent.

2.3 Averages in large N

We are interested in calculations of the averages of some functions of X, e.g. $\langle f(X, X^\dagger) \rangle$, with respect to distributions invariant under the adjoint action of the unitary group $P(X) = P(UXU^\dagger)$. We parameterize them by

$$P(X) \sim \exp\left(-N \mathrm{Tr} V(X, X^\dagger)\right). \tag{2.12}$$

$V(X, X^\dagger)$, often referred to as potential, has to be Hermitian and growing sufficiently fast at infinity. To simplify calculations, we split the potential into the Gaussian and the residual part. The Gaussian part can be conveniently parameterized with $\sigma > 0$ and $\tau \in [-1, 1]$ [47]

$$V_G(X, X^\dagger) = \frac{1}{\sigma^2(1-\tau^2)} \left(XX^\dagger - \frac{\tau}{2} \left(X^2 + (X^\dagger)^2 \right) \right). \tag{2.13}$$

Averages with respect to the Gaussian potential by the virtue of Wick's theorem reduce to products of pairwise expectations, called propagators

$$\langle X_{ab} X_{cd} \rangle_G = \frac{\sigma^2 \tau}{N} \delta_{ad} \delta_{bc}, \qquad \left\langle X_{ab} X^\dagger_{cd} \right\rangle_G = \frac{\sigma^2}{N} \delta_{ad} \delta_{bc}. \tag{2.14}$$

The exponent of the residual part of the potential is expanded into series, which produces additional terms, called vertices, to be averaged with respect to the Gaussian distribution. To cope with the multitude of terms, we represent them as diagrams (see table 1 for an overview). This introduces a natural hierarchy of diagrams according to their scaling with the size of the matrix. The dominant contribution, which is of the order of 1, comes from planar diagrams (see figure 1). The subleading corrections can be classified by the genus of the surface at which they can be drawn without the intersection [48].

2.4 Moment expansion of the quaternionic resolvent

To calculate the average of the quaternionic resolvent, we write it as

$$\mathcal{G} = \left\langle \left(\mathbf{1} - \mathcal{Q}^{-1} \mathcal{X} \right)^{-1} \right\rangle \mathcal{Q}^{-1}$$

and expand it into the geometric series

$$\mathcal{G} = \mathcal{Q}^{-1} + \left\langle \mathcal{Q}^{-1} \mathcal{X} \mathcal{Q}^{-1} \right\rangle + \left\langle \mathcal{Q}^{-1} \mathcal{X} \mathcal{Q}^{-1} \mathcal{X} \mathcal{Q}^{-1} \right\rangle + \ldots, \tag{2.15}$$

JHEP06(2018)152

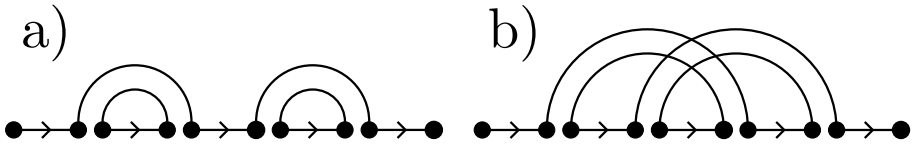

Figure 1. Examples of planar (a) and non-planar (b) diagrams in the diagrammatic expansion of the Gaussian model coming from the term $\left\langle \mathcal{Q}^{-1}(\mathcal{X}\mathcal{Q}^{-1})^4 \right\rangle$. For a general matrix model with an arbitrary potential the order of the diagram is given by N^{L+V-P}, where V is the number of vertices, L is the number of loops and P is the number of propagators comprising the diagram. This shows that the dominant contribution comes from the planar diagrams. The contribution from the non-planar diagram on (b) is of order N^{-2}, thus vanishes in the large N limit.

propagator	$\langle \mathcal{X}_{\alpha\beta,ij}\mathcal{X}_{\mu\nu,jk}\rangle_G$		Green's function	$G_{\alpha\beta} = \frac{1}{N}\mathrm{bTr}\mathcal{G}$	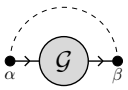
horizontal line	$(Q^{-1})_{\alpha\beta}\delta_{ij}$		vertex	$Ng_3X^{\alpha}_{ij}X^{\beta}_{jk}X^{\gamma}_{ki}$	
resolvent	$\mathcal{G} = \left\langle (\mathcal{Q}-\mathcal{X})^{-1}_{\alpha\beta,ij} \right\rangle$	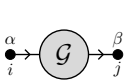	cumulant	$\left\langle X^{\alpha}_{ij}X^{\beta}_{jk}X^{\gamma}_{ki} \right\rangle_c$	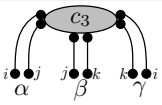

Table 1. Diagrammatic representation of the basic expressions in the moment expansion of the resolvent. The propagator represents the averages with respect to the Gaussian potential (2.14). An exemplary vertex is drawn for the theory which contains the cubic interaction $Ng_3\mathrm{Tr}X^{\alpha}X^{\beta}X^{\gamma}$ in the potential. A cumulant (dressed vertex) represents a sum over all connected diagrams connected to the baseline. Its structure in matrix indices (Latin letters) is the same as that of the vertex, because the propagators are the Kronecker deltas in this indices. The dashed line without arrows represent summation over Latin indices only.

and perform averages in the large N limit, as described in the previous section. The expansion is valid, provided that $||\mathcal{Q}^{-1}\mathcal{X}|| < 1$, thus for z inside the spectrum of X, we need to keep w finite. If the spectrum is bounded, one can always find sufficiently large w, so that this series is absolutely convergent. For the calculations with z outside the spectrum one can safely set $w = 0$.

It is convenient to introduce a notation, which incorporates the block structure of the duplicated matrices. We therefore endow each matrix with two sets of indices, writing for example $\mathcal{G}_{\alpha\beta,ij}$. The first two Greek indices, which we also refer to as quaternionic indices, enumerate blocks and take values 1 and $\bar{1}$. The Latin ones, running from 1 to N enumerate matrices within each block. The space described by the Latin indices we call simply the matrix space. The block trace operation can be represented as a partial trace over the matrix space $G(Q)_{\alpha\beta} = \frac{1}{N}\sum_{i=1}^{N}\mathcal{G}_{\alpha\beta,ii}$ (see also table 1). Due to the fact, that the propagators are expressed in terms of Kronecker deltas, all averaged expressions have trivial matrix structure, e.g. $\mathcal{G} = G \otimes \mathbf{1}$, but we need this notation for the next section.

Among all diagrams contributing to $\mathcal{G}$ (see figure 2 for an example) we distinguish a class of one-line irreducible diagrams (1LI), i.e. the ones that cannot be split into two

JHEP06(2018)152

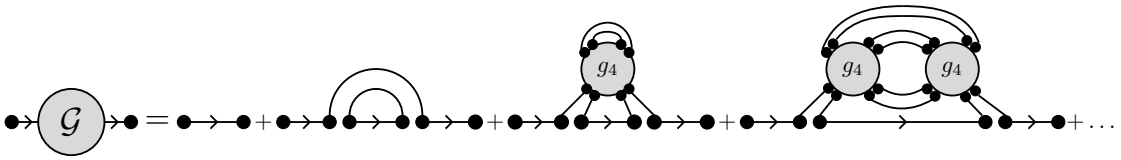

Figure 2. Some exemplary planar diagrams in a model with a quartic term g_4X^4 contributing to the Green's function. All diagrams (except for the first) are 1PI.

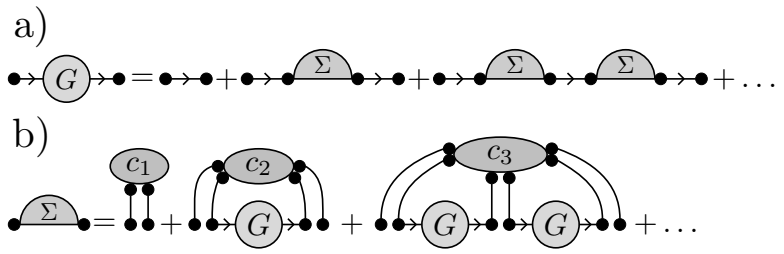

Figure 3. a) First Schwinger-Dyson equation. Diagrams contributing to the Green's function can be divided into one-particle irreducible (1PI) and the ones composed of 1PI connected by a horizontal line (corresponding to $\mathcal{Q}^{-1}$). b) Second Schwinger-Dyson equation. Any 1PI planar diagram can be represented as a certain connected subdiagram attached to the baseline (horizontal line from the graphical representation of the expansion (2.15)) via k propagators (this is the k-th cumulant). The diagrams between the legs of the cumulant can be of any type, which are in turn encoded in the Green's function. Since all cumulants are encoded in their generating function — the quaternionic R-transform (2.19), this relation leads to the equation $\Sigma(Q) = R(G(Q))$.

parts, connected only through $\mathcal{Q}^{-1}$. Let us denote as Σ a sum of all 1LI diagrams. This is a building block of the quaternionic resolvent, since any diagram can be decomposed into 1LI subdiagrams connected through $\mathcal{Q}^{-1}$. Having the absolute convergence of the series, we rearrange terms, obtaining the Schwinger-Dyson equation (here we restrict it only to the quaternionic part)

$$G(Q) = Q^{-1} + Q^{-1}\Sigma(Q)Q^{-1} + Q^{-1}\Sigma(Q)Q^{-1}\Sigma(Q)Q^{-1} + \dots, \tag{2.16}$$

presented also diagrammatically in figure 3a). This is a geometric series, which can be summed and written in a closed form

$$G(Q) = (Q - \Sigma(Q))^{-1}. \tag{2.17}$$

2.5 Quaternionic R-transform

To find G, one needs to relate Σ to G. To this end, let us consider diagrams contributing to averages of traced strings of X's and $X^\dagger$'s such that all X's and $X^\dagger$'s are connected with each other. Their sum we call a cumulant (in field theory language it is known as a dressed vertex) and endow the respective average with a subscript c. We adopt a convenient notation for cumulants in which $\dagger$ is associated with the $\bar{1}$ index and, trivially,

JHEP06(2018)152

lack of conjugation with 1. We also encode the length of the string. An example reads

$$c^{(k)}_{\alpha_1\alpha_2\ldots\alpha_k} = \left\langle \frac{1}{N}\mathrm{Tr}X^{\alpha_1}X^{\alpha_2}\ldots X^{\alpha_k}\right\rangle_c . \tag{2.18}$$

We also introduce the R-transform, which is a 2×2 matrix, defined through its expansion for small arguments

$$R_{\alpha\beta} = c^{(1)}_{\alpha}\delta_{\alpha\beta} + c^{(2)}_{\alpha\beta}Q_{\alpha\beta} + \sum_{\mu\in\{1,\bar{1}\}} c^{(3)}_{\alpha\mu\beta}Q_{\alpha\mu}Q_{\mu\beta} + \sum_{\mu,\nu\in\{1,\bar{1}\}} c^{(4)}_{\alpha\mu\nu\beta}Q_{\alpha\mu}Q_{\mu\nu}Q_{\nu\beta} + \ldots \tag{2.19}$$

This definition written in terms of indices may not seem to be intuitive, but in the matrix notation takes a clearer form

$$R(Q)\otimes\mathbf{1} = \langle\mathcal{X}\rangle_c + \langle\mathcal{X}\mathcal{Q}\mathcal{X}\rangle_c + \langle\mathcal{X}\mathcal{Q}\mathcal{X}\mathcal{Q}\mathcal{X}\rangle_c + \ldots, \tag{2.20}$$

which is the counterpart of (2.15). The matrix R is also a quaternion, so it is dubbed the quaternionic R-transform. Q is always associated with two consecutive indices in the cumulant and can be thought of as a transfer matrix. It is crucial for encoding all cumulants in the R-transform that matrices $\mathcal{X}$ and $\mathcal{Q}$ do not commute.

Consider now any 1LI diagram. Due to its irreducibility it can be depicted as a certain cumulant connecting the first and last $\mathcal{X}$ and possibly some others in between. The subdiagrams disconnected from the cumulant can be in any form, which is already encoded in the quaternionic Green's function. This allows us to write the second Schwinger-Dyson equation relating Σ and G via the quaternionic R-transform (see also figure 3b))

$$\Sigma(Q) = R(G(Q)). \tag{2.21}$$

The knowledge of all cumulants allows us to solve the matrix model, since equations (2.17) and (2.21) can be brought to a single 2×2 matrix equation

$$R(G(Q)) + G(Q)^{-1} = Q. \tag{2.22}$$

Once the averaging with respect to the ensemble was taken at the level of diagrams, we can safely remove the regularization and solve the above algebraic equation, setting first $w = 0$. We refer to [49, 50] for more detailed calculations in the diagrammatic formalism.

The construction presented in this section has been recently rigorously formalized in the framework of free probability [51].

3 2-point eigenvector correlation function

3.1 Preliminaries

In order to investigate the 2-point eigenvector correlation function associated with the off-diagonal overlap, we follow the paradigm outlined in the previous section for calculations of Green's function. A naive approach, i.e. calculation of $\mathfrak{h}(z_1,\bar{z}_2) = \left\langle \frac{1}{N}\mathrm{Tr}(z_1\mathbf{1}-X)^{-1}(\bar{z}_2\mathbf{1}-X^\dagger)^{-1}\right\rangle$, yields the result which is correct only outside of the

spectrum of X, which we refer to as the holomorphic solution. Inside the spectrum, we regularize each resolvent, using the rule

$$(z\mathbf{1} - X)^{-1} \to (\bar{z}\mathbf{1} - X^\dagger)M(z,w)^{-1}, \tag{3.1}$$

where $M(z,w) = (z\mathbf{1} - X)(\bar{z}\mathbf{1} - X^\dagger) + |w|^2\mathbf{1}$. We shall therefore study

$$h(z_1, w_1, z_2, w_2) = \left\langle \frac{1}{N}\mathrm{Tr}(\bar{z}_1\mathbf{1} - X^\dagger)M(z_1,w_1)^{-1}M(z_2,w_2)^{-1}(z_2\mathbf{1} - X) \right\rangle. \tag{3.2}$$

The weighted density is therefore given by

$$D(z_1, z_2) = \lim_{|w_1|,|w_2|\to 0} \frac{1}{\pi^2}\partial_{\bar{z}_1}\partial_{z_2}h(z_1, w_1, z_2, w_2). \tag{3.3}$$

In this paper we will calculate h by diagrammatic $1/N$ expansion in the planar limit. The singular part of $D(z_1, z_2)$ containing the Dirac delta is not accessible in perturbative calculations, so we get

$$O_2(z_1, z_2) = \lim_{|w_1|,|w_2|\to 0} \frac{1}{\pi^2}\partial_{\bar{z}_1}\partial_{z_2}h(z_1, w_1, z_2, w_2). \tag{3.4}$$

There exists a class of matrices which despite not being Hermitian have a real spectrum. A simple example is the product of two Hermitian matrices A, B, one of which (let us say A) is positive definite. The resulting matrix is not Hermitian, but isospectral to $A^{1/2}BA^{1/2}$, which must have real eigenvalues. The eigenvectors of AB are not orthogonal, which makes O_2 non-trivial. The realness of the spectrum facilitates calculations, as the knowledge of the traced resolvent is sufficient. By the virtue of the Sochocki-Plemelj formula valid for real x we can write

$$2\pi i\delta(x) = \lim_{\epsilon\to 0}\left(\frac{1}{x - i\epsilon} - \frac{1}{x + i\epsilon}\right), \tag{3.5}$$

and the two-point function can be calculated from the holomorphic function via

$$O_2(x,y) = \frac{-1}{4\pi^2}\left(\mathfrak{h}(+,+) - \mathfrak{h}(+,-) - \mathfrak{h}(-,+) + \mathfrak{h}(-,-)\right), \tag{3.6}$$

where

$$\mathfrak{h}(\pm,\pm) = \lim_{\epsilon_1,\epsilon_2\to 0}\mathfrak{h}(x \pm i\epsilon_1, y \pm i\epsilon_2) \tag{3.7}$$

and signs are uncorrelated.

3.2 Linearization

The expression for the regularized product of resolvents (3.2) contains two quadratic non-linearities. We overcome this difficulty, by using $2N \times 2N$ matrices $\mathcal{Q} = Q \otimes \mathbf{1}$, $\mathcal{P} = P \otimes \mathbf{1}$ and $\mathcal{X}$, where

$$Q = \begin{pmatrix} z_1 & i\bar{w}_1 \\ iw_1 & \bar{z}_1 \end{pmatrix}, \quad P = \begin{pmatrix} z_2 & i\bar{w}_2 \\ iw_2 & \bar{z}_2 \end{pmatrix}, \quad \mathcal{X} = \begin{pmatrix} X & 0 \\ 0 & X^\dagger \end{pmatrix}. \tag{3.8}$$

JHEP06(2018)152

As a natural generalization of the quaternionic resolvent to two-point functions, we define the average of the Kronecker product of two quaternionic resolvents

$$\mathcal{H} = \left\langle (\mathcal{Q} - \mathcal{X})^{-1} \otimes (\mathcal{P}^T - \mathcal{X}^T)^{-1} \right\rangle . \tag{3.9}$$

Such an object is quite unusual in Random Matrix Theory. A similar construction was used by Brezin and Zee for the calculation of the connected 2-point density in Hermitian models [52], but there one deals only with matrix indices. To the best of our knowledge the quaternionic approach to two-point functions for non-Hermitian matrices is considered for the first time, thus we will discuss it in more detail.

$\mathcal{H}$ is a $4N^2 \times 4N^2$ matrix with a very specific block structure. To keep track of it, we endow $\mathcal{H}$ with 8 indices. The upper ones refer to the first matrix in the Kronecker product, while the lower ones to the second. As in the case of the quaternionic Green's function, Greek indices, taking values in $\{1, \bar{1}\}$, enumerate blocks, while Latin indices ranging in $\{1, \ldots, N\}$ denote elements within each block. In the index notation, its components read (note the transpose of the second matrix)

$$\mathcal{H}^{\alpha\beta,ij}_{\mu\nu,kl} = \left\langle (\mathcal{Q} - \mathcal{X})^{-1}_{\alpha\beta,ij} \, (\mathcal{P} - \mathcal{X})^{-1}_{\nu\mu,lk} \right\rangle . \tag{3.10}$$

With the same assumptions as for one-point functions, the resolvents are then expanded into the power series

$$\mathcal{H} = \left\langle \left(\mathcal{Q}^{-1} + \mathcal{Q}^{-1}\mathcal{X}\mathcal{Q}^{-1} + \ldots\right) \otimes \left(\mathcal{P}^{-1} + \mathcal{P}^{-1}\mathcal{X}\mathcal{P}^{-1} + \ldots\right)^T \right\rangle , \tag{3.11}$$

and taking the expectation produces diagrams. The flow of Latin (matrix) indices in the diagrams follows the lines in the double line notation. The propagators are symmetric, thus the direction does not matter. The flow of quaternionic (Greek) indices is governed by their order in the expansion of the resolvent. Since the quaternion matrices Q and P are not symmetric, the direction of the line representing $\mathcal{Q}^{-1}$ matters and is depicted by an arrow. We draw diagrams in such a way that the terms in the expansion of the resolvents are in two rows, hereafter called baselines, with the first resolvent above. The quaternionic indices flow from left to right in the upper baseline and in the opposite direction below.

There are two ways of contracting matrix indices,[1] thus we define two functions

$$K^{\alpha\beta}_{\mu\nu} = \frac{1}{N} \sum_{i,j=1}^{N} \mathcal{H}^{\alpha\beta,ij}_{\mu\nu,ij}, \qquad L^{\alpha\beta}_{\mu\nu} = \frac{1}{N^2} \sum_{i,j=1}^{N} \mathcal{H}^{\alpha\beta,ii}_{\mu\nu,jj}, \tag{3.12}$$

which correspond to contractions presented in figure 4a). It will become clear later that K encodes correlations of eigenvectors and L of eigenvalues. These two possible contractions define two different classes of planar diagrams. The admissible diagrams have to be drawn in the region of the plane bounded by baselines and dashed lines depicting contractions. The diagrams contributing to K are of the ladder type (see figure 5), while the class of planar diagrams contributing to L, termed wheel diagrams, is broader, as it admits for

[1] In fact, there are $\frac{4!}{2^2 \cdot 2!} = 3$ ways, but $\sum_{ij} \mathcal{H}^{\alpha\beta,ij}_{\mu\nu,ji}$ leads to the same diagrams as $K^{\beta\alpha}_{\mu\nu}$.

JHEP06(2018)152

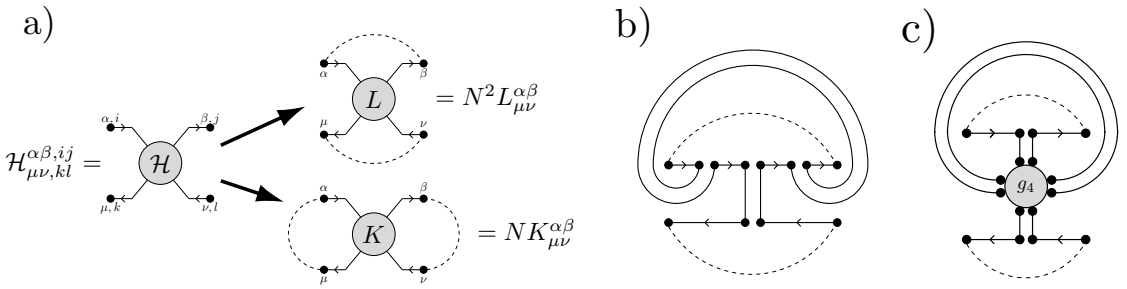

Figure 4. a) Possible contractions of matrix indices (dashed lines) of the Kronecker product of two quaternionic resolvents. The way one contracts indices determines the class dominant planar diagrams, which are drawn between dashed lines and the horizontal baselines. The upper choice corresponds to a class of double-trace two-point functions, see (5.2), while the lower possibility leads a single-trace two point function encoding correlations of eigenvectors. Diagrams contributing to L are of wheel type [52, 53] and K is given as a sum of ladder diagrams. b) An example of a diagram which contributes to L but is subleading in the calculation of K. c) An example of a diagram appearing during the calculation of L, which despite its planarity is subleading.

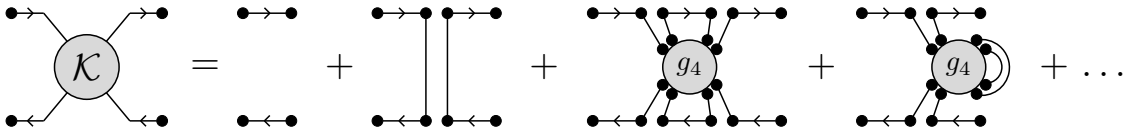

Figure 5. Some exemplary diagrams in a theory with quartic potential contributing to $\mathcal{K}$.

circumventing one of the baselines if the points on the baseline are connected through propagators and vertices, see figure 4b). Not all planar diagrams contribute equally to L. Diagrams in which a propagator connects two sides of a vertex and encircles a baseline is subleading, see figure 4c). In this section we concentrate on the ladder diagrams.

3.3 Ladder diagrams

In this section we are interested in the calculation of K. The contraction of matrix indices in $\mathcal{H}$, which leads to K, is in fact a summation of all N^4 elements within each 4×4 block. To make the notation of Greek indices even more explicit, we write the entries of K

$$K = \begin{pmatrix} K^{11}_{11} & K^{11}_{1\bar{1}} & K^{1\bar{1}}_{11} & K^{1\bar{1}}_{1\bar{1}} \\ K^{11}_{\bar{1}1} & K^{11}_{\bar{1}\bar{1}} & K^{1\bar{1}}_{\bar{1}1} & K^{1\bar{1}}_{\bar{1}\bar{1}} \\ K^{\bar{1}1}_{11} & K^{\bar{1}1}_{1\bar{1}} & K^{\bar{1}\bar{1}}_{11} & K^{\bar{1}\bar{1}}_{1\bar{1}} \\ K^{\bar{1}1}_{\bar{1}1} & K^{\bar{1}1}_{\bar{1}\bar{1}} & K^{\bar{1}\bar{1}}_{\bar{1}1} & K^{\bar{1}\bar{1}}_{\bar{1}\bar{1}} \end{pmatrix}. \tag{3.13}$$

An important consequence of this construction is that the $K^{11}_{\bar{1}\bar{1}}$ element is exactly the desired function h (3.2) for the calculation of the eigenvector correlation function.

Let us define $\mathcal{K}^{\alpha\beta,ij}_{\mu\nu,kl}$ the sum of all ladder diagrams contributing to K (before we contract indices). A vertex can connect two points on a baseline (a side rail of the ladder), dressing the part of the rail. There are also vertices connecting two baselines, which give rise to the rungs of the ladder. If we denote $\Gamma^{\alpha\beta,ij}_{\mu\nu,kl}$ a sum of all connected subdiagrams

JHEP06(2018)152

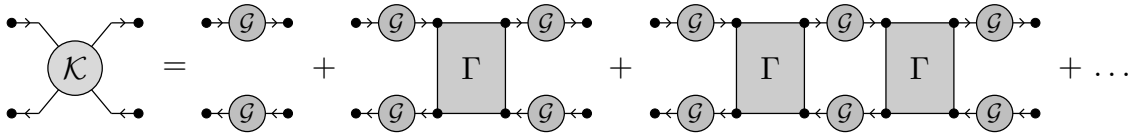

Figure 6. The general structure of planar ladder diagrams contributing to $\mathcal{K}$.

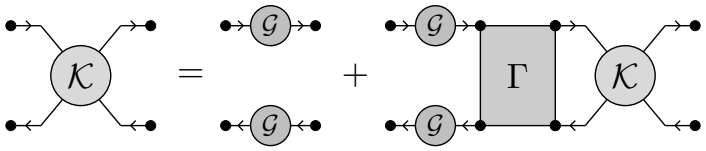

Figure 7. Matrix Bethe-Salpeter equation (3.14).

which connect two rails, one can express $\mathcal{K}$ in terms of Γ as a geometric series, presented in figure 6, which can be written in a closed form (a sum over repeating indices is implicit)

$$\mathcal{K}^{\alpha\beta,ab}_{\mu\nu,cd} = G^{\alpha\beta}G_{\mu\nu}\delta^{ab}\delta_{cd} + G^{\alpha\gamma}G_{\mu\rho}\delta^{ai}\delta_{cj}\Gamma^{\gamma\epsilon,ik}_{\rho\sigma,jl}\mathcal{K}^{\epsilon\beta,kb}_{\sigma\nu,ld}. \tag{3.14}$$

This relation, shown diagramatically in figure 7 and known as the matrix Bethe-Salpeter equation, is the counterpart of the Schwinger-Dyson equation for the two-point function, with Γ the counterpart of the self-energy.

A direct analysis of planar diagrams yields $\Gamma^{\alpha\beta,ij}_{\mu\nu,kl} = \frac{1}{N}B^{\alpha\beta}_{\mu\nu}\delta^i_k\delta^j_l$, where B is of order 1, see figure 8. Using the matrix structure of Γ, we trace out the matrix indices and find the equation for K, which in the matrix notation reads

$$K(Q,P) = G(Q)\otimes G^T(P) + \left[G(Q)\otimes G^T(P)\right]B(Q,P)K(Q,P). \tag{3.15}$$

We now turn our attention to the rungs. Any diagram contributing to Γ can be decomposed as a certain cumulant of length $n \geq 2$, the first k legs of which are attached to the upper rail, while the last legs are connected to the lower rail. The part of the rail between the legs of the cumulant gets dressed to the quaternionic Green's function $G(Q)$ above and $G(P)$ below. The space between k-th and $(k+1)$-th legs is left unfilled, because the quaternonic indices at the end of rails are not contracted. This decomposition of Γ is depicted in figure 9. As Γ is completely determined by the planar cumulants, $B^{\alpha\beta}_{\mu\nu}$ can be calculated from the quaternionic R transform (2.19). The rule is simple and goes as follows.

Consider the expansion of $R_{\alpha\mu}$ in Q (2.19) and differentiate it with respect to $Q_{\beta\nu}$. As a result for some $0 < k < n-1$ the k-th quaternion $Q_{\mu_k\mu_{k+1}}$ will be replaced by $\delta_{\mu_k\beta}\delta_{\nu\mu_{k+1}}$. Then all $Q_{\mu_l\mu_{l+1}}$'s from the l.h.s. of the removed Q (i.e. for $l < k$) are replaced by $G^{\mu_l\mu_{l+1}}(Q)$ and all $Q_{\mu_l\mu_{l+1}}$ on the right ($l > k$) by $G^T_{\mu_l\mu_{l+1}}(P)$. Then the sum over all possible positions (i.e. k's), where $\mathcal{Q}$ has been removed, is performed.

JHEP06(2018)152

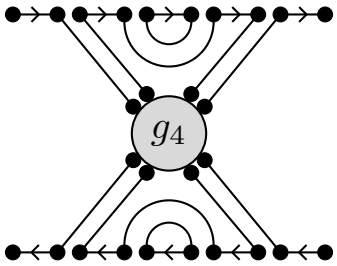

Figure 8. An example of a diagram contributing to Γ. It contributes to the second-to-last diagram in figure 9. Since the matrix indices follow the solid lines and propagators are given by Kronecker deltas, $\Gamma^{\alpha\beta,ij}_{\mu\nu,kl} = \frac{1}{N} B^{\alpha\beta}_{\mu\nu} \delta^i_k \delta^j_l$, allowing for the calculation of K.

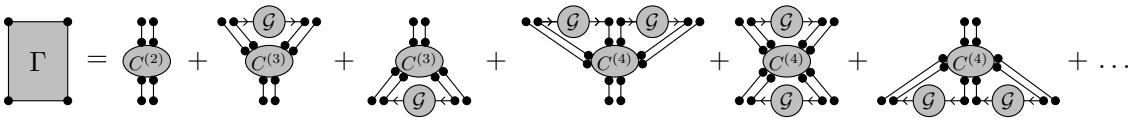

Figure 9. Γ given by the planar cumulants.

B can be therefore expressed in terms of cumulants as a power series

$$B^{\alpha\beta}_{\mu\nu}(Q,P) = \sum_{k,l=1}^{\infty} \sum_{\substack{\sigma_1,\ldots,\sigma_k \\ \rho_1,\ldots,\rho_l}} \delta^{\alpha\sigma_1}\delta^{\beta\sigma_k}\delta_{\mu\rho_l}\delta_{\nu\rho_1} c^{(k+l)}_{\sigma_1\ldots\sigma_k\rho_1\ldots\rho_l} G^{\sigma_1\sigma_2}(Q)\ldots G^{\sigma_{k-1}\sigma_k}(Q) G_{\rho_1\rho_2}(P)\ldots G_{\rho_{l-1}\rho_l}(P), \tag{3.16}$$

where all σ_i and ρ_j take values in $\{1,\bar{1}\}$ and for $k=1$ or $l=1$ $G_{\sigma_k\sigma_{k+1}}$ reduces to Kronecker delta. An application of this procedure to the quantum scattering ensemble is presented in appendix B.

We remark that the additivity of the quaternionic R-transform under the addition of unitarily invariant non-Hermitian matrices implies additivity of B.

3.4 Traced product of resolvents

In the holomorphic domain outside the spectrum the situation simplifies considerably, because one can set $|w| \to 0$ at the very beginning of calculations. Green's function is then diagonal, $G(z,\bar{z}) = \mathrm{diag}(\mathfrak{g}(z), \bar{\mathfrak{g}}(\bar{z}))$, where $\mathfrak{g}(z) = \left\langle \frac{1}{N}\mathrm{Tr}(z\mathbf{1} - X)^{-1} \right\rangle$ and $\bar{\mathfrak{g}}(\bar{z}) = \left\langle \frac{1}{N}\mathrm{Tr}(\bar{z}\mathbf{1} - X^\dagger)^{-1} \right\rangle$. Due to such a structure, B is also diagonal with components

$$B^{\alpha\beta}_{\mu\nu} = \delta^{\alpha\beta}\delta_{\mu\nu} \sum_{k,l=1}^{\infty} c^{(k+l)}_{\underbrace{\alpha\ldots\alpha}_{k}\underbrace{\mu\ldots\mu}_{l}} \left(\mathfrak{g}_\alpha(z_1)\right)^{k-1} \left(\mathfrak{g}_\mu(z_2)\right)^{l-1}, \tag{3.17}$$

where we assume the standard convention $\mathfrak{g}_1(z) = \mathfrak{g}(z)$ and $\mathfrak{g}_{\bar{1}}(z) = \bar{\mathfrak{g}}(\bar{z})$. A matrix equation (3.15) splits into decoupled scalar equations with the explicit solution for the component of our interest

$$K^{11}_{\bar{1}\bar{1}} = \frac{\mathfrak{g}(z_1)\bar{\mathfrak{g}}(\bar{z}_2)}{1 - \mathfrak{g}(z_1)\bar{\mathfrak{g}}(\bar{z}_2) B^{11}_{\bar{1}\bar{1}}}. \tag{3.18}$$

JHEP06(2018)152

The desired component of B obtained from (3.17) reads

$$B^{11}_{\bar{1}\bar{1}} = \sum_{k,l=1}^{\infty} c^{(k+l)}_{\underbrace{1\dots1}_{k}\underbrace{\bar{1}\dots\bar{1}}_{l}} \left(\mathfrak{g}(z_1)\right)^{k-1} \left(\bar{\mathfrak{g}}(\bar{z}_2)\right)^{l-1} . \tag{3.19}$$

Despite the fact that the mapping between cumulants and the R-transform is not one to one [49], some cumulants can be uniquely determined from the knowledge of $R(Q)$. The cumulants $c^{(n)}_{\underbrace{1\dots1}_{k}\underbrace{\bar{1}\dots\bar{1}}_{n-k}}$ are the coefficients at $Q_{11}^{k-1}Q_{1\bar{1}}Q_{\bar{1}\bar{1}}^{n-k-1}$ in the expansion of $R_{1\bar{1}}(Q)$. One can easily see that there are no other cumulants contributing to this term.

All cumulants contributing to $R_{1\bar{1}}$ have at least one $X^\dagger$ following X in the string, therefore $R_{1\bar{1}}$ is divisible by $Q_{1\bar{1}}$. Let us define $\tilde{R}_{1\bar{1}} = R_{1\bar{1}}/Q_{1\bar{1}}$, which is regular at 0. The considered cumulants are the only ones in which X is followed by $X^\dagger$ exactly once. To exclude all other possibilities in the expansion of $\tilde{R}_{1\bar{1}}$, we set $Q_{1\bar{1}} = 0 = Q_{\bar{1}1}$ in $\tilde{R}_{1\bar{1}}(Q)$. To reproduce (3.19) from $\tilde{R}_{1\bar{1}}$ one also needs to replace Q_{11} by $\mathfrak{g}(z_1)$ and $Q_{\bar{1}\bar{1}}$ by $\bar{\mathfrak{g}}(\bar{z}_2)$. Finally,

$$B^{11}_{\bar{1}\bar{1}} = \tilde{R}_{1\bar{1}}\left(\mathrm{diag}(\mathfrak{g}(z_1), \bar{\mathfrak{g}}(\bar{z}_2))\right) . \tag{3.20}$$

3.5 Biunitarily invariant ensembles

In this subsection we consider a class of ensembles, the pdf of which is invariant under multiplication by two unitary matrices, i.e. $P(X) = P(UXV^\dagger)$. In the large N limit the spectral density, which is rotationally invariant, is supported on either a disc or an annulus, a phenomenon termed 'the single ring theorem' [54, 55]. The enhanced symmetry allows one to relate the distribution of eigenvalues and singular values both in the $N \to \infty$ limit [56] and for finite N [40]. More precisely, the radial cumulative distribution function $F(r) = 2\pi \int_0^r \rho(s) s ds$ is given by the solution of the simple functional equation $S_{XX^\dagger}(F(r)-1) = \frac{1}{r^2}$, where $S_{XX^\dagger}$ is the Voiculescu S-transform of the density of squared singular values [56]. Recently, this result was extended to the one-point eigenvector correlation function, which is determined solely by F [29, 49]

$$O_1(r) = \frac{F(r)(1-F(r))}{\pi r^2}. \tag{3.21}$$

Such simple results in the large N limit are possible because of the exceptionally simple structure of cumulants. The only non-zero planar cumulants are the alternating ones [49], $\alpha_n = c^{(2n)}_{1\bar{1}\dots1\bar{1}} = c^{(2n)}_{\bar{1}1\dots\bar{1}1}$. They can be encoded in a function of a single scalar variable $A(x) = \sum_{k=1}^{\infty} \alpha_n x^{n-1}$, called the determining sequence [57]. Due to this, only four components of B (out of 16) do not vanish. These are $B^{11}_{\bar{1}\bar{1}} = B^{\bar{1}\bar{1}}_{11}$, $B^{1\bar{1}}_{11}$, $B^{\bar{1}1}_{1\bar{1}}$.

JHEP06(2018)152

A direct application of formula (3.16) leads to

$$B^{11}_{\bar{1}\bar{1}} = \sum_{k,l=1}^{\infty} \alpha_{k+l-1} \left[G_{1\bar{1}}(Q)G_{\bar{1}1}(Q)\right]^{k-1} \left[G_{1\bar{1}}(P)G_{\bar{1}1}(P)\right]^{l-1} \tag{3.22}$$

$$B^{1\bar{1}}_{\bar{1}1} = G_{1\bar{1}}(Q)G_{1\bar{1}}(P) \sum_{k,l=1}^{\infty} \alpha_{k+l} \left[G_{1\bar{1}}(Q)G_{\bar{1}1}(Q)\right]^{k-1} \left[G_{1\bar{1}}(P)G_{\bar{1}1}(P)\right]^{l-1} \tag{3.23}$$

$$B^{\bar{1}1}_{1\bar{1}} = G_{\bar{1}1}(Q)G_{\bar{1}1}(P) \sum_{k,l=1}^{\infty} \alpha_{k+l} \left[G_{1\bar{1}}(Q)G_{\bar{1}1}(Q)\right]^{k-1} \left[G_{1\bar{1}}(P)G_{\bar{1}1}(P)\right]^{l-1} \tag{3.24}$$

The components of B can be expressed through auxiliary functions

$$B^{11}_{\bar{1}\bar{1}} = B^{\bar{1}\bar{1}}_{11} = S\left(G_{1\bar{1}}(Q)G_{\bar{1}1}(Q), G_{1\bar{1}}(P)G_{\bar{1}1}(P)\right), \tag{3.25}$$

$$B^{1\bar{1}}_{\bar{1}1} = G_{1\bar{1}}(Q)G_{1\bar{1}}(P)T\left(G_{1\bar{1}}(Q)G_{\bar{1}1}(Q), G_{1\bar{1}}(P)G_{\bar{1}1}(P)\right), \tag{3.26}$$

$$B^{\bar{1}1}_{1\bar{1}} = G_{\bar{1}1}(Q)G_{\bar{1}1}(P)T\left(G_{1\bar{1}}(Q)G_{\bar{1}1}(Q), G_{1\bar{1}}(P)G_{\bar{1}1}(P)\right), \tag{3.27}$$

where

$$S(x,y) = \sum_{k,l=1}^{\infty} \alpha_{k+l-1} x^{k-1} y^{l-1} = \frac{xA(x) - yA(y)}{x-y}, \tag{3.28}$$

$$T(x,y) = \sum_{k,l=1}^{\infty} \alpha_{k+l} x^{k-1} y^{k-1} = \frac{A(x) - A(y)}{x-y}, \tag{3.29}$$

with A being the determining sequence.

We remark that the average over the ensemble has been already taken at the level of Feynman diagrams and at this moment, we can safely remove the regularization. There are further simplifications for the biunitarily invariant matrices [49]

$$G_{1\bar{1}}G_{\bar{1}1}A(G_{1\bar{1}}G_{\bar{1}1}) = F(r) - 1, \quad G_{1\bar{1}}G_{\bar{1}1} = -\pi O_1(r). \tag{3.30}$$

Having calculated B and knowing Green's function, we determine $K^{11}_{\bar{1}\bar{1}}$ from (3.15) and, after algebraic manipulations, we get a compact formula for the 2-point eigenvector correlation function from (3.4)

$$O_2(z_1,z_2) = \frac{1}{\pi}\partial_{\bar{z}_1}\partial_{z_2} \frac{\bar{z}_1(z_1-z_2)O_1(r_1) + z_2(\bar{z}_1-\bar{z}_2)O_1(r_2)}{|z_1-z_2|^2\left[F(r_1)-F(r_2)\right]}. \tag{3.31}$$

The quaternionic R-transform of biunitarily invariant ensembles takes a remarkably simple form [49], in particular $R_{1\bar{1}}(Q) = Q_{1\bar{1}}A(Q_{1\bar{1}}Q_{\bar{1}1})$. Moreover, due to the rotational symmetry of the spectrum, $\mathfrak{g}(z) = 1/z$. According to (3.18), the traced product of resolvents is given by

$$\mathfrak{h}(z_1,\bar{z}_2) = \frac{1}{z_1\bar{z}_2 - A(0)}. \tag{3.32}$$

Interestingly, $A(0) = r^2_{\text{out}}$, where r_{out} is the external radius of the spectrum. This result shows a high level of universality, since for any two functions f, g analytic in the spectrum the expectation in the $N \to \infty$ limit

$$\left\langle \frac{1}{N}\mathrm{Tr} f(X)g(X^\dagger) \right\rangle = \frac{1}{(2\pi i)^2}\int_\gamma dz_1 \int_{\bar{\gamma}} d\bar{z}_2 \frac{f(z_1)g(\bar{z}_2)}{z_1\bar{z}_2 - r^2_{\text{out}}} \tag{3.33}$$

JHEP06(2018)152

is given by the same formula, irrespectively of the specific biunitarily invariant ensemble. The only parameter — spectral radius r_{out} — can be set to 1 by rescaling the matrix. This result, appearing naturally in the language of cumulants, from the point of the spectral decomposition, $X = \sum_k |R_k\rangle \lambda_k \langle L_k|$, is far from being obvious and may explain the simplicity of formula (3.31).

4 Examples

4.1 Elliptic ensemble

As the first example of application of this formalism, we take the elliptic ensemble. Due to the fact that only the second cumulants do not vanish, the sum in (3.16) reduces to a single term and B is diagonal, $B_{ell} = \text{diag}(\sigma^2\tau, \sigma^2, \sigma^2, \sigma^2\tau)$. However, the equations (3.15) do not decouple, because Green's functions are not diagonal in the non-holomorphic regime. Denoting for $j = 1, 2$

$$G_j = \begin{pmatrix} \frac{\bar{z}_j - z_j\tau}{\sigma^2(1-\tau^2)} & \frac{i}{\sigma^2}\sqrt{1 - \frac{|z_j - \bar{z}_j\tau|^2}{\sigma^2(1-\tau^2)}} \\ \frac{i}{\sigma^2}\sqrt{1 - \frac{|z_j - \bar{z}_j\tau|^2}{\sigma^2(1-\tau^2)}} & \frac{z_j - \bar{z}_j\tau}{\sigma^2(1-\tau^2)} \end{pmatrix} \tag{4.1}$$

Green's function of the elliptic ensemble in the non-holomorphic regime (see appendix A), we find K, solving (3.15)

$$K = \left(\mathbf{1} - (G_1 \otimes G_2^T) B_{Ell}\right)^{-1} \left(G_1 \otimes G_2^T\right). \tag{4.2}$$

Then we focus on the component $K^{11}_{\bar{1}\bar{1}}$ and differentiate it twice, according to (3.4), obtaining

$$O_2(z_1, z_2) = \frac{1}{\pi^2}\partial_{\bar{z}_1}\partial_{z_2} K^{11}_{\bar{1}\bar{1}} = -\frac{\sigma^2(1-\tau^2)^2 - (z_1 - \bar{z}_2\tau)(\bar{z}_2 - z_1\tau)}{\pi^2\sigma^2(1-\tau^2)|z_1 - z_2|^4}. \tag{4.3}$$

This result was derived for the first time by Chalker and Mehlig [10].[2] For the Ginibre Ensemble ($\sigma = 1$, $\tau = 0$) it reduces to

$$O_2(z_1, z_2) = \frac{-1}{\pi^2}\frac{1 - z_1\bar{z}_2}{|z_1 - z_2|^4}. \tag{4.4}$$

For completeness, we remark that the holomorphic part of the two point function, calculated from (3.18), reads

$$\mathfrak{h}(z_1, \bar{z}_2) = \frac{4}{-4 + \left(z_1 + \sqrt{z_1^2 - 4\sigma^2\tau}\right)\left(\bar{z}_2 + \sqrt{\bar{z}_2^2 - 4\sigma^2\tau}\right)}. \tag{4.5}$$

4.2 Biunitarily invariant ensembles

We consider some examples where the two-point function can be easily calculated. This list is by no means exhaustive. In fact, biunitary invariance is preserved under addition and multiplication, thus one can easily generate new ensembles. We do not present results for products of the ensembles considered below, solely due to the fact that the expressions for $O_2(z_1, z_2)$ become lengthy.

- *Ginibre.* As a cross-check of correctness of our formula, let us first consider the Ginibre ensemble. Its spectral density is uniform on the unit disk, therefore $F(r) =$

[2] [10, eq. (94)] contains a small misprint in the constant factor, which does not affect validity of any other results therein.

JHEP06(2018)152

$2\pi \int_0^r s\frac{\theta(1-s)}{\pi} ds$ is equal to 1 for $r > 1$ and $F(r) = r^2$ for $r \leq 1$. Substitution to (3.31) reproduces the result derived earlier (4.4).

- *Induced Ginibre* [58]. Let us consider a rectangular $N \times M$ matrix X (without loss of generality, $M > N$) with iid Gaussian entries. There exists an $M \times M$ unitary matrix U so that $Y = XU$ can be represented in the block form $Y = (X', 0)$. The right $N \times (M - N)$ block consists of zeros, while X' is called the induced Ginibre matrix. In the limit $N, M \to \infty$ with $\alpha = \frac{M-N}{N}$ fixed, its radial cdf reads

$$F(r) = \begin{cases} 0 & \text{for } r < \sqrt{\alpha} \\ r^2 - \alpha & \text{for } \sqrt{\alpha} < r < \sqrt{\alpha + 1} \\ 1 & \text{for } r > \sqrt{1 + \alpha} \end{cases} \tag{4.6}$$

  Substitution into (3.31) yields, after some algebra

$$O_{Ind}(z_1, z_2) = \frac{1}{\pi^2} \frac{(1 + \alpha - z_1\bar{z}_2)(\alpha - z_1\bar{z}_2)}{z_1\bar{z}_2|z_1 - z_2|^4}. \tag{4.7}$$

  The Ginibre Ensemble corresponds to $\alpha = 0$.

- *Truncated Unitary* [59]. Let us consider a $(N + L) \times (N + L)$ random unitary matrix with a pdf given by the Haar measure on $\mathrm{U}(N + L)$ and remove its last L rows and columns. The radial cdf of the remaining square matrix in the limit $N, L \to \infty$, with $\kappa = \frac{L}{N}$ fixed, reads $F(r) = \kappa\frac{r^2}{1-r^2}$ for $r < (1 + \kappa)^{-1/2}$ and 1 otherwise [60]. Therefore the two-point eigenvector function reads

$$O_{TU}(z_1, z_2) = \frac{1}{\pi^2} \frac{-1 + z_1\bar{z}_2(1 + \kappa)}{|z_1 - z_2|^4}. \tag{4.8}$$

- *Spherical Ensemble.* Consider the product $Y = X_1X_2^{-1}$, where X_1 and X_2 are Ginibre matrices. Its radial cdf reads $F(r) = \frac{r^2}{1+r^2}$ and its spectrum is unbounded [61]. This ensemble is beyond the assumptions made for the derivation of (3.31). Nevertheless, motivated by the successful application of these methods for the one-point correlation function in this ensemble [29], we assume the correctness of our formulas and calculate the two-point function

$$O_{Sph}(z_1, z_2) = \frac{1}{\pi^2} \frac{-1}{|z_1 - z_2|^4}. \tag{4.9}$$

- *Product of two Ginibre.* We consider a matrix $Y = X_1X_2$, where X_1 and X_2 are Ginibre matrices. The radial cdf of Y is $F(r) = \min(r, 1)$, thus

$$O_{prod}(z_1, z_2) = -\frac{1}{\pi^2} \frac{2(|z_1| + |z_2|)(z_1\bar{z}_2 + |z_1z_2|) - |z_1 + z_2|^2 - 4|z_1z_2|}{4|z_1z_2||z_1 - z_2|^4}. \tag{4.10}$$

JHEP06(2018)152

4.3 Pseudohermitian matrix

Let us consider the product $X = AB$ of two Hermitian matrices A, B. The product is not Hermitian, $X^\dagger = BA \neq X$, but if one of the matrices, let us say A, is positive definite, X is isospectral to the Hermitian matrix $A^{1/2}BA^{1/2}$, thus X, despite its non-Hermiticity, has a real spectrum. The diagonalising matrix is, however, not unitary, resulting in non-orthogonality of eigenvectors. Such matrices can be toy-models for more complicated physical system described by Hamiltonians which are not Hermitian but possesses parity-time (PT) symmetry [62]. The most interesting models have a parameter which controls how far the system is from breaking of the symmetry. At a critical value, called the exceptional point, two real eigenvalues coalesce and move away in the imaginary direction, spontaneously breaking the PT-symmetry.

As an example we consider the matrix $X = (2+G_1)(2+G_2)$, where G_i's are independent matrices drawn from the Gaussian Unitary Ensemble, the spectral density of which in the large N limit is the Wigner semicircle, $\rho_{\mathrm{GUE}}(x) = \frac{1}{2\pi}\sqrt{4-x^2}$, supported on the interval $[-2, 2]$. This model has an exceptional point at $x = 0$.

The components of the quaternionic R-transform of X read [63]

$$R_{11} = \frac{4(1 - G_{1\bar{1}}G_{\bar{1}1})(1 - G_{\bar{1}\bar{1}})^2}{\left(1 + G_{1\bar{1}}G_{\bar{1}1}(G_{\bar{1}\bar{1}} - 2) - G_{\bar{1}\bar{1}} + G_{11}(G_{\bar{1}\bar{1}} + G_{1\bar{1}}G_{\bar{1}1} - 1)\right)^2}, \tag{4.11}$$

$$R_{1\bar{1}} = -\frac{G_{1\bar{1}}\left[-3 - G_{1\bar{1}}G_{\bar{1}1}(G_{\bar{1}\bar{1}} - 1) + G_{\bar{1}\bar{1}} + G_{11}(1 - G_{1\bar{1}}G_{\bar{1}1} + G_{\bar{1}\bar{1}})\right]^2}{(G_{1\bar{1}}G_{\bar{1}1} - 1)\left[1 + G_{1\bar{1}}G_{\bar{1}1}(G_{\bar{1}\bar{1}} - 2) - G_{\bar{1}\bar{1}} + G_{11}(G_{\bar{1}\bar{1}} - 1 + G_{1\bar{1}}G_{\bar{1}1})\right]^2}. \tag{4.12}$$

The other two components are given by the exchange of indices $1 \leftrightarrow \bar{1}$. Inserting them into (2.22) and focusing only on the holomorpic solution ($|w| = 0$), we arrive at the equation for Green's function

$$\frac{4}{(1 - \mathfrak{g}(z))^2} + \frac{1}{\mathfrak{g}(z)} = z. \tag{4.13}$$

We choose a branch which gives the asymptotic behavior $\mathfrak{g}(z) \sim 1/z$ for large z. The spectrum is supported on a single interval $[0, z_+]$, with $z_+ = \frac{1}{2}(11 + 5\sqrt{5})$. The Green's function infinitely close to the spectrum reads

$$\lim_{\epsilon \to 0} \mathfrak{g}(x \pm i\epsilon) = \frac{1 + 2x}{3x} - \frac{1}{6x}\left(\frac{a}{r^{1/3}}(1 \pm i\sqrt{3}) - r^{1/3}(1 \mp i\sqrt{3})\right), \tag{4.14}$$

where $a = 1 + 10x + x^2$ and $r = 1 + 15x + 39x^2 - z^3 - 6\sqrt{3}x\sqrt{x + 11x^2 - x^3}$. The imaginary part of Green's function yields the spectral density, calculated in [64]. The traced product of resolvents according to (3.18) satisfies the equation

$$\frac{1}{\mathfrak{h}(z_1, \bar{z}_2)} = \frac{1}{\mathfrak{g}(z_1)\bar{\mathfrak{g}}(\bar{z}_2)} - \frac{\left(1 - \mathfrak{g}(z_1)\right)^2\left(1 - \bar{\mathfrak{g}}(\bar{z}_2)\right)^2}{\left[-3 + \mathfrak{g}(\bar{z}_2) + \mathfrak{g}(z_1) + \mathfrak{g}(z_1)\mathfrak{g}(\bar{z}_2)\right]^2}, \tag{4.15}$$

where $\mathfrak{g}(z_1)$ and $\mathfrak{g}(\bar{z}_2)$ are the solutions of (4.13) with $1/z$ asymptotic behavior.

The two-point function is calculated from (3.6) and its cross-sections are juxtaposed with the numerical simulations in figure 10, showing an excellent agreement.

JHEP06(2018)152

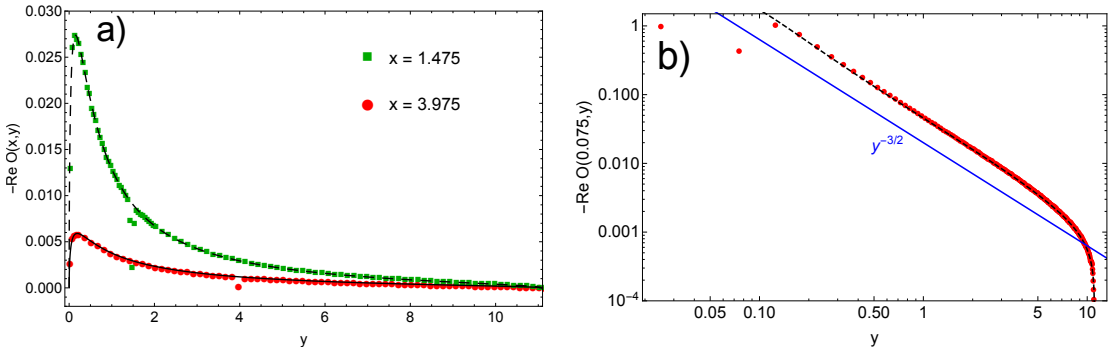

Figure 10. Cross sections of the two point eigenvector correlation function $O_2(x, y)$ for a) $x = 1.475$ (squares and dashed line), $x = 3.975$ (circles and solid line) and b) $x = 0.075$. The numerical data (points) are obtained by diagonalization of $5 \cdot 10^4$ matrices of size $N = 100$. Black lines are the solutions of (4.15) inserted into (3.7). Interestingly, if one of the arguments is close to the exceptional point $x = 0$, the large part of the function can be approximated by a power-law.

5 Towards microscopic universality of eigenvectors

Random matrices show the phenomenon of universality at certain regions of the spectra. In the case of Hermitian ensembles, such universalities appear in the bulk (the so-called sine kernel) and at the edges of the spectra (Airy, Bessel, Pearcey, etc.). For a given generic Hermitian ensemble represented by $N \times N$ matrices H, one of the tools for investigating the existence of universalities are the multi-trace correlation functions

$$G(z_1, z_2, \ldots, z_j) = \sum_{k_1,\ldots,k_j=1}^{\infty} N^{j-2} \frac{\left\langle \mathrm{tr} H^{k_1} \ldots \mathrm{tr} H^{k_j} \right\rangle_c}{z_1^{k_1+1} \ldots z_k^{k_j+1}}. \tag{5.1}$$

The subscript c denotes the connected part.

Such objects were studied extensively using various techniques including loop equations [37], Coulomb gas analogy [65] and Feynman diagrams [52, 53]. They were put into a formal mathematical formulation of the higher order freeness [66–68]. When the eigenvalues occupy a single interval, they obey the Ambjørn-Jurkiewicz-Makeenko universality [37]. The divergences of the double-trace correlation function signal the breakdown of the $1/N$ expansion and the need to resum the whole series and rescale its arguments. Different universal limits are manifested as different types of singularities.

A natural generalization of the two-point double-trace function to the non-Hermitian setting is the connected average of two copies of the electrostatic potential (2.5)

$$F(Q, P) = \left\langle \frac{1}{N} \ln \det(\mathcal{Q} - \mathcal{X}) \frac{1}{N} \ln \det(\mathcal{P} - \mathcal{X}) \right\rangle_c, \tag{5.2}$$

introduced in [42], where Gaussian models were also considered. As the quaternionic Green's function, encoding all expectations of the traces can be obtained from the potential (see (2.10)), the function above generates all covariances of traces

$$\left\langle \frac{1}{N} \mathrm{Tr} X^{\alpha_1} X^{\alpha_2} \ldots X^{\alpha_k} \frac{1}{N} \mathrm{Tr} X^{\beta_1} X^{\beta_2} \ldots X^{\beta_l} \right\rangle_c, \tag{5.3}$$

JHEP06(2018)152

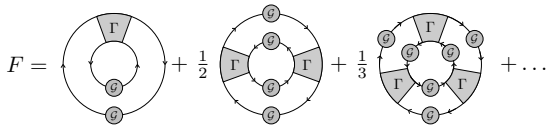

Figure 11. Hierarchy of wheel diagrams contributing to the two-point double-trace correlation function (5.2), which in turn corresponds to the contraction of indices in figure 4 leading to L. The combinatorial factor $1/m$ corresponds to rotational symmetry and prevents overcounting the diagrams.

being a natural extension of the second order freeness for large non-Hermitian matrices. Here $\alpha_i, \beta_j \in \{1, \dagger\}$.

As we mentioned earlier, the indices in the product of a resolvent can be contracted in two ways, see figure 4. One of them gives access to the eigenvector correlation function, while the second one yields F. More precisely, $F(Q,P) = \mathrm{Tr}L$.

Since we consider connected expectation, we may write $\ln\det(\mathcal{Q}-\mathcal{X}) = \ln\det(\mathbf{1} - \mathcal{X}\mathcal{Q}^{-1})$ and use the identity $\ln\det = \mathrm{Tr}\ln$. Then, logarithms are expanded in power series, $\ln(1+z) = \sum_{k=1}^{\infty}\frac{z^k}{k}$, which allows for convenient calculation of Feynman diagrams. Due to the presence of traces, the baselines from $(\mathcal{X}\mathcal{Q}^{-1})^k$ are now drawn as two concentric rings.[3] The dominant diagrams are the planar ones in which vertices and propagators are drawn between the two rings, but propagators connecting vertices do not encircle the inner ring (as in figure 4), see also [52, 53]. The diagrams have an additional symmetry, namely rotating each ring leads to a new admissible diagram contributing equally. The resulting symmetry factors exactly cancel coefficients in the expansion of logarithms.

Each diagram can be decomposed into m segments in which $\mathcal{X}$'s from two rings are connected through propagators and vertices. Segments are connected to each other through rings. As a result, each diagram looks like a wheel with m spokes. It turns out that the sum of all diagrams contributing to the spoke is exactly the rung, Γ, from the ladder diagrams in section 3.3. The $\mathcal{X}$'s on ring, which are not part of a spoke can be connected with each other through propagators and vertices in any way, thus contributing to the Green's function. The general structure of such diagrams is presented in figure 11.

The wheel diagrams with m spokes have an additional symmetry, namely they can be rotated by an angle $2\pi/m$. In order not to overcount the diagrams in the sum, we must include $1/m$ factor. Finally, we get

$$\begin{aligned} N^2 F(Q,P) &= \mathrm{Tr}\sum_{m=1}^{\infty}\frac{1}{m}\left[(G(Q)\otimes G^T(P))B(Q,P)\right]^m \\ &= -\log\det\left[\mathbf{1} - (G(Q)\otimes G^T(P))B(Q,P)\right]. \end{aligned} \tag{5.4}$$

This means that the result, derived in [42] and used for deducing the existence of the edge universality for the *spectral density* [69], holds for the entire class of non-Hermitian models.

[3] The rings could be equivalently drawn next to each other. This choice is just for convenience.

JHEP06(2018)152

The two-point single-trace correlation functions encoding correlations between eigenvectors also have their counterpart in the Hermitian case, but because of realness of the spectrum and orthogonality of eigenvectors it trivially reduces to the one-point Green's function

$$\left\langle \frac{1}{N}\mathrm{Tr}(z_1\mathbf{1}-H)^{-1}(z_2\mathbf{1}-H)^{-1}\right\rangle = \frac{\mathfrak{g}(z_1)-\mathfrak{g}(z_2)}{z_2-z_1}, \tag{5.5}$$

thus not attracting attention. Eigenvectors of non-normal matrices are no longer trivial, making such correlation functions meaningful quantities.

In the spirit of the above analysis, one is tempted to ask if we can probe hypothetical *eigenvector universality* using similar tools. We would like to stress that, even in the case of the simplest Ginibre ensemble, the direct analysis of the eigenvector correlation functions is very hard. Whereas the finite N expression for the one point function is known [10, 23], the only known non-perturbative results for the calculation of the two-point eigenvector correlation function are given implicitly [9, 10] as

$$O_2(z_1,z_2) = -\frac{N}{\pi^2\Gamma(N)}e^{-N(|z_1|^2+|z_2|^2)}\det\left[h_{ij}\right]_{i,j=0}^{N-2}, \tag{5.6}$$

where the matrix h is pentadiagonal with entries given by

$$h_{ij} = \frac{N^{j+3}}{\pi(j+1)!}\int d^2\lambda\bar{\lambda}^i\lambda^j\left[|z_1-\lambda|^2|z_2-\lambda|^2+\frac{1}{N}(z_1-\lambda)(\bar{z}_2-\bar{\lambda})\right]e^{-N|\lambda|^2}. \tag{5.7}$$

There is, however, a different possibility of inferring the existence of universality. Spectra of non-normal matrices are intimately linked with the properties of their eigenvectors. The completeness relation $\sum_{k=1}^{N}|R_k\rangle\langle L_k| = \mathbf{1}$ used in the weighted density (1.3) leads to the sum rule $\int_{\mathbb{C}} d\mu(w)D(z,w) = \rho(z)$, which imposes constraints on the eigenvector correlation functions

$$NO_1(z) + \int_{\mathbb{C}} d\mu(w)O_2(z,w) = \rho(z). \tag{5.8}$$

While the right hand side is of order 1, the one-point correlator gives a contribution of order N, thus there has to be a counterterm from the integral. As the region of integration is in fact compact in the large N limit, the divergence can stem only from the region when w is close to z. The exact calculations in this regime are not accessible within the diagrammatic approach, but below we give a qualitative argument that the microscopic scaling is responsible for the cancellation of divergences.

In RMT the microsopic universality can be probed on the scale of the typical distance between eigenvalues. Demanding that in the disk of radius δz centered at z we expect one eigenvalue, leads us to the scaling

$$w = z + \frac{u}{\sqrt{N\rho(z)}}, \tag{5.9}$$

where $u \sim 1$. We notice that in all examples presented in section 4 the two-point function can be expressed as

$$O_2(z,w) = -\frac{1}{\pi^2}\frac{P(z,w)}{|z-w|^4} \tag{5.10}$$

JHEP06(2018)152

with the same behavior in the denominator. The microscoping scaling (5.9) inserted in the denominator produces a term $(N\rho(z))^2$, while the Jacobian of the change of variables reduces the power to one, giving the desired behavior in N. Moreover, by the explicit evaluation of derivatives in (3.31) and the application of de l'Hospital's rule twice we get for biunitarily invariant ensembles $P(z,z) = \frac{O(z)}{\rho(z)}$, which cancels densities, eventually leaving only the one-point function, which produces the desired counterterm. We hypothesize that this phenomenon is universal across all non-Hermitian ensembles in the bulk.

Motivated by the ubiquitousness of the $|z-w|^{-4}$ divergence in the bulk we state the conjecture that in generic non-Hermitian matrices with complex entries for all points in the bulk at which the spectral density does not develop singularities, there exists a microscopic limit

$$\lim_{N\to\infty} N^{-2} O_2(z + \frac{x}{\sqrt{N}}, z + \frac{y}{\sqrt{N}}) = O_1(z)\Phi(|x-y|), \tag{5.11}$$

where

$$\Phi(|\omega|) = -\frac{1}{\pi^2|\omega|^4}\left(1 - (1+|\omega|^2)e^{-|\omega|^2}\right). \tag{5.12}$$

The function Φ was calculated in [9, 10] by evaluating $O_2(0,z)$ from the exact result (5.6) and taking the scaling limit $z = \frac{\omega}{\sqrt{N}}$. It is presented in figure 12a) and compared with the evaluation of the exact formula.

Interestingly, performing an analogous reasoning for the Ginibre ensemble (in which $P(z,w) = 1 - z\bar{w}$) when z is at the edge of the spectrum leads us to a different conclusion. When two arguments get close, the two-point function diverges, but it does so as $|z-w|^{-3}$, because P also vanishes, reducing the exponent. This suggests that at the edge the two-point function scales as $N^{3/2}$ instead of N^2 in the bulk. This stays in agreement with the sum rule (5.8), since O_1 at the edge scales as $N^{1/2}$ [23]. The limiting scaling function is not available to us, hence we evaluate numerically (5.6) and show the results in figure 12b). The divergence of the two-point function at the origin for the product of two Ginibre matrices (4.10) also suggests the existence of a different scaling there.

6 Summary

Using the methods of the quaternion formalism [70] for non-Hermitian random matrices, we have proposed the explicit calculational scheme for the two-point eigenvector correlation function (1.4). First, we have checked that our formalism reproduces all known examples in the literature, i.e. the complex Ginibre ensemble, an elliptic ensemble and the open chaotic scattering ensemble. Second, we considered two subclasses of non-normal random matrices: the pseudo-hermitian and the biunitarily invariant ensembles, which in the large N limit are described by the R-diagonal operators from free probability [71, 72]. In both cases we got new results for the two-point eigenvector correlation functions. In the case of the bi-unitarily invariant ensembles, the two-point function $O_2(z,w)$ has a particularly simple form. It is expressed solely as a function of the radial cumulative distribution function $F(r)$ and the one-point eigenvector correlation function $O_1(r)$.

JHEP06(2018)152

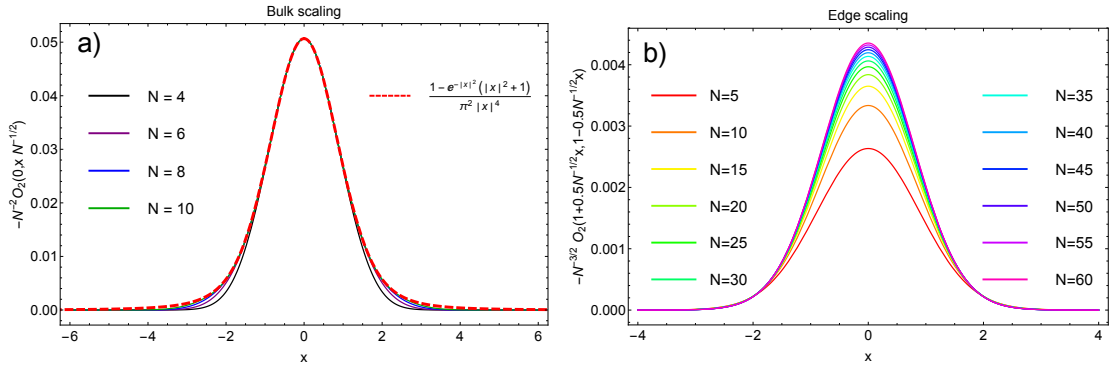

Figure 12. The two-point eigenvector correlation function $O_2(z_1, z_2)$ for the Ginibre ensemble in the microscopic a) bulk regime, $z_1 = 0$, $z_2 = \frac{x}{\sqrt{N}}$ and b) edge regime $z_1 = 1 + \frac{x}{2\sqrt{N}}$, $z_2 = 1 - \frac{x}{2\sqrt{N}}$. The red dashed line is Chalker and Mehlig's exact result (5.12). In the bulk microscopic regime O_2 scales as N^2 and at the edge as $N^{3/2}$. The rapid convergence to the limiting bulk scaling suggest that the corrections are exponentially small, while the hypothetical edge scaling seems to have $1/N$ corrections.

Recently, it was proven [29] that for biunitarily invariant ensmbles, $O_1(r)$ can be expressed in terms of $F(r)$ exclusively, which can be viewed as an extension of the single ring (Haagerup-Larsen) theorem [54, 56]. Combining this result with our formalism, we arrive at the conclusion, that the two-point eigenvector correlation function for general biunitarily invariant ensembles in the large N limit depends functionally solely on the spectral density. Such a situation resembles the Ambjørn-Jurkiewicz-Makeenko (known also as the Brezin-Zee) universality in the case of Hermitian random matrix models, where the two-point spectral Green's function depends solely on the one-point Green's function, irrespectively on the specific ensemble. Mathematical formulation of such a construction is known as the second order freeness [66]. We are therefore tempted to speculate that, by combining second order freeness and freeness with amalgamation [73], the notion of the non-orthogonality of eigenvectors can be extended into a broader context of operators in von Neumann algebras. Indeed, an equation similar to (3.15) has recently appeared in the description of fluctuations of Gaussian block matrices [74]. Moreover, the diagrammatic calculations of the traced product of resolvents resemble the partition structure diagrams introduced in [75].

The similarity of our result to AJM (BZ) universality has further consequences. In the case of the ABJ (BZ) universality, the singular points of the correlation functions identify the regions of the spectra where microscopic universality takes place. This includes both the cases of the bulk and edge universality. We are therefore inclined to apply a similar argument to our result, searching for the microscopic eigenvector universalities. An additional argument for the microscopic universality comes from a constraint on eigenvector correlation function (5.8), as originallly noted by Walters and Starr. The sum rules originating from this constraint strongly suggest the universal form of the microscopic two-point eigenvector correlations in analogy to a similar phenomenon for the sum rules of Dirac Euclidean operators found by Leutwyler and Smilga [76]. The latter lead the Stony Brook group to the discovery of the universal Bessel kernels for chiral random matrix models [77, 78].

JHEP06(2018)152

Our analysis, as well as explicit examples for the biunitarily invariant ensembles calculated in section 4.2, point at the generic shape of such universality, coming from the ubiquitous factor $|z-w|^4$ in the denominator. Explicitly, $O_2(z,w) = -\frac{1}{\pi^2}\frac{P(z,w)}{|z-w|^4}$, where $\lim_{z\to w} P(z,w) = O_1(z)/\rho(z)$ yields the Petermann factor. Such unique behavior is responsible for the crucial cancellation of the divergent terms in the leading order in N in the sum rules. The identification of this mechanism leads us to predict the existence of the universal microscopic scaling of the eigenvector correlation function $\Phi(|\omega|)$. Such a limit was obtained in the special case of the Ginibre ensemble [9, 10]. We conjecture that this universality extends to at least biunitarily invariant random ensembles.

Interestingly, the sum rule (5.8) leads also to interesting predictions at the edge. It is well known that correlations of eigenvalues of non-Hermitian matrices exhibit universal behavior at the edge, given by the error function. Our large N results for the eigenvector correlations show that the leading singularity weakens at the edge, $|z-w|^4 \to |z-w|^3$, leading to $N^{3/2}$ scaling of the two-point correlation function. The numerical evaluation of the implicit exact result (5.6) confirms this hypothesis, but the analytic form of the scaling function is not yet available, even in the case of the simplest, complex Ginibre ensemble.

Our results are only one step towards understanding the statistical properties of non-normal random operators and give rise to new questions. The matrix of overlaps O_{ij} is the simplest invariant object. It is natural to ask what kind of non-trivial higher order invariants can be built out of eigenvectors. This problem is even more cumbersome in the light of recent results [24, 33], because the distribution of the diagonal overlap O_{ii} is heavy tailed and some objects, for instance $\langle O_{ii}^2 \rangle$, do not exist. For the real Ginibre ensemble the situation is even more hopeless, since at the real axis the one-point function O_1 does not exist! While one expects the existence of certain correlation functions involving local averages of *distinct* eigenvectors, it is unclear whether their mathematical structure simplifies as it does for spectral statistics, which form determinantal point processes. Even though an event with two or more eigenvalues lying close to each other is unlikely to happen due to the eigenvalue repulsion, correlations between their eigenvectors do not decay, as can be seen from the microscopic scaling of O_2. It is therefore very appealing to study microscopic eigenvector correlations involving more than two eigenvalues.

Although the real eigenvalues and corresponding eigenvectors of the real Ginibre ensemble are beyond the scope of perturbative techniques, we expect that the results for the two-point function remain unchanged for the eigenvectors associated with complex eigenvalues of the real Ginibre. Despite that the eigenvector overlaps are heavy-tailed, the traces of powers of X and its conjugate transpose are localized around their mean value [23]. Such a big cancellation is possible due to the sum rule originating from the completeness relation. Based on this fact, we expect that the formula for the traced product of resolvents (3.18) holds also for matrices with real entries.

The issue of a hypothetical microscopic eigenvector universality for generic non-Hermitian ensembles is also of primary importance, since unraveling the unknown microscopic eigenvector correlations may give hope in the case of notorious sign problems by giving an insight into the properties of the Dirac operator in Euclidean QCD at non-zero chemical potential.

JHEP06(2018)152

Note added. After completing this manuscript, we became aware of a recent work by Bourgade and Dubach [24], which tackles the issue of eigenvector correlations in the complex Ginibre ensemble in the bulk using different probabilistic techniques. They found the full probability of the diagonal overlap as an inverse gamma distribution and also studied the first two moments of the off-diagonal overlap. Moreover they proved that the result for the macroscopic two-point function (4.4) extends to mesoscopic scales.

Acknowledgments

WT appreciates the financial support from the Polish Ministry of Science and Higher Education through the 'Diamond Grant' 0225/DIA/2015/44 and the scholarship of Marian Smoluchowski Research Consortium Matter Energy Future from KNOW funding. The authors thank Piotr Warchoł for discussions and are grateful to Yan Fyodorov, Paul Bourgade and Guillaume Dubach for correspondence and useful remarks. The authors are indebted to Janina Krzysiak for carefully reading this manuscript and helping to bring it to the current shape.

A One-point functions in elliptic ensemble

It is very instructive to show how the formalism described in section 2 works in practice. Let us consider a non-Hermitian matrix model given by the Gaussian potential (2.13). Due to the fact that there are no vertices in this model, the only cumulants are $c^{(2)}_{\alpha\beta}$, given by the propagators. This completely determines the quaternionic R-transform

$$R(Q) = \sigma^2 \begin{pmatrix} \tau Q_{11} & Q_{1\bar{1}} \\ Q_{\bar{1}1} & \tau Q_{\bar{1}\bar{1}} \end{pmatrix}. \tag{A.1}$$

Once we perform the average over the ensemble (i.e. we know the form of R), we can safely remove the regularization by setting $|w| = 0$ at the level of the algebraic equation (2.22), which in this case reads

$$\sigma^2 \begin{pmatrix} \tau G_{11} & G_{1\bar{1}} \\ G_{\bar{1}1} & \tau G_{\bar{1}\bar{1}} \end{pmatrix} + \frac{1}{G_{11}G_{\bar{1}\bar{1}} - G_{1\bar{1}}G_{\bar{1}1}} \begin{pmatrix} G_{\bar{1}\bar{1}} & -G_{1\bar{1}} \\ -G_{\bar{1}1} & G_{11} \end{pmatrix} = \begin{pmatrix} z & 0 \\ 0 & \bar{z} \end{pmatrix}. \tag{A.2}$$

Focusing on the $1\bar{1}$ component, one gets

$$G_{1\bar{1}} \left(\sigma^2 - \frac{1}{G_{11}G_{\bar{1}\bar{1}} - G_{1\bar{1}}G_{\bar{1}1}} \right) = 0. \tag{A.3}$$

There are two solutions, a trivial one $G_{1\bar{1}} = 0$ and a non-trivial one, $\sigma^2 = (G_{11}G_{\bar{1}\bar{1}} - G_{1\bar{1}}G_{\bar{1}1})^{-1}$. Let us focus on the trivial first. Inserting $G_{1\bar{1}} = 0$ into the equation given by the 11 component, we get $\sigma^2\tau G_{11} + 1/G_{11} = z$, with two solutions

$$G_{11}(z) = \frac{z \pm \sqrt{z^2 - 4\sigma^2\tau}}{2\sigma^2\tau} = \mathfrak{g}(z). \tag{A.4}$$

This is the holomorphic part, valid outside the spectrum and we have to choose the branch of the solution with a minus sign for correct asymptotic behavior at infinity $\mathfrak{g}(z) \sim 1/z$. In the holomorphic domain, the off-diagonal elements of Green's function vanish, because the one-point eigenvector correlation function is trivially zero as there are no eigenvalues there.

Considering the non-trivial solution of (A.3) and inserting it into the equations for 11 and $\bar{1}\bar{1}$ components, we obtain a system of two linear equations

$$\sigma^2\tau G_{11} + \sigma^2 G_{\bar{1}\bar{1}} = z,$$
$$\sigma^2\tau G_{\bar{1}\bar{1}} + \sigma^2 G_{11} = \bar{z},$$

with the solution

$$G_{11}(z) = \frac{\bar{z} - z\tau}{\sigma^2(1-\tau^2)}. \tag{A.5}$$

The spectral density is calculated according to (2.3):

$$\rho(z,\bar{z}) = \frac{1}{\pi}\partial_{\bar{z}} G_{11} = \frac{1}{\pi\sigma^2(1-\tau^2)}. \tag{A.6}$$

One can also calculate $G_{1\bar{1}}$ and get the following formula for the one-point eigenvector correlation function from (2.9)

$$O_1(z) = \frac{1}{\pi\sigma^2}\left(1 - \frac{|z-\bar{z}\tau|^2}{\sigma^2(1-\tau^2)^2}\right). \tag{A.7}$$

The boundary of the spectrum can be calculated in two ways: by requiring that the holomorphic and non-holomorphic solutions match at the boundary or by imposing vanishing of the one-point eigenvector correlation function. Both methods give

$$\frac{x^2}{(1+\tau)^2} + \frac{y^2}{(1-\tau)^2} = \sigma^2, \tag{A.8}$$

which is the equation for the ellipse with semi-axes $\sigma(1+\tau)$ and $\sigma(1-\tau)$, hence the name of the ensemble.

B Quantum scattering ensemble

Let us see how the procedure for determining the rung of the ladder works in practice. We consider the quantum scattering ensemble [79] given by

$$X = H + i\gamma\Gamma, \tag{B.1}$$

where H is a $N \times N$ complex matrix with Gaussian entries of zero mean and variance $\langle |H_{kl}|^2 \rangle = N^{-1}\delta_{kl}$ and $\Gamma = \sum_{a=1}^{M} V^a (V^a)^\dagger$. The components of N-dimensional vectors V^a are complex Gaussians with variance $\langle V_k^a \bar{V}_l^b \rangle = N^{-1}\delta_{kl}\delta_{ab}$. The two-point eigenvector correlation function in the limit $M, N \to \infty$ with $M/N = m$ fixed (planar limit) was studied by Mehlig and Santer [36]. We show how this result can be rederived within this formalism in a simpler way.

Γ is the complex Wishart matrix [80] multiplied by m. The planar cumulants of the Wishart matrix are stored in the Voiculecu's R-transform from free probability, which reads $R_\Gamma(z) = \frac{m}{1-z}$. The considered matrix X is non-Hermitian, therefore we need its quaternionic R-transform. Using the embedding of the complex R-transform into the quaternionic structure [70], we get $R_\Gamma(Q) = m(\mathbf{1}_2 - Q)^{-1}$. The Gaussian matrix is a particular instance of the elliptic ensemble corresponding to $\tau = 1$, therefore $R_H(Q) = Q$. Further, Γ is rescaled by a complex number $i\gamma$. The quaternionic R-transform of such a rescaled matrix is obtained from the relation [70] $R_{i\gamma\Gamma}(Q) = gR_\Gamma(Qg)$, where $g = \mathrm{diag}(i\gamma, -i\gamma)$. As the R-transform is additive under addition of two matrices, we have $R_X(Q) = Q + mg(\mathbf{1} - Qg)^{-1}$, which we then expand into a power series

$$R_X(Q) = Q + mg\sum_{k=0}^{\infty}(Qg)^k. \tag{B.2}$$

Then we perform the procedure with acting derivatives on the quaternionic R-transform and substituting the argument, as described in section 3.3. After summing up the resulting series, we get

$$B^{\alpha\beta}_{\mu\nu}(Q,P) = \delta^{\alpha\beta}\delta_{\nu\mu} + m\left(g^{-1} - G(Q)\right)^{-1}_{\alpha\beta}\left(g^{-1} - G^T(P)\right)^{-1}_{\mu\nu}. \tag{B.3}$$

This can we written in matrix form as

$$B(Q,P) = \mathbf{1} + m\left[g^{-1} - G(Q)\right]^{-1} \otimes \left[g^{-1} - G^T(P)\right]^{-1}. \tag{B.4}$$

Inserting this into (3.15), we reproduce the results of [36]. Green's function is calculated from (2.22).

References

[1] L.N. Trefethen and M. Embree, *Spectra and pseudospectra: the behavior of nonnormal matrices and operators*, Princeton University Press, (2005).

[2] V. Ratushnaya and R. Samtaney, *Non-modal stability analysis and transient growth in a magnetized vlasov plasma*, *Europhys. Lett.* **108** (2014) 55001.

[3] S. Rapaka, S. Chen, R.J. Pawar, P.H. Stauffer and D. Zhang, *Non-modal growth of perturbations in density-driven convection in porous media*, *J. Fluid Mech.* **609** (2008) 285.

[4] M.G. Neubert and H. Caswell, *Alternatives to resilience for measuring the responses of ecological systems to perturbations*, *Ecology* **78** (1997) 653.

[5] M. Asllani and T. Carletti, *Topological resilience in non-normal networked systems*, *Phys. Rev.* **E 97** (2018) 042302 [arXiv:1706.02703].

[6] A.E. Siegman, *Lasers without photons — or should it be lasers with too many photons?*, *Appl. Phys.* **B 60** (1995) 247.

JHEP06(2018)152

[7] B.F. Farrell and P.J. Ioannou, *Stochastic dynamics of baroclinic waves*, *J. Atmos. Sci.* **50** (1993) 4044.

[8] D. Borba, K.S. Riedel, W. Kerner, G.T.A. Huysmans, M. Ottaviani and P.J. Schmid, *The pseudospectrum of the resistive magnetohydrodynamics operator: Resolving the resistive alfvén paradox*, *Phys. Plasmas* **1** (1994) 3151.

[9] J. Chalker and B. Mehlig, *Eigenvector statistics in non-hermitian random matrix ensembles*, *Phys. Rev. Lett.* **81** (1998) 3367.

[10] B. Mehlig and J. Chalker, *Statistical properties of eigenvectors in non-hermitian gaussian random matrix ensembles*, *J. Math. Phys.* **41** (2000) 3233.

[11] R.A. Janik, W. Noerenberg, M.A. Nowak, G. Papp and I. Zahed, *Correlations of eigenvectors for nonHermitian random matrix models*, *Phys. Rev.* **E 60** (1999) 2699 [cond-mat/9902314] [INSPIRE].

[12] B.K. Murphy and K.D. Miller, *Balanced amplification: A new mechanism of selective amplification of neural activity patterns*, *Neuron* **61** (2009) 635 .

[13] G. Hennequin, T.P. Vogels and W. Gerstner, *Non-normal amplification in random balanced neuronal networks*, *Phys. Rev.* **E 86** (2012) 011909.

[14] G. Hennequin, T.P. Vogels and W. Gerstner, *Optimal control of transient dynamics in balanced networks supports generation of complex movements*, *Neuron* **82** (2014) 1394.

[15] T. Biancalani, F. Jafarpour and N. Goldenfeld, *Giant amplification of noise in fluctuation-induced pattern formation*, *Phys. Rev. Lett.* **118** (2017) 018101.

[16] L. Ridolfi, C. Camporeale, P. D'Odorico and F. Laio, *Transient growth induces unexpected deterministic spatial patterns in the turing process*, *Europhys. Lett.* **95** (2011) 18003.

[17] V. Klika, *Significance of non-normality-induced patterns: Transient growth versus asymptotic stability*, *Chaos* **27** (2017) 073120.

[18] Y.V. Fyodorov and D.V. Savin, *Statistics of resonance width shifts as a signature of eigenfunction non-orthogonality*, *Phys. Rev. Lett.* **108** (2012) 184101 [arXiv:1201.3357] [INSPIRE].

[19] J.-B. Gros, U. Kuhl, O. Legrand, F. Mortessagne, E. Richalot and D.V. Savin, *Experimental width shift distribution: A test of nonorthogonality for local and global perturbations*, *Phys. Rev. Lett.* **113** (2014) 224101.

[20] R. Movassagh, *Eigenvalue attraction*, *J. Stat. Phys.* **162** (2016) 615.

[21] Z. Burda, J. Grela, M.A. Nowak, W. Tarnowski and P. Warchoł, *Dysonian dynamics of the Ginibre ensemble*, *Phys. Rev. Lett.* **113** (2014) 104102 [arXiv:1403.7738] [INSPIRE].

[22] Z. Burda, J. Grela, M.A. Nowak, W. Tarnowski and P. Warchoł, *Unveiling the significance of eigenvectors in diffusing non-hermitian matrices by identifying the underlying Burgers dynamics*, *Nucl. Phys.* **B 897** (2015) 421 [arXiv:1503.06846] [INSPIRE].

[23] M. Walters and S. Starr, *A note on mixed matrix moments for the complex ginibre ensemble*, *J. Math. Phys.* **56** (2015) 013301.

[24] P. Bourgade and G. Dubach, *The distribution of overlaps between eigenvectors of ginibre matrices*, arXiv:1801.01219.

[25] K.M. Frahm, H. Schomerus, M. Patra and C.W.J. Beenakker, *Large petermann factor in chaotic cavities with many scattering channels*, *Europhys. Lett.* **49** (2000) 48.

JHEP06(2018)152

[26] H. Schomerus, K. Frahm, M. Patra and C. Beenakker, *Quantum limit of the laser line width in chaotic cavities and statistics of residues of scattering matrix poles*, *Physica* **A 278** (2000) 469.

[27] M. Patra, H. Schomerus and C.W.J. Beenakker, *Quantum-limited linewidth of a chaotic laser cavity*, *Phys. Rev.* **A 61** (2000) 023810.

[28] K. Petermann, *Calculated spontaneous emission factor for double-heterostructure injection lasers with gain-induced waveguiding*, *IEEE J. Quantum Electron.* **15** (1979) 566.

[29] S. Belinschi, M.A. Nowak, R. Speicher and W. Tarnowski, *Squared eigenvalue condition numbers and eigenvector correlations from the single ring theorem*, *J. Phys.* **A 50** (2017) 105204 [arXiv:1608.04923] [INSPIRE].

[30] J.H. Wilkinson, *The algebraic eigenvalue problem*, volume 87, Clarendon Press Oxford, (1965).

[31] Y.V. Fyodorov and B. Mehlig, *Statistics of resonances and nonorthogonal eigenfunctions in a model for single-channel chaotic scattering*, *Phys. Rev.* **E 66** (2002) 045202.

[32] Z. Burda, B.J. Spisak and P. Vivo, *Eigenvector statistics of the product of Ginibre matrices*, *Phys. Rev.* **E 95** (2017) 022134 [arXiv:1610.09184] [INSPIRE].

[33] Y.V. Fyodorov, *On statistics of bi-orthogonal eigenvectors in real and complex ginibre ensembles: combining partial schur decomposition with supersymmetry*, arXiv:1710.04699.

[34] D. Martí, N. Brunel and S. Ostojic, *Correlations between synapses in pairs of neurons slow down dynamics in randomly connected neural networks*, arXiv:1707.08337.

[35] D.V. Savin and V.V. Sokolov, *Quantum versus classical decay laws in open chaotic systems*, *Phys. Rev.* **E 56** (1997) R4911.

[36] B. Mehlig and M. Santer, *Universal eigenvector statistics in a quantum scattering ensemble*, *Phys. Rev.* **E 63** (2001) 020105.

[37] J. Ambjørn, J. Jurkiewicz and Yu. M. Makeenko, *Multiloop correlators for two-dimensional quantum gravity*, *Phys. Lett.* **B 251** (1990) 517 [INSPIRE].

[38] N. Dunford, J.T. Schwartz, W.G. Bade and R.G. Bartle, *Linear operators. Part I, general theory*, (1957).

[39] R.A. Horn and C.R. Johnson, *Matrix analysis*, Cambridge University Press, (1990).

[40] M. Kieburg and H. Kösters, *Exact relation between singular value and eigenvalue statistics*, *Random Matrices: Theory Appl.* **5** (2016) 1650015 [arXiv:1601.02586].

[41] L. Erdos, T. Krüger and D. Renfrew, *Power law decay for systems of randomly coupled differential equations*, arXiv:1708.01546.

[42] R.A. Janik, M.A. Nowak, G. Papp and I. Zahed, *NonHermitian random matrix models. 1.*, *Nucl. Phys.* **B 501** (1997) 603 [cond-mat/9612240] [INSPIRE].

[43] R.A. Janik, M.A. Nowak, G. Papp, J. Wambach and I. Zahed, *NonHermitian random matrix models: A free random variable approach*, *Phys. Rev.* **E 55** (1997) 4100 [hep-ph/9609491] [INSPIRE].

[44] J. Feinberg and A. Zee, *NonHermitian random matrix theory: Method of Hermitean reduction*, *Nucl. Phys.* **B 504** (1997) 579 [cond-mat/9703087] [INSPIRE].

JHEP06(2018)152

[45] J.T. Chalker and Z.J. Wang, *Diffusion in a Random Velocity Field: Spectral Properties of a Non-Hermitian Fokker-Planck Operator*, *Phys. Rev. Lett.* **79** (1997) 1797 [INSPIRE].

[46] A. Cayley, *A memoir on the theory of matrices*, *Phil. Trans. Roy. Soc. Lond.* **148** (1858) 17.

[47] Y.V. Fyodorov, B.A. Khoruzhenko and H.-J. Sommers, *Almost Hermitian random matrices: Eigenvalue density in the complex plane*, *Phys. Lett.* **A 226** (1997) 46 [cond-mat/9606173] [INSPIRE].

[48] B. Eynard et al., *Counting surfaces*, Springer Basel, (2016).

[49] M.A. Nowak and W. Tarnowski, *Complete diagrammatics of the single-ring theorem*, *Phys. Rev.* **E 96** (2017) 042149.

[50] M.A. Nowak and W. Tarnowski, *Spectra of large time-lagged correlation matrices from random matrix theory*, *J. Stat. Mech. Theor. Exp.* **2017** (2017) 063405.

[51] S.T. Belinschi, P. Śniady and R. Speicher, *Eigenvalues of non-hermitian random matrices and brown measure of non-normal operators: hermitian reduction and linearization method*, *Linear Algebra Appl.* **537** (2018) 48.

[52] E. Brézin and A. Zee, *Universal relation between Green's functions in random matrix theory*, *Nucl. Phys.* **B 453** (1995) 531 [cond-mat/9507032] [INSPIRE].

[53] J. Jurkiewicz, G. Łukaszewski and M.A. Nowak, *Diagrammatic approach to fluctuations in the wishart ensemble*, *Acta Phys. Polon.* **B 39** (2008) 799.

[54] J. Feinberg and A. Zee, *NonGaussian nonHermitian random matrix theory: Phase transition and addition formalism*, *Nucl. Phys.* **B 501** (1997) 643 [cond-mat/9704191] [INSPIRE].

[55] A. Guionnet, M. Krishnapur and O. Zeitouni, *The single ring theorem*, *Annals Math.* **174** (2011) 1189.

[56] U. Haagerup and F. Larsen, *Brown's spectral distribution measure for r-diagonal elements in finite von neumann algebras*, *J. Funct. Anal.* **176** (2000) 331.

[57] A. Nica and R. Speicher, *r-diagonal pairs-a common approach to haar unitaries and circular elements*, *Fields Inst. Commun.* **12** (1996).

[58] J. Fischmann, W. Bruzda, B.A. Khoruzhenko, H.-J. Sommers and K. Życzkowski, *Induced ginibre ensemble of random matrices and quantum operations*, *J. Phys.* **A 45** (2012) 075203.

[59] K. Zyczkowski and H.-J. Sommers, *Truncations of random unitary matrices*, *J. Phys.* **A 33** (2000) 2045.

[60] Z. Burda, M.A. Nowak and A. Swiech, *Spectral relations between products and powers of isotropic random matrices*, *Phys. Rev.* **E 86** (2012) 061137.

[61] U. Haagerup and H. Schultz, *Brown measures of unbounded operators affiliated with a finite von neumann algebra*, *Math. Scand.* **100** (2007) 209.

[62] C.M. Bender, *Making sense of non-Hermitian Hamiltonians*, *Rept. Prog. Phys.* **70** (2007) 947 [hep-th/0703096] [INSPIRE].

[63] M.A. Nowak and W. Tarnowski, in preparation.

[64] P. Warchoł, *Dynamics in random matrix theory — toy model with spectral phase transition*, (2010).

[65] F.D. Cunden and P. Vivo, *Universal covariance formula for linear statistics on random matrices*, *Phys. Rev. Lett.* **113** (2014) 070202.

JHEP06(2018)152

[66] J.A. Mingo and R. Speicher, *Second order freeness and fluctuations of random matrices: I. gaussian and wishart matrices and cyclic fock spaces*, *J. Funct. Anal.* **235** (2006) 226 .

[67] J.A. Mingo, P. Śniady and R. Speicher, *Second order freeness and fluctuations of random matrices: Ii. unitary random matrices*, *Adv. Math.* **209** (2007) 212 .

[68] B. Collins, J.A. Mingo, P. Śniady and R. Speicher, *Second order freeness and fluctuations of random matrices. iii. higher order freeness and free cumulants*, *Doc. Math* **12** (2007) 1.

[69] R.A. Janik, M.A. Nowak, G. Papp and I. Zahed, *Brezin-Zee universality: Why quenched QCD in matter is subtle?*, *Phys. Rev. Lett.* **77** (1996) 4876 [hep-ph/9606329] [INSPIRE].

[70] A. Jarosz and M.A. Nowak, *Random hermitian versus random non-hermitian operators — unexpected links*, *J. Phys.* **A 39** (2006) 10107.

[71] A. Nica and R. Speicher, *r-diagonal pairs-a common approach to haar unitaries and circular elements*, *Fields Inst. Commun.* **12** (1996) 149.

[72] F. Hiai and D. Petz, *The semicircle law, free random variables and entropy*, no. 77, American Mathematical Soc., (2006).

[73] D. Shlyakhtenko, *Random gaussian band matrices and freeness with amalgamation*, *Int. Math. Res. Not.* **1996** (1996) 1013.

[74] M. Diaz, J. Mingo and S. Belinschi, *On the global fluctuations of block gaussian matrices*, arXiv:1711.07140.

[75] U. Haagerup, T. Kemp and R. Speicher, *Resolvents of r-diagonal operators*, *Trans. Am. Math. Soc.* **362** (2010) 6029.

[76] H. Leutwyler and A.V. Smilga, *Spectrum of Dirac operator and role of winding number in QCD*, *Phys. Rev.* **D 46** (1992) 5607 [INSPIRE].

[77] E.V. Shuryak and J.J.M. Verbaarschot, *Random matrix theory and spectral sum rules for the Dirac operator in QCD*, *Nucl. Phys.* **A 560** (1993) 306 [hep-th/9212088] [INSPIRE].

[78] J.J.M. Verbaarschot and I. Zahed, *Spectral density of the QCD Dirac operator near zero virtuality*, *Phys. Rev. Lett.* **70** (1993) 3852 [hep-th/9303012] [INSPIRE].

[79] F. Haake, F. Izrailev, N. Lehmann, D. Saher and H.-J. Sommers, *Statistics of complex levels of random matrices for decaying systems*, *Z. Phys. B* **88** (1992) 359.

[80] R.A. Janik and M.A. Nowak, *Wishart and anti-Wishart random matrices*, *J. Phys.* **A 36** (2003) 3629 [math-ph/0112017] [INSPIRE].

JHEP06(2018)152

Condition numbers for real eigenvalues in real Elliptic Gaussian ensemble

Yan V. Fyodorov[1*] and Wojciech Tarnowski[2†]

[1]Department of Mathematics, King's College London Strand, London, WC2R 2LS, UK

[2]Marian Smoluchowski Institute of Physics,
Jagiellonian University, S. Łojasiewicza 11, PL 30-348 Kraków, Poland

October 22, 2019

Abstract

We study the distribution of the eigenvalue condition numbers $\kappa_i = \sqrt{(\mathbf{l}_i^*\mathbf{l}_i)(\mathbf{r}_i^*\mathbf{r}_i)}$ associated with real eigenvalues λ_i of partially asymmetric $N \times N$ random matrices from the Gaussian elliptic ensemble. The large values of κ_i signal about the non-orthogonality of (bi-orthogonal) set of left $\mathbf{l}_i$ and right $\mathbf{r}_i$ eigenvectors and enhanced sensitivity of the associated eigenvalues against perturbations of the matrix entries. We derive the general finite N expression for the joint probability density (JPD) $\mathcal{P}_N(z,t)$ of $t_i = \kappa_i^2 - 1$ for λ conditioned to have a value z and investigate its several scaling regimes in the limit $N \to \infty$. When the degree of asymmetry is fixed as $N \to \infty$, the number of real eigenvalues is $O(\sqrt{N})$, and in the bulk of the real spectrum $t_i = O(N)$, while on approaching the spectral edges the non-orthogonality is weaker: $t_i = O(\sqrt{N})$. In both cases the corresponding JPDs, after appropriate rescaling, coincide with those found in the earlier studied case of fully asymmetric (Ginibre) matrices, see [20]. A different regime of weak asymmetry arises when a finite fraction of N eigenvalues remain real as $N \to \infty$. In such a regime eigenvectors are weakly non-orthogonal, $t = O(1)$, and we derive the associated JPD, finding that the characteristic tail $\mathcal{P}(z,t) \sim t^{-2}$ survives for arbitrary weak asymmetry. As such, it is the most robust feature of the condition number density for real eigenvalues of asymmetric matrices.

1 Introduction

A (real-valued) square matrix X is asymmetric if it is different from its transpose X^T, and non-normal if $XX^T \neq X^TX$. Generically, asymmetric matrices are non-normal, and their eigenvalues are much more sensitive to the perturbations of the matrix entries than for their symmetric (hence selfadjoint and normal) counterparts. It is well-known, that non-normality may raise serious issues when calculating spectra of such matrices numerically: keeping fixed precision of calculations might not be sufficient as some eigenvalues can be "ill-conditioned".

To be more specific, we assume that X can be diagonalized (which for random matrices happens with probability one). Then to each eigenvalue λ_i, real or complex (in the latter case being always

*yan.fyodorov@kcl.ac.uk

†wojciech.tarnowski@doctoral.uj.edu.pl

accompanied by its complex conjugate partner $\overline{\lambda}_i$) correspond two sets of eigenvectors, left $\mathbf{l}_i$ and right $\mathbf{r}_i$ which always can be chosen *bi*-orthogonal: $\mathbf{l}_i^*\mathbf{r}_j = \delta_{ij}$, where $\mathbf{l}_i^* := \overline{\mathbf{l}_i^T}$ stands for Hermitian conjugation. The corresponding eigenproblems are $X\mathbf{r}_i = \lambda_i\mathbf{r}_i$ and $X^T\mathbf{l}_i = \lambda_i\mathbf{l}_i$. Consider now a matrix $X' = X + \epsilon P$, where second term represents an error one makes by storing the matrix entries with a finite precision, with $\epsilon > 0$ controlling the magnitude of the error and P reflecting the matrix structure of the perturbation. In the first order perturbation theory in parameter ϵ eigenvalues are shifted by

$$|\delta\lambda_i| = \epsilon|\mathbf{l}_i^* P\mathbf{r}_i| \leq \epsilon||P||\sqrt{(\mathbf{l}_i^*\mathbf{l}_i)(\mathbf{r}_i^*\mathbf{r}_i)}. \tag{1}$$

The latter quantity, $\kappa_i = \sqrt{(\mathbf{l}_i^*\mathbf{l}_i)(\mathbf{r}_i^*\mathbf{r}_i)}$, shows that the sensitivity of eigenvalues is essentially controlled by non-orthogonality of the corresponding left and right eigenvectors. Correspondingly, in the numerical analysis context κ_i is called the eigenvalue condition number of the eigenvalue λ_i [39, 40]. Note also that the Cauchy-Schwarz inequality implies $\kappa \geq 1$, with $\kappa = 1$ only when X is normal.

It is natural to ask how well-conditioned is a 'typical' asymmetric matrix. This question can be most meaningfully answered in the context of Random Matrix Theory (RMT), by defining 'typical' as randomly chosen according to a probability measure specified by a particular choice of the ensemble. The simplest yet nontrivial choice is to assume that all entries are mean zero independent, identically distributed Gaussian numbers. This defines the standard real Ginibre ensemble which we denote Gin_1. Note that the question is equally interesting for matrices whose entries are complex rather than real, defining complex Ginibre ensemble which we denote Gin_2. Note that for such ensemble eigenvalues λ_i are purely complex with probability one.

It is the latter ensemble for which the study of the eigenvalue condition numbers has been initiated two decades ago by Chalker and Mehlig [8,33]. More precisely, Chalker and Mehlig introduced a matrix of inner products $O_{ij} = (\mathbf{l}_i^*\mathbf{l}_j)(\mathbf{r}_j^*\mathbf{r}_i)$, which they called "eigenvector overlaps". The diagonal elements of that matrix are simply the squared eigenvalue condition numbers. They further associated with the diagonal elements of the overlap matrix the following single-point correlation function:

$$O_1(z) = \left\langle \frac{1}{N}\sum_{k=1}^{N} O_{kk}\delta(z-\lambda_k) \right\rangle_{Gin_2}. \tag{2}$$

where the angular brackets stand for the expectation with respect to the probability measure associated with complex Ginibre ensemble, and $\delta(z-\lambda_k)$ is the Dirac delta mass at the eigenvalue λ_k, so that the empirical density of eigenvalues in the complex plane z reads $\rho(z) = \frac{1}{N}\sum_{k=1}^{N}\delta(z-\lambda_k)$.

Such $O_1(z)$ gives the conditional expectations of (squared) κ as $\mathbb{E}(\kappa_i^2|z=\lambda_i) = \frac{O_1(z)}{\langle\rho(z)\rangle}$, where $\langle\rho(z)\rangle$ is the mean spectral density around z [3]. It turned out that in the bulk of the spectrum of the complex Ginibre ensemble the magnitude of a typical diagonal overlap O_{ii} grows linearly with the size of the matrix N, so one needs to consider a rescaled object $\tilde{O}_1(z) = \frac{1}{N}O_1(z)$ to obtain a non-trivial limit. In their influential papers [8, 33] Chalker and Mehlig used the "formal" perturbation theory expansion to evaluate asymptotically, for $N \gg 1$, both the diagonal overlap $O_1(z)$ and its more general off-diagonal counterpart

$$O_2(z_1,z_2) = \left\langle \frac{1}{N}\sum_{k\neq l}^{N} \mathcal{O}_{kl}\delta(z_1-\lambda_k)\delta(z_2-\lambda_l) \right\rangle_{Gin_2}.$$

The first mathematically rigorous verification of the Chalker and Mehlig result for the diagonal overlap has been done in [41]. Remarkably, the function $O_1(z)$ can be efficiently studied within the formalism of the free probability [31] which recently allowed to extend the Chalker-Mehlig formulas to a broad class of invariant ensembles beyond the Gaussian case [3, 35]. $O_1(z)$ is also known for finite size of the complex Ginibre matrix [8, 33] and products of small Ginibre matrices [7]. It has been recently shown that for complex Ginibre matrices the one and two-point functions conditioned on an arbitrary number of eigenvalues are related to determinantal point processes [2]. Various features characterising rich properties of eigenvectors of nonnormal random matrices have been also studied in [4] and [9].

Here it is necessary to mention that the interest in statistical properties of the overlap matrix O_{kl} and related objects extends much beyond the issues of eigenvalue stability under perturbation, and is driven by numerous applications in Theoretical and Mathematical Physics. In particular, non-orthogonality governs transient dynamics in complex systems [28,30,38], see also [15,32], analysis of spectral outliers in non-selfadjoint matrices [34], and, last but not least, the description of the Dyson Brownian motion for non-normal matrices [5, 6, 29]. Another steady source of interest in the statistics of eigenvector overlaps is due to its role in chaotic wave scattering. In that context $O_1(z)$ and $O_2(z_1, z_2)$ has been studied for a few special models different from Ginibre (both theoretically [18, 24, 25] and very recently experimentally [10, 11]) and in the associated models of random lasing [36, 37]. In the scattering context all eigenvalues are necessarily complex, and the lasing threshold is associated with an eigenvalue with the smallest imaginary part. For that special eigenvalue even the distribution of the overlap O_{ii} has been studied [37].

In fact, already Chalker and Mehlig not only analysed $O_1(z)$, but also put forward a conjecture on the tail for the density $\mathcal{P}(\mathcal{O}_{ii})$ of the distribution of diagonal overlaps $\mathcal{O}_{ii}$. Namely, based on exactly solvable case of 2×2 matrices and numerical simulations for complex Ginibre case they predicted that for large overlaps the density will show a tail $\mathcal{P}(\mathcal{O}_{ii}) \sim \mathcal{O}_{ii}^{-3}$ making all the positive integer moments beyond $O_1(z)$ divergent. This conjecture has been settled only recently with two different methods, by Bourgade and Dubach in [5] (where some information about $\mathcal{O}_{l\neq k}$ was also provided) and by Fyodorov [20]. The latter paper also revealed that for real eigenvalues of a real Ginibre matrices Gin_1 the diagonal overlaps $\mathcal{O}_{ii}$ are distributed with even heavier tail: $\mathcal{P}(\mathcal{O}_{ii}) \sim \mathcal{O}_{ii}^{-2}$, making even the mean of the overlap divergent.

To address the above distributions it is convenient to introduce the following natural generalization of the equation (2)

$$\mathcal{P}_N(z,t) = \left\langle \sum_{i=1}^{N} \delta(O_{ii} - 1 - t)\delta(z - \lambda_i) \right\rangle \tag{3}$$

interpreted as the (conditional) probability density function of the 'diagonal' (or 'self-overlap') non-orthogonality factor $t = O_{ii} - 1$ for the right and left eigenvectors corresponding to eigenvalues in the vicinity of a point $z = x + iy$ in the complex plane. We will call it for brevity the joint probability density (JPD) of the two variables, t and z. As was shown in [5, 20] the JPD $\mathcal{P}_N(z,t)$ tends (after appropriate rescaling of the variables z and t with the size N) to the inverse gamma distribution as $N \gg 1$:

$$\lim_{N\to\infty} N\,\mathcal{P}_N(z\sqrt{N}, Nt) = \frac{\langle\rho(z)\rangle}{t} e^{-\frac{\tilde{O}_1(z)}{t\langle\rho(z)\rangle}} \left(\frac{\tilde{O}_1(z)}{t\langle\rho(z)\rangle}\right)^{\beta}, \quad |z| < 1. \tag{4}$$

Here parameter $\beta = 1$ corresponds to the real eigenvalues of the real Ginibre matrices (in which case the parameter z should be chosen real) and $\beta = 2$ to the complex Ginibre case. Recall that in the above the limiting spectral density of real eigenvalues for $\beta = 1$ is $\langle \rho(z) \rangle = \frac{1}{2\sqrt{2\pi}}$ for the interval $|z| < 1$, whereas the limiting spectral density of real eigenvalues for $\beta = 2$ is $\langle \rho(z) \rangle = \pi^{-1}$ inside the unit circle $|z| < 1$.

The limiting expression (4) naturally incorporates for complex Ginibre case the Chalker-Mehlig result. In the formula above $\tilde{O}(z) = \pi^{-1}(1 - |z|^2)$, which is the large N limit of the rescaled one-point correlation function. Interestingly, despite the fact that for $\beta = 1$ the mean value defined via $O_1(z)$ does not exist, its rescaled version, $\tilde{O}_1(z) = \frac{1}{2\sqrt{2\pi}}(1 - z^2)$, appears as a parameter in the inverse γ_1 distribution and defines therefore the *typical* value of the diagonal overlap. Further calculations in a few non-Gaussian rotationally-invariant matrix ensembles (in particular, associated with "truncations" of unitary matrices) done very recently in [12] suggest that (4) might exhibit a certain degree of universality. Note that the statistics of O_{ii} for complex eigenvalues of real Ginibre matrices remains an outstanding problem, though it would be natural to expect that also in that case for a fixed z with nonvanishing imaginary part the limit should be the same as for the complex Ginibre case.

Returning to the original question of eigenvalue condition numbers for real-valued matrices, the above results in particular imply that in contrast to well-conditioned eigenvalues of symmetric matrices with $\kappa = 1$ the typical condition numbers in fully asymmetric random matrices grow with matrix size as $\sqrt{N}$ [20] and show strong fluctuations. One of natural questions is then to ask how those properties evolve for matrices with a controlled degree of asymmetry in their entries. The aim of this work is to answer this question. To this end we consider matrices with i.i.d. real Gaussian entries, such that the entries X_{ij} and X_{ji} are correlated. The joint pdf for the elements of this ensemble, known in the literature either as real partly symmetric Ginibre ensemble, or alternatively as the Real Elliptic Gaussian Ensemble, is given by

$$P(X)dX = C_N^{-1} \exp\left[-\frac{1}{2(1-\tau^2)}\mathrm{Tr}(XX^T - \tau X^2)\right] dX. \tag{5}$$

Here $dX = \prod_{i,j=1}^{N} dX_{ij}$ is the flat Lebesgue measure over all matrix elements and the normalization constant reads $C_N = (2\pi)^{N^2/2}(1+\tau)^{N/2}(1-\tau^2)^{\frac{N(N-1)}{4}}$. The parameter $\tau \in [0,1]$ tunes the degree of correlation, $\mathbb{E}(X_{ij}X_{ji}) = \tau$ for $i \neq j$, and (5) interpolates between the Real Ginibre Ensemble for $\tau = 0$ and real symmetric matrices (Gaussian Orthogonal Ensemble) for $\tau = 1$. In particularly, it is well-known that for large sizes $N \gg 1$ a nontrivial scaling regime of *weak non-Hermiticity* arises as long as the product $N(1-\tau)$ is kept of the order of unity [14, 21–23, 26]. It is this regime when non-normality gradually develops and the condition numbers κ_i start growing away from the value $\kappa_i = 1$. Our considerations allow us to address this regime in a quantitative way.

2 Statement of the main results

It turns out that the method of evaluating the JPD in eq. (3) suggested for Ginibre case in [20] works for the Elliptic ensemble as well, though actual calculations turn out to be significantly more involved. Relegating technical detail to the rest of the paper, in this section we present our main findings.

Our main theorem gives the joint probability density function of the eigenvalue λ_i and the shifted overlap $t = O_{ii} - 1$ for elliptic matrices of a given size N distributed according to (5). It takes more compact form when the rescaled variable $q = (1-\tau)t$ is considered.

Theorem 2.1. *Let X_N be $N \times N$ random matrix with the probability density function given by* (5). *Let us define the rescaled and shifted eigenvalue condition number $q = (1-\tau)(\kappa^2 - 1)$. The joint pdf* (3) *of real eigenvalue z and associated squared condition number expressed via the variable q is given by*

$$\mathcal{P}_N(z,q) = \frac{1}{2(1+\tau)\sqrt{2\pi}\Gamma(N-1)} \frac{e^{-\frac{z^2}{2(1+\tau)}\left(1+\frac{q}{1+q}\right)}}{\sqrt{q(1+q)}} \left(\frac{q}{q+1+\tau}\right)^{\frac{N}{2}-1} \times \left[\frac{(1+\tau-2z^2)P_{N-2} + 2z[R_{N-2} + \tau(N-2)R_{N-3}]}{1+q} + \frac{P_{N-2}z^2}{(1+q)^2} + \frac{\tau^2(1+\tau)^2N(N-2)P_{N-3}}{(1+\tau+q)^2} + \frac{(1+\tau)(1-\tau^2)(N-2)((N-2)P_{N-3} - T_{N-3})}{1+\tau+q} - \frac{2\tau(1+\tau)(N-2)zR_{N-3}}{(1+q)(1+\tau+q)}\right], \quad (6)$$

where the functions: $P_m := P_m(z)$, $R_m := R_m(z)$, $T_m := T_m(z)$ are defined in terms of the Hermite polynomials

$$\mathrm{He}_m(z) = \frac{(\pm i)^m}{\sqrt{2\pi}} e^{\frac{z^2}{2}} \int_{\mathbb{R}} t^m e^{-\frac{t^2}{2} \mp izt} dt, \quad (7)$$

as

$$P_N(z) = N! \sum_{k=0}^{N} \frac{\tau^k}{k!} \left((k+1)\mathrm{He}_k^2\left(\frac{z}{\sqrt{\tau}}\right) - k\mathrm{He}_{k-1}\left(\frac{z}{\sqrt{\tau}}\right)\mathrm{He}_{k+1}\left(\frac{z}{\sqrt{\tau}}\right)\right), \quad (8)$$

$$R_N(z) = \frac{N!}{2} \sum_{k=0}^{N} \frac{\tau^{k+\frac{1}{2}}}{k!} \left((k+2)\mathrm{He}_{k+1}\left(\frac{z}{\sqrt{\tau}}\right)\mathrm{He}_k\left(\frac{z}{\sqrt{\tau}}\right) - k\mathrm{He}_{k+2}\left(\frac{z}{\sqrt{\tau}}\right)\mathrm{He}_{k-1}\left(\frac{z}{\sqrt{\tau}}\right)\right), \quad (9)$$

$$T_N(z) = N! \sum_{k=0}^{N} \frac{k\tau^k}{k!} \left((k+1)\mathrm{He}_k^2\left(\frac{z}{\sqrt{\tau}}\right) - k\mathrm{He}_{k-1}\left(\frac{z}{\sqrt{\tau}}\right)\mathrm{He}_{k+1}\left(\frac{z}{\sqrt{\tau}}\right)\right). \quad (10)$$

Remark 2.2. Note that for $\tau = 0$ these quantities simplify to $P_N = e^{z^2}\Gamma\left(N+1, z^2\right)$, $R_N = zP_N$ and $T_N = Nz^2P_{N-1}$, with $\Gamma(N+1,z) = \int_z^\infty u^N e^{-x} du$, and the known result [20, eq. 2.5] is recovered.

Remark 2.3. The exact mean density of purely real eigenvalues $\rho_N^{(r)}(z)$ for real Elliptic matrices of even size N is known due to Forrester and Nagao [17]. It is given by $\rho_N^{(r)}(z) = \rho_N^{(1)}(z) + \rho_N^{(2)}(z)$ with

$$\rho_N^{(1)}(z) = \frac{1}{\sqrt{2\pi}} e^{-\frac{z^2}{1+\tau}} \sum_{k=0}^{N-2} \frac{\tau^k}{k!} He_k^2\left(\frac{z}{\sqrt{\tau}}\right), \quad (11)$$

$$\rho_N^{(2)}(z) = \frac{1}{\sqrt{2\pi}(1+\tau)\Gamma(N-1)} e^{-\frac{z^2}{2(1+\tau)}} \tau^{N-3/2} He_{N-1}\left(\frac{z}{\sqrt{\tau}}\right) \int_0^z e^{-\frac{u^2}{2(1+\tau)}} He_{N-2}\left(\frac{u}{\sqrt{\tau}}\right) du. \quad (12)$$

For N odd the density can be obtained using the method from [16]. Our expression (6) by its very definition must reproduce the Forrester-Nagao result after integration over the variable t. Performing such an integration analytically is, however, a challenging task which we managed to complete for $N = 2, 3, 4$. However, we checked that performing such integral numerically for moderate values of N gives indistinguishable results from the density of real eigenvalues, see Appendix A.

Being exact, the expression (6) can be further analyzed in interesting scaling limits as $N \to \infty$. The first of such limits is the so-called 'bulk scaling' corresponding to the eigenvalues inside the limiting support of the spectrum which (after appropriate rescaling $z \to \sqrt{N}z$) for a fixed z and $0 \leq \tau < 1$ represents an ellipse in the complex plane (hence the name for the ensemble) centered at the origin, with semi-axis $1-\tau$ along imaginary axis and $1+\tau$ along the real axis. Since we are dealing only with real eigenvalues, we restrict ourselves to real z such that $|z| < 1+\tau$, where the following asymptotics holds:

Corollary 2.4. *(bulk scaling) Define for a fixed $0 \leq \tau < 1$ and real z satisfying $|z| < 1+\tau$ the limiting scaled JPD as $\mathcal{P}_{bulk}(z,t) = \lim_{N\to\infty} N\mathcal{P}_N(\sqrt{N}z, Nt)$. Then*

$$\mathcal{P}_{bulk}(z,t) = \frac{\sqrt{1-\tau^2}}{2\sqrt{2\pi}} \frac{\left[1-\frac{z^2}{(1+\tau)^2}\right]}{t^2} e^{-\frac{1-\tau^2}{2t}\left[1-\frac{z^2}{(1+\tau)^2}\right]}. \tag{13}$$

This asymptotics shows that the typical value of the diagonal overlap $t = O_{ii} - 1$ in this regime is always of the order N as $N \gg 1$, similarly to the behaviour for the Ginibre case $\tau = 0$. Moreover, by recalling that the asymptotic density of real eigenvalues in elliptic case is $\langle \rho(z) \rangle = \frac{1}{\sqrt{2\pi(1-\tau^2)}}$ and introducing $\tilde{O}_1(z) = \frac{\sqrt{1-\tau^2}}{2\sqrt{2\pi}}(1 - \frac{z^2}{(1+\tau)^2})$, we see that (13) is exactly of the form (4) for $\beta = 1$.

When approaching the boundary $|z| = 1+\tau$ of the eigenvalue support the typical diagonal overlap $\tilde{O}_1(z)$ tends to zero, and in the appropriate scaling vicinity of the boundary it becomes parametrically weaker, as the variable t in such a regime becomes of the order $\sqrt{N}$:

Corollary 2.5. *(edge scaling) Take a fixed $0 \leq \tau < 1$ and parametrize z and q as $z = \sqrt{N}(1+\tau) + \delta_\tau\sqrt{1-\tau^2}$ and $q = \sigma\sqrt{N(1-\tau^2)}$. Then the limit $\mathcal{P}_{edge}(\delta_\tau, q) = \lim_{N\to\infty} \sqrt{N}\mathcal{P}_N(z,q)$ exists and is equal to*

$$\mathcal{P}_{edge}(\delta_\tau, \sigma) = \frac{1}{4\pi\sigma^2(1-\tau^2)} e^{-\frac{1}{4\sigma^2}+\frac{\delta_\tau}{\sigma}} \left[e^{-2\delta_\tau^2} + \left(\frac{1}{\sigma} - 2\delta_\tau\right) \int_{2\delta_\tau}^{\infty} e^{-\frac{u^2}{2}} du \right]. \tag{14}$$

Note that this form is essentially the same as found for real Ginibre case in [20].

Finally, the ultimate goal of our study is to investigate the *weak non-Hermiticity* regime occuring for $N \to \infty$ when τ approaches unity with the rate $O(N^{-1})$, so that the parameter $2N(1-\tau) = a^2$ is fixed. Such parameter therefore controls the deviation from the fully symmetric limit. In this regime of "almost symmetric" matrices already a finite fraction of order of N eigenvalues are real, and their mean density asymptotically is given by [14, 23]

$$\langle \rho(z) \rangle = \rho_{sc}(z) \int_0^1 e^{-\frac{1}{2}As^2} ds, \qquad |z| < 2, \tag{15}$$

where $\rho_{sc}(z) = \frac{1}{2\pi}\sqrt{4-z^2}$ is the standard Wigner semicircle density characterizing real symmetric GOE matrices, and $A = (\pi\rho_{sc}(z)a)^2$.

As anticipated, such regime turns out to be not only "weakly non-Hermitian", but also "weakly non-normal" as the typical value of the diagonal overlap $t = O_{ii} - 1$ turns out to be of the order of unity in the bulk of the spectrum, namely

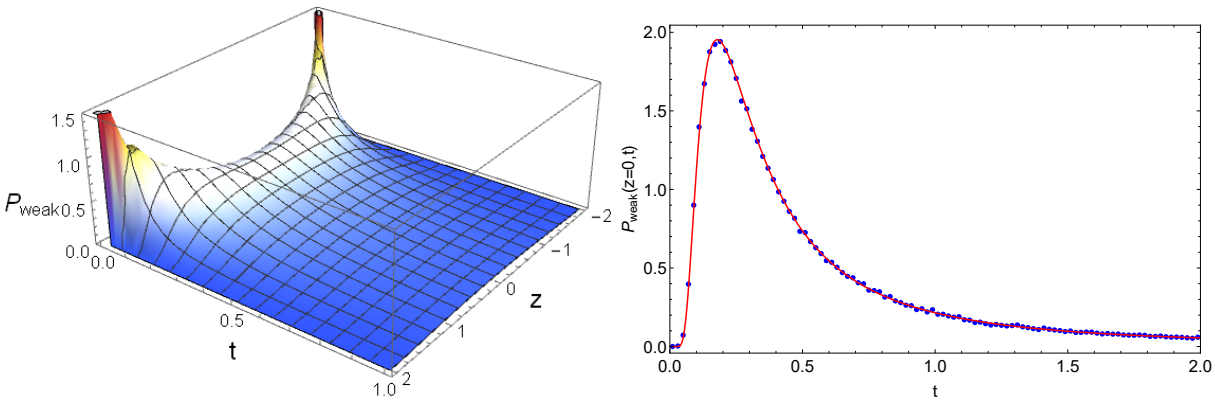

Figure 1: (left) 3D plot of $\mathcal{P}_{weak}(z,t)$. (right) Section of the plot at $z=0$ (red line) juxtaposed numerical diagonalization of $2\cdot 10^4$ matrices of size $N=500$.

Corollary 2.6. *Let $|z|<2$ and $t\geq 1$ be fixed. Consider the limit $\mathcal{P}_{weak}(z,t)=\lim_{N\to\infty} N^{-1/2}\mathcal{P}_N(z\sqrt{N},t)$ with $2N(1-\tau)=a^2$ fixed. Then*

$$\mathcal{P}_{weak}(z,t)=\frac{A}{2}\rho_{sc}(z)\frac{e^{-\frac{A}{2t}}}{t^2}\int_0^1 e^{-\frac{1}{2}As^2}\left(1+A+\frac{A}{t}-As^2\right)s^2ds, \tag{16}$$

where $A=(\pi\rho_{sc}(z)a)^2$ and $\rho_{sc}(z)=\frac{1}{2\pi}\sqrt{4-z^2}$.

Remark 2.7. After integration by parts one can rewrite the above as

$$\mathcal{P}_{weak}(z,t)=\frac{A}{2}\rho_{sc}(z)\frac{e^{-\frac{A}{2t}}}{t^2}\left[\left(\frac{2}{A}-\frac{1}{t}\right)e^{-\frac{A}{2}}+\left(1+\frac{1}{t}-\frac{2}{A}\right)\int_0^1 e^{-\frac{1}{2}As^2}ds\right]. \tag{17}$$

From this form it is easy to check that $\int_0^\infty \mathcal{P}_{weak}(z,t)dt$ agrees with the mean density (15), as expected.

We thus conclude that the characteristic tail $\mathcal{P}_{weak}(z,t)\sim t^{-2}$ is the most robust feature of the condition number density for real eigenvalues of asymmetric matrices, as it survives in the regime of arbitrary weak asymmetry as long as $a>0$,

Acknowledgments. WT appreciates the support of Polish Ministry of Science and Higher Education through the 'Diamond Grant' 0225/DIA/2015/44 and the doctoral scholarship ETIUDA UMO-2018/28/T/ST1/00470 from National Science Center. WT is grateful to King's College London for warm hospitality during his stay.

3 Derivation of the main results

We briefly outline an adaptation of the method of evaluating the JPD in eq. (3) following [20] with necessary modifications.

3.1 Partial Schur decomposition

Let λ be a real eigenvalue of a $N \times N$ real matrix X_N. Then it is well-known, see e.g. [13], that the matrix X_N can be decomposed as

$$X_N = O \begin{pmatrix} \lambda & \mathbf{w}^T \\ 0 & X_{N-1} \end{pmatrix} O^T = O \tilde{X}_N O^T, \tag{18}$$

where $\mathbf{w}$ is a column vector with $N-1$ components and X_{N-1} is a matrix of size $(N-1)\times(N-1)$. The matrix O is known in the literature as the Hausholder reflection matrix. Note that although the left/right eigenvectors of $\tilde{X}_N$ corresponding to λ are different from those of X_N, the inner products (hence, the eigenvalue condition numbers) are the same. Parameterizing these eigenvectors as $\tilde{\mathbf{r}}_\lambda = (1, 0, \ldots, 0)^T$ and $\tilde{\mathbf{l}}_\lambda = (1, b_1, \ldots, b_{N-1}) = (1, \mathbf{b}^T)$, we immediately obtain for the associated condition number $\kappa_\lambda^2 = 1 + \mathbf{b}^T\mathbf{b}$. Demanding that $\tilde{\mathbf{l}}_\lambda$ is the left eigenvector of $\tilde{X}_N$ leads us to the relation $\mathbf{b} = (\lambda - X_{N-1}^T)^{-1}\mathbf{w}$. As a consequence [20]

$$\kappa_\lambda^2 = 1 + \mathbf{w}^T(\lambda - X_{N-1})^{-1}(\lambda - X_{N-1}^T)^{-1}\mathbf{w}. \tag{19}$$

The Lebesgue measure on X_N can be decomposed as $dX_N = \tilde{C}_N |\det(\lambda - X_{N-1})| d\lambda d\mathbf{w} dX_{N-1} dO$, with the known proportionality constant $\tilde{C}_N$.

It turns out to be more technically convenient to concentrate on evaluating a characteristic function $\mathcal{L}(z,p) = \left\langle \delta(z-\lambda) e^{-p\mathbf{b}^T\mathbf{b}} \right\rangle_N$ representing the Laplace transform of the JPD $\mathcal{P}(z,t)$. Hereafter by $\langle \ldots \rangle_N$ we denote the expected value with respect to the probability measure (5) for matrices X_N of size N.

Lemma 3.1. *The characteristic function $\mathcal{L}(z,p)$ can be represented in the form*

$$\mathcal{L}(z,p) = \frac{e^{-\frac{z^2}{2(1+\tau)}}}{2^{\frac{N}{2}}\Gamma\left(\frac{N}{2}\right)\sqrt{1+\tau}} \left\langle \frac{\det(z-X)(z-X^T)}{\det{}^{1/2}\left[2p(1-\tau^2) + (z-X)(z-X^T)\right]} \right\rangle_{N-1}. \tag{20}$$

Proof. Substituting the decomposition (18) together with the associated decomposition of the Lebesgue measure into the probability measure of the elliptic ensemble (5) one can easily see that the ensemble average in (20) amounts to performing the following integral:

$$\begin{aligned} \mathcal{L}(z,p) = C_N^{-1} e^{-\frac{z^2}{2(1+\tau)}} \int \exp\left[-\frac{1}{2(1-\tau^2)}\mathrm{Tr}(X_{N-1}X_{N-1}^T - \tau X_{N-1}^2)\right] \times \\ \exp\left[-\frac{1}{2(1-\tau^2)}\mathbf{w}^T\left(1 + 2p(1-\tau^2)(z-X_{N-1})^{-1}(z-X_{N-1}^T)^{-1}\right)\mathbf{w}\right] |z - X_{N-1}| dX_{N-1} d\mathbf{w} dO \end{aligned} \tag{21}$$

The integral over O yields the volume of the space of Hausholder transformations $V_O = \frac{\pi^{N/2}}{\Gamma(\frac{N}{2})}$ [13]. The integral over $\mathbf{w}$ is Gaussian and can be easily performed, giving the factor

$$\frac{\left[2\pi(1-\tau^2)\right]^{\frac{N-1}{2}}}{\det{}^{1/2}[1 + 2p(1-\tau^2)(z-X_{N-1})^{-1}(z-X_{N-1}^T)^{-1}]} = \frac{\left[2\pi(1-\tau^2)\right]^{\frac{N-1}{2}} \det{}^{1/2}(z-X_{N-1})(z-X_{N-1}^T)}{\det{}^{1/2}\left[(2p(1-\tau^2) + (z-X_{N-1})(z-X_{N-1}^T)\right]}. \tag{22}$$

Taking all the multiplicative numerical constants into account and the factor $|\det(z - X_{N-1})|$ from the Jacobian, we arrive at (20). □

3.2 Ratio of determinants

The problem has been therefore reduced to the calculation of the expectation for the ratio of two random determinants

$$D_N := \left\langle \frac{\det(z-X)(z-X^T)}{\det{}^{1/2}\left[(2p(1-\tau^2)+(z-X)(z-X^T)\right]} \right\rangle_N , \tag{23}$$

which is evaluated as

Theorem 3.2.

$$D_N = \frac{2^{-\frac{N}{2}}}{\sqrt{1+\tau}\,\Gamma\left(\frac{N}{2}\right)} \int_0^\infty \frac{dt}{t} e^{-pt(1-\tau)} e^{-\frac{z^2 t}{2(1+\tau)(1+t)}} \left(\frac{t}{1+t}\right)^{1/2} \left(\frac{t}{1+\tau+t}\right)^{\frac{N-1}{2}} \times$$
$$\left[\frac{P_{N-1}(1+\tau-2z^2)+2z(R_{N-1}+\tau(N-1)R_{N-2})}{1+t} + \frac{P_{N-1}z^2}{(1+t)^2} + \frac{\tau^2(1+\tau)^2(N^2-1)P_{N-2}}{(1+\tau+t)^2} + \right.$$
$$\left. \frac{(1+\tau)(1-\tau^2)(N-1)[(N-1)P_{N-2}-T_{N-2}]}{1+\tau+t} - \frac{2\tau(1+\tau)(N-1)zR_{N-2}}{(1+t)(1+\tau+t)} \right], \tag{24}$$

where P_N, R_N and T_N are defined in (8)-(10).

Remark 3.3. The Theorem 3.2 immediately implies our main statement, Theorem 2.1: Indeed, by inserting (24) into (20) we see that $\mathcal{L}(z,p)$ is already represented as a Laplace transform and (6) follows.

The proof of Theorem 3.2 proceeds via employing the supersymmetry approach to ratios of determinants.

Proof. Let χ, ρ, θ, η denote N-component vectors in anticommuting (Grassmann) variables. This allows us to rewrite the determinant in the numerator as a standard Berezin Gaussian integral

$$\det(z-X)(z-X^T) = \int d\chi d\rho d\theta d\eta \exp\left[-\chi^T(z-X)\eta - \theta^T(z-X^T)\rho\right]. \tag{25}$$

The inverse square root of the determinant of a symmetric positive definite matrix A can be represented as a standard Gaussian integral. Namely, introducing N-component real vectors S_1, S_2 we can write

$$\det{}^{-\frac{1}{2}}\left[2p(1-\tau^2)+(z-X)(z-X^T)\right] =$$
$$\frac{1}{(2\pi)^N} \int dS_1 dS_2 \exp\left[-\frac{1}{2}(S_1^T S_2^T) \begin{pmatrix} u & i(z-X) \\ i(z-X^T) & u \end{pmatrix} \begin{pmatrix} S_1 \\ S_2 \end{pmatrix} \right], \tag{26}$$

where we denoted $u^2 = 2p(1-\tau^2)$. This provides a representation of the right-hand side in (24) in the form

$$D_N = \frac{1}{(2\pi)^N} \int d\chi d\rho d\theta d\eta dS_1 dS_2 \exp\left[-z(\chi^T\eta + \theta^T\rho) - \frac{1}{2}(uS_1^T S_1 + uS_2^T S_2 + 2izS_1^T S_2) \right] \times$$
$$\left\langle e^{\mathrm{Tr} X(\theta\rho^T - \eta\chi^T + iS_2 S_1^T)} \right\rangle_N . \tag{27}$$

The identity $\left\langle e^{-\mathrm{Tr}XA}\right\rangle_N = e^{\frac{1}{2}\mathrm{Tr}(AA^T+\tau A^2)}$ allows us to perform the ensemble average. This in turn produces terms that are quartic in Grassmann variables, which we further bilinearize by employing a few auxilliary Gaussian integrals, the step known as the Hubbard-Stratonovich transformation:

$$e^{\theta^T\eta\rho^T\chi} = \frac{1}{\pi}\int_{\mathbb{C}} d^2a e^{-|a|^2+a\theta^T\eta+\bar{a}\rho^T\chi}, \qquad e^{\tau\chi^T\theta\rho^T\eta} = \frac{1}{\pi}\int_{\mathbb{C}} d^2b e^{-|b|^2+\sqrt{\tau}b\chi^T\theta+\sqrt{\tau}\bar{b}\rho^T\eta}, \quad (28)$$

$$e^{-\frac{\tau}{2}(\rho^T\theta)^2} = \frac{1}{\sqrt{2\pi}}\int_{\mathbb{R}} e^{-\frac{c^2}{2}+ic\sqrt{\tau}\rho^T\theta}dc, \qquad e^{-\frac{\tau}{2}(\chi^T\eta)^2} = \frac{1}{\sqrt{2\pi}}\int_{\mathbb{R}} e^{-\frac{f^2}{2}-if\sqrt{\tau}\chi^T\eta}df, \quad (29)$$

where we use the notation $d^2z = dx\,dy$ for $z = x + iy$.

Applying these transformations converts all integrations over anticommuting variables into a Gaussian Berezin integral which we can write as $\int d\chi d\rho d\theta d\eta e^{-\frac{1}{2}\xi^T M\xi}$, where $\xi^T = (\chi^T\eta^T\theta^T\rho^T)$ and the antisymmetric matrix M is given by

$$M = \begin{pmatrix} 0 & g - iA^T & -b\sqrt{\tau} & \bar{a} \\ -g + iA & 0 & a & \bar{b}\sqrt{\tau} \\ b\sqrt{\tau} & -a & 0 & h - iA \\ -\bar{a} & -\bar{b}\sqrt{\tau} & -h + iA^T & 0 \end{pmatrix}. \quad (30)$$

Here we denoted $g = z + if\sqrt{\tau}$, $h = z + ic\sqrt{\tau}$ for brevity, and introduced the rank-two matrix $A = S_1 \otimes S_2^T + \tau S_2 \otimes S_1^T$, where $a \otimes b^T$ stands for the matrix with entries $a_i b_j$.

The Berezin Gaussian integration yields Pfaffian of the matrix M, evaluating which explicitly gives

$$\mathrm{Pf}(M) = (|a|^2 + \tau|b|^2 + gh)^{N-2}\left[(|a|^2 + \tau|b|^2 + gh)^2 - (|a|^2 + \tau|b|^2 + gh)i(g+h)\mathrm{Tr}A - |a|^2\mathrm{Tr}AA^T - \tau|b|^2\mathrm{Tr}A^2 - (g^2+h^2)\det A - gh(\mathrm{Tr}A)^2 - i(g+h)\det A\,\mathrm{Tr}A + \det{}^2 A\right]. \quad (31)$$

We then see that the resulting integrand depends on the vectors S_1 and S_2 only via their scalar products, so it is convenient to parameterize integrals by the entries of the associated Gram matrix [19]

$$\hat{Q} = \begin{pmatrix} Q_1 & Q \\ Q & Q_2 \end{pmatrix}, \qquad \hat{Q}_{ij} = (S_i^T S_j), \qquad i,j = 1,2. \quad (32)$$

The Jacobian of this change of variables is $(\det\hat{Q})^{\frac{N-3}{2}}$, while the integration over redundant angular variables yields the factor $C^{(o)}_{N,2} = \frac{2^{N-2}\pi^{N-1}}{\Gamma(N-1)}$ [27]. The range of integration is restricted by the non-negativity conditions $Q_1 \geq 0$, $Q_2 \geq 0, \det\hat{Q} = Q_1Q_2 - Q^2 \geq 0$. Following [20] it convenient to change variables into $r = (\det\hat{Q})^{1/2}$, and parameterize the integration region by $Q_2 = \frac{r^2+Q^2}{Q_1}$. The change of measure reads $dQ_1dQ_2dQ = 2\frac{dQ_1}{Q_1}rdrdQ$. After rescaling $Q_1 \to uQ_1$, we have

$$D_N = \frac{1}{4\pi^4\Gamma(N-1)}\int_{\mathbb{C}} d^2a\int_{\mathbb{C}} d^2b\, e^{-|a|^2-|b|^2}\int_{\mathbb{R}^2} dc\,df\, e^{-\frac{c^2}{2}-\frac{f^2}{2}} \times \int_{-\infty}^{\infty} dQ\int_0^{\infty}\frac{dQ_1}{Q_1}\int_0^{\infty} r^{N-2}dr\, e^{-\frac{1}{2}\left(u^2Q_1+\frac{r^2+Q^2}{Q_1}+2izQ+r^2+Q^2(1+\tau)\right)}\mathrm{Pf(M)}. \quad (33)$$

Noticing that $\mathrm{Tr}A = (1+\tau)Q$, $\mathrm{Tr}A^2 = (1+\tau^2)Q^2 + 2\tau Q_1 Q_2$, $\mathrm{Tr}AA^T = (1+\tau^2)Q_1Q_2 + 2\tau Q^2$ and $\det A = -\tau \det Q$, the Pfaffian $\mathrm{Pf}(M)$ can be expressed as

$$(|a|^2+\tau|b|^2+gh)^{N-2}\left[(|a|^2+\tau|b|^2+gh)^2 - (|a|^2+\tau|b|^2+gh)(iQ(1+\tau)(g+h)+Q^2(1+\tau)^2) - \right.$$
$$\left. -|a|^2(1+\tau^2)r^2 - 2\tau^2 r^2|b|^2 + \tau r^2(g^2+h^2) - i\tau(g+h)Q(1+\tau)r^2 + \tau^2 r^4\right]. \quad (34)$$

The integrals over a, b, c, f are performed in the following way. Let us denote

$$P_N = \frac{1}{2\pi^3}\int d^2a d^2b dc df e^{-|a|^2-|b|^2-\frac{c^2}{2}-\frac{f^2}{2}}(|a|^2+\tau|b|^2+gh)^N. \quad (35)$$

Expanding the expression in the bracket and using the binomial theorem twice, we obtain

$$P_N = N!\sum_{k=0}^{N}\tau^k\sum_{m=0}^{k}\frac{1}{m!}\mathrm{He}_m^2\left(\frac{z}{\sqrt{\tau}}\right), \quad (36)$$

where $\mathrm{He}_m(x) = (2\pi)^{-1/2}\int_{-\infty}^{\infty}e^{-\frac{y^2}{2}}(x+iy)^m dy$ are the monic Hermite polynomials. The internal sum can be performed via the Cristoffel-Darboux formula, finally yielding

$$P_N = N!\sum_{k=0}^{N}\frac{\tau^k}{k!}\left((k+1)\mathrm{He}_k^2\left(\frac{z}{\sqrt{\tau}}\right) - k\mathrm{He}_{k-1}\left(\frac{z}{\sqrt{\tau}}\right)\mathrm{He}_{k+1}\left(\frac{z}{\sqrt{\tau}}\right)\right). \quad (37)$$

Note that P_N can be interpreted as the expectation of the squared characteristic polynomial $\left\langle \det(z-X)(z-X^T)\right\rangle_N$, and in this capacity has been already studied for the elliptic ensemble [1]. All other integrals over a, b, c, f in (33) are performed in a similar way. After exploiting the three term recurrence for Hermite polynomials $\mathrm{He}_{N+1}(x) = x\mathrm{He}_N(x) - N\mathrm{He}_{N-1}(x)$, the integrals are evaluated to

$$P_N - P_{N-1}Q^2(1+\tau)^2 + r^4\tau^2 P_{N-2} - r^2[(N-1)(1+\tau^2)+4\tau^2]P_{N-2} - 2iQ(1+\tau)R_{N-1} +$$
$$2r^2\tau(z - iQ(1+\tau))R_{N-2} + (1-\tau^2)r^2 T_{N-2}, \quad (38)$$

where R_N and T_N are defined by (9) and (10). Note also that $R_N(z) = \frac{1}{2(N+1)}\frac{dP_{N+}(z)}{dz}$. It is convenient to exploit the structure of (38) and exponent in (33) and rescale further $Q \to \frac{Q}{1+\tau}$ and, similarly, $Q_1 \to \frac{Q_1}{1+\tau}$. Recalling that $u^2 = 2p(1-\tau^2)$, one then arrives at

$$D_N = \frac{1}{2\pi(1+\tau)\Gamma(N-1)}\int_0^\infty \frac{dQ_1}{Q_1}e^{-pQ_1(1-\tau)}\int_{\mathbb{R}}dQ e^{-\frac{1}{2(1+\tau)}\left(Q^2\frac{1+Q_1}{Q_1}+2izQ\right)}$$
$$\int_0^\infty r^{N-2}dr e^{-\frac{r^2}{2}\frac{Q_1+1+\tau}{Q_1}}\left[P_N - P_{N-1}Q^2 + r^4\tau^2 P_{N-2} - r^2[(N-1)(1+\tau^2)+4\tau^2]P_{N-2} - \right.$$
$$\left. 2iQR_{N-1} + 2r^2\tau(z-iQ)R_{N-2} + (1-\tau^2)r^2T_{N-2}\right]. \quad (39)$$

The remaining integration over Q is Gaussian, while the one over r is of the type $\int_0^\infty r^{N-2}e^{-ar^2/2}dr = \frac{1}{2}\left(\frac{2}{a}\right)^{\frac{N-1}{2}}\Gamma\left(\frac{N-1}{2}\right)$. The integral over Q_1 formally looks like logarithmically divergent. To see the cancellation of the divergent part one should exploit a non-trivial identity

$$P_N - P_{N-1}(1+\tau-z^2) - (N-1)[2\tau^2+N-1]P_{N-2} - 2zR_{N-1} + (1-\tau^2)(N-1)T_{N-2} = 0, \quad (40)$$

which is verified in the Appendix B. After further algebraic manipulations with the help of *Mathematica* we finally obtain

$$D_N = \frac{2^{-\frac{N}{2}}}{\sqrt{1+\tau}\Gamma\left(\frac{N}{2}\right)} \int_0^\infty \frac{dQ_1}{Q_1} e^{-pQ_1(1-\tau)} e^{-\frac{z^2 Q_1}{2(1+\tau)(1+Q_1)}} \left(\frac{Q_1}{1+Q_1}\right)^{\frac{1}{2}} \left(\frac{Q_1}{1+\tau+Q_1}\right)^{\frac{N-1}{2}} \times$$
$$\left[\frac{P_{N-1}(1+\tau-2z^2)+2z(R_{N-1}+\tau(N-1)R_{N-2})}{1+Q_1} + \frac{P_{N-1}z^2}{(1+Q_1)^2} + \frac{\tau^2(1+\tau)^2(N^2-1)P_{N-2}}{(1+\tau+Q_1)^2} + \right.$$
$$\left. \frac{(1+\tau)(1-\tau^2)(N-1)[(N-1)P_{N-2}-T_{N-2}]}{1+\tau+Q_1} - \frac{2\tau(1+\tau)(N-1)zR_{N-2}}{(1+Q_1)(1+\tau+Q_1)}\right]. \quad (41)$$

□

3.3 Asymptotic analysis

As P_N, R_N and T_N are the building blocks of the determinant, we consider here their large-N asymptotics. First, we find convenient integral representations which should allow the use of the Laplace method. For this we start from (37) and using the integral representation for Hermite polynomials in (7) we obtain

$$P_N = \frac{N!}{2\pi\tau} e^{\frac{z^2}{\tau}} \sum_{k=0}^{N} \frac{1}{k!} \int_{\mathbb{R}^2} dtds e^{-\frac{t^2+s^2}{2\tau} - \frac{iz}{\tau}(t-s)} [(k+1)t^k s^k - kt^{k+1}s^{k-1}]. \quad (42)$$

The sum is evaluated using $\sum_{k=0}^{N} \frac{x^k}{k!} = e^x \frac{\Gamma(N+1,x)}{\Gamma(N+1)}$, where $\Gamma(N+1,x) = \int_x^\infty u^N e^{-u} du$. This yields

Lemma 3.4.

$$P_N(z) = \frac{N!}{2\pi\tau} e^{\frac{z^2}{\tau}} \int_{\mathbb{R}^2} dtds e^{-\frac{t^2+s^2}{2\tau} - \frac{iz}{\tau}(t-s)+ts} \left(\frac{\Gamma(N+1,ts)}{N!} + t(s+t)\frac{\Gamma(N,ts)}{(N-1)!}\right). \quad (43)$$

An analogous procedure applied to T_N gives

Lemma 3.5.

$$T_N = \frac{N!}{2\pi\tau} e^{\frac{z^2}{\tau}} \int_{\mathbb{R}^2} dtds e^{-\frac{t^2+s^2}{2\tau} - \frac{iz}{\tau}(t-s)+ts} \left((t^2+2ts)\frac{\Gamma(N,ts)}{(N-1)!} + t^2 s(t+s)\frac{\Gamma(N-1,ts)}{(N-2)!}\right). \quad (44)$$

3.3.1 Bulk scaling

Let us give the proof of the **Corollary 2.4**.

Proof. After rescaling $z \to z\sqrt{N}$, $t \to t\sqrt{N}$ and $s \to s\sqrt{N}$, and then changing the integration variables $(t,s) \to (p,q)$ as $(t+s)/\sqrt{2} = p$ and $(t-s)/\sqrt{2} = q$ the equation (43) takes the following form:

$$P_N(z\sqrt{N}) = \frac{N!N}{2\pi\tau} e^{N\frac{z^2}{\tau}} \int_{\mathbb{R}} dp\, e^{-N\frac{p^2}{2}\left(\frac{1}{\tau}-1\right)} \int_{\mathbb{R}} dq e^{-N\left(\frac{q^2}{2}\left(\frac{1}{\tau}+1\right)+\frac{iz\sqrt{2}}{\tau}q\right)} \quad (45)$$
$$\times \left(\theta_N\left(\frac{p^2-q^2}{2}\right) + Np^2\theta_{N-1}\left(\frac{p^2-q^2}{2}\frac{N}{N-1}\right)\right),$$

where we denoted $\theta_N(x) = \frac{\Gamma(N+1,Nx)}{\Gamma(N+1)}$. Note that for any N this function is bounded: $\theta_N(x) \leq 1$, and in the limit $N \to \infty$ for a fixed real x we have $\theta_N(x) \to \theta_\infty(x)$, where $\theta_\infty(x) = 1$ for $x < 1$ and 0 otherwise.

For $N \gg 1$ the integral over p can be most straightforwardly evaluated by the Laplace method, yielding that the leading contribution to $P_N(z\sqrt{N})$ can be written as

$$P_N(z\sqrt{N}) \sim \frac{N!\sqrt{N}}{\sqrt{2\pi\tau(1-\tau)}} e^{N\frac{z^2}{\tau}} \int_{\mathbb{R}} dq e^{-N\left(\frac{q^2}{2}\left(\frac{1}{\tau}+1\right)+\frac{iz\sqrt{2}}{\tau}q\right)} \left(\theta_N\left(\frac{-q^2}{2}\right) + \frac{\tau}{1-\tau}\theta_{N-1}\left(\frac{-q^2}{2}\right)\right). \tag{46}$$

For large N the $q-$integral above can be performed (for a fixed, $N-$independent real value of z) by the standard saddle point method, with the saddle point position given by $q = q_* := -\frac{iz\sqrt{2}}{1+\tau}$ yielding the required asymptotic formula:

$$P_N(z\sqrt{N}) \sim \frac{N!}{\sqrt{1-\tau^2}(1-\tau)} e^{\frac{Nz^2}{1+\tau}} \theta_\infty\left(z^2/(1+\tau)^2\right) \tag{47}$$

The same type of reasoning applied to (44) gives

$$T_N(z\sqrt{N}) \sim \frac{N!}{(1-\tau^2)^{3/2}} \frac{Nz^2}{1+\tau} e^{\frac{Nz^2}{1+\tau}} \theta_\infty\left(z^2/(1+\tau)^2\right). \tag{48}$$

Finally, the asymptotics

$$R_N(z\sqrt{N}) \sim \frac{N!z\sqrt{N}}{(1-\tau^2)^{3/2}} e^{\frac{Nz^2}{1+\tau}} \theta_\infty\left(z^2/(1+\tau)^2\right) \tag{49}$$

is obtained from (47) using the fact that $R_N(z) = \frac{1}{2(N+1)} \frac{dP_{N+1}(z)}{dz}$.

Upon inserting this asymptotics into (6) and rescaling $q \to Nq$ it is clear that only the second to last term in the square bracket provides the leading order contribution, which happens to be

$$\frac{(1+\tau)(1-\tau^2)(N-1)[(N-1)P_{N-2} - T_{N-2}]}{1+\tau+Nq} \sim \frac{(N-1)![(1+\tau)^2 - z^2]}{q\sqrt{1-\tau^2}} e^{\frac{Nz^2}{1+\tau}}. \tag{50}$$

As a consequence, the joint pdf reads

$$N\mathcal{P}(z\sqrt{N}, Nq) = \frac{\sqrt{\frac{1+\tau}{1-\tau}}(1 - \frac{z^2}{(1+\tau)^2})}{2\sqrt{2\pi}q^2} e^{-\frac{1+\tau}{2q}\left(1-\frac{z^2}{(1+\tau)^2}\right)}. \tag{51}$$

Changing variables to $t = \frac{q}{1-\tau}$, one immediately recovers Corollary 2.4. □

3.3.2 Edge scaling

When z is tuned to values parametrically close to $z = \pm(1+\tau)$ where the step-function argument in equations (47)-(50) is close to unity by a distance $O(N^{-1/2})$, the correponding asymptotics need to be evaluated with higher accuracy. Such regime is known as the *edge scaling*, which features in the **Corollary 2.5** which we now prove.

Proof. In the proof we choose the vicinity of $z = 1 + \tau$. Correspondingly, in (45) we now scale $z = 1+\tau+\frac{w}{\sqrt{N}}$, where w is of order 1. The transition from (45) to (46) remains the same as before. Now we use the integral representation of the incomplete gamma function $\Gamma(N, x) = x^N \int_1^\infty u^{N-1} e^{-ux} du$ helps to rewrite the integral (46) in the form

$$P_N(z) \sim \frac{N! N^{N+1}}{4\pi\tau\Gamma(N)} e^{N\frac{z^2}{\tau}} \int_{\mathbb{R}} dq\, e^{-\frac{N(1+\tau)}{2\tau}(q^2+i2\sqrt{2}q)-\frac{iqw\sqrt{2N}}{\tau}} \int_1^\infty du\, e^{-\frac{Nu}{2}(-q^2)+N\ln\left[\frac{u}{2}(-q^2)\right]} \times \left(\frac{-q^2}{2} + \frac{\tau}{1-\tau}\frac{1}{u}\right). \quad (52)$$

An inspection shows that whereas the $q-$integration is dominated by the contribution from the saddle point $q = -\sqrt{2}i$ the last $u-$integral is dominated by the vicinity of $u = 1$ of the widths $O(N^{-1/2})$. Parametrizing in such a vicinity $u = 1 + \frac{v}{\sqrt{N}}$ one then arrives at the leading -order asymptotic

$$P_N \sim \frac{N! N^{N-1/2}}{(1-\tau)^2\Gamma(N)} e^{\frac{w^2}{1+\tau}+2w\sqrt{N}+N\tau} \int_0^\infty e^{-\frac{1+\tau}{2(1-\tau)}\left(v+\frac{2w}{1+\tau}\right)^2} dv. \quad (53)$$

After the change of variables $u = \sqrt{\frac{1+\tau}{1-\tau}}(v+\frac{2w}{1+\tau})$ and the use of Stirling's approximation $\Gamma(N+1) \sim \sqrt{2\pi}N^{N+\frac{1}{2}}e^{-N}$, we obtain

$$P_N = \frac{N! e^{\frac{z^2}{1+\tau}}}{(1-\tau)\sqrt{2\pi(1-\tau^2)}} \int_{\frac{2w}{\sqrt{1-\tau^2}}}^\infty e^{-\frac{u^2}{2}} du. \quad (54)$$

The last integral is related to the complementary error function $\mathrm{erfc}(x) = \frac{2}{\sqrt{\pi}}\int_x^\infty e^{-t^2} dt$. Using $R_N(z) = \frac{1}{2(N+1)}\frac{dP_{N+1}(z)}{dz}$ we obtain that in such regime asymptotically $R_N \sim \sqrt{N}P_N$. From the asymptotics of (50) one expects that the leading order contributions from $(N+1)P_N$ and T_N cancel, therefore one needs to work with the appropriate integral representation. Combining (43) and (44) and following the analogous reasoning as above we obtain

$$(N+1)P_N - T_N = \frac{N!\sqrt{N}}{\sqrt{2\pi}(1-\tau^2)} e^{\frac{z^2}{1+\tau}} \left[e^{-\frac{2w^2}{1-\tau^2}} - \frac{2w}{\sqrt{1-\tau^2}} \int_{\frac{2w}{\sqrt{1-\tau^2}}}^\infty e^{-\frac{u^2}{2}} du \right], \quad (55)$$

which is of the same order as $\sqrt{N}P_N$, as expected. To get the correct asymptotic at the edge, we rescale $q \to q\sqrt{N}$ in (6). It is now clear that the first term in square bracket in (6) is subleading and contribution of other terms is of the same order. The asymptotics of $\left(\frac{q\sqrt{N}}{1+\tau+q\sqrt{N}}\right)^{\frac{N}{2}-1}$ is calculated as

$$e^{-\frac{N}{2}\ln\left(1+\frac{1+\tau}{q\sqrt{N}}\right)} \sim e^{-\frac{(1+\tau)\sqrt{N}}{2q}+\frac{(1+\tau)^2}{4q^2}} \quad (56)$$

and we obtain

$$\mathcal{P} \sim \frac{1}{4\pi q^2\sqrt{N}} e^{\frac{w}{q}-\frac{1-\tau^2}{4q^2}} \left[e^{-\frac{2w^2}{1-\tau^2}} + \left(\frac{\sqrt{1-\tau^2}}{q} - \frac{2w}{\sqrt{1-\tau^2}}\right) \int_{\frac{2w}{1-\tau^2}}^\infty e^{-\frac{u^2}{2}} du \right]. \quad (57)$$

After denoting $w = \delta_\tau\sqrt{1-\tau^2}$ and $q = \sigma\sqrt{1-\tau^2}$, the statement of the Corollary 2.5 follows.

□

3.3.3 Weak nonhermiticity

Our final goal is to provide the proof of **Corollary 2.6**.

Proof. We start again from (45) keeping z fixed and $N-$independent like before in the bulk case, but for the weak nonhermiticity regime replace $\tau = 1 - \frac{a^2}{2N}$. It is then immediately obvious that $p-$integral is no longer dominated by the small vicinity $p \sim N^{-1/2}$, but rather by the integration range of order unity. Then a quick inspection shows that for extracting the leading asymptotics in the large N limit one can effectively replace (45) by

$$P_N(z\sqrt{N}) \sim \frac{N!N^2}{2\pi\tau} e^{N\frac{z^2}{\tau}} \int_{\mathbb{R}} dp\, p^2 e^{-\frac{p^2a^2}{4}} \int_{\mathbb{R}} dq e^{-N\left(q^2+iz\sqrt{2}q\right)} \theta_\infty\left(\frac{p^2-q^2}{2}\right). \tag{58}$$

Performing the integral over q by the saddle point method we see that the range of integration over p is given by $|p| < \frac{\sqrt{4-z^2}}{\sqrt{2}}$. After a few simple changes of variables and straightforward manipulations one arrives at

$$P_N(z\sqrt{N}) \sim \frac{N!N^{3/2}(4-z^2)^{3/2}}{2\sqrt{2\pi}} e^{\frac{Nz^2}{2}} \int_0^1 e^{-\frac{s^2a^2}{2}\left(1-\frac{z^2}{4}\right)} s^2 ds. \tag{59}$$

The asymptotic behavior of R_N simply follows from the relation $R_N(z) = \frac{1}{2(N+1)} \frac{dP_{N+1}(z)}{dz}$ and is related to the asymptotics of P_N as $R_N = \frac{z\sqrt{N}}{2} P_N$. Asymptotics of T_N analogously follows from its integral representation and reads

$$T_N(z\sqrt{N}) = \frac{N!N^{5/2}(4-z^2)^{3/2}}{2\sqrt{2\pi}} e^{\frac{Nz^2}{2}} \int_0^1 e^{-\frac{s^2a^2}{2}\left(1-\frac{z^2}{4}\right)} \frac{4s^4 - z^2s^4 + z^2s^2}{4} ds. \tag{60}$$

Note that in (6) we used the rescaled quantity $q = (1-\tau)t$, therefore for the correct asymptotics, we need to rescale $q \to \frac{2N}{a^2}t$. This shows that all terms in square bracket are of the same order. Direct use of the asymptotic forms (59) and (60) leads to (16). □

Appendix A Density of real eigenvalues for moderate matrix size

For $N = 2$ the joint pdf (6) reads

$$\mathcal{P}_{N=2}(z,q) = \frac{1}{2\sqrt{2\pi}(1+\tau)} \frac{e^{-\frac{z^2}{2(1+\tau)}\left(1+\frac{q}{1+q}\right)}}{\sqrt{q(1+q)}} \left(\frac{z^2}{(1+q)^2} + \frac{1+\tau}{1+q}\right). \tag{61}$$

The substitution $t^2 = \frac{q}{q+1}$ allows one to calculate the integral. After integration by parts, we obtain

$$\int_0^\infty \mathcal{P}_{N=2}(z,q)dq = \frac{e^{-\frac{z^2}{1+\tau}}}{\sqrt{2\pi}} + \frac{e^{-\frac{z^2}{2(1+\tau)}}}{\sqrt{2\pi}} \frac{z}{1+\tau} \int_0^z e^{-\frac{u^2}{2(1+\tau)}} du, \tag{62}$$

which agrees with (11)-(12) when we substitute $N = 2$. This way, with the help of *Mathematica* software, we were also able to perform integration for $N = 3, 4$. For $N = 4$ we again see agreement with Forrester-Nagao result, while for $N = 3$ we compared the results of integration with the numerical diagonalizations of random matrices, see Fig. 2. For moderate matrix sizes, where the symbolic calculations were not possible, we numerically integrated (6) and compared with numerical diagonalization, observing good agreement, see Fig. 2.

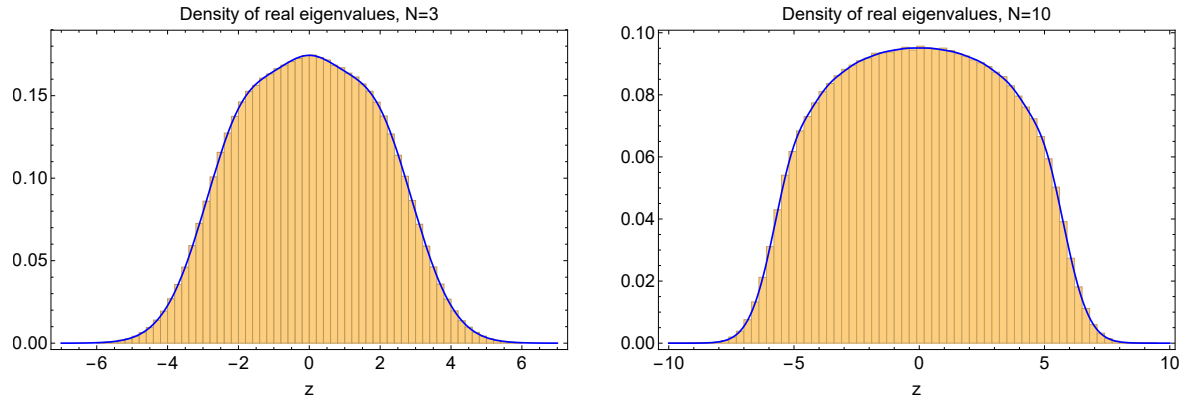

Figure 2: Histograms of the density of real eigenvalues for the elliptic ensemble with $\tau = 0.9$ obtained by direct diagonalization of 10^6 matrices of size $N = 3$ (left) and $2 \cdot 10^5$ matrices of size $N = 10$ (right). Blue solid lines present the formula obtained by analytical (left) and numerical (right) integration of $\mathcal{P}(z, q)$ (6). Formulas are rescaled so that the density is normalized to 1.

Appendix B Proof of the identity (40)

We shall prove (40) by induction.

Proof. The first step is trivial as this identity can be verified by substituting Hermite polynomials for low N. Let us assume that (40) holds for $N-1$. Using formulas (8)-(10) it is easy to find the recurrence relations

$$P_N = NP_{N-1} + A_N, \tag{63}$$
$$R_N = NR_{N-1} + B_N, \tag{64}$$
$$T_N = NT_{N-1} + NA_N, \tag{65}$$

with

$$A_N = \tau^N[(N+1)\mathrm{He}_N^2 - N\mathrm{He}_{N+1}\mathrm{He}_{N-1}], \tag{66}$$
$$2B_N = \tau^{N-1/2}[(N+1)\mathrm{He}_N\mathrm{He}_{N-1} - (N-1)\mathrm{He}_{N+1}\mathrm{He}_{N-2}, \tag{67}$$

where for simplicity we omitted the argument $\frac{z}{\sqrt{\tau}}$ of Hermite polynomials. These recursions allow us to rewrite lhs of (40) as

$$(N-1)[P_{N-1} - P_{N-2}(1+\tau-z^2) - (N-2)(2\tau^2+N-2)P_{N-3} - 2zR_{N-2} + (1-\tau^2)(N-2)T_{N-3}] + A_N + (z^2-\tau)A_{N-1} - N(N-1)\tau^2 A_{N-2} - 2zB_{N-1}. \tag{68}$$

The the expression in square brackets is zero by the induction assumption. Verification that the second line equals 0 relies on the substitution of (66) and (67) and consecutive use of the three term recursion $\mathrm{He}_{N+1}(x) = x\mathrm{He}_N(x) - N\mathrm{He}_{N-1}(x)$. □

References

[1] G. Akemann, M. J. Phillips and H.-J. Sommers, *Characteristic polynomials in real Ginibre ensembles.* J. Phys. A: Math. Theor. **42**, 012001 (2008).

[2] G. Akemann, R. Tribe, A. Tsareas, O. Zaboronski, *On the determinantal structure of conditional overlaps for the complex Ginibre ensemble.* arXiv:1903.09016 [math-ph] (2019).

[3] S. Belinschi, M. A. Nowak, R. Speicher and W. Tarnowski, *Squared eigenvalue condition numbers and eigenvector correlations from the single ring theorem.* J. Phys. A: Math. Theor. **50**, 105204 (2017).

[4] F. Benaych-Georges and O. Zeitouni, *Eigenvectors of non normal random matrices.* Electron. Commun. Probab. **23**(70), 1-12 (2018).

[5] P. Bourgade, G. Dubach, *The distribution of overlaps between eigenvectors of Ginibre matrices.* arXiv:1801.01219 [math.PR] (2018).

[6] Z. Burda, J. Grela, M. A. Nowak, W. Tarnowski and P. Warcho, *Dysonian dynamics of the Ginibre ensemble.* Phys. Rev. Lett. **113**, 104102 (2014).

[7] Z. Burda, B. J. Spisak and P. Vivo, *Eigenvector statistics of the product of Ginibre matrices.* Phys. Rev. E **95**, 022134 (2017).

[8] J. T. Chalker and B. Mehlig, *Eigenvector Statistics in Non-Hermitian Random Matrix Ensembles.* Phys. Rev. Lett. **81**, 3367 (1998).

[9] N. Crawford and R. Rosenthal, *Eigenvector correlations in the complex Ginibre ensemble.* arXiv:1805.08993 (2018).

[10] M. Davy and A. Z. Genack, *Selectively exciting quasi-normal modes in open disordered systems.* Nature Comm. **9**, 4714 (2018).

[11] M. Davy and A. Z. Genack, *Impact of non-Hemiticity on modal strength and correlation in transmission through random open cavities.* arXiv:1905.08301 (2019).

[12] G. Dubach, *On eigenvector statistics in the spherical and truncated unitary ensembles.* arXiv:1908.06713 [math.PR] (2019).

[13] A. Edelman, E. Kostlan and M. Shub, *How many eigenvalues of a random matrix are real?*, J. Amer. Math. Soc. **7**, 247-267 (1994).

[14] K. B. Efetov, *Directed quantum chaos.* Phys. Rev. Lett. **79**, 491 (1997).

[15] L. Erdös, T. Krüger and D. Renfrew, *Randomly coupled differential equations with correlations.* arXiv:1908.05178 (2019).

[16] P. J. Forrester and A. Mays, *A Method to Calculate Correlation Functions for $\beta = 1$ Random Matrices of Odd Size.* J. Stat. Phys. **134**, 443462 (2009).

[17] P. J. Forrester and T. Nagao, *Skew orthogonal polynomials and the partly symmetric real Ginibre ensemble.* J. Phys. A: Math. Theor. **41**, 375003 (2008).

[18] K. M. Frahm, H. Schomerus, M. Patra and C. W. J. Beenakker, *Large petermann factor in chaotic cavities with many scattering channels.* Europhys. Lett. **49**, 48 (2000).

[19] Y. V. Fyodorov, *Negative moments of characteristic polynomials of random matrices: Ingham-Siegel integral as an alternative to HubbardStratonovich transformation.* Nucl. Phys. B **621**(3), 643674 (2002).

[20] Y. V. Fyodorov, *On statistics of bi-orthogonal eigenvectors in real and complex Ginibre ensembles: combining partial Schur decomposition with supersymmetry.* Commun. Math. Phys. **363**, 579603 (2018).

[21] Y. V. Fyodorov, B. Khoruzhenko and H. – J. Sommers, *Almost-Hermitian Random Matrices: Eigenvalue Density in the Complex Plane.* Phys. Lett. A **226**, 46–52 (1997).

[22] Y. V. Fyodorov, B. Khoruzhenko and H. – J. Sommers, *Almost-Hermitian Random Matrices: Crossover from Wigner-Dyson to Ginibre Eigenvalue Statistics.* Phys. Rev. Lett. **79**, 557–560 (1997).

[23] Y. V. Fyodorov, B. Khoruzhenko and H. – J. Sommers, *Universality in the random matrix spectra in the regime of weak non-Hermiticity.* Ann. Inst. Henri Poincaré [Physique Theorique] **68**, 449-489 (1998).

[24] Y. V. Fyodorov and B. Mehlig, *Statistics of resonances and nonorthogonal eigenfunctions in a model for single-channel chaotic scattering.* Phys. Rev. E **66**, 045202 (2002).

[25] Y. V. Fyodorov and D. V. Savin, *Statistics of resonance width shifts as a signature of eigenfunction non-orthogonality.* Phys. Rev. Lett. **108**, 184101 (2012).

[26] Y. V. Fyodorov and H. – J. Sommers, *Random matrices close to Hermitian or unitary: overview of methods and results.* J. Phys. A: Math. Theor. **36**, 3303–3347 (2003).

[27] Y. V. Fyodorov and E. Strahov, *Characteristic polynomials of random Hermitian matrices and Duistermaat – Heckman localization on non-compact Kähler manifolds.* Nucl. Phys. B **630**, 453–491 (2002).

[28] J. Grela, *What drives transient behavior in complex systems?* Phys. Rev. E **96**, 022316 (2017).

[29] J. Grela, P. Warcho, *Full Dysonian dynamics of the complex Ginibre ensemble.* J. Phys. A: Math. Theor. **51**, 42 (2018).

[30] E. Gudowska-Nowak, J. Ochab, D. Chialvo, M. A. Nowak and W. Tarnowski, *From synaptic interactions to collective dynamics in random neuronal networks models: critical role of eigenvectors and transient behavior.* arXiv:1805.03592v1 [q-bio.NC] (2018).

[31] R. A. Janik, W. Noerenberg, M. A. Nowak, G. Papp and I. Zahed, *Correlations of eigenvectors for nonHermitian random matrix models.* Phys. Rev. E **60**, 2699 (1999).

[32] D. Martí, N. Brunel and S. Ostojic, *Correlations between synapses in pairs of neurons slow down dynamics in randomly connected neural networks.* Phys. Rev. E **97**, 062314 (2018).

[33] B. Mehlig and J. T. Chalker, *Statistical properties of eigenvectors in non-Hermitian Gaussian random matrix ensembles*. J. Math. Phys. **41**, 3233 (2000).

[34] I. Neri and F. L. Metz, *Eigenvalue Outliers of Non-Hermitian Random Matrices with a Local Tree Structure.* Phys. Rev. Lett. **117**, 224101 (2016); Erratum in: Phys. Rev. Lett. **118**, 019901 (2017).

[35] M. A. Nowak and W. Tarnowski, *Probing non-orthogonality of eigenvectors in non-Hermitian matrix models: diagrammatic approach*. JHEP **2018** 152 (2018).

[36] M. Patra, H. Schomerus and C. W. J. Beenakker, *Quantum-limited linewidth of a chaotic laser cavity*. Phys. Rev. A **61**, 023810 (2000).

[37] H. Schomerus, K. Frahm, M. Patra and C. W. J. Beenakker, *Quantum limit of the laser line width in chaotic cavities and statistics of residues of scattering matrix poles*. Physica A **278**, 469 (2000).

[38] W. Tarnowski, I. Neri and P. Vivo, *Universal transient behavior in large dynamical systems on networks*. arXiv:1906.10634 [nlin.AO] (2019).

[39] L. N. Trefethen and M. Embree, *Spectra and Pseudospectra. The Behavior of Nonnormal Matrices and Operators*. Princeton University Press, Princeton (2005).

[40] J. H. Wilkinson, *The Algebraic Eigenvalue Problem*. Oxford University Press, Oxford (1965).

[41] M. Walters and S. Starr, *A note on mixed matrix moments for the complex Ginibre ensemble.* J. Math. Phys. **56**, 013301 (2015).

Available online at www.sciencedirect.com

ScienceDirect

Nuclear Physics B 955 (2020) 115051

NUCLEAR PHYSICS B

www.elsevier.com/locate/nuclphysb

Narain transform for spectral deformations of random matrix models

M.A. Nowak *, W. Tarnowski

Institute of Theoretical Physics and Mark Kac Complex Systems Research Center, Jagiellonian University, S. Łojasiewicza 11, PL 30-348 Kraków, Poland

Received 2 October 2019; received in revised form 29 April 2020; accepted 9 May 2020
Available online 15 May 2020
Editor: Hubert Saleur

Abstract

We start from applying the general idea of spectral projection (suggested by Olshanski and Borodin and advocated by Tao) to the complex Wishart model. Combining the ideas of spectral projection with the insights from quantum mechanics, we derive in an effortless way all spectral properties of the complex Wishart model: first, the Marchenko-Pastur distribution interpreted as a Bohr-Sommerfeld quantization condition for the hydrogen atom; second, hard (Bessel), soft (Airy) and bulk (sine) microscopic kernels from properly rescaled radial Schrödinger equation for the hydrogen atom. Then, generalizing the ideas based on Schrödinger equation to the case when Hamiltonian is non-Hermitian, we propose an analogous construction for spectral projections of universal kernels for bi-orthogonal ensembles. In particular, we demonstrate that the Narain transform is a natural extension of the Hankel transform for the products of Wishart matrices, yielding an explicit form of the universal kernel at the hard edge. We also show how the change of variables of the *rescaled* kernel allows us to make the link to the universal kernel of the Muttalib-Borodin ensemble. The proposed construction offers a simple alternative to standard methods of derivation of microscopic kernels. Finally, we speculate, that a suitable extension of the Bochner theorem for Sturm-Liouville operators may provide an additional insight into the classification of microscopic universality classes in random matrix theory.

* Corresponding author.
E-mail addresses: maciej.a.nowak@uj.edu.pl (M.A. Nowak), wojciech.tarnowski@doctoral.uj.edu.pl (W. Tarnowski).

https://doi.org/10.1016/j.nuclphysb.2020.115051

1. Introduction

Determinantal point processes [1] appear in several areas of mathematics, physics and applied sciences, ranging from random matrix theory (RMT) to combinatorics and theory of representations. The unique feature of such processes relies on the fact, that the N-point joint probability distribution function is expressed as a determinant of a matrix built from a single, two-point correlation function known as a kernel. Celebrated examples of such kernels in high energy physics include "hard-edge" Bessel kernels [2–4], observed in numerous lattice calculations [5], or Pearcey kernels appearing at strong-weak coupling phase transition in Yang-Mills theories in the limit of large number of colors [6,7]. The calculation of kernels and their asymptotic limits became therefore an area of vigorous studies using advanced mathematical tools, like supersymmetry [8–11], orthogonal [12] and bi-orthogonal polynomials [13], Riemann-Hilbert problem [14–16] and Plancherel-Rotach [17] limiting procedures for integral representations, to mention most popular.

Borodin and Olshanski [18] offered a different point of view at kernels built from orthogonal polynomials in random matrix theory. When treated as an integral operator, the kernel is a projection – a consequence of a finite number of eigenvalues and orthogonality of polynomials. This idea was later advocated by Tao [19], who also used physical intuition by the mapping between Gaussian Unitary Ensemble and the quantum harmonic oscillator. In this quantum mechanical picture the projection stems from the fact that the first N energy levels are occupied. Using these techniques, Bornemann elaborated the Sturm-Liouville problem and showed that all three classical limiting kernels can be obtained in this way [20]. The joint probability density functions in RMT can be mapped onto various physical systems, including point charges with logarithmic interaction [21–23] and spinless fermions [24]. The latter equivalence proved to be a fertile ground of applications of RMT to cold atom systems [25–28].

It is intriguing to investigate the chronological intertwining of the ideas in quantum mechanics, mathematics and statistics from the perspective of the contemporary random matrix theory. In 1926, Schrödinger has solved his equation for Coulomb potential, obtaining among others the radial part of the wave function in terms of Laguerre functions.[1] Two years later (1928) Wishart introduced his ensemble in multivariate statistics, as a generalization of the χ^2 ensemble [29]. The original paper deals with the real random variables, but his ideas were later generalized to complex variables [30]. A year later (1929), Bochner has proven his theorem [31] (see section 3.1) for Sturm–Liouville operators, without any direct references to Schrödinger equation. At that time spectral properties of random matrices were not considered at all. Laguerre polynomials appeared explicitly in random matrix theory only after Mehta and Gaudin used the orthogonal polynomial method to disentangle the Van der Monde determinant [32]. This technique has also paved the way for classical universal kernels. However, the link to the uniqueness of the determinantal triality of soft, edge and bulk microscopic universalities of Sturm–Liouville operators have been cleared out only recently [20].

With introducing non-trivial initial conditions for Dyson Brownian motion, new universality classes emerged in random matrix theory. In the 90's of the previous century, collision of soft edges in GUE led Brezin and Hikami [33] to the Pearcey kernel. In a similar collision of chiral fronts at the hard edge of the chiral random matrix model one of the authors found the Bessoid kernel universality [34]. While still determinantal [35], such models break rotational invariance,

[1] Year earlier, Pauli has quantized algebraically hydrogen atom, using the hidden symmetry (Runge-Lenz vector) of the Coulomb potential, therefore treating this problem as a free problem on S_3 hypersphere.

and require non-standard tools. Later it was discovered that such ensembles can be solved by polynomials that are orthogonal with respect to more than one weight [36].

The bi-orthogonality method of Muttalib and Borodin [13,37] opened a new way for treating a broader class of random matrix models, to which the orthogonal polynomial method does not apply. Historically, it is again puzzling that bi-orthogonality was not linked to random matrices earlier. Already in 1951, Fano and Spencer [38] studying propagation of the X-rays through the matter, have introduced bi-orthogonal Laguerre polynomials. These ideas were further developed in mathematics by Preiser [39] and Konhauser [40]. In particular, Preiser's construction corresponds exactly to the case of Muttalib-Borodin ensemble.

The aim of this work is to further elaborate the spectral projection method, with the use of insights from elementary quantum mechanics. In section 2, we pedagogically introduce the spectral projection method and demonstrate its easiness in taking the microscopic limits by recalculating all limiting kernels in the complex Wishart ensemble. We link the Marchenko-Pastur distribution [41] to the Bohr-Sommerfeld quantization condition. We also notice that the threeness of the classical universal kernels can be linked to the strictures originating from the Bochner theorem for Sturm-Liouville problem [31].

Recent developments on the integrable structure of products of random matrices and the multitude of new microscopic kernels in biorthogonal ensembles naturally pose a question whether the spectral projection method can be extended to incorporate these universality classes. In section 3 we discuss the possibilities to circumvent the constrains of Bochner's theorem and consider an analog of a quantum-mechanical Hamiltonian, but with higher number of derivatives. Although such an operator may not be self-adjoint, still, due the fact that its left and right eigenvectors form a bi-orthogonal basis, it is possible to infer the microscopic limit of the kernels, using the spectral projection method. The power of this approach – easiness of calculation of microscopic kernel without the need of Plancherel-Rotach asymptotics – is demonstrated on two examples: singular values of products of Gaussian matrices [42] and the Muttalib-Borodin ensemble [13,37]. In both cases the Narain transform [43–45] allows one to recover the Meijer-G hard edge universality, generalizing Bessel kernel. Again, the spectral projection translates to the truncation of the phase space of the associated transform.

Section 4 concludes the paper. In appendix A, we show an alternative mapping of the Wishart ensemble to the 2-dimensional hydrogen atom problem [46]. In appendix B we recover the Marchenko-Pastur distribution from the WKB approximation. In appendix C we recall some properties of the Meijer-G functions.

2. Spectral projections from hydrogen atom problem

2.1. Complex Wishart ensemble

Let us consider Hermitian matrix $M = XX^\dagger$, where X is the complex $N \times T$ matrix with entries given by the probability density function $P(X)dX = Z_{NT}^{-1} e^{-\frac{1}{\sigma^2}\sum_{\alpha,j}^{N,T} |X_{\alpha,j}|^2} \prod_{\alpha j}^{N,T} d\Re X_{\alpha j} \times d\Im X_{\alpha j}$. Here Z_{NT}^{-1} provides the normalization and σ^2 is the variance of the complex Gaussian distribution, which we set to 1, to simplify the expressions. This defines complex Wishart matrix [29]. Switching to eigenvalues, we arrive, using standard methods [47], at their joint probability density

$$P(\lambda_1, ..., \lambda_N) = Q_N^{-1} \prod_{j=1}^{N} \lambda_j^{\alpha} e^{-\lambda_j} \prod_{1 \leq i < j \leq N} |\lambda_i - \lambda_j|^2, \tag{1}$$

with $\alpha = T - N$, and the Vandermonde determinant (last term) is the price for switching from elements of X to eigenvalues λ_i of matrix M. Standard orthogonal polynomials method [12] allows one to rewrite the probability distribution as

$$P_N(\lambda_1, ..., \lambda_N) = \frac{1}{N!} \left(\det \left[\psi_{j-1}(\lambda_k) \right]_{j,k=1}^{N} \right)^2 = \frac{1}{N!} \left[\det K_N(\lambda_i, \lambda_j) \right], \tag{2}$$

with the correlation *kernel*

$$K_N(\lambda, \mu) = \sum_{l=0}^{N-1} \psi_l(\lambda) \psi_l(\mu), \tag{3}$$

where $\psi_l(\lambda) = e^{-\lambda/2} \lambda^{\alpha/2} P_l(\lambda)$ and P_l are monic polynomials. This form already suggests links to quantum mechanics. The first equality in (2) represents the joint probability of eigenvalues as the square of the Slater determinant, therefore can be interpreted as the quantum probability density of non-interacting spinless fermions (see [28] for a review). This also explains why the eigenvalue density is expressed solely in terms of a two-point function (second expression on the r.h.s. of (2)). Next, we see that the most natural choice of polynomials is dictated by the weight $w_\alpha(\lambda) = \lambda^\alpha e^{-\lambda}$. Such polynomials, orthonormal on the positive part of the real axis, are the associated Laguerre polynomials and appear in the radial part of the Schrödinger equation. Indeed, upon standard separation of variables in the wavefunction, $\varphi(\vec{r}) = R(r) Y_l^m(\theta, \psi)$, it reads

$$\frac{d^2 y(r)}{dr^2} + \left[\frac{2\mu e^2}{r\hbar^2} - \frac{l(l+1)}{r^2} \right] y(r) = -\frac{2\mu E}{\hbar^2} y(r), \tag{4}$$

where $y(r) = r R(r)$. Switching to dimensionless variable $x = r\epsilon$, where $(\epsilon/2)^2 = -2\mu E/\hbar^2$, putting $2\mu = 1$ and all other physical constants to 1, we recover [48]

$$\frac{d^2 y(x)}{dx^2} + \left[-\frac{1}{4} + \frac{1}{\epsilon x} - \frac{l(l+1)}{x^2} \right] y(x) = 0, \tag{5}$$

where $y = y_n^l = e^{-x/2} x^{(k+1)/2} L_j^k(x)$. Here $k = 2l + 1$ and the principal quantum number is related to the order of Laguerre polynomial as $n = j + l + 1$. Note, that $\epsilon = 1/n$, or, equivalently, $E_n = -1/4n^2$, since in our units Bohr's radius equals to 2. To map this random matrix problem to the hydrogen atom we associate $\psi_l(\lambda) = \sqrt{x}\, y(x)$. This completes the dictionary between hydrogen atom problem and the Wishart kernel. In Appendix A we also present a mapping into 2D hydrogen atom with $1/r$ potential [46], in which the relation between eigenfunctions of the radial part of the Schrödinger equation and ψ is even more explicit.

The Schrödinger equation for ψ expressed in terms of the parameters of the Wishart ensemble reads

$$\frac{d^2 \psi_k}{dx^2} + \frac{1}{x} \frac{d\psi_k}{dx} + \frac{1 + 2k + \alpha}{2x} \psi_k - \frac{\alpha^2}{4x^2} \psi_k = \frac{1}{4} \psi_k. \tag{6}$$

Finally, let us note that in the bra-ket notations the kernel can be rewritten as $\hat{K}_N = \sum_{k=0}^{N-1} |\psi_k\rangle \langle \psi_k|$, thus it is the operator projecting onto the set of N lowest eigenstates. Indeed, due to the orthonormality of eigenfunctions $\hat{K}_N^2 = \hat{K}_N$, last equation, when calculated in coordinate representation, yields well-known reproducing property $\langle x | \hat{K}_N | y \rangle \equiv K_N(x, y) = \int K_N(x, z) K_N(z, y) dz$.

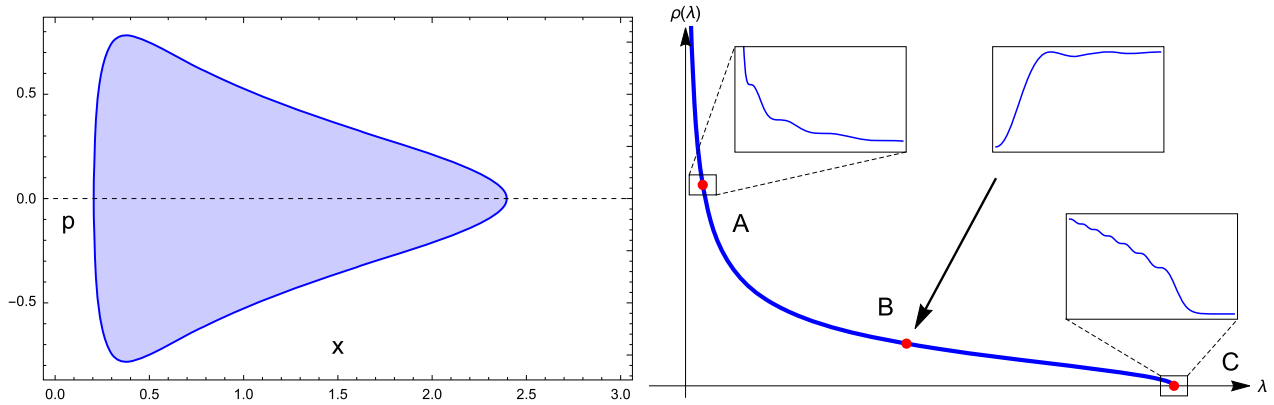

Fig. 1. (left) A region in the phase space where the Wigner function is nonzero. We took c=0.3. (right) Identification of three regions of the Marchenko-Pastur distribution that give rise to different microscopic scalings.

2.2. *Macroscopic density from the semiclassical approximation*

To have the finite support of the spectral density in the large N limit, we rescale $x \to Tx$. Upon this scaling and identifying momentum[2] as $p = -\frac{i}{T}\frac{d}{dx}$ (in analogy to $\hbar \leftrightarrow 1/T$) in the limit $N, T \to \infty$ with $c = N/T$ fixed we obtain the Schrödinger equation $(p^2 + V_{eff})\psi = -\frac{1}{4}\psi$ with the effective potential

$$V_{eff} = \frac{(1-c)^2}{4x^2} - \frac{1+c}{2x}. \tag{7}$$

The probability density function can be obtained from the Wigner quasiprobability distribution, defined as

$$W(x,p) = \frac{1}{\pi\hbar}\int_{-\infty}^{\infty} \overline{\psi}(x+y)\psi(x-y)e^{2ipy/\hbar}dy, \tag{8}$$

by integrating out the momentum. In the large N limit the Wigner function is constant in the region of the phase space $p^2 + V(x) \leq \frac{1}{4}$ and zero outside [49] (see Fig. 1). As a consequence, the density of eigenvalues is proportional to the momentum and the Bohr-Sommerfeld quantization condition

$$T\oint p(xT)dx = \left(N + \frac{1}{2}\right)2\pi \tag{9}$$

on the RMT side corresponds to the normalization of the density

$$\int_{r_-}^{r_+} \rho(x)dx = 1. \tag{10}$$

This allows us to obtain the density of eigenvalues

$$\rho(x) = \frac{1}{2\pi cx}\sqrt{(r_+ - x)(x - r_-)}. \tag{11}$$

[2] For this analogy it is even better to take the 2D radial momentum $p_r = \frac{i}{T}\left(\frac{d}{dx} + \frac{1}{x}\right)$, but this eventually leads to the same result in large T limit.

Here $r_\pm = (1 \pm \sqrt{c})^2$ are classical turning points in WKB approximation. In Appendix B we provide another derivation of this result based on the explicit WKB analysis of (6).

We have therefore obtained Marchenko-Pastur distribution as an *exact, semiclassical limit of the quantum mechanical hydrogen atom problem*. It is intriguing to speculate why such a link has not been exploited (to the authors knowledge) in the literature. Perhaps the reason is that the Bohr-Sommerfeld quantization condition does not reproduce correctly the ground state of the hydrogen atom, and not even the Bohr quantization condition [50]. It is amusing to notice, that if one replaced $l(l+1)$ by $(l+1/2)^2$ in the numerator of the centrifugal potential, this would be the case and B-S approximation would lead to the exact result for the hydrogen spectra [51]. Of course, in the large l limit it does not matter which of the equations (5) or (6) we use, however, at the microscopic level, the additional square root in Laguerre function for the Wishart will play the crucial role in getting the proper scaling of the hard edge.

We complete this part with the observation, that in the case of harmonic oscillator, similar construction is ambiguities free, since Bohr-Sommerfeld quantization condition yields exact spectrum. The Wigner semicircle, or rather semi-ellipse, is just the similar projection of the ellipse $p^2 + x^2/4 = 1$ onto the x axis in the phase space. The Bohr-Sommerfeld quantization condition just reads $\int \rho(x)dx = 1$, where $\rho = \frac{1}{2\pi}\sqrt{4-x^2}$ (in units where $2\mu = 1$) [19]. Again, the rigid argument comes from the fact, that the Wigner function for harmonic oscillator is explicitly known [49], and yields a direct relation between the momenta and positions at the semi-classical level.

2.3. Microscopic scaling as a spectral deformation

Correlations of eigenvalues probed on the scale of the typical separation between them are independent on the probability density function of matrix elements. They fall into several universality classes, depending on the point x_0 of the spectrum at which their behavior is probed. The shape of the spectral density, in turn, determines the microscopic scale s by demanding that in the interval $[x_0, x_0 + s]$ one expects one eigenvalue to occur. Looking at the form of the Marchenko-Pastur distribution (see Fig. 1), we immediately identify three distinct regions corresponding to microscopic scalings.

A **Hard edge.** In the limit when $N, T \to \infty$ but $\alpha = T - N$ remains fixed ($c \to 1$), the turning point r_- approaches zero, and the eigenvalue density near this point behaves like $1/\sqrt{x}$. Asking how many out of original N eigenvalues will appear in a narrow bin of size s around zero, we get

$$n_{hard} \sim N \int_0^s \frac{dx}{\sqrt{x}} \sim N\sqrt{s}. \tag{12}$$

Demanding that $n_{hard} \sim 1$, we set the proper microscopic scale to $s \sim N^{-2}$.

B **Bulk.** Between the endpoints, at some x_0, when counting the number of eigenvalues in a narrow interval of length s, one can approximate the density as locally constant $\rho(x_0)$. This leads to

$$n_{bulk} \sim N \int_{x_0 - s/2}^{x_0 + s/2} \rho(x_0)dx \sim Ns\rho(x_0), \tag{13}$$

which implies that the bulk microscopic scale is $s \sim \frac{1}{N\rho(x_0)}$.

C **Soft edge.** When $c \neq 1$, the macroscopic spectral density around both turning points vanishes like $\sqrt{|r_\pm - x|}$. Counting the eigenvalues close to the edge, leads to

$$n_{soft} \sim N \int_0^s \sqrt{x} dx \sim N s^{3/2}, \tag{14}$$

thus the edge microscopic scale is set to $s \sim N^{-2/3}$.

Following the generic arguments by Borodin and Olshanski [52] and inspired by Tao [19] presentation for the Gaussian Unitary Ensemble, we will now obtain the microscopic, universal kernels for the complex Wishart ensemble. We remark that this case belongs to the generic class of Sturm-Liouville operators, considered recently by Bornemann [20]. However, in this note, we attempt to use the insights from quantum mechanics rather than abstract mathematics.

The complete set of eigenfunctions provides a resolution of identity $\mathbf{1} = \sum_{k=0}^{\infty} |\psi_k\rangle \langle\psi_k|$. The random matrix kernel is obtained by truncating this sum to first N eigenstates and is therefore a projection. Formally, we project the Hilbert space to the space of functions $|\psi\rangle$ that satisfy $\langle\psi| \hat{H} |\psi\rangle \leq E_{N-1}$. Using the explicit form of (6), we write is less formally as

$$\frac{d^2}{dx^2} + \frac{1}{x}\frac{d}{dx} + \frac{1+2k+\alpha}{2x} - \frac{\alpha^2}{4x^2} \geq \frac{1}{4} \tag{15}$$

and later we are looking for a convenient representation of functions that span such space.

The microscopic scalings provide further deformations of the projection range, which in the large N, T limit gives rise to the universal microscopic kernels, which we work out in details beneath.

A **Bessel kernel.** Using the hard edge scaling $x/T \to sN^{-2}$, and performing the large N limit (note that $k \sim N$), we obtain the equation

$$\frac{d^2}{ds^2} + \frac{1}{s}\frac{d}{ds} + \frac{1}{s} - \frac{\alpha^2}{4s^2} \geq 0. \tag{16}$$

Changing variables $z = 2\sqrt{s}$ converts the above bound into the more familiar form

$$\Delta_\alpha \equiv -\frac{d^2}{dz^2} - \frac{1}{z}\frac{d}{dz} + \frac{\alpha^2}{z^2} \leq 1, \tag{17}$$

where on the l.h.s. we recognize the Bessel operator, appearing in quantum mechanical problems with polar angle symmetry. To see the deformation caused by the microscopic scaling at the hard edge, we invoke the *Hankel transform*

$$F(t) = H_\alpha[f(z)] = \int_0^\infty J_\alpha(tz) f(z) z dz \tag{18}$$

and its inverse

$$f(z) = \int_0^\infty J_\alpha(tz) F(t) t dt. \tag{19}$$

The Hankel transform of the Bessel operator reads $H_\alpha[\Delta_\alpha f(z)] = t^2 F(t)$ [53], thus the spectral deformation in dual variable t (note that t cannot be negative) reads simply

$$t \leq 1. \tag{20}$$

Hankel transform and its inverse give a representation of the identity operator

$$f(z') = \int_0^\infty \int_0^\infty zt J_\alpha(z't) J_\alpha(tz) f(z) dz dt. \tag{21}$$

The deformation condition (20) restricts the range of the parameter t and therefore turns the above identity operator into the projection

$$\mathbf{P}[f(z')] = \int_0^\infty \left[\int_0^1 zt J_\alpha(z't) J_\alpha(tz) dt \right] f(z) dz. \tag{22}$$

Changing variables once more as $t = \sqrt{s}$ and introducing $z = \sqrt{y}$ and $z' = \sqrt{x}$, we rewrite the above as

$$\mathbf{P}[f(x)] = \int_0^\infty \left[\frac{1}{4} \int_0^1 J_\alpha(\sqrt{xs}) J_\alpha(\sqrt{sy}) ds \right] f(y) dy \equiv \int_0^\infty K(x, y) f(y) dy, \tag{23}$$

so the kernel, understood as a projection, reads

$$K_{Bessel}(x, y) = \frac{1}{4} \int_0^1 J_\alpha(\sqrt{xs}) J_\alpha(\sqrt{ys}) ds = \frac{J_\alpha(\sqrt{x}) J'_\alpha(\sqrt{y}) \sqrt{y} - \sqrt{x} J'_\alpha(\sqrt{x}) J_\alpha(\sqrt{y})}{2(x - y)}, \tag{24}$$

where on the r.h.s. we presented the more familiar form of the kernel based on the Lommel integral and primes denote differentiation with respect to the argument. Hard edge scaling deforms the upper half plane in s variable onto the strip between the parallel lines $s = 0$ and $s = 1$.

B **Sine kernel.** Combining the rescaling needed for the finite support and the microsopic scaling, we define the new variable s as $x/T = x_0 + \frac{s}{N\rho(x_0)}$. Upon taking the large N, T limit, the bound (15) in this new variable reads

$$\frac{d^2}{ds^2} \geq \frac{(x_0 - r_+)(x_0 - r_-)}{4c^2 x_0^2 \rho^2(x_0)}. \tag{25}$$

Using the explicit form of the Marchenko-Pastur density (11), the above bound is simplified to

$$-\frac{d^2}{ds^2} \leq \pi^2. \tag{26}$$

On the l.h.s. we recognize the Schrödinger operator for a free particle, therefore the natural procedure for resolving this bound is to use plane waves, i.e. to move to the momentum space via the Fourier transformation:

$$F(q) = \int_{-\infty}^{\infty} e^{2\pi i t q} f(t) dt,$$

$$f(t) = \int_{-\infty}^{\infty} e^{-2\pi i t q} F(q) dq. \tag{27}$$

The spectral deformation in the momentum space reads therefore

$$q^2 \leq \frac{\pi^2}{(2\pi)^2} = \frac{1}{4}. \tag{28}$$

Combination of Fourier transforms provides a representation of an identity operator

$$f(t') = \int_{-\infty}^{\infty} \int_{-\infty}^{\infty} e^{-2\pi i t' q} e^{2\pi i t q} f(t) dt dq. \tag{29}$$

The deformation (28) projects the above identity operator onto

$$\mathbf{P}[f(t')] = \int_{-\infty}^{\infty} \left[\int_{-\frac{1}{2}}^{\frac{1}{2}} e^{-2\pi i t' q} e^{2\pi i t q} dq \right] f(t) dt, \tag{30}$$

Microscopic scaling in the bulk restricts the range of momenta to the interval $-\frac{1}{2} \leq q \leq \frac{1}{2}$. Calculation of the integral in square brackets yields the projection in the position basis, which is the sine kernel

$$K_{Sine}(t, t') = \frac{\sin(\pi(t' - t))}{\pi(t' - t)}. \tag{31}$$

C **Airy kernel.** At the soft edge we introduce the scaling variable s as $x/T = r_{\pm} \pm \frac{s}{\sqrt{c}(r_{\pm} N)^{2/3}}$. In the large N and T limit generic bound (15) is transformed into

$$-\frac{d^2}{ds^2} + s \leq 0. \tag{32}$$

On the l.h.s. we recognize the Schrödinger operator with the linear potential. This condition in the position-momentum space (s, q) restricts the range of integration to the parabola $4\pi^2 q^2 + s \leq 0$, which is not well suited for reading out the limiting kernel. To circumvent this problem, Tao introduced a similarity transformation in the momentum space [19]. Alternatively, since we identify the differential Airy operator in (32), we can directly resort to *the Airy transform* [54]

$$F(z) = A[f(t)] = \int_{-\infty}^{\infty} Ai(z - t) f(t) dt \tag{33}$$

and its inverse

$$f(t) = \int_{\infty}^{\infty} F(z) Ai(z - t) dz. \tag{34}$$

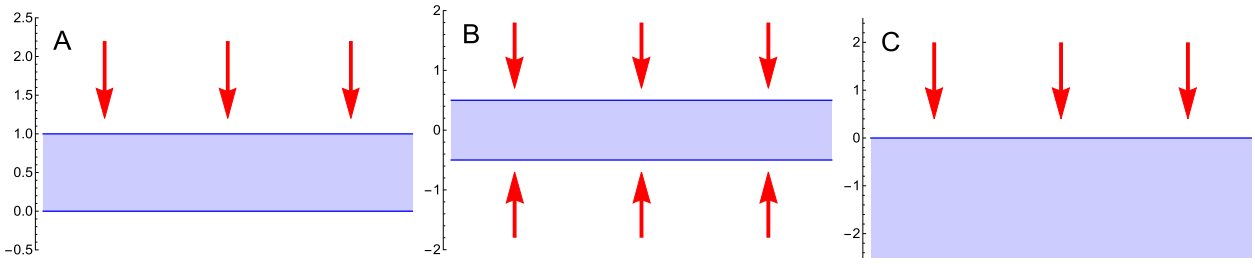

Fig. 2. Regions in the phase space after microscopic scaling at the hard edge (A), in bulk (B) and at the soft edge (C). Red arrows point at the direction of deformation. (For interpretation of the colors in the figure(s), the reader is referred to the web version of this article.)

Using the Airy transform for the operator bound (32), and the fact that the Airy function fulfills $Ai''(x) = x\,Ai(x)$ we express the spectral deformation in dual variable t simply as

$$z \leq 0. \tag{35}$$

Combining both Airy transforms we obtain the identity operator

$$f(t') = \int_{-\infty}^{\infty}\int_{-\infty}^{\infty} Ai(t'-z)Ai(t-z)f(t)dtdz \tag{36}$$

The deformation condition (35) turns the above identity operator into a projection

$$\mathbf{P}[f(t')] = \int_{-\infty}^{\infty}\left[\int_{-\infty}^{0} Ai(t'-z)Ai(t-z)dz\right] f(t)dt, \tag{37}$$

so the kernel reads

$$K_{Airy}(t,t') = \int_{-\infty}^{0} Ai(t'-z)Ai(t-z)dz = \frac{Ai(t')Ai'(t) - Ai'(t')Ai(t)}{t'-t}, \tag{38}$$

where on the r.h.s. we presented the more familiar form of the Airy kernel based on relation

$$\frac{d}{dz}\left[\frac{Ai(t'-z)Ai'(t-z) - Ai'(t'-z)Ai(t-z)}{t'-t}\right] = Ai(t'-z)Ai(t-z). \tag{39}$$

We summarize this section in Fig. 2, by plotting the domain of the projection operator before and after the pertinent microscopic scalings.

3. Bochner theorem and beyond - non-Hermitian Hamiltonians

3.1. Bochner theorem

In a short paper written in 1929 [31] Salomon Bochner has noticed that if an infinite sequence of polynomials $P_n(x)$ satisfies an eigenequation to the second order self-adjoint differential operator

$$p(x)P_n''(x) + q(x)P_n'(x) + r(x)P_n(x) = \lambda_n P_n(x), \tag{40}$$

then $p(x), q(x), r(x)$ must be polynomials of degree 2, 1, and 0, respectively. If additionally polynomials are orthogonal and their support is real, the only solutions are polynomials of Jacobi, Laguerre or Hermite type.

These orthogonal polynomials are associated with classical random matrix ensembles: Gaussian Unitary Ensemble (Hermite), Laguerre Unitary Ensemble (also known as complex Wishart) and Jacobi Unitary Ensemble (null hypothesis in the complex multivariate analysis of variance). They do not lead to any new universality class than what is known for Wishart ensemble. Recently, Bornemann [20], using the spectral projection method, classified the scaling limits of determinantal processes arising from Sturm-Liouville operators.[3] They do not lead to any new universality class than what is known for Wishart ensemble. On the other hand, it is known that there are other scaling limits of the kernel in unitary matrix models. These are related to different vanishing of the spectral density at the edge or at the closing gap in the bulk, see [55] for a review. This raises a question whether such limits can be related to spectral projections. To avoid limitations of the Bochner theorem one may look at the class of Hamiltonians with higher powers of momentum operator. Self-adjointness constrains these Hamiltonians to have only even powers of momentum and Krall [56] provided complete classification of orthogonal polynomials to the problem with quartic momenta. However, classification of higher order Bohner-Krall polynomial systems remains still an open problem. While there are some particular examples of sixth [57] and eighth order systems [58], the corresponding weights are only modifications of classical Gaussian, Laguerre and Jacobi weights by Heaviside theta and Dirac delta functions (see [59] for review), which makes them uninteresting from the random matrix theory perspective.

3.2. Non-Hermitian 'Hamiltonians'

Relaxing the self-adjointness condition admits a broader class of operators. Then one deals with non-Hermitian 'Hamiltonian' and two eigenequations to each eigenvalue:

$$\mathcal{H}\,|P_k\rangle = \lambda_k\,|P_k\rangle \quad \text{and} \quad \mathcal{H}^\dagger\,|Q_k\rangle = \lambda_k\,|Q_k\rangle\,. \tag{41}$$

Here $|P_k\rangle$ and $\langle Q_k|$ are called left and right eigenfunctions, in the analogy to non-Hermitian matrices. They are no longer orthogonal, but bi-orthogonal

$$\langle Q_k|P_l\rangle = \int Q_k(x)P_l(x)dx = \delta_{kl}. \tag{42}$$

The adjoint Hamiltonian $\mathcal{H}^\dagger$ is defined in a standard way

$$\int f(x)\mathcal{H}g(x)dx = \int (\mathcal{H}^\dagger f(x))g(x)dx. \tag{43}$$

Now, because of biorthogonality the two sets of eigenfunctions cannot be both polynomials, enlarging the space of possible solutions.

Preiser [39] considered a higher order generalization of Bochner-Krall theorem with restriction that $P_k(x)$ are polynomials in x, while $Q_k(x)$ are polynomials in x^m multiplied by some weight. He found that for the Hamiltonian with third derivative there exists only one such set, which was discovered earlier by Spencer and Fano [38].

Biorthogonal structures appear in multi matrix models, where the correlation kernel is built from biorthogonal functions P_k and Q_k

[3] He did not used explicitly Bochner theorem.

$$K_N(x,y) = \sum_{k=0}^{N-1} Q_k(x) P_k(y). \tag{44}$$

Biorthogonality ensures that the kernel is a projection. It is therefore tempting to ask whether such kernels are built of eigenfunctions of a certain 'Hamiltonian' and if so, is it possible to obtain the microscopic scaling using spectral projections?

3.3. Singular values of products of complex Gaussian matrices

Let us consider X_k - rectangular matrices of size $(N+\nu_{k-1}) \times (N+\nu_k)$ with complex Gaussian iid entries of zero mean and unit variance. Without loss of generality we assume $\nu_0 = 0$ and $\nu_k > 0$ for $k > 0$. The squared singular values of the product $Y_M = X_1 X_2 \dots X_M$ form a biorthogonal ensemble with the correlation kernel (44). The biorthogonal functions are explicitly given by [42]

$$P_k(x) = G^{1,0}_{1,M+1}\left(\begin{matrix} k+1 \\ 0, -\nu_M, \dots, -\nu_1 \end{matrix} \middle| x \right), \tag{45}$$

$$Q_k(x) = G^{M,1}_{1,M+1}\left(\begin{matrix} -k \\ \nu_M, \dots, \nu_1, 0 \end{matrix} \middle| x \right). \tag{46}$$

Here G stands for the Meijer-G function (see Appendix C). From the differential equation (88) we deduce that polynomials P_k satisfy the eigenproblem ($\mathcal{H}_M P_k = \lambda_k P_k$ with $\lambda_k = k$) of the following differential operator (Hamiltonian)

$$\mathcal{H}_M = x\frac{d}{dx} - \frac{d}{dx}\prod_{j=1}^{M}\left(x\frac{d}{dx} + \nu_j\right). \tag{47}$$

With the help of the identity $\left(\frac{d}{dx}x - \nu_j\right)\frac{d}{dx} = \frac{d}{dx}\left(x\frac{d}{dx} - \nu_j\right)$ we immediately obtain its adjoint

$$\mathcal{H}_M^\dagger = -x\frac{d}{dx} - 1 + (-1)^M \frac{d}{dx}\prod_{j=1}^{M}\left(x\frac{d}{dx} - \nu_j\right). \tag{48}$$

The explicit form (46) and the differential equation (88) prove that Q_k satisfy the eigenequation $\mathcal{H}_M^\dagger Q_k = k Q_k$. Therefore P_k and Q_k are left and right eigenfunctions of a non-Hermitian Hamiltonian.

To probe the microscopic scaling at the edge, we rescale $x = \frac{z}{N}$, which turns the eigenequation for $\mathcal{H}_M$ into

$$\left[\frac{1}{N} z\frac{d}{dz} - \frac{d}{dz}\prod_{j=1}^{M}\left(z\frac{d}{dz} + \nu_j\right)\right] P_k = \frac{k}{N} P_k. \tag{49}$$

As k is always smaller than N, in the large N limit we look for the functions that satisfy $\langle\psi|\,\Delta_{\vec{\nu}}^{(M+1)}\,|\psi\rangle \leq 1$, with

$$\Delta_{\vec{\nu}}^{(M+1)} := -\frac{d}{dz}\prod_{j=1}^{M}\left(z\frac{d}{dz} + \nu_j\right). \tag{50}$$

In order to continue the analogy to the deformation of the phase-space of Hermitian operators, we have to find the suitable transformation, which will convert the above inequality into an algebraic constraint.

3.4. The Narain transform

In a series of papers [43–45] Narain introduced a broad class of asymmetric transforms, which include many known classical transforms. The Narain transform and its inverse are defined as

$$g(s) = \int_0^\infty k(s,y) f(y) dy, \qquad f(y) = \int_0^\infty h(y,s) g(s) ds, \tag{51}$$

where the integral kernels read

$$k(s,y) = 2\gamma x^{\gamma-1/2} G^{m,p}_{p+q,m+n}\left(\begin{matrix} a_1,\ldots,a_p,b_1,\ldots,b_q \\ c_1,\ldots,c_m,d_1,\ldots,d_n \end{matrix} \middle| (sy)^{2\gamma} \right), \tag{52}$$

$$h(y,s) = 2\gamma x^{\gamma-1/2} G^{n,q}_{p+q,m+n}\left(\begin{matrix} -b_1,\ldots,-b_q,-a_1,\ldots,-a_p \\ -d_1,\ldots,-d_n,-c_1,\ldots,-c_m \end{matrix} \middle| (ys)^{2\gamma} \right). \tag{53}$$

If f has a discontinuity at x, then $\int_0^\infty h(x,s)ds \int_0^\infty k(s,y) f(y) dy$ takes the value $\frac{1}{2}(f(x+0) + f(x-0))$, provided that $\sum a_k + \sum b_k = \sum c_k + \sum d_k$.

3.5. Spectral projection for products of Wishart Matrices

We use the following kernels in the Narain transformation

$$k(s,y) = G^{M,0}_{0,M+1}\left(\begin{matrix} - \\ \nu_1,\ldots,\nu_M,0 \end{matrix} \middle| sy \right), \tag{54}$$

$$h(y,s) = G^{1,0}_{0,M+1}\left(\begin{matrix} - \\ 0,-\nu_1,\ldots,-\nu_M \end{matrix} \middle| sy \right). \tag{55}$$

In the space of the dual variable s, the operator $\Delta^{(M+1)}_{\vec{\nu}}$ acts by multiplying by s, as can be easily proven, using identities from Appendix C. The hard edge scaling of the kernel reduces therefore the range of parameter s to $s \leq 1$. Alike in the Hermitian case, the identity operator

$$g(x) = \int_0^\infty \left[\int_0^\infty h(x,s) k(s,y) ds \right] g(y) dy \tag{56}$$

is deformed to

$$\mathbf{P}[f(x)] = \int_0^\infty \left[\int_0^1 h(x,s) k(s,y) ds \right] f(y) dy. \tag{57}$$

We obtain this way the limiting form of the microscopic kernel at the hard edge

$$K_M^{hard}(x,y) = \int_0^1 G^{1,0}_{0,M+1}\left(\begin{matrix} - \\ 0,-\nu_1,\ldots,-\nu_M \end{matrix} \middle| sx \right) G^{M,0}_{0,M+1}\left(\begin{matrix} - \\ \nu_1,\ldots,\nu_M,0 \end{matrix} \middle| sy \right) ds. \tag{58}$$

Note that $G^{1,0}_{0,2}\left(\begin{matrix}-\\ \nu, 0\end{matrix}\,\middle|\, x\right) = x^{\nu/2} J_\nu(2\sqrt{x})$ and $G^{1,0}_{0,2}\left(\begin{matrix}-\\ 0, -\nu\end{matrix}\,\middle|\, x\right) = x^{-\nu/2} J_\nu(2\sqrt{x})$, which yields

$$K_1^{hard}(x,y) = \left(\frac{y}{x}\right)^{\nu/2} \int_0^1 J_\nu(2\sqrt{sx}) J_\nu(2\sqrt{sy}) ds. \tag{59}$$

This form slightly differs from (24). To understand this discrepancy, let us note that biorthogonal functions can be rescaled as $P_k(x) \to f(x) P_k(x)$ and $Q_k(x) \to \frac{1}{f(x)} Q_k(x)$ without altering their biorthogonality. Under such a rescaling kernel is transformed $K(x,y) \to \frac{1}{f(x)} K(x,y) f(y)$. In our case it is sufficient to take $f(x) = x^{\nu/2}$ and further rescale $(x,y) \to \frac{1}{4}(x,y)$. The Narain transform can therefore be viewed as a generalization of the Hankel transform at the hard edge.

3.6. Muttalib-Borodin ensemble with the Laguerre weight

As another example we consider the joint pdf of eigenvalues introduced by Muttalib [37] and elaborated later by Borodin [13]

$$P(\lambda_1, \ldots, \lambda_n) = C_N \prod_{1 \le i < j \le N} |\lambda_i - \lambda_j| \prod_{1 \le i < j \le N} |\lambda_i^\theta - \lambda_j^\theta| \prod_{k=1}^N \lambda_k^\alpha e^{-\lambda_k} d\lambda_k, \tag{60}$$

with $\alpha > -1$, and $\theta \ge 0$. Eigenvalues form a determinantal point process with a correlation kernel given by the bi-orthogonal functions (44). Here P_k is a polynomial of order k, while Q_k is a polynomial in x^θ multiplied by the Laguerre weight. For integer values of θ Konhauser provides the explicit form of Q [40, eq. (5)]

$$Q_k(x) = x^\alpha e^{-x} \sum_{j=0}^k (-1)^j \binom{k}{j} \frac{x^{j\theta}}{\Gamma(j\theta + \alpha + 1)}, \tag{61}$$

while Carlitz gives the explicit form of polynomials [60, eq. (9)]

$$P_k(x) = \frac{1}{k!} \sum_{i=0}^k \frac{x^i}{i!} \sum_{j=0}^i (-1)^j \binom{i}{j} \frac{\Gamma(k + \frac{j+\alpha+1}{\theta})}{\Gamma(k)}. \tag{62}$$

For $\theta = 1$ this reduces to the Laguerre orthogonal polynomials, while the case $\theta = 2$ was considered by Preiser [39] in an attempt to extend Bohner-Krall theorem. Polynomials satisfy the eigenvalue equation $\mathcal{H} P_k = \lambda_k P_k$, with $\lambda_k = \theta k$ of the following differential operator [40]

$$\mathcal{H} = \left(\frac{d}{dx} x + \alpha - x\right) \left[\left(1 - \frac{d}{dx}\right)^\theta - 1\right]. \tag{63}$$

Konhauser showed also that $Z_k = x^{-\alpha} e^x Q_k(x)$, a polynomial in x^θ, satisfies [40, eq. (10)]

$$\left(\frac{d}{dx}\right)^\theta x^{\alpha+1} \frac{d}{dx} Z_k - x^{\alpha+1} \frac{d}{dx} Z_k = -x^\alpha \theta k Z_k. \tag{64}$$

Then it is easy to show that Q_k satisfies the eigenequation $\mathcal{H}^\dagger Q_k = \lambda_k Q_k$ to the same eigenvalues as P_k. The differential operator

$$\mathcal{H}^\dagger = \left[1 - \left(1 + \frac{d}{dx}\right)^\theta\right]\left(-\alpha + x + x\frac{d}{dx}\right) \tag{65}$$

is the adjoint of $\mathcal{H}$. We probe the hard edge by introducing a new variable $x = uN^{-\frac{1}{\theta}}$. In the large N limit, having in mind that $k < N$, from the eigenequation for $\mathcal{H}^\dagger$ we obtain

$$-\frac{1}{\theta}\left(\frac{d}{du}\right)^\theta\left(u\frac{d}{du} - \alpha\right) \leq 1. \tag{66}$$

A change of variable $u = \theta z^{1/\theta}$ turns this condition into a more familiar form

$$-\frac{d}{dz}\prod_{j=1}^{\theta}\left(z\frac{d}{dz} + \nu_j\right) \leq 1, \tag{67}$$

with

$$\nu = -\frac{1}{\theta}, -\frac{2}{\theta}, -\frac{3}{\theta}, \ldots, -\frac{\theta-1}{\theta}, -\frac{\alpha}{\theta}. \tag{68}$$

We now take

$$k(s,y) = G^{\theta,0}_{0,\theta+1}\left(\begin{matrix} - \\ 0, -\frac{1}{\theta}, \ldots, -\frac{\theta-1}{\theta}, -\frac{\alpha}{\theta}\end{matrix}\middle| sy\right), \tag{69}$$

$$h(y,s) = G^{1,0}_{0,\theta+1}\left(\begin{matrix} - \\ \frac{\alpha}{\theta}, 0, \frac{1}{\theta}, \ldots, \frac{\theta-1}{\theta}\end{matrix}\middle| sy\right). \tag{70}$$

Again, using the identities from Appendix C one can show the identity $\int_0^\infty k(s,z)(\mathcal{H}^\dagger f(z))dz = \int_0^\infty sk(s,z)f(z)dz$. This means that the condition (67) in the dual space is equivalent to $s \leq 1$. This allows us to read out the form of the kernel

$$K(y,x) = \int_0^1 G^{1,0}_{0,\theta+1}\left(\begin{matrix} - \\ \frac{\alpha}{\theta}, 0, \frac{1}{\theta}, \ldots, \frac{\theta-1}{\theta}\end{matrix}\middle| sx\right)G^{\theta,0}_{0,\theta+1}\left(\begin{matrix} - \\ 0, -\frac{1}{\theta}, \ldots, -\frac{\theta-1}{\theta}, -\frac{\alpha}{\theta}\end{matrix}\middle| sy\right)ds. \tag{71}$$

Note also that the truncation condition $s \leq 1$ was obtained from the consideration of $\mathcal{H}^\dagger$, therefore the kernel has now interchanged arguments. Using (87) we also write an equivalent kernel

$$\left(\frac{y}{x}\right)^{\frac{\alpha}{\theta}} K(y,x) = \int_0^1 G^{1,0}_{0,\theta+1}\left(\begin{matrix} - \\ 0, -\frac{\alpha}{\theta}, -\frac{\alpha-1}{\theta}, \ldots, -\frac{\alpha-\theta+1}{\theta}\end{matrix}\middle| sx\right)G^{\theta,0}_{0,\theta+1}\left(\begin{matrix} - \\ \frac{\alpha}{\theta}, \frac{\alpha-1}{\theta}, \ldots, \frac{\alpha-\theta+1}{\theta}, 0\end{matrix}\middle| sy\right)ds, \tag{72}$$

which corresponds to the form obtained by Kuijlaars and Stivigny [61, Theorem 5.1].

4. Summary

We explained the spectral projection method on the example of Wishart ensemble, rederiving three classical microscopic universalities. We also linked the Marchenko-Pastur distribution with

the Bohr-Sommerfeld quantization condition of the hydrogen atom. Such a link is intuitively expected, because the Dyson electrostatic analogy in the limit of large matrices allows one to solve random matrix models using the saddle point approximation - the same mathematical method which gives the WKB approximation in quantum mechanics, with the correspondence $\frac{1}{\hbar} \leftrightarrow N$. To the best of our knowledge such an interpretation was not emphasized in the literature.

Bochner theorem provides limitations on the applications of spectral projection method to orthogonal polynomials. We demonstrated that the spectral projection method can be extended to biorthogonal systems. To demonstrate the power of this approach, we recalculated the hard edge Meijer-G kernel. In the paper [42], where all correlations functions for products of Wishart matrices were found for the first time, the problem of calculating the microscopic limit at the hard edge was not tackled, despite that such a result was expected. This task was performed several months later as a subject of a separate work [62]. This impressive calculation required refined integral representations and careful saddle point analysis. In this work we show how the calculations can be reduced to just a few lines. Moreover, to the best of our knowledge, the Narain transform was not used before in random matrix theory.

Rapid progress in random matrix theory in last three decades has brought plethora of new microscopic universality classes. Despite of many examples of microscopic universalities, there is lack of their systematic classification. The spectral projection method adopted to non-Hermitian Hamiltonians and possible generalizations of Bochner theorem for higher order differential operators[4] offer a new perspective on this problem. Certainly, this program is a challenging mathematical problem, which we do not attempt to solve in this work.

This work raises a series of fundamental questions related to possible generalization of Bochner theorem in the context of random matrix theory. Is it possible to reframe all universality classes in this language? Will this classification be predictive for constructing new types of random matrix models? Can one infer the microscopic kernels of non-Hermitian ensembles from a 'complex version' of Bochner theorem? Can one mimic this construction for pfaffian processes for $\beta = 1, 4$? If so, is there a link to Quantum Hall Effect [64]? We leave these questions open but we think that the presented method has also pedagogical value. It offers an easy and intuitive way to recover not only the classical universality classes, but also more involving Meijer-G functions. Combining physical intuition with mathematics may provide in such a way new insights even in standard problems.

Declaration of competing interest

The authors declare that they have no known competing financial interests or personal relationships that could have appeared to influence the work reported in this paper.

Acknowledgements

The research was supported by the MAESTRO DEC-2011/02/A/ST1/00119 grant of the National Center of Science. WT also appreciates the financial support from the Polish Ministry of Science and Higher Education through "Diamond Grant" 0225/DIA/2015/44 and the doctoral scholarship ETIUDA UMO-2018/28/T/ST1/00470 from National Science Center.

[4] After completion of the paper, Oleg Evnin has pointed to us a recent paper [63], proposing the classification of cubic extension of Bochner theorem. This construction, however, does not refer to random matrix theory.

Appendix A. Mapping Wishart onto 2D hydrogen atom

The time-independent Schrödinger equation in 2D with the potential $V(r) = -Ze^2/r$ in the cylindrical coordinates reads

$$\left[-\frac{\hbar^2}{2m}\left(\frac{\partial^2}{\partial r^2}+\frac{1}{r}\frac{\partial}{\partial r}+\frac{1}{r^2}\frac{\partial^2}{\partial \varphi^2}\right)-Ze^2/r\right]\phi(r,\varphi)=E\varphi(r,\varphi). \tag{73}$$

An Ansatz $\phi(r,\varphi) = R(r)e^{il\varphi}/\sqrt{2\pi}$ separates variables. Setting the physical constants $Ze^2 = 1$, $2m = 1$, $\hbar = 1$ and changing variables as $\rho = \lambda r$, $E = -1/4\lambda^2$ we arrive at the equation for the radial part

$$\left(\frac{d^2}{d\rho^2}+\frac{1}{\rho}\frac{d}{d\rho}+\frac{\lambda}{\rho}-\frac{l^2}{\rho^2}-\frac{1}{4}\right)R(\rho)=0. \tag{74}$$

Upon identification $2l = |\alpha|$ and $2\lambda = 1 + 2k + \alpha$ we obtain the equation (6) for the function building the kernel.

Appendix B. WKB analysis of the macroscopic spectral density

The spectral density is calculated from the kernel as

$$\rho(x) = \frac{1}{N}K(x,x) = \frac{1}{N}\sum_{k=0}^{N-1}\psi_k^2(x). \tag{75}$$

In the large N limit the sum can be approximated by an integral over the variable $t = k/N$

$$\rho(x) \xrightarrow{N\to\infty} \int_0^1 \psi_t^2(x)dt. \tag{76}$$

Taking the equation (6) for ψ_k, rescaling $x \to Tx$ and setting $t = k/N$, we obtain

$$\frac{1}{T^2}\left(\frac{d^2}{dx^2}+\frac{1}{x}\frac{d}{dx}\right)\psi_t(x) = \left(\frac{1}{4}+\frac{(1-c)^2}{4x^2}-\frac{ct}{x}-\frac{1-c}{2x}\right)\psi_t(x) \equiv (V(x)-E)\psi_t(x). \tag{77}$$

We also note that up to a term $1/4x^2$, which is irrelevant in the asymptotic analysis, the operator on the lhs of (77) is minus square of the radial momentum $p_r(x) = -i\hbar\left(\frac{1}{r}+\frac{d}{dr}\right)$. Using the WKB Ansatz $\psi(x) = A(x)e^{T\phi(x)}$, we obtain the general solution

$$\psi_t(x) = \frac{1}{\sqrt{xp_r(x)}}\left(C_+e^{iT\int^x p_r(x')dx'}+C_-e^{-iT\int^x p_r(x')dx'}\right). \tag{78}$$

Matching condition at each of the turning points gives two forms of the solution

$$\psi(x) = \frac{C}{\sqrt{xp_r(x)}}\cos\left[-\frac{\pi}{4}+T\int_{x_-}^{x}dx'p_r(x')\right] = \frac{C'}{\sqrt{xp_r(x)}}\cos\left[-\frac{\pi}{4}+T\int_{x}^{x_+}dx'p(x')\right]. \tag{79}$$

Uniqueness of the solution irrespective of the choice of turning point leads to the quantization condition

$$T \oint p_r(x)dx = 2\pi \left(n + \frac{1}{2}\right), \quad n \in \mathbb{N}. \tag{80}$$

Note that for the calculation of the spectral density, ψ_t^2 is needed. For large T it is a rapidly oscillating function and the oscillations average out and only the average of $\cos^2$, which is $1/2$, is relevant[5]

$$\psi_t^2(x) = \begin{cases} 0 & \text{for} \quad x < x_- \text{ or } x > x_+ \\ \frac{C}{2xp(x,t)} & \text{for} \quad x_- < x < x_+ \end{cases}. \tag{81}$$

The turning points are

$$x_\pm(t) = 1 - c + 2ct \pm 2\sqrt{ct(1 + ct - c)}. \tag{82}$$

The spectral density is therefore given by

$$\rho(x) = \int_0^1 dt \frac{C}{\sqrt{2c(1 + 2tx - x) - c^2 - (x-1)^2}} \chi_{x_- < x < x_+} = \frac{C}{2cx}\sqrt{(x - (1 - \sqrt{c})^2)((1 + \sqrt{c})^2 - x)}, \tag{83}$$

where χ_A is equal to 1 when A is true and 0 for A false. Setting $C = \frac{1}{\pi}$ normalizes the density.

Appendix C. Some properties of Meijer-G functions

The Meijer-G functions are defined as an integral

$$G_{p,q}^{m,n}\left(\begin{matrix} a_1, \ldots, a_p \\ b_1, \ldots, b_q \end{matrix} \middle| z\right) = \frac{1}{2\pi i} \int_L \frac{\prod_{j=1}^m \Gamma(b_j - s) \prod_{j=1}^n \Gamma(1 - a_j + s)}{\prod_{j=m+1}^q \Gamma(1 - b_j + s) \prod_{j=n+1}^p \Gamma(a_j - s)} z^s ds, \tag{84}$$

where $\Gamma(z)$ is the Euler gamma function. The integration contour L is chosen to separate all poles of $\prod_{j=1}^m \Gamma(b_j - s)$ from the poles of $\prod_{j=1}^n \Gamma(1 - a_j + s)$ (see also [65], §5.2 for details). By definition, they are symmetric in its first m and last $q - m$ lower parameters. When first and the last lower parameter differ by an integer number, they can be interchanged

$$G_{p,q}^{m,n}\left(\begin{matrix} a_1, \ldots, a_p \\ b_1, b_2, \ldots, b_{q-1}, b_q \end{matrix} \middle| z\right) = (-1)^{b_q - b_1} G_{p,q}^{m,n}\left(\begin{matrix} a_1, \ldots, a_p \\ b_q, b_2, \ldots, b_{q-1}, b_1 \end{matrix} \middle| z\right). \tag{85}$$

The following differential operator acts by increasing first lower indices

$$\left(-z\frac{d}{dz} + b_1\right) G_{p,q}^{m,n}\left(\begin{matrix} a_1, \ldots, a_p \\ b_1, b_2, \ldots, b_q \end{matrix} \middle| z\right) = G_{p,q}^{m,n}\left(\begin{matrix} a_1, \ldots, a_p \\ b_1 + 1, b_2, \ldots, b_q \end{matrix} \middle| z\right). \tag{86}$$

Combining this with (85), we obtain the operator $z\frac{d}{dz} - b_q$, which increases last lower indices. Multiplication by the argument allows one to increase all indices

[5] This can be rephrased more rigorously in terms of weak convergence.

$$z^{\alpha} G^{m,n}_{p,q}\left(\begin{matrix} a_1,\ldots,a_p \\ b_1,\ldots,b_q \end{matrix}\,\middle|\, z\right) = G^{m,n}_{p,q}\left(\begin{matrix} a_1+\alpha,\ldots,a_p+\alpha \\ b_1+\alpha,\ldots,b_q+\alpha \end{matrix}\,\middle|\, z\right). \tag{87}$$

Meijer-G functions satisfy the following differential equation

$$\left[(-1)^{p-m-n} z \prod_{j=1}^{p}\left(z\frac{d}{dz}-a_j+1\right) - \prod_{j=1}^{q}\left(z\frac{d}{dz}-b_j\right)\right] G^{m,n}_{p,q}\left(\begin{matrix} a_1,\ldots,a_p \\ b_1,\ldots,b_q \end{matrix}\,\middle|\, z\right) = 0. \tag{88}$$

References

[1] O. Macchi, The coincidence approach to stochastic point processes, Adv. Appl. Probab. 7 (1) (1975) 83–122.
[2] E.V. Shuryak, J. Verbaarschot, Random matrix theory and spectral sum rules for the Dirac operator in QCD, Nucl. Phys. A 560 (1) (1993) 306–320.
[3] J. Verbaarschot, I. Zahed, Random matrix theory and three-dimensional QCD, Phys. Rev. Lett. 73 (17) (1994) 2288.
[4] J. Verbaarschot, Spectrum of the QCD Dirac operator and chiral random matrix theory, Phys. Rev. Lett. 72 (16) (1994) 2531.
[5] U.M. Heller, Low-lying Dirac operator eigenvalues, lattice effects and random matrix theory, PoS (Lattice) (2011) 103.
[6] R. Narayanan, H. Neuberger, Universality of large N phase transitions in Wilson loop operators in two and three dimensions, J. High Energy Phys. 2007 (12) (2007) 066.
[7] R. Lohmayer, H. Neuberger, T. Wettig, Eigenvalue density of Wilson loops in 2D $SU(N)$ YM, J. High Energy Phys. 2008 (05) (2009) 107.
[8] K. Efetov, Supersymmetry and theory of disordered metals, Adv. Phys. 32 (1) (1983) 53–127.
[9] J. Verbaarschot, M. Zirnbauer, Critique of the replica trick, J. Phys. A, Math. Gen. 18 (7) (1985) 1093.
[10] J. Verbaarschot, H.A. Weidenmüller, M. Zirnbauer, Grassmann integration in stochastic quantum physics: the case of compound-nucleus scattering, Phys. Rep. 129 (6) (1985) 367–438.
[11] T. Guhr, Dyson's correlation functions and graded symmetry, J. Math. Phys. 32 (2) (1991) 336–347.
[12] M.L. Mehta, Random Matrices, vol. 142, Elsevier, 2004.
[13] A. Borodin, Biorthogonal ensembles, Nucl. Phys. B 536 (3) (1998) 704–732.
[14] P. Bleher, A. Its, Semiclassical asymptotics of orthogonal polynomials, Riemann-Hilbert problem, and universality in the matrix model, Ann. Math. 150 (1999) 185–266.
[15] P. Deift, T. Kriecherbauer, K.-R. McLaughlin, New results on the equilibrium measure for logarithmic potentials in the presence of an external field, J. Approx. Theory 95 (3) (1998) 388–475.
[16] P. Deift, Orthogonal Polynomials and Random Matrices: A Riemann-Hilbert Approach, vol. 3, American Mathematical Soc., 1999.
[17] M. Plancherel, W. Rotach, Sur les valeurs asymptotiques des polynomes d'Hermite, Comment. Math. Helv. 1 (1) (1929) 227–254.
[18] A. Borodin, G. Olshanski, Asymptotics of Plancherel-type random partitions, J. Algebra 313 (1) (2007) 40–60.
[19] T. Tao, Topics in Random Matrix Theory, vol. 132, American Mathematical Soc., 2012.
[20] F. Bornemann, On the scaling limits of determinantal point processes with kernels induced by Sturm–Liouville operators, SIGMA 12 (2016) 083.
[21] F.J. Dyson, Statistical theory of the energy levels of complex systems. I, J. Math. Phys. 3 (1) (1962) 140–156.
[22] A. Zabrodin, P. Wiegmann, Large-N expansion for the 2D Dyson gas, J. Phys. A, Math. Gen. 39 (28) (2006) 8933.
[23] P.J. Forrester, Log-Gases and Random Matrices (LMS-34), Princeton University Press, 2010.
[24] E. Kanzieper, V. Freilikher, Random-matrix models with the logarithmic-singular level confinement: method of fictitious fermions, Philos. Mag. B 77 (5) (1998) 1161–1171.
[25] D.S. Dean, P. Le Doussal, S.N. Majumdar, G. Schehr, Finite-temperature free fermions and the Kardar-Parisi-Zhang equation at finite time, Phys. Rev. Lett. 114 (11) (2015) 110402.
[26] D.S. Dean, P. Le Doussal, S.N. Majumdar, G. Schehr, Universal ground-state properties of free fermions in a d-dimensional trap, Europhys. Lett. 112 (6) (2015) 60001.
[27] J. Grela, S.N. Majumdar, G. Schehr, Kinetic energy of a trapped Fermi gas at finite temperature, Phys. Rev. Lett. 119 (13) (2017) 130601.
[28] D.S. Dean, P. Le Doussal, S.N. Majumdar, G. Schehr, Noninteracting fermions in a trap and random matrix theory, J. Phys. A, Math. Theor. 52 (14) (2019) 144006.

[29] J. Wishart, The generalised product moment distribution in samples from a normal multivariate population, Biometrika 20 (1928) 32–52.
[30] N.R. Goodman, Statistical analysis based on a certain multivariate complex Gaussian distribution (an introduction), Ann. Math. Stat. 34 (1) (1963) 152–177.
[31] S. Bochner, Über Sturm-Liouvillesche Polynomsysteme, Math. Z. 29 (1) (1929) 730–736.
[32] M.L. Mehta, M. Gaudin, On the density of eigenvalues of a random matrix, Nucl. Phys. 18 (1960) 420–427.
[33] E. Brezin, S. Hikami, Universal singularity at the closure of the gap in random matrix theory, Phys. Rev. E 57 (1998) 4140.
[34] R. Janik, M.A. Nowak, G. Papp, I. Zahed, Critical scaling at zero virtuality in QCD, Phys. Lett. B 446 (1999) 9.
[35] P. Zinn-Justin, Random Hermitian matrices in an external field, Nucl. Phys. B 497 (3) (1997) 725–732.
[36] P. Bleher, A. Kuijlaars, Random matrices with external source and multiple orthogonal polynomials, Int. Math. Res. Not. 2004 (3) (2004) 109–129.
[37] K.A. Muttalib, Random matrix models with additional interactions, J. Phys. A, Math. Gen. 28 (5) (1995) L159.
[38] L.V. Spencer, U. Fano, Penetration and diffusion of X-rays. Calculation of spatial distributions by polynomial expansion, J. Res. Natl. Bur. Stand. 46 (1951) 446.
[39] S. Preiser, An investigation of biorthogonal polynomials derivable from ordinary differential equations of the third order, J. Math. Anal. Appl. 4 (1) (1962) 38–64.
[40] J.D. Konhauser, Biorthogonal polynomials suggested by the Laguerre polynomials, Pac. J. Math. 21 (2) (1967) 303–314.
[41] V.A. Marchenko, L.A. Pastur, Distribution of eigenvalues for some sets of random matrices, Math. USSR Sb. 1 (4) (1967) 457.
[42] G. Akemann, J.R. Ipsen, M. Kieburg, Products of rectangular random matrices: singular values and progressive scattering, Phys. Rev. E 88 (5) (2013) 052118.
[43] R. Narain, The G-functions as unsymmetrical Fourier kernels. I, Proc. Am. Math. Soc. 13 (6) (1962) 950–959.
[44] R. Narain, The G-functions as unsymmetrical Fourier kernels. II, Proc. Am. Math. Soc. 14 (1) (1963) 18–28.
[45] R. Narain, The G-functions as unsymmetrical Fourier kernels. III, Proc. Am. Math. Soc. 14 (2) (1963) 271–277.
[46] X.L. Yang, S.H. Guo, F.T. Chan, K.W. Wong, W.Y. Ching, Analytic solution of a two-dimensional hydrogen atom. I. Nonrelativistic theory, Phys. Rev. A 43 (1991) 1186–1196.
[47] L.A. Pastur, M. Shcherbina, Eigenvalue Distribution of Large Random Matrices, vol. 171, American Mathematical Soc., 2011.
[48] S. Weinberg, Lectures on Quantum Mechanics, Cambridge University Press, 2015.
[49] D.S. Dean, P. Le Doussal, S.N. Majumdar, G. Schehr, Wigner function of noninteracting trapped fermions, Phys. Rev. A 97 (6) (2018) 063614.
[50] Simple exercise shows that WKB approximation yields the formula $E_{WKB} = E_0/[(n-1/2)^2 + \sqrt{l(l+1)}]^2$, where $E_0 = -13.6$ eV.
[51] R.E. Langer, On the connection formulas and the solutions of the wave equation, Phys. Rev. 51 (8) (1937) 669.
[52] A. Borodin, G. Olshanski, Asymptotics of Plancherel-type random partitions, J. Algebra 313 (1) (2007) 40–60.
[53] R. Piessens, The Hankel transform, in: The Transforms and Applications Handbook, CRC Press Second, Boca Raton, 2000, Ch. 9.
[54] O. Vallée, M. Soares, Airy Functions and Applications to Physics, World Scientific Publishing Company, 2010.
[55] A. Kuijlaars, Universality, preprint, arXiv:1103.5922, 2011.
[56] H.L. Krall, On Orthogonal Polynomials Satisfying a Certain Fourth Order Differential Equation, vol. 6, Pennsylvania State College, 1940.
[57] L.L. Littlejohn, An application of a new theorem on orthogonal polynomials and differential equations, Quaest. Math. 10 (1) (1986) 49–61.
[58] H. Azad, A. Laradji, M.T. Mustafa, Higher order self-adjoint operators with polynomial coefficients, preprint, arXiv: 1409.2523, 2014.
[59] L.L. Littlejohn, A.M. Krall, Orthogonal polynomials and higher order singular Sturm-Liouville systems, Acta Appl. Math. 17 (2) (1989) 99–170.
[60] L. Carlitz, A note on certain biorthogonal polynomials, Pac. J. Math. 24 (3) (1968) 425–430.
[61] A.B. Kuijlaars, D. Stivigny, Singular values of products of random matrices and polynomial ensembles, Random Matrices: Theory Appl. 03 (2014) 450011.
[62] A.B. Kuijlaars, L. Zhang, Singular values of products of Ginibre random matrices, multiple orthogonal polynomials and hard edge scaling limits, Commun. Math. Phys. 332 (2) (2014) 759–781.
[63] E. Horozov, B. Shapiro, M. Tater, In search of higher Bochner theorem, preprint, arXiv:1807.01558, 2018.
[64] G. Moore, N. Read, Nonabelions in the fractional quantum Hall effect, Nucl. Phys. B 360 (2–3) (1991) 362–396.
[65] Y.L. Luke, Special Functions and Their Approximations, vol. 2, Academic Press, 1969.

LETTER **Communicated by Johnatan Aljadeff**

From Synaptic Interactions to Collective Dynamics in Random Neuronal Networks Models: Critical Role of Eigenvectors and Transient Behavior

E. Gudowska-Nowak
gudowska@th.if.uj.edu.pl
Marian Smoluchowski Institute of Physics and Mark Kac Complex Systems Research Center, Jagiellonian University, PL 30-348 Kraków, Poland

M. A. Nowak
maciej.a.nowak@uj.edu.pl
Marian Smoluchowski Institute of Physics and Mark Kac Complex Systems Research Center, Jagiellonian University, PL 30-348 Kraków, Poland

D. R. Chialvo
dchialvo@gmail.com
Center for Complex Systems and Brain Sciences, Escuela de Ciencia y Tecnología, Universidad Nacional de San Martín, San Martín, 1650 Buenos Aires, Argentina and Consejo Nacional de Investigaciones Científicas y Tecnológicas, 1650 Buenos Aires, Argentina

J. K. Ochab
jeremi.ochab@uj.edu.pl
Marian Smoluchowski Institute of Physics and Mark Kac Complex Systems Research Center, Jagiellonian University, PL 30-348 Kraków, Poland

W. Tarnowski
wojciech.tarnowski@doctoral.uj.edu.pl
Marian Smoluchowski Institute of Physics and Mark Kac Complex Systems Research Center, Jagiellonian University, PL 30-348 Kraków, Poland

The study of neuronal interactions is at the center of several big collaborative neuroscience projects (including the Human Connectome Project, the Blue Brain Project, and the Brainome) that attempt to obtain a detailed map of the entire brain. Under certain constraints, mathematical theory can advance predictions of the expected neural dynamics based solely on the statistical properties of the synaptic interaction matrix. This work explores the application of free random variables to the study of large synaptic interaction matrices. Besides recovering in a straightforward way known results on eigenspectra in types of models of neural networks proposed by Rajan and Abbott (2006), we extend them to

Neural Computation **32, 395–423** (2020)
https://doi.org/10.1162/neco_a_01253

heavy-tailed distributions of interactions. More important, we analytically derive the behavior of eigenvector overlaps, which determine the stability of the spectra. We observe that on imposing the neuronal excitation/inhibition balance, despite the eigenvalues remaining unchanged, their stability dramatically decreases due to the strong nonorthogonality of associated eigenvectors. This leads us to the conclusion that understanding the temporal evolution of asymmetric neural networks requires considering the entangled dynamics of both eigenvectors and eigenvalues, which might bear consequences for learning and memory processes in these models. Considering the success of free random variables theory in a wide variety of disciplines, we hope that the results presented here foster the additional application of these ideas in the area of brain sciences.

1 Introduction

Contemporary neuroscience focuses on detailed studies of the neuronal connections across the entire human brain. Large-scale collaborative efforts (Insel, Landis, & Collins, 2013; Van Essen et al., 2013), including the BRAIN Initiative in the United States, Brainome in China, and the Blue Brain Project in the European Union were launched with the objective of mapping the connectivity of the entire brain at different resolutions. At a certain point, a theory will be desperately needed to analyze these very large maps, describing the adjacency matrix of the brain. The work presented here enters into this uncharted and challenging territory.

Under certain constraints, mathematical theory can advance predictions of the expected neural dynamics based solely on the statistical properties of their synaptic interaction matrix. In that sense, randomly connected networks of neurons are one of the classical tools of theoretical neuroscience. Only recently it was observed that the nonnormality of the synaptic connectivity matrix (i.e., the matrix does not commute with its transpose) has dramatic consequences for the temporal dynamics of stochastic equations, which can mimic the dynamics of the network (Hennequin, Vogels, & Gerstner, 2012; Ganguli, Huh, & Sompolinsky, 2008; Ahmadian, Fumarola, & Miller, 2015). In particular, the work of Martí, Brunel, and Ostojic (2018) shows that increasing the symmetry of the connectivity leads to a systematic slowing down of the dynamics, and vice versa, decreasing the symmetry of the matrix leads to the speed-up of the dynamics. This asymmetry not only forces matrices to have complex spectra (which challenges several traditional tools of random matrix theory), but, more important, its study sheds new light on the role of the Bell-Steinberger (Bell & Steinberger, 1965) matrix of overlaps between the left and right eigenvectors of the connectivity matrix.

Contemporarily, the pivotal role of overlaps is understood in the simplest case of the spectral dynamics of the complex Ginibre matrix—in either Smoluchowski-Fokker-Planck formalism (Burda, Grela, Nowak, Tarnowski, & Warchoł, 2014; Gudowska-Nowak, Janik, Jurkiewicz, & Nowak, 2003) or in Langevin formalism (Bourgade & Dubach, 2018; Grela & Warchoł, 2018), following pioneering work (Chalker & Mehlig, 1998; Mehlig & Chalker, 2000). The effects of the overlaps of the Ginibre matrix for the temporal autocorrelation function of randomly connected networks was recently addressed analytically (Martí et al., 2018), confirming the numerical simulations in the weakly coupled regime of synaptic models.

In this letter, we study the nonnormality aspects of the popular model with excitatory-inhibitory structure (Wehr & Zador, 2003; Higley & Contreras, 2006; Haider, Duque, Hasenstaub, & McCormick, 2006), proposed by Rajan and Abbott (2006). An important ingredient of this model is the introduction of the balance condition, which stabilizes the fluctuating spectra of the network. Later, the numerical study of the full nonlinear dynamics in the Rajan-Abbott model (del Molino, Pakdaman, Touboul, & Wainrib, 2013) has shown the emergence of a transition leading to synchronized (stationary or periodic) states. This phenomenon cannot be explained solely by the spectral features of the connectivity matrix, which motivates our study of missing nonspectral properties of nonnormal networks, such as sensitivity to perturbations and transient dynamics induced by the nonorthogonality of eigenvectors. Recently, it was also hypothesized that the nonnormality is universal in real complex networks (Asllani & Carletti, 2018).

Free random variables (hereafter FRV) theory is a relatively young mathematical theory, originating from the work of Voiculescu, Dykema, and Nica (1992). Partly due to the connection with large, random matrices, in the past decade it has made a huge impact on physics (Gopakumar & Gross, 1995), statistical inference (El Karoui, 2008; Rao, Mingo, Speicher, & Edelman, 2008), engineering of information and communication technologies (Couillet & Debbah, 2011), and finances (Potters, Bouchaud, & Laloux, 2005; Burda, Jurkiewicz, Nowak, Papp, & Zahed, 2004; Burda, Jarosz, Nowak, & Snarska, 2010; Burda et al., 2011). In brief, FRV can be viewed as a noncommutative probability theory for big-data problems, where the information is hidden in statistical properties of eigenvalues and eigenvectors. As such, it is ideally suited for disentangling signals from noise in various kinds of complex systems. Another advantage comes from the fact that at the operational level, the formalism is simple and powerful, often getting results on the basis of back-of-the-envelope calculations.

From this perspective, it is rather bewildering that FRV so far has not been broadly applied to the most challenging complex problem of understanding the brain. Thus, in this letter, we consider FRV applications to understand the neuronal networks as represented by the synaptic strength matrix. A direct application of FRV not only allows us to recover in a

straightforward way well-known results from the literature (Rajan & Abbott, 2006), but also to address quantitatively such issues as the stability of the network with respect to the change of weight and to extend the existing formalisms for the heavy-tailed distributions.

The letter is organized as follows. In section 2, we discuss two important effects caused by the nonorthogonality of eigenvectors of nonnormal matrices: high sensitivity of the spectra and the transient behavior of the linearized dynamics. We briefly describe free probability theory in section 3, showing how it allows one to calculate spectral density and gives a access to eigenvector nonorthogonality. In section 4, we reframe the model introduced by Rajan and Abbott in this language. Applying the theoretical toolbox explained in appendixes A to C, we recover and generalize their main results for the unbalanced network. In doing so, we uncover the analytic formulas for the one-point eigenvector correlation function for this model, which is crucial for determining its stability. Since FRV also works in the case of heavy-tailed distributions (Bercovici, Pata, & Biane, 1999), we present results for the spectra and eigenvectors of the Rajan-Abbott model adapted for the case of Cauchy noise. We successfully confirm our analytic predictions with numerical simulations.

In section 5, we show explicitly that the excitation/inhibition balance condition not only tames the spectral outliers, but also exerts dramatic effects on the nonorthogonality of eigenvectors, increasing the networks' eigenvalue condition number by several orders of magnitude. Section 6 closes the letter with a summary of the main results and their implications. It also outlines promising directions for further studies using the formalism presented here.

2 Nonnormality of Synaptic Interactions in Neural Networks

Adjacency matrices of directed networks and synaptic strength matrices are nonnormal. This not only influences their spectra, as the eigenvalues can be complex but also has a strong effect on the eigenvectors. A diagonalizable nonnormal matrix possesses two eigenvectors: left and right for each eigenvalue. They satisfy the eigenproblems

$$\langle L_i| X = \langle L_i| \lambda_i, \qquad X |R_i\rangle = \lambda_i |R_i\rangle . \tag{2.1}$$

Here we use physicists' "bra-ket notation," where $|R_i\rangle$ is a column and $\langle L_i|$ is a row vector. The scalar product is denoted as $\langle L_i|R_j\rangle$, and we define the conjugated left vector $|L_i\rangle = (\langle L_i|)^\dagger$.

Eigenvectors are normalized to $\langle L_i|R_j\rangle = \delta_{ij}$, but they are not orthogonal among themselves $\langle R_i|R_j\rangle \neq \delta_{ij} \neq \langle L_i|L_j\rangle$. Chalker and Mehlig (1998; Mehlig & Chalker, 2000) introduced a matrix of scalar products of eigenvectors:

$$O_{ij} = \langle L_i | L_j \rangle \langle R_j | R_i \rangle . \tag{2.2}$$

We next describe two phenomena important in neural networks, in which the nonorthogonality of eigenvectors captured in the matrix of overlaps plays an essential role.

2.1 Perturbations of a Network. Considering the perturbation of the matrix X by some ϵP, the change of the spectrum in the first order in ϵ reads

$$\delta\lambda_i = \epsilon \langle L_i | P | R_i \rangle \leq \epsilon \sqrt{\langle L_i | L_i \rangle \langle R_i | R_i \rangle} \|P\|_F . \tag{2.3}$$

The inequality follows from the Cauchy inequality, and $\|P\|_F$ denotes the Frobenius norm $\|P\|_F^2 = \mathrm{Tr} PP^\dagger$. This inequality is saturated (equality holds) by the rank one Wilkinson matrix $P = |L_i\rangle \langle R_i|$. The inequality, equation 2.3, shows that spectra of networks represented by nonnormal matrices are more sensitive to changes in their connectivity. This enhanced sensitivity is driven by the nonorthogonality of eigenvectors. The quantity $\kappa(\lambda_i) = \sqrt{O_{ii}}$ is known in the numerical analysis community as the eigenvalue condition number (Wilkinson, 1965; Trefethen & Embree, 2005).

2.2 Eigenvector Nonorthogonality in Transient Dynamics. Stability analysis and the linear response of the dynamic systems with respect to external perturbations are among the most popular methods for describing complex systems (Guckenheimer & Holmes, 2013). Let us consider dynamics obtained from the linearization of the system in the vicinity of a fixed point:

$$\frac{d}{dt} |\psi\rangle = (-\mu + X) |\psi\rangle + \left|\xi(t)\right\rangle . \tag{2.4}$$

Here, ξ represents the external drive, and μ ensures stability in the absence of coupling (X) between components. In the context of neural networks, μ represents the current leakage due to membrane capacitance (Sompolinsky, Crisanti, & Sommers, 1988). Choosing it as a "spike" $\left|\xi(t)\right\rangle = \delta(t) \left|\psi(0)\right\rangle$ or, equivalently, choosing an initial condition $\left|\psi(0)\right\rangle$, we formally solve the system for $t > 0$:

$$\left|\psi(t)\right\rangle = \exp[(X - \mu)t] \left|\psi(0)\right\rangle . \tag{2.5}$$

The long-time dynamics is governed by the eigenvalue with the largest real part. However, if X is nonnormal, this analysis is incomplete. The behavior of the linearized dynamics can be drastically different at its early stage. In particular, the system may initially move away from the fixed point. This sometimes invalidates the linear approximation and renders the fixed point unstable, even though the linearized dynamics predicts stability.

To describe this transient dynamics, we consider the squared Euclidean distance from the fixed point, which is the squared norm of the solution, equation 2.5:

$$D(t) = \langle \psi(t)|\psi(t)\rangle = e^{-2\mu t} \left\langle \psi(0)\right| e^{X^\dagger t} e^{Xt} \left|\psi(0)\right\rangle$$
$$= \sum_{i,j=1}^{N} \langle \psi(0)|L_i\rangle \langle R_i|R_j\rangle \langle L_j|\psi(0)\rangle e^{-2\mu t + t(\bar{\lambda}_i + \lambda_j)}. \quad (2.6)$$

If we consider $\left|\psi(0)\right\rangle$ as a particular vector of unit norm, averaging over all directions uniformly distributed on the hypersphere (real or complex) $\|\psi(0)\|^2 = 1$ leads to

$$\bar{D}(t) = e^{-2\mu t} \frac{1}{N} \mathrm{Tr} e^{X^\dagger t} e^{Xt} = e^{-2\mu t} \frac{1}{N} \sum_{ij} e^{t(\lambda_i + \bar{\lambda}_j)} O_{ij}. \quad (2.7)$$

We see that all elements of the overlaps of left and right eigenvectors drive the behavior of the squared distance. First, they enhance the contributions of the eigenmodes, which is responsible for amplifying the response to the external driving. Second, since the matrix is not diagonal, they couple different eigenmodes during the evolution. This results in an interference between eigenmodes, which is reflected as an oscillatory behavior of the squared norm of the solution (see Figure 7). Note that for normal matrices, such effects do not exist, since left and right vectors are orthogonal and the "coupling matrix" is an identity. Recently, transient growth was proposed as an amplification mechanism of neural signals (Murphy & Miller, 2009; Hennequin, Vogels, & Gerstner, 2012, 2014). We also remark here that even in the systems in which the average trajectory is not amplified, one can still observe transient trajectories, provided that the initial condition is chosen from the subspace spanned by the eigenvectors of $e^{X^\dagger t} e^{Xt}$ to eigenvalues greater than 1 (Bondanelli & Ostojic, 2018).

Usually the matrix X is modeled as random. We remark that the averaging over all initial conditions is equivalent to fixing an initial vector $\left|\psi(0)\right\rangle$ and averaging over the vectors $U\left|\psi(0)\right\rangle$, where U is uniformly distributed (according to the Haar measure) on the orthogonal (unitary) group. This implies that the average over initial conditions is already included when averaging over randomness in X when its probability density function is invariant under orthogonal (unitary) transformations, $P(X) = P(UXU^\dagger)$. Although the matrix X may not admit this invariance, the averaging over initial conditions is equivalent to rotating the matrix $e^{X^\dagger t} e^{Xt} \to U^\dagger e^{X^\dagger t} e^{Xt} U$, thus acting as if X were invariant. Although biologically plausible models break the unitary invariance of the synaptic connectivity matrix, the above argument and equation 2.7 apply to a broad class of models.

3 Theory of Free Random Variables

3.1 Spectral Density and Eigenvector Correlations. Unitarily (and orthogonally) invariant random matrices in the large size limit are described by free probability. Its power relies on the easiness of obtaining analytical formulas, which are very good approximations even for a relatively small matrix size.

An important class of matrices, the so-called bi-unitarily invariant, which generalizes the gaussian distribution (described in section 3.2), is important in models of neural networks. In this class, the unitary symmetry of the distribution is enhanced to $P(UXV) = P(X)$ for U, V independent unitary matrices—hence, the name. Despite the fact that they are genuinely non-Hermitian, due to enhanced symmetry the spectral problem is effectively one-dimensional, because the spectrum is rotationally invariant on the complex plane. In this case, a powerful result holds in FRV, known as the Haagerup-Larsen theorem (Haagerup & Larsen, 2000). It states that the radial cumulative distribution function, $F(r) = \int_0^r 2\pi\,\rho(r')r'dr'$, of the ensemble X can be inferred from the simple functional equation,

$$S_{X^\dagger X}(F(r) - 1) = \frac{1}{r^2}, \tag{3.1}$$

where $S_X(z)$ is the so-called S-transform for the ensemble X. In appendix A, we explain the probabilistic interpretation of S and provide a simple example. Spectra of bi-unitarily invariant ensembles in large N limit are supported on either a disc or an annulus, a phenomenon dubbed "the single ring theorem" (Feinberg & Zee, 1997; Feinberg, Scalettar, & Zee, 2001). The inner radius of the spectrum is deduced from the condition $F(r_{in}) = 0$, while the outer one is given by $F(r_{out}) = 1$.

The applicability of free probability to non-Hermitian matrices is not limited to spectra only. It gives also access to the averages of the overlap matrix conditioned on eigenvalues. The one-point function

$$O(z) = \frac{1}{N^2}\left\langle \sum_{i=1}^{N} \delta^{(2)}(z - \lambda_i)\,\langle L_i|L_i\rangle\,\langle R_i|R_i\rangle \right\rangle, \tag{3.2}$$

associated with the diagonal elements of the overlap matrix, can be calculated for any type of unitarily invariant probability (Janik, Nörenberg, Nowak, Papp, & Zahed, 1999).[1] For bi-unitarily invariant ensembles, it takes a remarkably simple form (Belinschi, Nowak, Speicher, & Tarnowski,

[1] In the original formulation, Chalker and Mehlig chose normalization $1/N$ and showed that the correlator for the Ginibre-Girko ensemble grows like N. Our normalization $1/N^2$ ensures the finite limit for large N.

2017):

$$O(r) = \frac{1}{\pi r^2} F(r)(1 - F(r)). \tag{3.3}$$

The ratio of the one-point correlation function and the spectral density gives the conditional expectation of the squared eigenvalue condition number (Belinschi et al., 2017):

$$\mathbb{E}\left(\kappa^2(\lambda_i)|r = |\lambda_i|\right) = \frac{NO(r)}{\rho(r)}. \tag{3.4}$$

Recently, the two-point function associated with off-diagonal elements of the overlap matrix has become accessible within free probability (Nowak & Tarnowski, 2018).

3.2 Example: Ginibre-Girko Ensemble. We conclude this section with an example of the above construction by considering the so-called Ginibre-Girko matrix G, the entries of which are independently taken from the real/complex gaussian distribution with zero mean and $1/N$ variance. Such a case was considered in the model of randomly connected neural networks by Sompolinsky et al. (1988).

According to equation 3.1, we need the S-transform for $G^\dagger G$. This matrix belongs to the Wishart ensemble (Wishart, 1928; Anderson, 1958). Its S-transform reads $S_{G^\dagger G}(z) = \frac{1}{1+z}$ (see appendix A). This completes the calculation, since now replacing $z \to F(r) - 1$ and using equation 3.1, we get

$$F(r) = r^2. \tag{3.5}$$

The spectrum is therefore uniform, $\rho(r) = \frac{1}{2\pi r}\frac{dF(r)}{dr} = \frac{1}{\pi}$, on the unit disc ($F(r_{in}) = 0, F(r_{out}) = 1$), reproducing the Ginibre-Girko result. The eigenvector correlator comes from equation 3.3, $O(r) = \frac{1}{\pi}(1 - r^2)$, in agreement with Chalker and Mehlig (1998), where it was calculated using much more laborious techniques. In the next section, we show that this computational simplicity is preserved when considering the ensembles, taking into account physiological restrictions imposed on the neural networks models.

4 Reframing the Rajan-Abbott Model

The strength of synapses between all pairs of N neurons in a network is represented by the weighted adjacency (synaptic) matrix. Contrary to the Ginibre matrices, the structure of its elements is more complicated. In the minimal model (Rajan & Abbott, 2006), there are two kinds of neurons with a fraction $f_E N$ representing excitatory (E), and $f_I N = (1 - f_E)N$ the remaining inhibitory (I) neurons. Their strengths are sampled from gaussian ensembles, with means μ_i and variances σ_i^2/N, where $i = I, E$. The matricial

representation of the synaptic strength matrix therefore reads $X = M + W$. Here, the deterministic matrix M represents the average synaptic activity. In this model, it is a rank one matrix with identical rows, each containing $f_E N$ consecutive means μ_E, followed by $f_I N$ consecutive means μ_I. The random part W models variability across the population. It is assumed to be of the form $W = G\Lambda$, where G is the Girko-Ginibre matrix and Λ is diagonal with its first $f_E N$ elements equal to σ_E and last $f_I N$ ones equal to σ_I.

Several studies (Shadlen & Newsome, 1994; Troyer & Miller, 1997; Haider et al., 2006) show that the amount of excitation and inhibition of a neuron is the same (the so-called E/I balance) even on the scale of few milliseconds (Wehr & Zador, 2003; Higley & Contreras, 2006). To incorporate this fact in the model, the balance condition is imposed on two levels. The global condition $f_E\mu_E + f_I\mu_I = 0$ means that neurons are balanced on average. This forces the last nonzero eigenvalue of M to vanish. Even in the case of a null spectrum of M, its nonnormal character causes the eigenvalues of $M + G\Lambda$ to differ much from that of $G\Lambda$. As a result a few eigenvalues lie far beyond the spectrum of $G\Lambda$ (Rajan & Abbott, 2006; Tao, 2013; see Figure 1).

The local E/I balance is imposed on this model by demanding that the sum of strengths coupled independently to each neuron vanishes. Mathematically, we subtract the $1/N$ of a sum of each row from any element in that row. As a consequence, the elements within each row sum to zero. This condition brings the outliers back to the disc of radius $R = \sqrt{f_I\sigma_I^2 + f_E\sigma_E^2}$; now the spectra of W and $M + W$ are identical (Rajan & Abbott, 2006; see also Figure 1). Whenever we indicate E/I balance in the figures, we assume such local balance.

4.1 Rajan-Abbott Results from FRV. Having known that the E/I balance causes the spectrum to be insensitive to the matrix of average strengths M, we consider a more general model of m types of neurons, each with multiplicity $f_k N$ and the synaptic strength variance σ_k^2/N. The random part of the synaptic strength matrix can be written as $W = G\Lambda$, where G is a Ginibre-Girko matrix as before, while Λ is diagonal with a generic structure $\mathrm{diag}(\sigma_1\mathbf{1}_{f_1 N}, \ldots, \sigma_m\mathbf{1}_{f_m N})$. The multiplicities are normalized as $\sum_{i=1}^m f_i = 1$. In appendix B, using free probability, we obtain the algebraic equation for the radial cumulative distribution function $F(r)$:

$$1 = \sum_{i=1}^{m} \frac{f_i\sigma_i^2}{r^2 - \sigma_i^2(F(r) - 1)}. \tag{4.1}$$

Explicit solutions exist for $m = 2, 3, 4$ types of neurons, corresponding to the quadratic, cubic, or quartic algebraic equation for $F(r)$, but other cases are easily tractable numerically. The case solved by Rajan and Abbott corresponds to the quadratic equation. Solution 4.1 is also equivalent to the

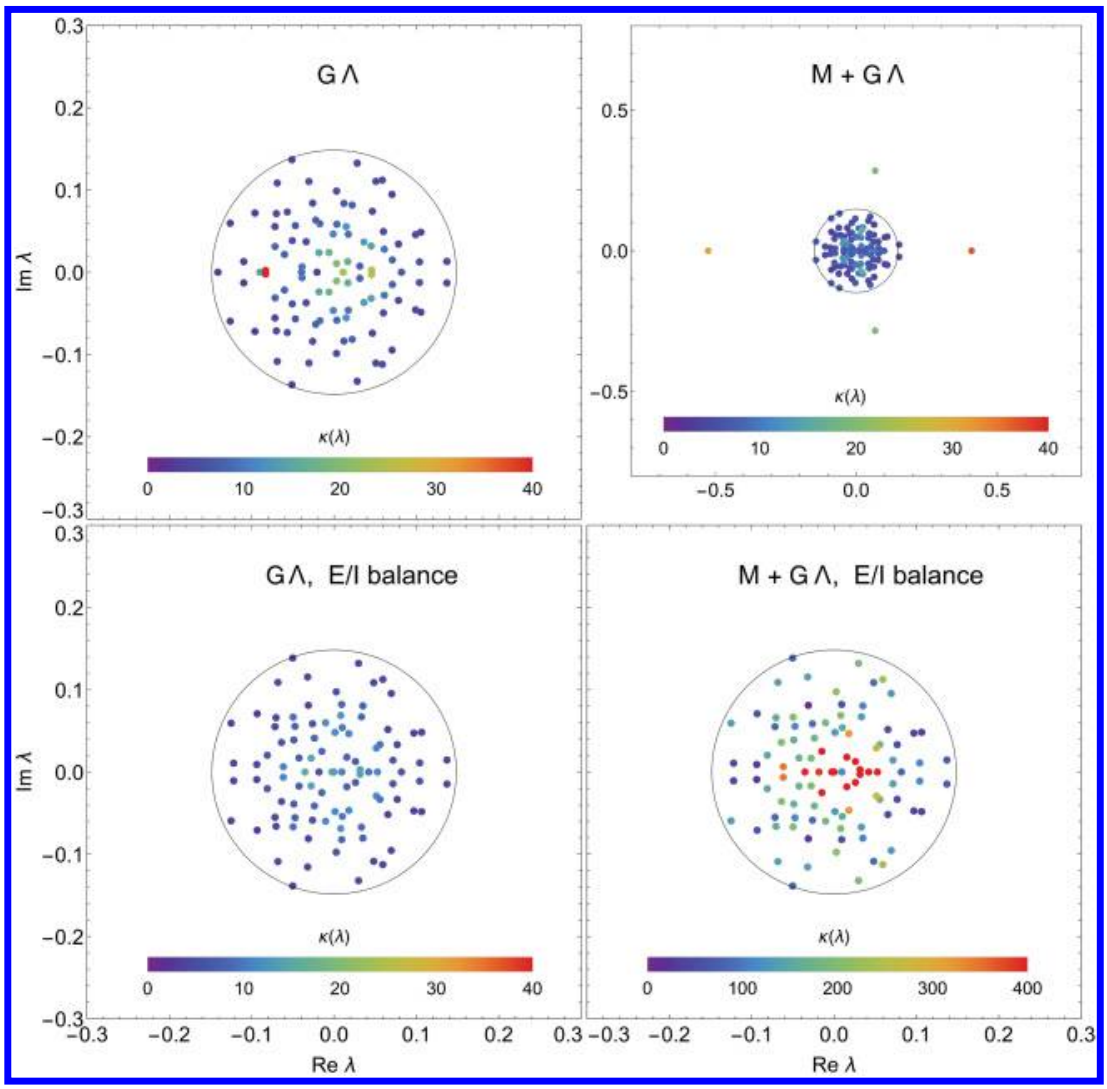

Figure 1: Eigenvalues and their condition numbers of the matrix of variances $G\Lambda$ (top left), the Rajan-Abbott neural network model (top right), matrix of variances with the E/I balance imposed (bottom left), and the Rajan-Abbott model with E/I balance (bottom right). We observed in many realizations that the outliers of the unconstrained Rajan-Abbott model have a higher condition number than the average of eigenvalues within the circle. The spectra in the panels on the left differ only slightly. The eigenvalues presented in bottom panels are exactly the same, but the presence of a highly nonnormal matrix M causes the eigenvalues on the bottom right to be conditioned much more poorly. Note the tenfold ($\sqrt{N}$, as predicted by equation 5.3) broader scale in that panel. The same realization of the gaussian matrix G was taken for all plots. We used parameters $\sigma_I = 0.3, \sigma_E = 0.1, f_I = 0.15, f_E = 0.85, \mu_I = 0.85, \mu_E = 0.15$, and matrix size $N = 100$.

diagrammatic construction of Wei (2012) but more explicit. The spectrum is always confined within the disc of radius $r_{out}^2 = \sum_{i=1}^{m} f_i \sigma_i^2$, as visible from the condition $F(r_{out}) = 1$.

We argue in section 5 that the presence of the deterministic matrix M and the balance condition exert a dramatic effect on the eigenvectors of the synaptic strength matrix. Knowing $F(r)$, free probability allows us to calculate via equation 3.3 the eigenvector correlation function $O(r)$ for its random part W. In the case of the minimal model considered by Rajan and Abbott, it reads explicitly

$$O_W(r) = \frac{1}{2\pi\sigma_E^4\sigma_I^4}\left((f_I - f_E)\sigma_I^2\sigma_E^2(\sigma_E^2\sigma_I^2) - r^2(\sigma_E^4 + \sigma_I^4) + (\sigma_E^2 + \sigma_I^2)\sqrt{K}\right), \tag{4.2}$$

where

$$K = r^4(\sigma_E^2 - \sigma_I^2)^2 + \sigma_I^4\sigma_E^4 + 2r^2(f_E - f_I)\sigma_E^2\sigma_I^2(\sigma_E^2 - \sigma_I^2). \tag{4.3}$$

This result is inaccessible within the framework of Wei (2012).

4.2 Heavy-Tailed Noise. Cauchy noise, belonging to the regime of Lévy stable distributions, is used here as the simplest mechanism to mimic the nongaussianity of the realistic synaptic matrices. Since learning rules could change the initial random network structure into a small-world network (Watts & Strogatz, 1998; Yu, Huang, Singer, & Nikolić, 2008; Downes et al., 2012; Pastore, Massobrio, Godjoski, & Martinoia, 2018) by dynamic modification of synaptic weights, the possibility of obtaining analytic benchmarks for heavy-tailed distributions is appealing. Spatial and temporal Lévy processes are omnipresent in biological time series, but the fact that they do not possess finite moments invalidates several standard tools of statistical analysis. In the case of matrices exhibiting heavy-tailed distributions of elements, the underlying mathematical structure is quite involved (Cizeau & Bouchaud, 1994; Burda, Jurkiewicz, Nowak, Papp, & Zahed, 2007). Here, for simplicity, we focus on the Cauchy matrix distribution, given by the probablity density function $P(X) \sim \det(XX^\dagger + 1)^{-2N}$.

Application of FRV techniques to the spectral Cauchy distribution leads (see appendix C) to the simple result

$$\rho(r) = \frac{1}{2\pi r}\frac{dF(r)}{dr} = \frac{1}{\pi}\sum_{i=1}^{m}\frac{f_i\sigma_i^2}{(r^2 + \sigma_i^2)^2}, \tag{4.4}$$

$$O(r) = \frac{1}{\pi r^2}F(r)(1 - F(r)) = \frac{1}{\pi}\sum_{i=1}^{m}\frac{f_i}{r^2 + \sigma_i^2}\sum_{j=1}^{m}\frac{f_j\sigma_j^2}{r^2 + \sigma_j^2}. \tag{4.5}$$

In this case, the spectrum spreads over the whole complex plane, reflecting the large fluctuation of Lévy-type noise. In the case of more realistic Lévy

noise, one loses the simple analytic structure presented above, but the formalism stays; the resulting equations are usually of a transcendental type but can be easily solved numerically.

We also remark that in models with heavy-tailed randomness, Dale's principle cannot be tightly satisfied in this model. Irrespective of the mean of this distribution, there is always a nonnegligible probability of obtaining the value with the opposite sign as the mean because of the infinite variance of such distributions.

5 Nonnormality in the Rajan-Abbott Model

We argue that imposing the E/I balance not only confines the eigenvalues to a disc but, more important, induces a very strong nonorthogonality of eigenvectors. This in turn causes the spectra to be highly sensitive to perturbations and strengthen the transient effects.

Let us assume that the matrix W is diagonalizable. If we denote $|u\rangle = (1, 1, \ldots, 1)^T$, the E/I balance is equivalent to the fact that $|u\rangle$ is the right eigenvector of W to the eigenvalue $\lambda_1 = 0$. Let $\langle L_1|$ be the left eigenvector to this eigenvalue. For brevity, we also denote $\langle m| = (\underbrace{\mu_1, \ldots, \mu_1}_{f_1 N \text{ times}}, \ldots, \underbrace{\mu_m, \ldots, \mu_m}_{f_m N \text{ times}})$, which allows us to write $M = |u\rangle \langle m|$. The spectral decomposition of W reads

$$W = 0 \cdot |u\rangle \langle L_1| + \sum_{j=2}^{N} \left|R_j\right\rangle \lambda_j \left\langle L_j\right| . \tag{5.1}$$

Since $\langle m|u\rangle = 0$, $\langle m|$ has a decomposition into the left eigenvectors of W, except for $\langle L_1|$, $\langle m| = \sum_{j=2}^{N} \left\langle L_j\right| \alpha_j$ with $\alpha_j = \left\langle m|R_j\right\rangle$. Hence, the total synaptic strength matrix is decomposed as

$$M + W = 0 \cdot |u\rangle \langle L_1| + \sum_{j=2}^{N} \left(\left|R_j\right\rangle + \frac{\alpha_j}{\lambda_j} |u\rangle \right) \lambda_j \left\langle L_j\right| . \tag{5.2}$$

We explicitly constructed the eigenvectors of the synaptic strength matrix. The left eigenvectors are not altered when M is taken into consideration due to the E/I balance. The bi-orthogonality condition $\left\langle L_i|R_j\right\rangle = \delta_{ij}$ leaves freedom of rescaling each pair of eigenvectors by a nonzero complex number $\left|R_j\right\rangle \to c_j \left|R_j\right\rangle$ and $\left\langle L_j\right| \to \left\langle L_j\right| c_j^{-1}$. These transformations allow us to set the length of left eigenvectors $\left\langle L_j|L_j\right\rangle = 1$. The diagonal elements of the overlap matrix in the presence of the matrix M and E/I balance read

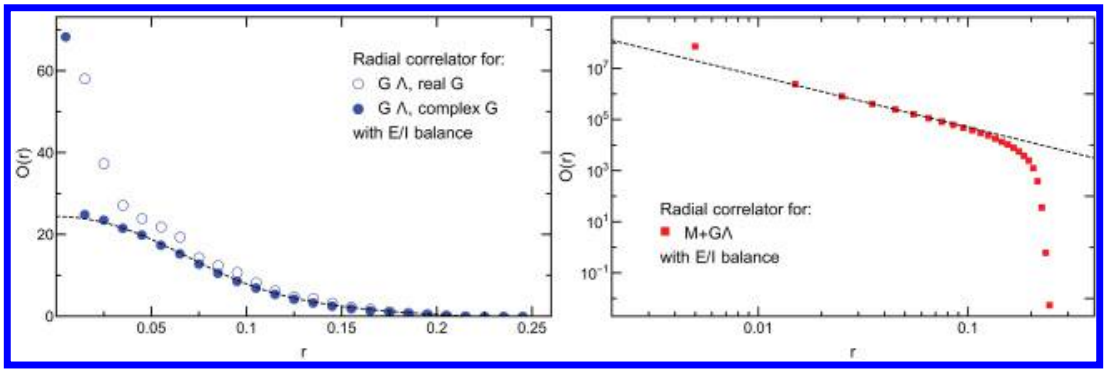

Figure 2: (Left) The eigenvector correlation function for the matrix of variances $G\Lambda$ with the E/I balance imposed. The random matrix G was generated from the complex and real Ginibre ensembles. The dashed line presents the analytical solutions from FRV. Numerical results (circles) were obtained by diagonalizing 1500 matrices of size $N = 1000$. The discrepancies for real matrices come from the real eigenvalues. The fluctuations of the diagonal overlaps associated with them are so strong that the mean of their distribution does not exist (Fyodorov, 2018). (Right, log-log scale) Eigenvector correlator of $M + G\Lambda$, where G is complex Ginibre. The solid line presents the power law, $O(r) \sim r^{-2}$, predicted by equation 5.3 for small r. In both panels, we took the parameters $\sigma_I = 0.4$, $\sigma_E = 0.1$, $f_I = 0.25$, $f_E = 0.75$. For the picture on the right, we also set $\mu_E = 0.25$, $\mu_I = 0.75$.

$$O'_{jj} = O_{jj} + 2\mathrm{Re}\left(\frac{\langle m|R_j\rangle\langle R_j|u\rangle}{\lambda_j}\right) + N\frac{|\langle m|R_j\rangle|^2}{|\lambda_j|^2}, \tag{5.3}$$

where we have used $\langle u|u\rangle = N$ and denoted O_{jj} the overlap matrix in the absence of deterministic weights M. Note that O_{jj} also grows linearly with N. This shows that the condition numbers grow with the size of a matrix, and the effect of the matrix of averages is stronger for eigenvalues close to the origin.

Analogous reasoning for the full overlap matrix leads to the conclusion that all of its elements O_{ij} for $i, j \geq 2$ are affected by the E/I balance and the deterministic matrix. The dominant term in large N is given by

$$O'_{ij} - O_{ij} \sim N\langle L_i|L_j\rangle\frac{\langle m|R_i\rangle\langle R_j|m\rangle}{\lambda_i\bar{\lambda}_j}. \tag{5.4}$$

To study the statistics of the eigenvalue condition numbers, we performed numerical simulations by diagonalizing matrices, the random part of which was generated from either a real or complex Ginibre ensemble. The eigenvector correlation function is juxtaposed with equation 4.2 from free probability (see Figure 2). The presence of the matrix M and the E/I

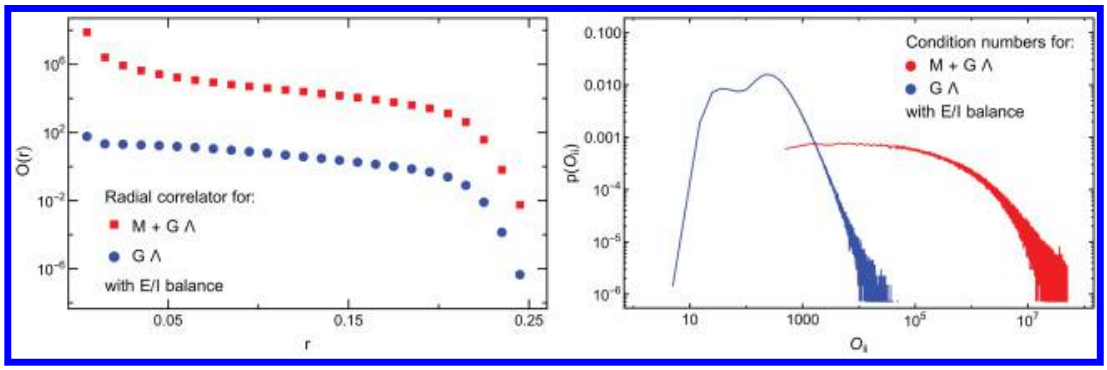

Figure 3: (Left, Log Scale) The eigenvector correlation function of the synaptic strength matrices with the E/I balance condition. Despite unchanged spectra, the squared condition numbers differ significantly. (Right, log-log scale) The distribution of the squared eigenvalue condition numbers of the eigenvalues of the synaptic strength matrix with and without the matrix M.

balance is manifested in the scaling $O(r) \sim r^{-2}$ for small r, as observed in Figure 2, in accordance with equation 5.3.

There is a visible mismatch between numerics for real matrices and the results from free probability, particularly evident for eigenvalues with small moduli. This fact is explained in the light of the recent result of Fyodorov (2018), who showed that the distribution of the overlap for gaussian matrices is heavy-tailed. This distribution conditioned on real eigenvalues of the real Ginibre ensemble is so fat-tailed that even the mean does not exist; thus, $O(z)$ can be considered only outside the real axis. Being aware of this fact, we have performed further simulations only for complex matrices, which do not suffer from this problem.

We studied the effect of the deterministic matrix M by juxtaposing the eigenvector correlation function in Figure 3 and noticed the significant increase in its magnitude. This enhancement of nonnormality is visible not only at the level of the mean value, but also on the full distribution of the overlap (see Figure 3, right).

These conclusions are strengthened by the similar study based on Cauchy synaptic matrices. Figure 4 shows perfect agreement of our predictions with the numerics. Due to the local E/I balance, the spectra are unchanged. This does not hold, however, for the squared eigenvalue condition numbers; they dramatically increase (several orders of magnitude; note the scales in Figures 5 and 6). Finally, the unperturbed eigenvector correlator approaches the predicted slope (compare the predicted slope 4 to the measured 3.84). The perturbed correlator reproduces small r behavior (compare the predicted exponent 2 to the measured 2.03), whereas large r numerical simulations provide asymptotic slope 5.25, as compared to the predicted slope equal to 4.

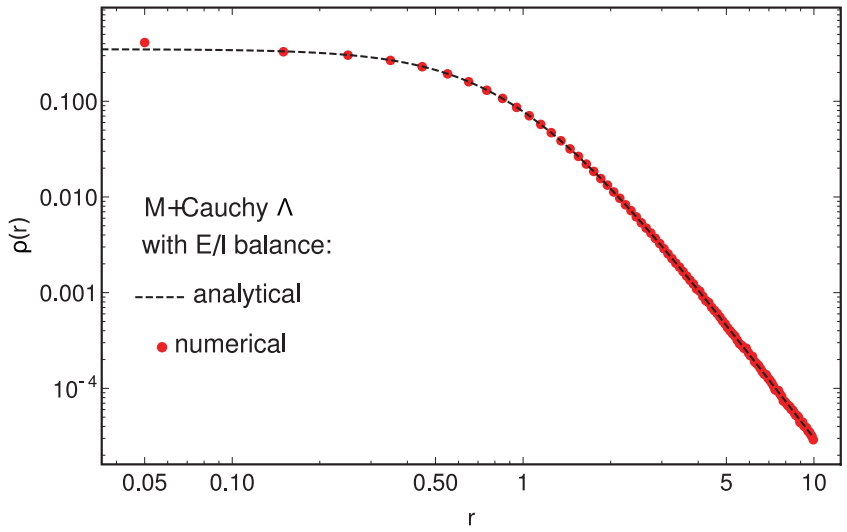

Figure 4: A cross-check of the numerical results with the analytical prediction of the spectral density for the Cauchy synaptic matrix on a log-log scale.

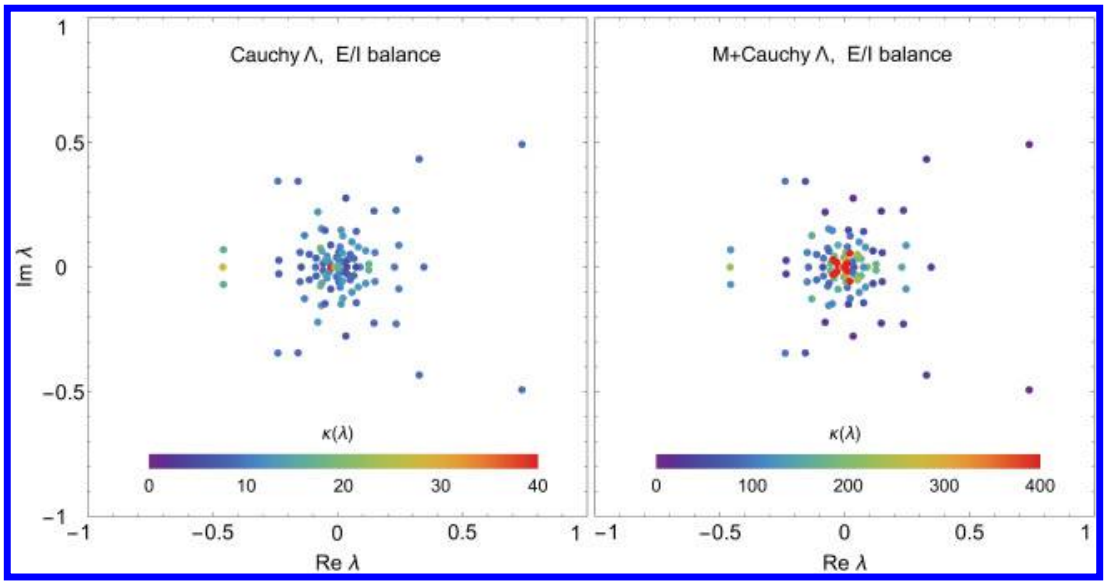

Figure 5: Eigenvalues and their condition numbers for the synaptic matrix, the random part of which is generated from the matrix Cauchy distribution without (left) and with (right) the deterministic connection, M, reflecting Dale's principle. Note the increase of condition numbers caused by addition of M (the scale is resized by an order of magnitude). Matrices M and Λ are the same as in Figure 1.

Although the presence of the matrix M breaks the unitary invariance of the synaptic strength matrix, it is still worth considering the squared norm averaged over initial conditions as a quantity measuring the transient response. The deterministic connections and the E/I balance cause an increase of all elements of the overlap matrix O_{ij}, as equation 5.4 predicts. To elucidate the importance of this fact, we studied the squared norm of the

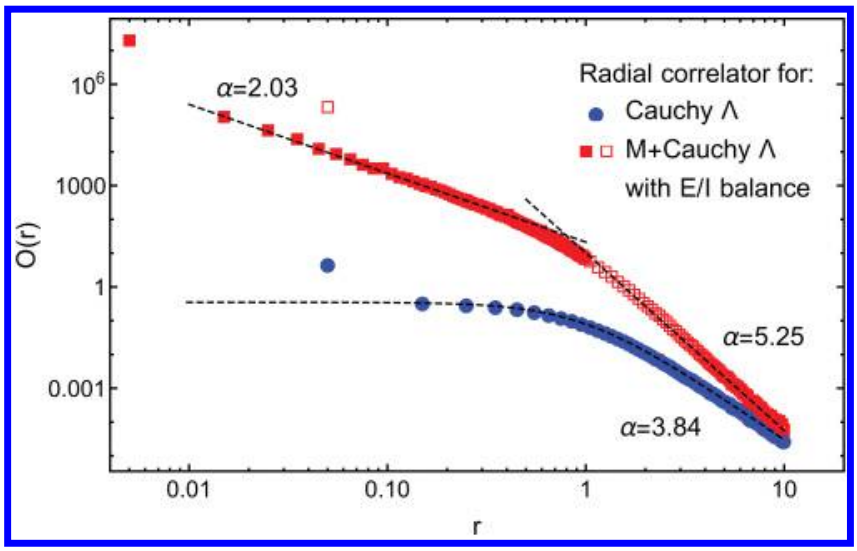

Figure 6: The radial eigenvector correlator for Cauchy synaptic matrices on a log-log scale. Blue circles approximate the analytic prediction ($\alpha = 4$, dashed curve) for the unperturbed model. The red slope is the perturbed model, with filled squares reflecting the universal inverse squared behavior for small r (exponent $\alpha = 2$). Dashed straight lines are numerical fits for small and large r. Matrix size used: $N = 500$.

solution to the linearized dynamics, equation 2.6, with $X = W$ and $X = M + W$, where initial conditions were generated randomly from the uniform distribution on the unit sphere. This dynamics is obtained by the linearization of the model considered in del Molino et al. (2013). Results presented in Figure 7 show that the deterministic connections in the network followed by the E/I balance significantly enhance the norm of the solution, and all presented trajectories are transient. This would not be the case if the connections were fully random. Moreover, the strong oscillations of the squared norm indicate interference between the eigenmodes. It is worth stressing the accuracy of qualitative predictions based on equation 2.7 despite the fact that the presence of the matrix M and the E/I balance break the rotational symmetry of the ensemble.

To further explore the effect of the matrix M, we study the linear dynamics governed by the synaptic connectivity matrix $X = W + qM$ and imposed E/I balance. The parameter $0 \leq q \leq 1$ allows one to tune the strength of the deterministic weights and the level of nonnormality. For $q = 1$, it coincides with the Rajan-Abbott model. Numerical simulations show that for small values of q, the squared norm decays monotonically. As q increases, $\bar{D}(t)$ becomes nonmonotonic with a local maximum (see Figure 8). For a quantitative study, as a measure of the transient amplification, we consider the maximum of the squared norm over the entire time span, $\max_{t>0} D(t)$, as a function of q. Equation 2.7 shows that the transient dynamics is governed by the full overlap matrix and—according to equation 5.4, where the matrix

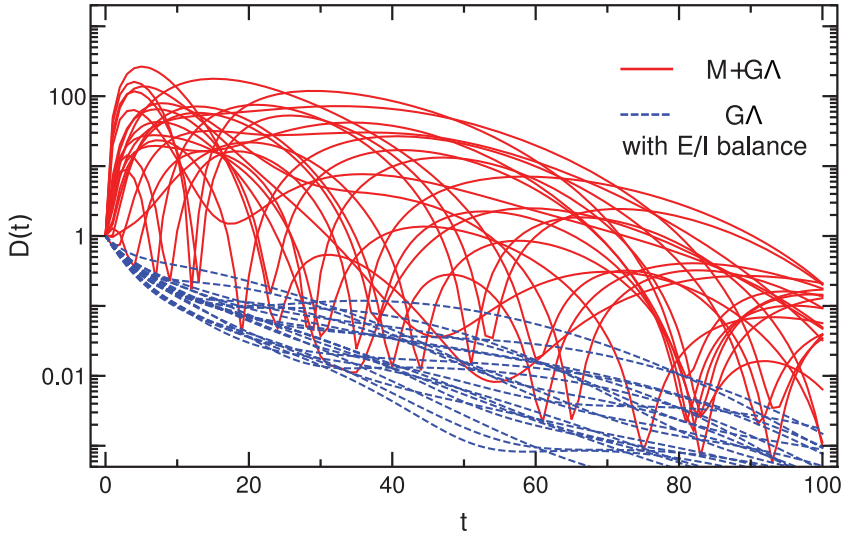

Figure 7: The squared Euclidean distance from the fixed point in the linearized dynamics of del Molino et al. (2013). The presence of M induces transient behavior and strong oscillations. These effects are caused by strong nonnormality. Numerical results were obtained for the minimal Rajan-Abbott model. The matrix is of size $N = 100$ with the same parameters as in Figure 1. We chose $\mu = r_{out} + 0.02$ to ensure stability. Each blue and red curve corresponds to a single initial condition generated randomly from the set of vectors of unit norm. The solid purple line represents an average of $D(t)$ taken over the presented realizations, while the green dashed line is the theoretical average over all initial conditions, equation 2.7.

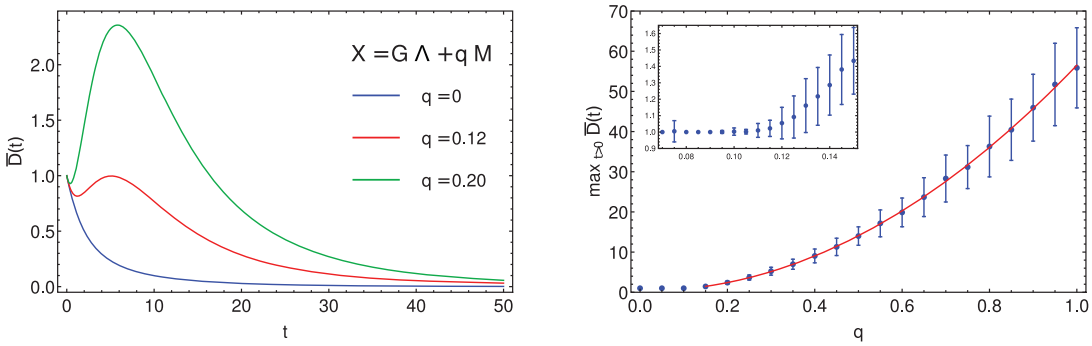

Figure 8: (left) The average squared norm, equation 2.7, in the system, equation 2.4, with the connectivity matrix $X = G\Lambda + qM$. The parameter $0 \leq q \leq 1$ tunes the strength of deterministic connections. We chose $\mu = r_{out} + 0.05$, $N = 100$ and averaged over 200 realizations of the matrix X. (right) Maximum of the squared norm averaged over initial conditions, equation 2.7, further averaged over 200 realizations of the matrix X. Error bars denote standard deviation. The red line depicts the quadratic fit $0.38 - 1.35q + 57.48q^2$ for data with $q \geq 0.15$, confirming predictions based on equation 5.4. In the inset, we show a close-up of the region around q^*, where the transition between the constant and quadratic behavior takes place.

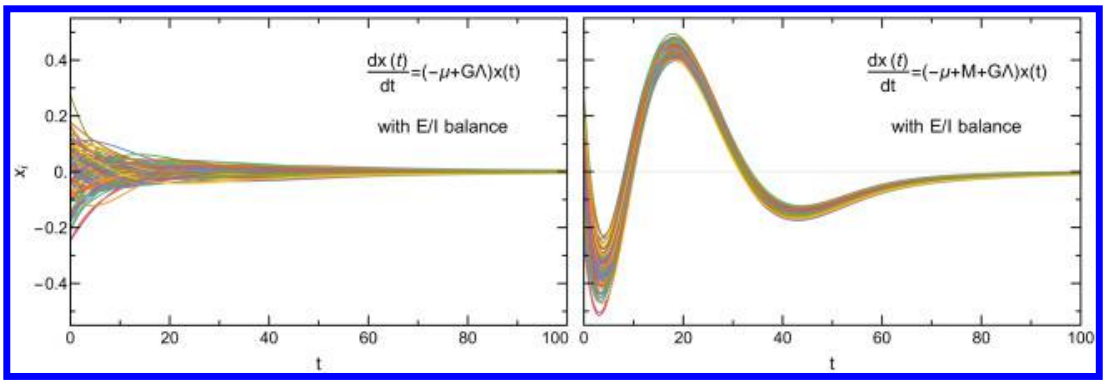

Figure 9: The activity of each neuron in the linearized dynamics. In the right panel we can see the onset of collective dynamics driven by the matrix M and the balance condition. Both simulations started from exactly the same initial condition randomly chosen from the N-dimensional hypersphere. Parameters are the same as in Figure 7.

M enters twice—we expect that the maximal amplification grows quadratically with q. This behavior is verified in Figure 8 and is true only for q exceeding a certain threshold q^*. For $q < q^*$, the transient effects are small, and the maximal value is the initial value, 1.

One expects these dramatic effects to be visible in the activity of individual neurons. We therefore studied the temporal dynamics of the components of the vector of neural activities, equation 2.5, for randomly chosen initial conditions. The results, presented in Figure 9, show that in the presence of M, the neuronal activity is not only transiently enhanced; it is also more synchronized, as observed numerically in the full dynamics by del Molino et al. (2013). This effect, which is persistent in the nonlinear model, is observed as transient in the linearized dynamics.

Spectra of heavy-tailed random matrices are unbounded, and there is a nonzero probability for arbitrarily large eigenvalues. This challenges the model, equation 2.4, with fixed μ. We adapt it to the heavy-tailed spectra, noticing that for each realization of the random matrix, the corresponding eigenvalues are finite. To ensure the stability of the linear system, we choose $\mu = 0.02 + \max \mathrm{Re}\lambda$ for each realization of randomness. Similar to the case of the gaussian disorder, we observe an initial growth of $D(t)$, which is two orders of magnitude stronger in the presence of the matrix M, followed by relaxation toward the fixed point and oscillations resulting from the interference between eigenmodes. The spectral radius of the Cauchy matrix grows with its size like $\sqrt{N}$ (Jiang & Qi, 2017); therefore, to ensure stability, μ needs to be of the same order, while for the gaussian noise, μ is of order one. This difference of scales is equivalent to different timescales of the dynamics; therefore, the transient effects are much shorter with Cauchy noise. This effect is magnified because of the low value of the spectral

density for large r. Eigenvalues with large real parts are more separated from each other, and a single mode quickly dominates equation 2.7, ending the transient phase.

6 Discussion and Conclusion

In this letter, we explored the use of FRV in the study of large synaptic interaction matrices. Besides straightforwardly recovering known results on the application of random matrices to neural networks, we have addressed the issue of large fluctuations, most probably relevant to the dynamics of learning and memory in biological neural networks (Beggs & Plenz, 2003; Benayoun, Cowan, van Drongelen, & Wallace, 2010). Using recent results on the properties of eigenvectors in nonnormal matrices, we have quantitatively linked the strength of the fluctuation of the outliers to a certain eigenvector correlator. We presented our analysis for the simplest gaussian case; nevertheless, we also pointed out how one can consider other distributions (e.g., heavy-tailed). The formalism stays the same, but in the case of more general PDFs (apart form the Cauchy disorder, which we solved analytically), one may need to rely on numerical solutions. In the case of heavy tails, one needs to redefine the dynamical model, equation 2.4, in such a way that the fixed point is stable. For the finite size of matrices, it is possible by adjusting the parameter μ.

Previous work on dynamical random matrices (Burda et al., 2014; Gudowska-Nowak et al., 2003; Grela & Warchoł, 2018) shows that the understanding of the temporal evolution of nonnormal matrix models requires considering the entangled dynamics of both eigenvectors and eigenvalues, contrary to the simple evolution of the spectra of normal matrices, for which the eigenvectors decouple in the presence of the spectral evolution.

The synaptic strengths of real neuronal networks are not static (Kandel, Schwartz, & Jessell, 2000). Neural activity itself, in the course of time, allows neurons to form new connections, strengthening or weakening the existing synapses. This synaptic plasticity, on which biological learning is based, is not captured in many models. Nonetheless, the change of the synaptic strengths in a short time interval can be treated as a small, additive perturbation of the initial matrix. This results in reorganization of the spectrum on a complex plane.

Our results indicate that for balanced networks, the sensitivity of eigenvalues to additive perturbation is dramatic and increases several orders of magnitude in the networks with a heavy-tailed spectrum of adjacency matrices (small worlds). Since it is commonly accepted that spike-timing-dependent plasticity in small-world networks is a hypothetical learning mechanism (for a recent experimental study, see Kim & Lim, 2018), one may worry how synchronization of the network is possible at all. We

emphasize here that the E/I balance is put into this model by hand. In the real brain, the E/I balance is maintained on the scale of hundreds of milliseconds (Haider et al., 2006), and periods during which the balance is violated are not longer than few milliseconds (Wehr & Zador, 2003; Higley & Contreras, 2006). More complete models of neural networks must incorporate the E/I balance as a dynamical process.

Networks adapting to the changing external conditions may change their structure in a controlled way. The high sensitivity of eigenvalues to these changes in this case might be desired because it can facilitate the adaptation. We hypothesize that such high sensitivity in the models with dynamical E/I balance can emerge through a process of a kind of self-regulated criticality (Chialvo, 2010). Although the specifics of such a process are not certain yet, there is evidence both empirical (Turrigiano & Nelson, 2004; Liu, 2004; Pu, Gong, Li, & Luo, 2013; Shew, Yang, Yu, Roy, & Plenz, 2011) and theoretical (Levina, Herrmann, & Geisel, 2007; Magnasco, Piro, & Cecchi, 2009; Schneidman, Berry, Segev, & Bialek, 2006) of its plausibility. In addition, the connection of the E/I balance with criticality has already been observed at the level of neuronal avalanche analysis in EEG or MEG data (Poil, Hardstone, Mansvelder, & Linkenkaer-Hansen, 2012).

Since the balance condition leads to a dramatic increase of eigenvector overlaps, conditioning the spectra, which further take crucial part in driving mechanisms of temporal evolution of the networks, one needs a powerful, stabilizing mechanism preventing the transition to the chaotic behavior in the full nonlinear dynamics.

We envision one a priori mechanism that can tame such a behavior: transient behavior. This conclusion is consistent with the model of del Molino et al. (2013) for nonnormal balanced networks, who have observed synchronization inexplicable by solely spectral properties of the networks. Transient behavior means that even stable trajectories may initially diverge before reaching the fixed point for long periods. This implies that transient behavior is complementary to the stability analysis and may signal nonlinear features already on the linear level (Grela, 2017). Since analytic tools allowing the study of transient behavior for balanced networks are still missing, we have performed sample simulations for gaussian networks. The results are shown in Figures 7 to 9. These simulations confirm qualitatively the presence of transient behavior.

Nevertheless, they raise more quantitative questions: What are the statistical features of transient behavior in balanced neuronal networks? How do the effects of transient behavior scale with the size of the network? What are the timescales in the transient behavior? How does the transient behavior depend on the type of adjacency matrix? We hope to provide some analytic answers to these questions in the sequel to this work. Finally, considering the success of FRV analysis in a variety of disciplines, we hope that the ideas presented in this letter trigger more interdisciplinary interactions in the area of brain studies.

Appendix A: A Guide Through Free Random Variables

Free random variables can be viewed as a probability theory, where the basic random variable is represented by an infinite matrix. It is therefore most convenient to explain the cornerstones of the theory of free probability using concepts from the classical theory of probability (CTP). (For a more detailed treatment of the problem, see Mingo & Speicher, 2017.)

Consider the following problem. We have two random variables x_1 and x_2 drawn from independent probability distributions $p_1(x_1)$ and $p_2(x_2)$. The distribution of the random variable s being the sum of x_1 and x_2 therefore reads

$$p(s) = \int dx_1 dx_2 p_1(x_1) p_2(x_2) \delta(s - (x_1 + x_2)) = \int dx p_1(x) p_2(s - x). \tag{A.1}$$

One can easily unravel the convolution using the Fourier transform (characteristic function). Then $\hat{p}(k) \equiv \int p(s) e^{iks} ds = \hat{p}_1(k)\hat{p}_2(k)$, where $\hat{p}_i(k)$ are Fourier transforms corresponding to the original densities $p_i(x)$. Note that a characteristic function generates moments of the respective distribution. We can further simplify the problem if instead of characteristic functions, we consider their natural logarithms $\phi(k) \equiv \ln \hat{p}(k)$. Then we get the addition law, which linearizes the convolution

$$\phi_{1+2}(k) = \phi_1(k) + \phi_2(k). \tag{A.2}$$

Since ϕ is another generating function—this time for cumulants of the distribution—the above relation means the additivity of the corresponding cumulants. The algorithm of convolution is therefore straightforward. First, knowing $p_i(x)$, we construct $\phi_i(k)$. Then we perform the addition law, equation A.2. Finally, we reconstruct $p_{1+2}(s)$ from $\phi_{1+2}(k)$, performing the first step in reversed order. A pedagogical and simple example is represented by the convolution of two independent gaussian distributions, $N_1(0, \sigma_1^2)$ and $N_2(0, \sigma_2^2)$. The first step shows that in both cases, only one cumulant—the second one, $\kappa_2 = \sigma^2$—is nonvanishing. The addition law and the last step of the logarithm immediately lead to the the resulting distribution, which is also gaussian, $N_{1+2}(0, \sigma^2 = \sigma_1^2 + \sigma_2^2)$.

In free probability, the notion of independence is replaced by the notion of freeness. Two large (infinite) matrices are mutually free if their eigenvectors are maximally decorrelated—for example, matrices X and $UYU^\dagger$, where U is the Haar measure, are free.

The role of the characteristic function is played by the complex valued Green's function,

$$G_X(z) = \int \frac{\rho_X(\lambda)}{z-\lambda} d\lambda, \tag{A.3}$$

where $\rho_X(\lambda)$ is the average spectral density of the matrix X, here playing the role of the probability density function in CTP. Indeed, expanding $G_X(z)$ around $z = \infty$, we get spectral moments $m_k^{(X)} = \int \lambda^k \rho_X(\lambda) d\lambda$. Note that knowing $G_X(z)$, we can easily reconstruct $\rho_X(\lambda)$. Indeed,

$$-\frac{1}{\pi} \lim_{\epsilon \to 0} \Im G(z)|_{z=\lambda'+i\epsilon} = \lim_{\epsilon \to 0} \int \rho(\lambda) \frac{1}{\pi} \frac{\epsilon}{(\lambda'-\lambda)^2 + \epsilon^2} d\lambda =$$

$$= \int \rho(\lambda) \delta(\lambda - \lambda') d\lambda = \rho(\lambda'). \tag{A.4}$$

The role of the generating function for free cumulants is played by the so-called R-transform, $R(z) = \sum_{k=1}^{\infty} \kappa_k z^{k-1}$. The crucial relation between $R(z)$ and $G(z)$ reads $R(G(z)) + \frac{1}{G(z)} = z$ or $G(R(z) + 1/z)) = z$; the function $R(z) + \frac{1}{z}$ is the functional inverse of Green's function. Let us return to the problem of addition. Imagine that we now have the spectral measures $\rho_{X_i}(\lambda)$, corresponding to two matricial ensembles with the measures $P(X_i)dX_i$, where $i = 1, 2$. We are now asking what the spectral density of the ensemble $X_{1+2} = X_1 + X_2$ is. This is a highly nontrivial and nonlinear problem, since X_1 and X_2 do not commute, but free calculus allows solving this case in full analogy to CTP. The algorithm is as follows. First, from ρ_i corresponding to X_i we construct matching $G_i(z)$ and $R_i(z)$. Then

$$R_{X_1+X_2} = R_1(z) + R_2(z), \tag{A.5}$$

which supersedes equation A.2. Finally, we proceed in reverse order, reconstructing from $R_{X_1+X_2}(z)$ Green's function $G_{X_1+X_2}(z)$ and, finally, the spectral density $\rho_{X_1+X_2}(\lambda)$. As an example, we consider the "gaussian" distribution in free theory—the spectral distribution where the only nonvanishing cumulant is the variance σ^2. Thus, $R(z) = \sigma^2 z$. Reconstructing Green's function gives $\sigma^2 G + 1/G = z$, with the solution $G(z) = \frac{1}{2\sigma^2}(z - \sqrt{z^2 - 4\sigma^2})$. Taking the imaginary part, we reconstruct the celebrated Wigner semicircle $\rho(\lambda) = \frac{1}{2\pi\sigma^2}\sqrt{4\sigma^2 - \lambda^2}$. We see that the addition algorithm for two free Wigner semicircles precisely mimics the addition algorithm of two gaussians.

Similarly to addition, one can consider multiplication laws for random variables $x_1 \cdot x_2$. In CTP, such a problem is unraveled with the help of the Mellin transform (see Epstein, 1948). In free calculus, the role of the Mellin transform is played by the S-transform, related to the R-transform by $S_X(z)R_X(zS_X(z)) = 1$. The multiplication law reads

$$S_{X_1X_2}(z) = S_{X_1}(z) \cdot S_{X_2}(z), \tag{A.6}$$

and the algorithm for multiplication follows the algorithm for addition. However, one should be aware that the product of two symmetric (Hermitian) matrices may be nonsymmetric (non-Hermitian). In such a case, the eigenvalues can appear on the whole complex plane, and the methods of $R(z)$ and $S(z)$ transforms, based on analyticity, require substantial modifications. Luckily, there exists one powerful case, governed by the Haagerup-Larsen theorem (known also as the single-ring theorem), when analytic methods hold for complex spectra. If the complex matrix X can be decomposed as $X = PU$, where P is positive, U is Haar-measured, and P and U are mutually free, the spectrum on the complex plane has a polar symmetry and the radial distribution can be easily read out from the singular values of X, that is, the real eigenvalues of $X^\dagger X$. In free probability theory, such ensembles are known as R-diagonal. To infer the information about the spectra and some correlations between left and right eigenvectors, one needs only the explicit form of $S_{X^\dagger X}(z)$. In the case of the Ginibre ensemble G (where G_{ij} are drawn from either real or complex gaussian distributions), this is particularly easy, since matrix $G^\dagger G$ is known as a Wishart ensemble. To avoid obscure mathematics, let us recall that the Wishart ensemble is a free analogue of the Poisson distribution from classical probability (Voiculescu et al., 1992). This implies that all cumulants are the same, and if normalized to 1 for convenience, its R-transform is by definition $R_{G^\dagger G}(z) = \sum_{i=1}^{\infty} z^{i-1} = \frac{1}{1-z}$. Using the above-mentioned functional relation between R and S transforms, we arrive at $S_{G^\dagger G} = \frac{1}{1+z}$. Similar techniques can be applied for generic randomness in Rajan-Abbott type models, as we show below.

Appendix B: The Rajan-Abbott Model with Gaussian Noise

We use the theorem from free probability, which states that the product of an R-diagonal operator with any operator is R-diagonal (Nica & Speicher, 2006); therefore, W is subject to the Haagerup-Larsen theorem. Then $W^\dagger W = \Lambda G^\dagger G \Lambda \overset{\mathrm{Tr}}{=} G^\dagger G \Lambda^2$, where the last equation expresses the fact that the spectral properties are invariant under the cyclic permutations of matrices under the trace. Green's function (resolvent) for Λ^2 therefore reads

$$G_{\Lambda^2}(z) = \sum_{i=1}^{m} \frac{f_i}{z - \sigma_i^2}. \tag{B.1}$$

Substituting $z \to R_{\Lambda^2}(z) + \frac{1}{z}$ in equation B.1 and using the fundamental FRV relation $G(R(z) + \frac{1}{z}) = z$, we arrive at

$$1 = \sum_{i=1}^{m} \frac{f_i}{zR_{\Lambda^2}(z) - z\sigma_i^2 + 1}. \tag{B.2}$$

Now we replace in equation B.2 $z \to tS_{\Lambda^2}(t)$, and using the relation between S and R transforms, we arrive at

$$1 = \sum_{i=1}^{m} \frac{f_i}{1 + t - \sigma_i^2 t S_{\Lambda^2}(t)}. \tag{B.3}$$

We note that $\frac{1}{1+t}$ is the S-transform for the Wishart ensemble (calculated above), and the multiplication law gives us the final S-transform for $W^\dagger W$, that is, $\frac{1}{1+t} S_{\Lambda^2}(t) = S_{G^\dagger G}(t) S_{\Lambda^2}(t) = S_{W^\dagger W}(t)$, so we arrive at

$$1 + t = \sum_{i=1}^{m} \frac{f_i}{1 - \sigma_i^2 t S_{W^\dagger W}(t)}. \tag{B.4}$$

In the last step, we substitute $t \to F(r) - 1$ and use the Haagerup-Larsen theorem, arriving at

$$F(r) = \sum_{i=1}^{m} \frac{f_i}{1 - \sigma_i^2 (F(r) - 1)/r^2}. \tag{B.5}$$

Subtracting $1 = \sum_i f_i$ from both sides, we simplify it to

$$1 = \sum_{i=1}^{m} \frac{f_i \sigma_i^2}{r^2 - \sigma_i^2 (F(r) - 1)}. \tag{B.6}$$

Appendix C: The Rajan-Abbott Model with Cauchy Noise

FRV calculus is a powerful technique, and the range of its applications is not confined to the basin of attraction of the gaussian type. In particular, for random matrices X belonging to the free Lévy class (spectral density decays like $1/\lambda^{\alpha-1}$), the S-transform for the Wishart-Lévy matrix $X^\dagger X$ reads $S_{X^\dagger X}(t) = \frac{1}{t(1+t)} \left(\frac{t}{b}\right)^{t/\alpha}$, with $b = \exp[i\pi(\alpha/2 - 1)]$ (Burda, Jurkiewicz, Nowak, Papp, & Zahed, 2001). The stability index $\alpha = 2$ reproduces the gaussian case, but a simple form can be obtained also for the Cauchy disorder $\alpha = 1$. In this case, $S_{X^\dagger X}(t) = -\frac{t}{1+t}$, and when applied to equation B.3, yields

$$1 + t = \sum_{i=1}^{m} \frac{f_i}{1 + S_{W^\dagger W}(t) \sigma_i^2}. \tag{C.1}$$

The final substitution $t \to F(r) - 1$ and the use of the Haagerup-Larsen theorem give an explicit, linear equation for an arbitrary number of types of

neurons:

$$F(r) = \sum_{i=1}^{m} \frac{f_i}{1 + \sigma_i^2/r^2}. \tag{C.2}$$

Contrary to the previous case, the spectrum is unbounded and stretches up to infinity. Explicitly, the spectral density and the eigenvector correlator read

$$\rho(r) = \frac{1}{2\pi r}\frac{dF(r)}{dr} = \frac{1}{\pi}\sum_{i=1}^{m} \frac{f_i \sigma_i^2}{\left(r^2 + \sigma_i^2\right)^2}, \tag{C.3}$$

$$O(r) = \frac{1}{\pi r^2} F(r)(1 - F(r)) = \frac{1}{\pi}\sum_{i=1}^{m} \frac{f_i}{r^2 + \sigma_i^2} \sum_{j=1}^{m} \frac{f_j \sigma_j^2}{r^2 + \sigma_j^2}. \tag{C.4}$$

In the case of arbitrary α, the resulting transcendental equations can be easily solved numerically. Other types of neural network randomness can also be modeled (e.g., by considering Student-Fisher spectral distributions).

Acknowledgments

The research was supported by the MAESTRO DEC-2011/02/A/ST1/00119 grant of the National Center of Science. W.T. also appreciates the financial support from the Polish Ministry of Science and Higher Education through Diamond Grant 0225/DIA/2015/44 and the scholarship of Marian Smoluchowski Research Consortium Matter Energy Future from KNOW funding. We thank Jacek Grela and Piotr Warchoł for discussions and critical remarks, and Janina Krzysiak for carefully reading the manuscript.

References

Ahmadian, Y., Fumarola, F., & Miller, K. D. (2015). Properties of networks with partially structured and partially random connectivity. *Physical Review E*, *91*(1), 012820.

Anderson, T. W. (1958). *An introduction to multivariate statistical analysis*, vol. 2. New York: Wiley.

Asllani, M., & Carletti, T. (2018). *Universality of non-normality in real complex networks*. arXiv:1803.11542.

Beggs, J. M., & Plenz, D. (2003). Neuronal avalanches in neocortical circuits. *Journal of Neuroscience*, *23*(35), 11167–11177.

Belinschi, S., Nowak, M. A., Speicher, R., & Tarnowski, W. (2017). Squared eigenvalue condition numbers and eigenvector correlations from the single ring theorem. *Journal of Physics A: Mathematical and Theoretical*, *50*(10), 105204.

Bell, J., & Steinberger, J. (1965). Weak interactions of kaons. In *Proceedings of the International Conference on Elementary Particles*.

Benayoun, M., Cowan, J. D., van Drongelen, W., & Wallace, E. (2010). Avalanches in a stochastic model of spiking neurons. *PLOS Computational Biology*, *6*(7), e1000846.

Bercovici, H., Pata, V., & Biane, P. (1999). Stable laws and domains of attraction in free probability theory. *Annals of Mathematics*, *149*, 1023–1060.

Bondanelli, G., & Ostojic, S. (2018). *Coding with transient trajectories in recurrent neural networks*. arXiv:1811.07592.

Bourgade, P., & Dubach, G. (2018). *The distribution of overlaps between eigenvectors of Ginibre matrices*. arXiv:1801.01219.

Burda, Z., Grela, J., Nowak, M. A., Tarnowski, W., & Warchoł, P. (2014). Dysonian dynamics of the Ginibre ensemble. *Physical Review Letters*, *113*(10), 104102.

Burda, Z., Jarosz, A., Nowak, M. A., Jurkiewicz, J., Papp, G., & Zahed, I. (2011). Applying free random variables to random matrix analysis of financial data. Part I: The gaussian case. *Quantitative Finance*, *11*(7), 1103–1124.

Burda, Z., Jarosz, A., Nowak, M. A., & Snarska, M. (2010). A random matrix approach to Varma processes. *New Journal of Physics*, *12*(7), 075036.

Burda, Z., Jurkiewicz, J., Nowak, M. A., Papp, G., & Zahed, I. (2001). Free random Lévy variables and financial probabilities. *Physica A: Statistical Mechanics and Its Applications*, *299*(1), 181–187.

Burda, Z., Jurkiewicz, J., Nowak, M. A., Papp, G., & Zahed, I. (2004). Free Lévy matrices and financial correlations. *Physica A: Statistical Mechanics and Its Applications*, *343*, 694–700.

Burda, Z., Jurkiewicz, J., Nowak, M. A., Papp, G., & Zahed, I. (2007). Free random Lévy and Wigner-Lévy matrices. *Physical Review E*, *75*(5), 051126.

Chalker, J. T., & Mehlig, B. (1998). Eigenvector statistics in non-Hermitian random matrix ensembles. *Physical Review Letters*, *81*(16), 3367.

Chialvo, D. R. (2010). Emergent complex neural dynamics. *Nature Physics*, *6*(10), 744.

Cizeau, P., & Bouchaud, J.-P. (1994). Theory of Lévy matrices. *Physical Review E*, *50*(3), 1810.

Couillet, R., & Debbah, M. (2011). *Random matrix methods for wireless communications*. Cambridge: Cambridge University Press.

del Molino, L. C. G., Pakdaman, K., Touboul, J., & Wainrib, G. (2013). Synchronization in random balanced networks. *Physical Review E*, *88*(4), 042824.

Downes, J. H., Hammond, M. W., Xydas, D., Spencer, M. C., Becerra, V. M., Warwick, K., Whalley, B. J., & Nasuto, S. J. (2012). Emergence of a small-world functional network in cultured neurons. *PLOS Computational Biology*, *8*(5), e1002522.

El Karoui, N. (2008). Spectrum estimation for large dimensional covariance matrices using random matrix theory. *Annals of Statistics*, *36*(6), 2757–2790.

Epstein, B. (1948). Some applications of the Mellin transform in statistics. *Ann. Math. Statist.*, *19*(3), 370–379.

Feinberg, J., Scalettar, R., & Zee, A. (2001). "Single ring theorem" and the disk-annulus phase transition. *Journal of Mathematical Physics*, *42*(12), 5718–5740.

Feinberg, J., & Zee, A. (1997). Non-gaussian non-Hermitian random matrix theory: Phase transition and addition formalism. *Nuclear Physics B*, *501*(3), 643–669.

Fyodorov, Y. V. (2018). On statistics of bi-orthogonal eigenvectors in real and complex Ginibre ensembles: Combining partial Schur decomposition with supersymmetry. *Communications in Mathematical Physics*, *363*(2), 579–603.

Ganguli, S., Huh, D., & Sompolinsky, H. (2008). Memory traces in dynamical systems. *Proceedings of the National Academy of Sciences*, *105*(48), 18970–18975.

Gopakumar, R., & Gross, D. J. (1995). Mastering the master field. *Nuclear Physics B*, *451*(1–2), 379–415.

Grela, J. (2017). What drives transient behavior in complex systems? *Physical Review E*, *96*(2), 022316.

Grela, J., & Warchoł, P. (2018). Full Dysonian dynamics of the complex Ginibre ensemble. *Journal of Physics A: Mathematical and Theoretical*, *51*(42), 425203.

Guckenheimer, J., & Holmes, P. (2013). *Nonlinear oscillations, dynamical systems, and bifurcations of vector fields*. New York: Springer Science & Business Media.

Gudowska-Nowak, E., Janik, R. A., Jurkiewicz, J., & Nowak, M. A. (2003). Infinite products of large random matrices and matrix-valued diffusion. *Nuclear Physics B*, *670*(3), 479–507.

Haagerup, U., & Larsen, F. (2000). Brown's spectral distribution measure for *r*-diagonal elements in finite von Neumann algebras. *Journal of Functional Analysis*, *176*(2), 331–367.

Haider, B., Duque, A., Hasenstaub, A. R., & McCormick, D. A. (2006). Neocortical network activity in vivo is generated through a dynamic balance of excitation and inhibition. *Journal of Neuroscience*, *26*(17), 4535–4545.

Hennequin, G., Vogels, T. P., & Gerstner, W. (2012). Non-normal amplification in random balanced neuronal networks. *Physical Review E*, *86*(1), 011909.

Hennequin, G., Vogels, T. P., & Gerstner, W. (2014). Optimal control of transient dynamics in balanced networks supports generation of complex movements. *Neuron*, *82*(6), 1394–1406.

Higley, M. J., & Contreras, D. (2006). Balanced excitation and inhibition determine spike timing during frequency adaptation. *Journal of Neuroscience*, *26*(2), 448–457.

Insel, T. R., Landis, S. C., & Collins, F. S. (2013). The NIH brain initiative. *Science*, *340*(6133), 687–688.

Janik, R. A., Nörenberg, W., Nowak, M. A., Papp, G., & Zahed, I. (1999). Correlations of eigenvectors for non-Hermitian random-matrix models. *Physical Review E*, *60*(3), 2699.

Jiang, T., & Qi, Y. (2017). Spectral radii of large non-Hermitian random matrices. *Journal of Theoretical Probability*, *30*(1), 326.

Kandel, E. R., Schwartz, J. H., & Jessell, T. M. (2000). *Principles of neural science*, vol. 4. New York: McGraw-Hill.

Kim, S.-Y., & Lim, W. (2018). Stochastic spike synchronization in a small-world neural network with spike-timing-dependent plasticity. *Neural Networks*, *97*, 92–106.

Levina, A., Herrmann, J. M., & Geisel, T. (2007). Dynamical synapses causing self-organized criticality in neural networks. *Nature Physics*, *3*(12), 857.

Liu, G. (2004). Local structural balance and functional interaction of excitatory and inhibitory synapses in hippocampal dendrites. *Nature Neuroscience*, *7*(4), 373.

Magnasco, M. O., Piro, O., & Cecchi, G. A. (2009). Self-tuned critical anti-Hebbian networks. *Physical Review Letters*, *102*(25), 258102.

Martí, D., Brunel, N., & Ostojic, S. (2018). Correlations between synapses in pairs of neurons slow down dynamics in randomly connected neural networks. *Physical Review E*, *97*(6), 062314.

Mehlig, B., & Chalker, J. T. (2000). Statistical properties of eigenvectors in non-Hermitian gaussian random matrix ensembles. *Journal of Mathematical Physics*, *41*(5), 3233–3256.

Mingo, J. A., & Speicher, R. (2017). *Free probability and random matrices*. Berlin: Springer.

Murphy, B. K., & Miller, K. D. (2009). Balanced amplification: A new mechanism of selective amplification of neural activity patterns. *Neuron*, *61*(4), 635–648.

Nica, A., & Speicher, R. (2006). *Lectures on the combinatorics of free probability*. Cambridge: Cambridge University Press.

Nowak, M. A., & Tarnowski, W. (2018). Probing non-orthogonality of eigenvectors in non-Hermitian matrix models: Diagrammatic approach. *Journal of High Energy Physics*, *2018*(6), 152.

Pastore, V. P., Massobrio, P., Godjoski, A., & Martinoia, S. (2018). Identification of excitatory-inhibitory links and network topology in large-scale neuronal assemblies from multi-electrode recordings. *PLOS Computational Biology*, *14*(8), e1006381.

Poil, S.-S., Hardstone, R., Mansvelder, H. D., & Linkenkaer-Hansen, K. (2012). Critical-state dynamics of avalanches and oscillations jointly emerge from balanced excitation/inhibition in neuronal networks. *Journal of Neuroscience*, *32*(29), 9817–9823.

Potters, M., Bouchaud, J.-P., & Laloux, L. (2005). *Financial applications of random matrix theory: Old laces and new pieces*. arXiv preprint physics/0507111.

Pu, J., Gong, H., Li, X., & Luo, Q. (2013). Developing neuronal networks: Self-organized criticality predicts the future. *Scientific Reports*, *3*, 1081.

Rajan, K., & Abbott, L. (2006). Eigenvalue spectra of random matrices for neural networks. *Physical Review Letters*, *97*(18), 188104.

Rao, N. R., Mingo, J. A., Speicher, R., & Edelman, A. (2008). Statistical eigeninference from large Wishart matrices. *Annals of Statistics*, *36*(6), 2850–2885.

Schneidman, E., Berry II, M. J., Segev, R., & Bialek, W. (2006). Weak pairwise correlations imply strongly correlated network states in a neural population. *Nature*, *440*(7087), 1007.

Shadlen, M. N., & Newsome, W. T. (1994). Noise, neural codes and cortical organization. *Current Opinion in Neurobiology*, *4*(4), 569–579.

Shew, W. L., Yang, H., Yu, S., Roy, R., & Plenz, D. (2011). Information capacity and transmission are maximized in balanced cortical networks with neuronal avalanches. *Journal of Neuroscience*, *31*(1), 55–63.

Sompolinsky, H., Crisanti, A., & Sommers, H. J. (1988). Chaos in random neural networks. *Physical Review Letters*, *61*, 259–262.

Tao, T. (2013). Outliers in the spectrum of IID matrices with bounded rank perturbations. *Probability Theory and Related Fields*, *155*, 231–263.

Trefethen, L. N., & Embree, M. (2005). *Spectra and pseudospectra: The behavior of nonnormal matrices and operators*. Princeton, NJ: Princeton University Press.

Troyer, T. W., & Miller, K. D. (1997). Physiological gain leads to high ISI variability in a simple model of a cortical regular spiking cell. *Neural Computation*, *9*(5), 971–983.

Turrigiano, G. G., & Nelson, S. B. (2004). Homeostatic plasticity in the developing nervous system. *Nature Reviews Neuroscience*, *5*(2), 97.

Van Essen, D. C., Smith, S. M., Barch, D. M., Behrens, T. E., Yacoub, E., Ugurbil, K., & WU-Minn HCP (2013). The WU-Minn Human Connectome Project: An overview. *NeuroImage*, *80*, 62–79.

Voiculescu, D. V., Dykema, K. J., & Nica, A. (1992). *Free random variables*. Providence, RI: American Mathematical Society.

Watts, D. J., & Strogatz, S. H. (1998). Collective dynamics of "small-world" networks. *Nature*, *393*(6684), 440.

Wehr, M., & Zador, A. M. (2003). Balanced inhibition underlies tuning and sharpens spike timing in auditory cortex. *Nature*, *426*(6965), 442.

Wei, Y. (2012). Eigenvalue spectra of asymmetric random matrices for multicomponent neural networks. *Physical Review E*, *85*(6), 066116.

Wilkinson, J. H. (1965). *The algebraic eigenvalue problem*. Oxford: Clarendon Press.

Wishart, J. (1928). The generalised product moment distribution in samples from a normal multivariate population. *Biometrika*, *20A*(1–2), 32–52.

Yu, S., Huang, D., Singer, W., & Nikolić, D. (2008). A small world of neuronal synchrony. *Cerebral Cortex*, *18*(12), 2891–2901.

Received November 30, 2018; accepted July 13, 2019.

Dynamical Isometry is Achieved in Residual Networks in a Universal Way for any Activation Function

Wojciech Tarnowski **Piotr Warchoł** **Stanisław Jastrzębski** **Jacek Tabor** **Maciej A. Nowak**
Jagiellonian University in Kraków Jagiellonian University in Kraków

Abstract

We demonstrate that in residual neural networks (ResNets) dynamical isometry is achievable irrespective of the activation function used. We do that by deriving, with the help of Free Probability and Random Matrix Theories, a universal formula for the spectral density of the input-output Jacobian at initialization, in the large network width and depth limit. The resulting singular value spectrum depends on a single parameter, which we calculate for a variety of popular activation functions, by analyzing the signal propagation in the artificial neural network. We corroborate our results with numerical simulations of both random matrices and ResNets applied to the CIFAR-10 classification problem. Moreover, we study consequences of this universal behavior for the initial and late phases of the learning processes. We conclude by drawing attention to the simple fact, that initialization acts as a confounding factor between the choice of activation function and the rate of learning. We propose that in ResNets this can be resolved based on our results by ensuring the same level of dynamical isometry at initialization.

1 Introduction

Deep Learning has achieved unparalleled success in fields such as object detection and recognition, language translation, and speech recognition (LeCun et al., 2015). At the same time, models achieving these state-of-the-art results are increasingly deep and complex (Canziani et al., 2016), which often leads to optimization challenges such as vanishing gradients. Many solutions to this problem have been proposed. In particular, Residual Neural Networks remedy this to some extent (He et al., 2016; Veit et al., 2016) by using skip connections in the network architecture, which improve gradient flow. As a result, Residual Neural Networks outmatched other competing models in the 2015 ILSVRC and COCO competitions. Yet another approach towards solving this problem is to tailor fit the networks weight initialization to facilitate training, for example by ensuring dynamical isometry (Pennington et al., 2017). In this latter case, the insights are based on an analysis of the statistical properties of information propagation in the network and a study of the full singular spectrum of a particular matrix, namely the input-output Jacobian, via the techniques of Free Probability and Random Matrix Theories (FPT & RMT). This perspective has recently led to successfully training a 10000 layer vanilla convolutional neural network (Xiao et al., 2018).

RMT is a versatile tool that, since its inception, saw a substantial share of applications, from the earliest in nuclear physics (Wigner, 1993) to the latest in game theory (Carmona et al., 2018) (see (Akemann et al., 2011) for some of the use cases discovered in the mean time). It is thus not surprising that it found its way to be used to understand artificial neural networks. In particular, to study their loss surface (Choromanska et al., 2015; Pennington and Bahri, 2017), the associated Gram matrix (Louart et al., 2018; Pennington and Worah, 2017) and in the case of single layer networks, their dynamics (Liao and Couillet, 2018). Our main contribution is extending the theoretical analysis of (Pennington et al., 2017; Schoenholz et al., 2016; Pennington et al., 2018) to residual networks. In particular, we find that residual networks can achieve dynamical isometry for many different activation functions provided that the variance of weight initialization scale is inversely proportional to the number of skip-connections. This is in contrast to feedforward networks, where orthogonal weights and antisymmetric sigmoidal activation functions (like tanh) are required. These theoretical results are supported by an empirical investigation on the popular CIFAR-10 benchmark.

Proceedings of the 22nd International Conference on Artificial Intelligence and Statistics (AISTATS) 2019, Naha, Okinawa, Japan. PMLR: Volume 89.

1.1 Related work

The framework of dynamical mean field theory, we will apply to study signal propagation in neural networks, was first used in this context in (Poole et al., 2016). There, the authors showed the existence of an order-to-chaos expressivity transition for deep feedforward neural networks with random initial weights, on the plane spanned by the variances of the network weights and biases. This in turn led to the insight of (Schoenholz et al., 2016), that arbitrary deep networks can be trained as long as they are close to the criticality associated with that transition. The techniques developed in these works, together with methods of FPT and RMT, allowed, for the first time, to analytically compute the singular value distribution of the input-output Jacobian of a deep feedforward network with nonlinear activation function and at criticality (Pennington et al., 2017). Finally, (Pennington et al., 2018) showed, that for feedforward neural networks, in their large depth limit and at a special point of the above mentioned critical line, the singular spectrum of the Jacobian is given by a universal distribution depending on the form of the activation function used. In particular they distinguish the *Bernoulli* and the *smooth* universality classes corresponding to piecewise linear and some nonlinear activation functions. In fact, in this paper, we take the approach of that last work and apply it to fully connected residual neural networks. We find a single universality class for this architecture.

Let us also mention some recent, important developments in the area of residual neural network initialization. One of the earlier developments, is the introduction of layer-sequential unit-variance (LSUV) initialization (Mishkin and Matas, 2015). The two step process involved normalizing the outputs of the neurons on the first forward run and showed promising results. In another, very relevant paper (Taki, 2017), analyzing the signal propagation in a similar manner to that mentioned in the paragraph above, shows for ResNets, with piecewise linear, symmetric as well as ReLU activation functions, that the proper variance for network weight initialization is of order $\frac{1}{NL}$, where L is the number of layers and N the number of neurons in each layer. A similar conclusion is reached by (Balduzzi et al., 2017). We corroborate this result with our analysis. Another contribution shows that adding skip connections to the network, eliminates the critical behavior described above (Yang and Schoenholz, 2017). Finally, the importance of initialization in ResNets is shown by (Zhang et al., 2019), where it is demonstrated that initializing to a zero function enables training state of the art residual networks without the use of batch normalization (Ioffe and Szegedy, 2015). Note that ResNet with this initialization achieves in fact an ideal isometry.

When finishing this manuscript, we have learned of a recent paper tackling the same problem of ResNets initialization by studying the singular spectrum properties of the Jacobian with the tools of Free Probability. While the analysis of (Ling and Qiu, 2018) is related, it is crucial to note that the authors do not observe the universal character of the singular spectrum - the main result of our paper, and treat only piecewise linear activation functions. It is also worth mentioning that, similar to us, they rediscover the importance of $\frac{1}{LN}$ scaling of (Balduzzi et al., 2017) and (Taki, 2017).

1.2 Our results

Our contributions are the following. We show that the singular spectrum of the input-output Jacobian, in the the networks large width and depth limit, is given by a universal formula - with the dependence on the type of activation function encapsulated in a single parameter. Furthermore, we calculate the layer dependent statistical properties of the pre-activations for a variety of activation functions. All together, this gives the associated singular spectra of the Jacobian, which we compare with random matrix and artificial neural network numerical simulations corroborating our theoretical results. The singular values of the input-output Jacobian concentrate around 1 for a wide range of parameters, which shows that fine-tuning the initialization is not required for achieving dynamical isometry in ResNets. Interestingly, the universal formula for the singular spectrum of the Jacobian is valid also in the case when batch normalization is used. Even though the final results of the theoretical calculations are derived in the limit $L, N \to \infty$, the numerical experiments match them already for $L = 10$ (with $N = 500$). As a practical application of our work and the universality property it uncovers, we propose a framework for setting up weight initialization in experiments with residual neural networks.

1.3 Structure of the paper

We follow this introductory section by defining the model of ResNets we will work with and with a short note on the relevance of the input-output Jacobian. Then, in subsection 3.1, we derive the equation governing the Green's function and hence the spectrum of the Jacobian, which depends on a single parameter, which we denote by c. Proceeding is the analysis of the propagation of the information in the network via an analysis of the probability density function describing the pre-activations across the layers at network initialization. This allows us to calculate c for many different activation functions in Appendix D. We close the second section of the paper by revealing the random matrix experiments confirming our results. Sec. 4 is devoted to the outcome of associated residual neural network numerical calculations. There, we showcase the resulting, experimental, universal spectrum of the Jacobian and the outcomes of the learning processes. We close the paper with a discussion section. In Appendix A we give a brief comment on the influence of batch normalization on the presented

setup. In the rest of the Appendices, we show the results of numerical experiments validating the signal propagation recurrence relations and some baseline (based on using the same weight matrix variances, irrespective of the choice of activation functions) simulations of the learning process.

2 The model

In this paper, we consider a deep, residual network of L layers of a constant width of N neurons. We follow the typical nomenclature of the literature and therefore the real-valued, synaptic matrix for the l-th layer is denoted by $\boldsymbol{W}^l$, whereas the real-valued bias vectors are $\boldsymbol{b}^l$. The information propagates in this network according to:

$$\boldsymbol{x}^l = \phi(\boldsymbol{h}^l) + a\boldsymbol{x}^{l-1}, \quad \boldsymbol{h}^l = \boldsymbol{W}^l\boldsymbol{x}^{l-1} + \boldsymbol{b}^l, \tag{1}$$

where $\boldsymbol{h}^l$ and $\boldsymbol{x}^l$ are pre- and post-activations respectively and ϕ is the activation function itself, acting entry-wise on the vector of pre-activations. We have introduced the parameter a to track the influence of skip connections in the calculations, however we do not study its influence on the Jacobian's spectrum or learning in general. By $\boldsymbol{x}^0$ we denote the input of the network and by $\boldsymbol{x}^L$ its output. Our primary interest will lay in exploring the singular value spectral properties of the input-output Jacobian:

$$J_{ik} = \frac{\partial x_i^L}{\partial x_k^0}, \tag{2}$$

known to be useful in studying initialization schemes of neural networks at least since the work of (Glorot and Bengio, 2010). It in particular holds the information on the severity of the exploding gradients problem.

2.1 Relevance of the input-output Jacobian

To understand why we are interested in the Jacobian, consider the neural network adjusting its weights during the learning process. In a simplified, example by example scenario, this happens according to

$$\Delta W_{ij}^l = -\eta \frac{\partial E(\boldsymbol{x}^L, \boldsymbol{y})}{\partial W_{ij}^l}, \tag{3}$$

where $E(\boldsymbol{x}^L, \boldsymbol{y})$ is the error function depending on $\boldsymbol{x}^L$ - the output of the network, $\boldsymbol{y}$ - the correct output value associated with that example and, implicitly through $\boldsymbol{x}^L$, on the parameters of the model, namely the weights and biases. Here, for simplicity, we consider only the adjustments of the weights - an analogous reasoning applies to the biases. η is the learning rate. By use of the chain rule we can rewrite this as:

$$\Delta W_{ij}^l = -\eta \sum_{k,t} \frac{\partial x_t^l}{\partial W_{ij}^l} \frac{\partial x_k^L}{\partial x_t^l} \frac{\partial E(\boldsymbol{x}^L, \boldsymbol{y})}{\partial x_k^L}, \tag{4}$$

For the learning process to be stable, all three terms need to be bounded. Out of those, the middle one can become problematic if a poor choice of the initialization scheme is made. We can rewrite it as:

$$\frac{\partial x_k^L}{\partial x_t^l} = \left[\prod_{i=l+1}^{L} \left(\boldsymbol{D}^i \boldsymbol{W}^i + \mathbf{1}a \right) \right]_{kt} \tag{5}$$

and see the larger the difference between L and l, the more terms we have in the product, and (in general) the less control there is over its behavior. Here $\mathbf{1}$ is an identity matrix and, $\boldsymbol{D}^l$ is a diagonal matrix such that $D_{ij}^l = \phi'(h_i^l)\delta_{ij}$. Indeed, it was proposed by (Glorot and Bengio, 2010), that learning in deep feed-forward neural networks can be improved by keeping the mean singular value of the Jacobian associated with layer i (in our setup $\boldsymbol{J}^i = \boldsymbol{D}^i\boldsymbol{W}^i + \mathbf{1}a$), close to 1 for all i's. It is also important for the dynamics of learning to be driven by data, not by the random initialization of the network. The latter may take place if the Jacobian to the l-th layer possesses very large singular values which dominate the learning or very small singular values suppressing it. In the optimal case all singular values should be concentrated around 1 regardless of how deep is the considered layer. One therefore examines the case of $l = 0$, namely $\partial x_k^L / \partial x_t^0$ - the input-output Jacobian, as the most extreme object of (5). The feature that in the limit of large depth all singular values of $\boldsymbol{J}$ concentrate around 1, irrespective of the depth of the network, was coined as dynamical isometry (Saxe et al., 2013).

Note, that the spectral problem for the full Jacobian

$$\boldsymbol{J} = \prod_{l=1}^{L} \left(\boldsymbol{D}^l \boldsymbol{W}^l + \mathbf{1}a \right) \tag{6}$$

belongs to the class of matrix-valued diffusion processes (Gudowska-Nowak et al., 2003; Janik and Wieczorek, 2004), leading to a complex *eigenvalue* spectrum. We note that the large N limit, spectral properties of (6) with $\boldsymbol{D} = \mathbf{1}$ (deep linear networks), and different symmetry classes of $\boldsymbol{W}$, was derived already by (Gudowska-Nowak et al., 2003). Due to non-normality of the Jacobian, singular values cannot be easily related to eigenvalues. Therefore we follow (Pennington et al., 2017, 2018) and tackle the full *singular spectrum* of the Jacobian (or equivalently the eigenvalue spectrum of $\boldsymbol{J}\boldsymbol{J}^T$), extending these works to the case of the Residual Neural Network model.

3 Spectral properties of the Jacobian

3.1 Spectral analysis

Free Probability Theory, or Free Random Variable (FRV) Theory (Voiculescu et al., 1992), is a powerful tool for the spectral analysis of random matrices in the limit of their large size. It is a counterpart of the classical Probability

Theory for the case of non-commuting observables. For a pedagogical introduction to the subject, see (Mingo and Speicher, 2017) - here we start by laying out the basics useful in the derivations of this subsection. The fundamental objects of the theory are the Green's functions (a.k.a. Stieltjes transforms in mathematical literature):

$$G_H(z) = \left\langle \frac{1}{N}\mathrm{Tr}\,(z\mathbf{1} - \boldsymbol{H})^{-1} \right\rangle = \int_{-\infty}^{\infty} \frac{\rho_H(\lambda)d\lambda}{z-\lambda}, \qquad (7)$$

which generate spectral moments and where the subscript H indicates, that his formulation is proper for self-adjoint matrices. The eigenvalue density can be recovered via the Sochocki-Plemelj formula

$$\rho_H(x) = -\frac{1}{\pi}\lim_{\epsilon\to 0} G_H(x+i\epsilon). \qquad (8)$$

The associated free cumulants are generated by the so-called R-transform, which plays the role of the logarithm of the characteristic function in the classical probability. By this correspondence, the R-transform is additive under addition, i.e. $R_{X+Y}(z) = R_X(z) + R_Y(z)$ for mutually free, but non-commuting random ensembles X and Y. Moreover, it is related to G via the functional equations

$$G\left(R(z) + \frac{1}{z}\right) = z, \qquad R(G(z)) + \frac{1}{G(z)} = z. \qquad (9)$$

On the other hand, the so-called S-transform facilitates calculations of the spectra of products of random matrices, as it satisfies $S_{AB}(z) = S_A(z)S_B(z)$, provided A and B are mutually free and at least one is positive definite. If additionally, the ensemble has a finite mean, the S-transform can be easily obtained from the R-transform, and vice versa, through a pair of the following, mutually inverse maps $z = yS(y)$ *and* $y = zR(z)$. Explicitly:

$$S(zR(z)) = \frac{1}{R(z)}, \quad R(zS(z)) = \frac{1}{S(z)}. \qquad (10)$$

Denoting now $\boldsymbol{J}_L$ the Jacobian across L layers and $\boldsymbol{Y}_l = (a\mathbf{1} + \boldsymbol{D}^l\boldsymbol{W}^l)$, one can write the recursion relation $\boldsymbol{J}_L\boldsymbol{J}_L^T = \boldsymbol{Y}_L\boldsymbol{J}_{L-1}\boldsymbol{J}_{L-1}^T\boldsymbol{Y}_L$. The latter matrix is isospectral to $\boldsymbol{Y}_L^T\boldsymbol{Y}_L\boldsymbol{J}_{L-1}\boldsymbol{J}_{L-1}^T$, which leads to the equation for the S-transform $S_{J_LJ_L^T}(z) = S_{Y_L^TY_L}(z)S_{J_{L-1}J_{L-1}^T}(z)$. Proceeding inductively, we arrive at

$$S_{JJ^T}(z) = \prod_{l=1}^{L} S_{Y_lY_l^T}(z). \qquad (11)$$

To find the S-transform of the single layer Jacobian, we will first consider its Green's function

$$G(z) = \left\langle \frac{1}{N}\mathrm{Tr}(z\mathbf{1} - \boldsymbol{Y}_l\boldsymbol{Y}_l^T)^{-1} \right\rangle, \qquad (12)$$

with the averaging over the ensemble of weight matrices $\boldsymbol{W}^l$. To facilitate the study of G, in particular to cope with $\boldsymbol{Y}\boldsymbol{Y}^T$, one linearizes the problem by introducing matrices of size $2N \times 2N$

$$\mathcal{Z} := \begin{pmatrix} -a & 1 \\ z & -a \end{pmatrix}, \qquad \mathcal{X} := \begin{pmatrix} \boldsymbol{X} & 0 \\ 0 & \boldsymbol{X}^T \end{pmatrix}, \qquad (13)$$

with $\boldsymbol{X} = \boldsymbol{D}^l\boldsymbol{W}^l$. Another crucial ingredient is the block trace operation (bTr), which is the trace applied to each $N \times N$ block. The generalized Green's function is defined as a block trace of the generalized resolvent $(\mathcal{Z}\otimes\mathbf{1} - \mathcal{X})^{-1}$

$$\mathcal{G} := \begin{pmatrix} G_{11} & G_{12} \\ G_{21} & G_{22} \end{pmatrix} = \left\langle \frac{1}{N}\mathrm{bTr}\begin{pmatrix} -a-\boldsymbol{X} & 1 \\ z & -a-\boldsymbol{X}^T \end{pmatrix}^{-1} \right\rangle. \qquad (14)$$

Remarkably, the Green's function of $\boldsymbol{Y}\boldsymbol{Y}^T$ is the G_{12} entry of the generalized Green's function. This construction is a slight modification of the quaternionization approach to large non-Hermitian matrices developed by (Janik et al., 1997), therefore we adapt these concepts here for calculations in the large width limit of the network. Furthermore, the generalized Green's function (14) is given implicitly by the solution of the Schwinger-Dyson equation

$$\mathcal{G}(\mathcal{Z}) = (\mathcal{Z} - \mathcal{R}(\mathcal{G}(\mathcal{Z})))^{-1}. \qquad (15)$$

Here $\mathcal{R}$ is the generalized R-transform of FRV theory. This construction is a generalization of standard FRV tools to the matrix-valued functions. In particular, (15) is such a generalization of (9) to 2×2 matrices.

To study two common weight initializations, Gaussian and scaled orthogonal, on the same footing, we assume that W belongs to the class of biunitarily invariant random matrices, i.e. its pdf is invariant under multiplication by two orthogonal matrices, $P(\boldsymbol{U}\boldsymbol{W}\boldsymbol{V}^T) = P(\boldsymbol{W})$ for $\boldsymbol{U},\boldsymbol{V} \in O(N)$. In the large N limit these matrices are known in free probability as R-diagonal operators (Nica and Speicher, 1996). A product of R-diagonal operator with an arbitrary operator remains R-diagonal (Nica and Speicher, 2006), thus the matrix $\boldsymbol{X}$ is R-diagonal too.

The generalized $\mathcal{R}$-transform of R-diagonal operators takes a remarkably simple form (Nowak and Tarnowski, 2017)

$$\mathcal{R}(\mathcal{G}) = A(G_{12}G_{21})\begin{pmatrix} 0 & G_{12} \\ G_{21} & 0 \end{pmatrix}. \qquad (16)$$

Here, $A(x) = \sum_{k=1}^{\infty} c_{2k}x^{k-1}$ is the determining sequence, which generates cumulants c_{2k}, it is a Taylor expansion of $A(x)$ at 0. For the later use we mention a simple relation for the determining sequence of a scaled matrix $A_{aX}(z) = a^2A_X(a^2z)$, which generalizes the Hermitian case $G_{aH}(z) = \frac{1}{a}G_H(\frac{z}{a})$ or, equivalently, $R_{aH}(z) = aR_H(az)$.

We derive the equation for the Green's function (with $G(z) = G_{12}$) by substituting the $\mathcal{R}$-transform (16) into (15) and eliminating irrelevant variables. It thus reads:

$$G = \frac{GA(zG^2) - 1}{a^2 - z(1 - GA(zG^2))^2}, \qquad (17)$$

where for clarity we omitted the argument of the Green's function. In the next step we substitute $z \to R(z) + \frac{1}{z}$ and use (9) to obtain

$$z = \frac{zA(z^2R + z) - 1}{a^2 - (R + \frac{1}{z})(1 - zA(z^2R + z))^2}. \tag{18}$$

Then, we substitute $z \to zS(z)$ and use (10), which leads us to

$$1 = \frac{zSA(z(z+1)S) - 1}{a^2zS - (z+1)(1 - zSA(z(z+1)S))^2}. \tag{19}$$

This equation is exact. To incorporate the additional scaling of weights variances by $1/L$ in our considerations, as proposed by (Taki, 2017) and (Balduzzi et al., 2017), we rescale $\boldsymbol{X} \to \boldsymbol{X}/\sqrt{L}$ and since we are interested in deep networks, we keep only the leading term in $1/L$ (see also (Janik and Wieczorek, 2004)). This leads to $A(z(z+1)S) \to \frac{1}{L}A\left(\frac{1}{L}z(z+1)S\right) = \frac{c_2}{L} + O\left(\frac{1}{L^2}\right)$, which simplifies (19) to a quadratic equation for S. Choosing the appropriate branch of the solution, we see that

$$S_{Y_lY_l^T}(z) = \frac{1}{a^2}\left(1 - \frac{c_2^l}{a^2L}(1+2z) + O\left(\frac{1}{L^2}\right)\right). \tag{20}$$

Here

$$c_2^l = \left\langle \frac{1}{N}\mathrm{Tr}\boldsymbol{W}^l\boldsymbol{D}^l\boldsymbol{D}^l(\boldsymbol{W}^l)^T \right\rangle = \frac{\sigma_w^2}{N}\sum_i^N \left(\phi'(h_i^l)\right)^2 \tag{21}$$

is the squared spectral radius of the matrix $\boldsymbol{D}^l\boldsymbol{W}^l$. In general, c_2^l can vary across the depth of the network due to non-constant variance of preactivations. Assuming that this variability is bounded, we can consider the logarithm of (11) and write:

$$\ln S_{JJ^T}(z) = -2L\ln a - \frac{(1+2z)}{a^2}c, \tag{22}$$

where we defined the effective cumulant $c = \frac{1}{L}\sum_{l=1}^L c_2^l$ and used $\ln(1+x) \approx x$. This allows us to deduce the form of the S-transform, assuming that a does not scale with L

$$S_{JJ^T}(z) = \frac{1}{a^{2L}}e^{-\frac{c}{a^2}(1+2z)}. \tag{23}$$

Substituting $z \to zR(z)$ and using (10), we obtain

$$a^{2L} = R(z)\exp\left[-\frac{c}{a^2}(1 + 2zR(z))\right]. \tag{24}$$

Then, we substitute $z \to G(z)$ and use (9) to finally get

$$a^{2L}G(z) = (zG(z) - 1)e^{\frac{c}{a^2}(1-2zG(z))}, \tag{25}$$

an equation for the Green's function characterizing the square singular values of the Jacobian, which can be solved numerically. We do that for a range of different activation functions and present the results with numerical simulations to corroborate them in Fig. 1.

We close this section with a remark that the above analysis is not restricted only to the model (1), but analogous reasoning can be performed for networks in which skip connections bypass more than one fully connected block. The qualitative results remain unaltered provided that L is replaced by the number of skip connections.

3.2 Signal propagation

The formulas we have derived until now were given in terms of a single parameter c, which is the squared derivative of the activation function averaged within each layer and across the depth of the network. Thus, we now need to address the behavior of preactivations. In the proceeding paragraph, we closely follow a similar derivation done in (Schoenholz et al., 2016), for fully connected feed forward networks.

For the simplicity of our arguments, we consider here W_{ij}^l and b_i^l as independent identically distributed (iid) Gaussian random variables with 0 mean and variances $\frac{(\sigma_W)^2}{LN}$ and $(\sigma_b)^2$, respectively. Here, $(\sigma_W)^2$ is of order one, and the additional scaling is meant to reflect those introduced in the previous paragraphs. At the end of this section we provide an argument that the same results hold for scaled orthogonal matrices.

In this subsection, we will denote the averaging over variables W_{ij}^l and b_i^l, at a given layer l, by $\langle\cdot\rangle_{wbl}$. By $\langle u\rangle_l$ we denote the sample average, of some variable u in the l-th layer: $\langle u\rangle_l \equiv \frac{1}{N}\sum_{i=1}^N u_i^l$. Note that the width ($N$) is independent of the layer number, however the derivation can be easily generalized to the opposite case, when the architecture is more complicated. Unless stated otherwise explicitly, all integrals are calculated over the real line.

We are interested in the distribution of h_i^l in our model, depending on the input vectors and the probability distributions of W_{ij}^l and b_i^l. If we assume they are normal (as can be argued using the Central Limit Theorem), we just need the first two moments. It is clear that $\langle h_i^l\rangle_{wbl} = 0$. Furthermore, we assume ergodicity, i.e. that averaging some quantity over a layer of neurons is equivalent to averaging this quantity for one neuron over an ensemble of neural networks with random initializations. We assume this is true for h_i, x_i, W_{ij} and b_i. Thus, we can say that $\langle h\rangle_l = 0$ and moreover, as we work in the limit of wide networks, $\langle f(h)\rangle_l$ (where f is some function of h_l) can be replaced with an averaging over a normal distribution of variance $q^l \equiv \left\langle \left(h^l\right)^2 \right\rangle_{wbl}$. This is the crux of the dynamical mean field theory approach (Poole et al., 2016) for feed-forward neural networks. We have in particular:

$$c_2^l = \sigma_W^2\left\langle(\phi'(h))^2\right\rangle_l = \sigma_W^2\int \mathcal{D}z\phi'^2\left(\sqrt{q^l}z\right), \tag{26}$$

where $\mathcal{D}z = \exp(-z^2/2)dz/\sqrt{2\pi}$. To calculate the effective cumulant, we need to know how the variance of the distribution of the preactivations changes as the input information propagates across consecutive layers of the network. It is shown in Appendix C, that q^l satisfy the recurrence equation

$$q^{l+1} = a^2 q^l + \left(1-a^2\right)\sigma_b^2 + \frac{(\sigma_W)^2}{L}\int \mathcal{D}z\phi^2\left(\sqrt{q^l}z\right) + 2\frac{(\sigma_W)^2}{L}\left[\sum_{k=1}^{l-1} a^k \int \mathcal{D}z\phi\left(\sqrt{q^{l-k}}z\right)\right]\int \mathcal{D}z\phi\left(\sqrt{q^l}z\right), \quad (27)$$

with the initial condition $q^1 = \sigma_b^2 + \frac{\sigma_W^2}{L}$.

We remark here that the above reasoning concerning signal propagation holds also when the weights are scaled orthogonal matrices, i.e. $\boldsymbol{W}\boldsymbol{W}^T = \frac{\sigma_W^2}{L}\mathbf{1}$. In such a case $\left\langle W_{ij}\right\rangle = 0$ and $\left\langle W_{ij}W_{kl}\right\rangle = \frac{\sigma_W^2}{NL}\delta_{ik}\delta_{jl}$ (Collins and Śniady, 2006) and the entries of $\boldsymbol{W}$ can be approximated as independent Gaussians (Chatterjee and Meckes, 2007).

3.3 Random matrix simulations

To thoroughly test the theoretical predictions of Section 3, we run numerical simulations using *Mathematica*. The initial condition, input vector $\boldsymbol{x}^0$ of length $N = 500$, filled with iid Gaussian random variables of zero mean and unit variance, is propagated according to the recurrence (1), for various activation functions. The network weights and biases are generated from normal distribution of zero mean and σ_W^2/NL and σ_b^2 variances, respectively, with $N = 500$ The propagation of variance of preactivations, post-activations as well as the calculation of the second cumulants c^l for the studied activation functions, across the network, is presented in Appendix E. All numerical simulations corroborate our theoretical results. Here, for clarity and as a generic example, in Fig. 1 (upper), we show the distribution of singular values of the input-output Jacobian (defined in (6)) for the tanh nonlinearity for various network depths. In this example the Jacobian in not independent of the signal propagation, contrary to the case of piecewise linear activation functions. Similarly, in the lower panel of Fig. 1, we showcase the outcome of numerical experiments and the associated, matching, theoretical results for the most popular ReLU activation function, for various initializations resulting in different values of the effective cumulant c.

4 Experiments on image classification

The goal of this section is to test our theoretical predictions on real data via the popular CIFAR-10 benchmark (Krizhevsky, 2009). To this end we will use a single representation fully connected residual network, see Fig. 2.

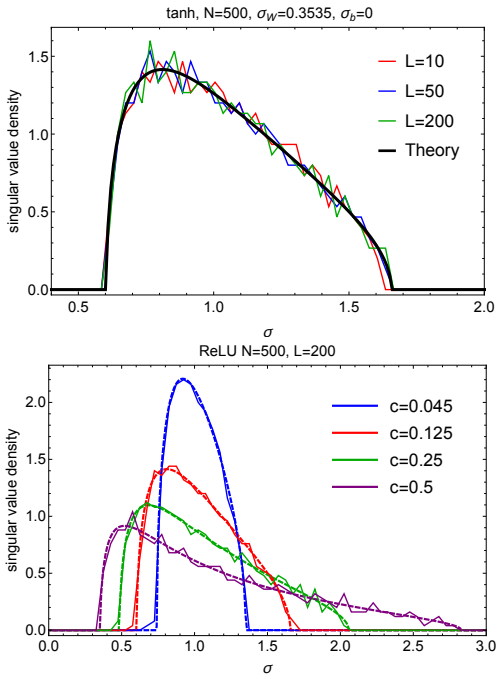

Figure 1: (Top) density of singular values of the input-output Jacobian for the residual network with tanh nonlinearity. Note that the asymptotic theoretical result describes remarkably well not very deep ($L = 10$) networks. (Bottom) asymptotic distribution of singular values for various values of parameter c (dashed) juxtaposed with the numerical simulations for ReLU nonlinearity (solid). Note that histograms were calculated from a single random initialisation. The smaller c, the narrower the spectrum and the closer to the ideal isometry.

This simplified version of the model of (He et al., 2016) does not use (i) multiple stages with different dimension of hidden representation, and (ii) two layers within residual block. We leave study of a more general version of ResNets for future work.

4.1 Achieving dynamical isometry for any activation function

Perhaps the most interesting prediction of our theory is that ResNets, in contrast to fully connected networks, can achieve dynamical isometry for many different activation functions. We will study this empirically by looking at $\mathbf{J}$, at initialization, for different activation functions and number of residual blocks. Please note that by $\mathbf{J}$ we refer to Jacobian of the output of the last residual block with respect to the input of the first one, see also Fig. 2.

We consider the following popular activation functions: ReLU (Nair and Hinton, 2010), Tanh, Hard Tanh, Sigmoid, SeLU (Klambauer et al., 2017) and Leaky ReLU (Maas

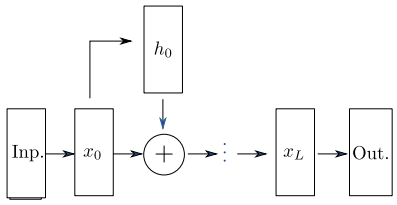

Figure 2: Residual network architecture used in the paper.

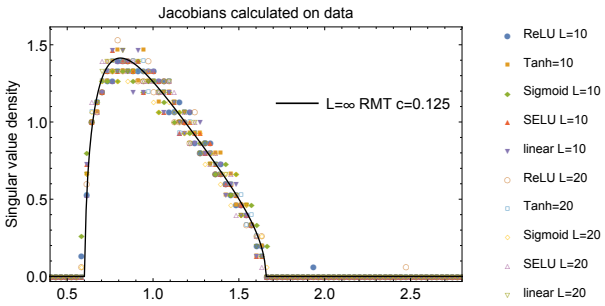

Figure 3: Singular spectra obtained for various activation functions and depth $L = 10, 20$. The network was fed with examples from CIFAR10 dataset.

et al., 2013) with the leaking constant 0.05 and 0.25. For each activation function we consider the number of blocks L to be 10 and 20. All weights of the network are initialized from a zero-centered normal distribution whereas biases are initialized to zero. The weights of the residual blocks are initialized using standard deviation $\sigma_W/\sqrt{NL}$, other weights are initialized as by (Taki, 2017). For the given activation function and the number of blocks L, we set σ_W in such a way that the effective cumulant $c = 0.125$, which ensures the concentration of eigenvalues of the Jacobian around one, and hence dynamical isometry (see Appendix D for more details and Fig. 1 for the shape of the singular value densities).

For each pair of activation function and number of blocks we compute the empirical spectrum of $\mathbf{J}$ at initialization, the results are reported in Fig. 3. Indeed, we observe that upon scaling the initializations standard deviation, in such a way that c is kept constant, the empirical spectrum of $\mathbf{J}$ is independent of the number of residual blocks or the choice of activation functions.

4.2 Learning dynamics are more similar at universality under dynamical isometry

Our next objective is to investigate whether networks achieving dynamical isometry share similar learning dynamics. While this is outside of the scope of our theoretical investigation, it is inspired by studies such as (Pennington et al., 2017), which demonstrate the importance of dynam-

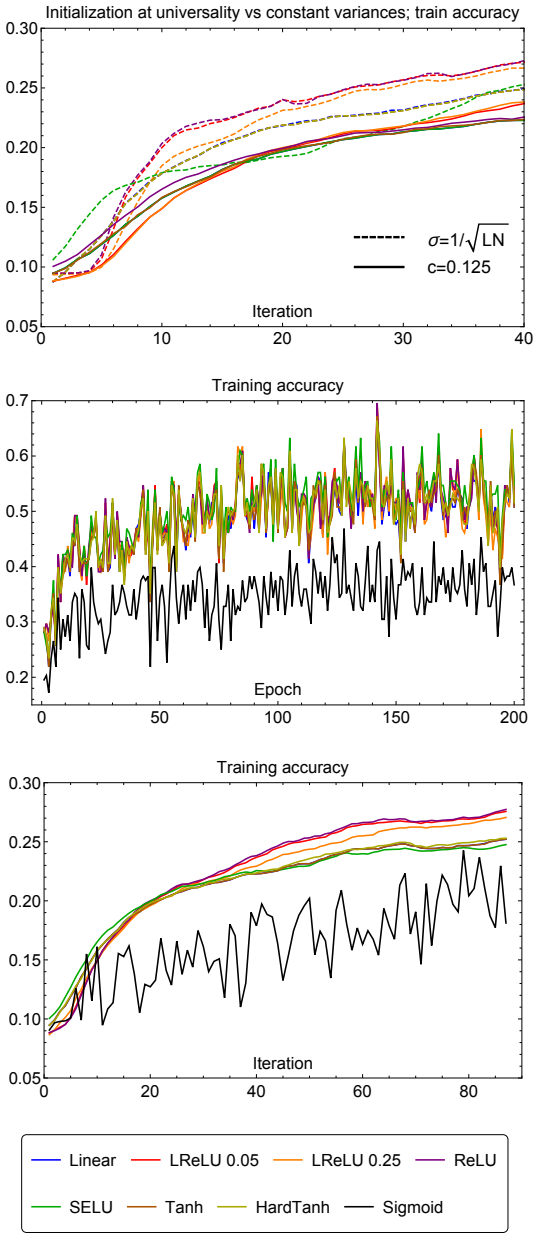

Figure 4: Training accuracy during first 200 epochs (middle) and first 100 iterations (bottom) of residual networks with various activation functions. The weight initialization was chosen for each activation function in such a way that the effective cumulant is $c = 0.125$. In the top panel, the dynamics with this initialization was juxtaposed with analogous training of networks in which the variance of weights was chosen to be $\frac{1}{LN}$ for all activation functions. We used leaky ReLU with $\alpha = 0.05, 0.25$.

ical isometry at the initialization for the subsequent optimization.

We consider the same set of experiments as in the previous section, and follow a similar training protocol to (He et al., 2016). We train for 200 epochs and drop the learning rate by a factor of 10 after epochs 80, 120, and 160. We use batch-size 128 and a starting learning rate of either 10^{-3} or 10^{-4} [1].

First, we look at the learning dynamics on the training set. We can observe that most of the activation functions exhibit similar training accuracy evolution, see Fig. 4 (middle). Using the sigmoid activation, led however to significantly slower optimization. This is due to a faster growth of the variances of post- and pre- activations (which can be observed in Fig. 5), which exacerbates the neuron saturation problem.

Overall our results suggest that the singular spectrum of $\mathbf{J}$ at initialization does not fully determine generalization and training performance. Nonetheless, setting the same effective cumulant for the experiments with different activation functions results in a markedly coinciding behavior of neural networks using activation functions of similar characteristics. This is in contrast to a setup in which the variances of the weight matrix entries are set to be equal. To demonstrate this we run another set of training experiments, this time with all standard deviations $\sigma = 1/\sqrt{LN}$. The plots depicting the full results are relegated to Fig. 7 in Appendix F. Here, in Fig. 4 (top) we showcase the training accuracy during the first 40 iterations for these two setups (excluding, for clarity, the networks with the sigmoid activation function). With different effective cumulants, the network learning dynamics, differs among experiments with different activation functions, especially at the beginning of learning.

This suggests that the spectrum of the input-output Jacobian at initialization can be treated as a confounding variable in such experiments. Ensuring that the level of dynamic isometry, and hence the value of the effective cumulant is kept the same, provides the possibility of a more meaningful comparison of the effect of activation functions on learning dynamics.

5 Synopsis and discussion

The main focus of this paper was the singular spectrum of the input-output Jacobian of a simple model of residual neural networks. We have shown that in the large network depth limit, it is described by a single, universal equation. This holds irrespective of the activation function used, for biunitarily invariant weight initializations matrices, a set covering Gaussian and scaled orthogonal initialization schemes. The singular value density depends on a single parameter called the effective cumulant, which can be calculated by considering the propagation of information in the network, via a dynamical mean field theory approach. This parameter depends on the activation function used, variance of biases and the entries of the weight matrices, and, for some activation functions, also on the depth of the network. We demonstrated the validity of our theoretical results in numerical experiments, both by generating random matrices adhering to the assumptions of the model and by evaluating the Jacobians of residual networks (at initialization) on the CIFAR10 dataset.

For a given activation function and/or network depth, it is always possible to set the weight matrix entries variances in such a way, that the resulting singular spectra of the Jacobians not only fulfill the conditions for dynamical isometry, but also are exactly the same, irrespective of the activation function used. This observation allows us to eliminate the singular spectrum of the Jacobian treated as a confounding factor in experiments with the learning process of simple residual neural networks for different activation functions. As an example of how this approach can be applied, we examined how accuracies of simple residual neural networks, employing a variety of activation functions, change during the learning process. When using the same variances of weight matrices entries, the learning curves of similar activation functions differed between each other more than when the networks were initialized with the same input-output Jacobian spectra. This allows, in our opinion, for a more meaningful comparison between the effects of choosing the activation function. We hope this observation will help with the research of deep neural networks.

[1] We use relatively low learning rates, largely because we omit batch normalization layers in the architecture.

Acknowledgements

PW would like to acknowledge the funding of the Polish National Science Centre, through the project SONATA number 2016/21/D/ST2/01142. WT appreciates the financial support from the Polish Ministry of Science and Higher Education through "Diamond Grant" 0225/DIA/2015/44. SJ was supported by the Polish National Science Centre through ETIUDA stipend No. 2017/24/T/ST6/00487.

References

Akemann, G., Baik, J., and Di Francesco, P. (2011). *The Oxford handbook of random matrix theory*. Oxford University Press.

Balduzzi, D., Frean, M., Leary, L., Lewis, J., Ma, K. W.-D., and McWilliams, B. (2017). The shattered gradients problem: If resnets are the answer, then what is the question? *arXiv preprint arXiv:1702.08591*.

Canziani, A., Paszke, A., and Culurciello, E. (2016). An analysis of deep neural network models for practical applications. *arXiv preprint arXiv:1605.07678*.

Carmona, R., Cerenzia, M., and Palmer, A. Z. (2018). The dyson game. *arXiv preprint arXiv:1808.02464*.

Chatterjee, S. and Meckes, E. (2007). Multivariate normal approximation using exchangeable pairs. *arXiv preprint math/0701464*.

Choromanska, A., Henaff, M., Mathieu, M., Arous, G. B., and LeCun, Y. (2015). The loss surfaces of multilayer networks. In *Artificial Intelligence and Statistics*, pages 192–204.

Collins, B. and Śniady, P. (2006). Integration with respect to the haar measure on unitary, orthogonal and symplectic group. *Communications in Mathematical Physics*, 264(3):773–795.

Glorot, X. and Bengio, Y. (2010). Understanding the difficulty of training deep feedforward neural networks. In *Proceedings of the thirteenth international conference on artificial intelligence and statistics*, pages 249–256.

Gudowska-Nowak, E., Janik, R. A., Jurkiewicz, J., and Nowak, M. A. (2003). Infinite products of large random matrices and matrix-valued diffusion. *Nuclear Physics B*, 670(3):479–507.

He, K., Zhang, X., Ren, S., and Sun, J. (2016). Deep residual learning for image recognition. In *Proceedings of the IEEE conference on computer vision and pattern recognition*, pages 770–778.

Ioffe, S. and Szegedy, C. (2015). Batch normalization: Accelerating deep network training by reducing internal covariate shift. In Bach, F. R. and Blei, D. M., editors, *ICML*, volume 37 of *JMLR Workshop and Conference Proceedings*, pages 448–456. JMLR.org.

Janik, R. A., Nowak, M. A., Papp, G., Wambach, J., and Zahed, I. (1997). Non-hermitian random matrix models: Free random variable approach. *Physical Review E*, 55(4):4100.

Janik, R. A. and Wieczorek, W. (2004). Multiplying unitary random matrices—universality and spectral properties. *Journal of Physics A: Mathematical and General*, 37(25):6521.

Klambauer, G., Unterthiner, T., Mayr, A., and Hochreiter, S. (2017). Self-normalizing neural networks. In *Advances in Neural Information Processing Systems*, pages 971–980.

Krizhevsky, A. (2009). Learning Multiple Layers of Features from Tiny Images. Master's thesis.

LeCun, Y., Bengio, Y., and Hinton, G. (2015). Deep learning. *nature*, 521(7553):436.

Liao, Z. and Couillet, R. (2018). The dynamics of learning: A random matrix approach. *arXiv preprint arXiv:1805.11917*.

Ling, Z. and Qiu, R. C. (2018). Spectrum concentration in deep residual learning: a free probability appproach. *arXiv preprint arXiv:1807.11694*.

Louart, C., Liao, Z., Couillet, R., et al. (2018). A random matrix approach to neural networks. *The Annals of Applied Probability*, 28(2):1190–1248.

Maas, A. L., Hannun, A. Y., and Ng, A. Y. (2013). Rectifier nonlinearities improve neural network acoustic models. In *Proc. icml*, volume 30, page 3.

Mingo, J. A. and Speicher, R. (2017). *Free probability and random matrices*, volume 4. Springer.

Mishkin, D. and Matas, J. (2015). All you need is a good init. *arXiv preprint arXiv:1511.06422*.

Nair, V. and Hinton, G. E. (2010). Rectified linear units improve restricted boltzmann machines. In *Proceedings of the 27th international conference on machine learning (ICML-10)*, pages 807–814.

Nica, A. and Speicher, R. (1996). *r*-diagonal pairs-a common approach to haar unitaries and circular elements. *arXiv preprint funct-an/9604012*.

Nica, A. and Speicher, R. (2006). *Lectures on the combinatorics of free probability*, volume 13. Cambridge University Press.

Nowak, M. A. and Tarnowski, W. (2017). Complete diagrammatics of the single-ring theorem. *Physical Review E*, 96(4):042149.

Pennington, J. and Bahri, Y. (2017). Geometry of neural network loss surfaces via random matrix theory. In *International Conference on Machine Learning*, pages 2798–2806.

Pennington, J., Schoenholz, S., and Ganguli, S. (2017). Resurrecting the sigmoid in deep learning through dynamical isometry: theory and practice. In *Advances in Neural Information Irocessing Systems*, pages 4785–4795.

Pennington, J., Schoenholz, S. S., and Ganguli, S. (2018). The emergence of spectral universality in deep networks. *arXiv preprint arXiv:1802.09979*.

Pennington, J. and Worah, P. (2017). Nonlinear random matrix theory for deep learning. In *Advances in Neural Information Processing Systems*, pages 2637–2646.

Poole, B., Lahiri, S., Raghu, M., Sohl-Dickstein, J., and Ganguli, S. (2016). Exponential expressivity in deep neural networks through transient chaos. In *Advances in neural information processing systems*, pages 3360–3368.

Saxe, A. M., McClelland, J. L., and Ganguli, S. (2013). Exact solutions to the nonlinear dynamics of learning in deep linear neural networks. *arXiv preprint arXiv:1312.6120*.

Schoenholz, S. S., Gilmer, J., Ganguli, S., and Sohl-Dickstein, J. (2016). Deep information propagation. *arXiv preprint arXiv:1611.01232*.

Taki, M. (2017). Deep residual networks and weight initialization. *arXiv preprint arXiv:1709.02956*.

Veit, A., Wilber, M. J., and Belongie, S. (2016). Residual networks behave like ensembles of relatively shallow networks. In *Advances in Neural Information Processing Systems*, pages 550–558.

Voiculescu, D. V., Dykema, K. J., and Nica, A. (1992). *Free random variables*. Number 1. American Mathematical Soc.

Wigner, E. P. (1993). Characteristic vectors of bordered matrices with infinite dimensions i. In *The Collected Works of Eugene Paul Wigner*, pages 524–540. Springer.

Xiao, L., Bahri, Y., Sohl-Dickstein, J., Schoenholz, S. S., and Pennington, J. (2018). Dynamical isometry and a mean field theory of cnns: How to train 10,000-layer vanilla convolutional neural networks. *arXiv preprint arXiv:1806.05393*.

Yang, G. and Schoenholz, S. (2017). Mean field residual networks: On the edge of chaos. In *Advances in Neural Information Processing Systems*, pages 7103–7114.

Zhang, H., Dauphin, Y. N., and Ma, T. (2019). Residual learning without normalization via better initialization. In *International Conference on Learning Representations*.